AGED MUSCLE ECM RECAPITULATES ALTERED HOST RESPONSE OBSERVED IN AGED MUSCLE INJURY

by

Samuel T. LoPresti

Bachelor of Science in Biomedical Engineering

University of Rochester, 2012

Submitted to the Graduate Faculty of

Swanson School of Engineering in partial fulfillment

of the requirements for the degree of

Doctor of Philosophy

University of Pittsburgh

2018

UNIVERSITY OF PITTSBURGH

SWANSON SCHOOL OF ENGINEERING

This dissertation was presented

by

Samuel T. LoPresti

It was defended on

October 22, 2018

and approved by

Fabrisia Ambrosio, Ph.D., MPT, Associate Professor
Department of Physical Medicine & Rehabilitation

Stephen F. Badylak, DVM., Ph.D., MD, Professor
Department of Surgery

Bryan N. Brown, Ph.D., Assistant Professor
Department of Bioengineering

Jon D. Piganelli, Ph.D., Associate Professor
Department of Surgery

William R. Wagner, Ph.D., Professor
Department of Surgery

Cecelia C. Yates, Ph.D., Associate Professor
Department of Nursing

Dissertation Director: Bryan N. Brown, Ph.D., Assistant Professor
Department of Bioengineering

**AGED MUSCLE ECM RECAPITULATES ALTERED HOST RESPONSE
OBSERVED IN AGED MUSCLE INJURY**

Samuel Traxler LoPresti, Ph.D.

University of Pittsburgh, 2018

Extracellular matrix acts as the supporting structure of a tissue and dynamically changes in a reciprocal relationship with cells of that tissue. ECM changes with aging and disease and can affect the responses of cells in these altered states. ECM can be used as a model for aged microenvironments to more fully understand their effect on cellular function. Macrophage polarization has been shown to be necessary for appropriate skeletal muscle healing. This study used decellularized skeletal muscle ECM from young and aged mice to determine microenvironmental effects on macrophage phenotype both *in vitro* and *in vivo* using an abdominal wall injury reconstruction model.

The first objective of this work was to characterize muscle ECM from young and aged mice and to observe its effect on macrophage phenotype and function. Bone marrow-derived macrophages treated with muscle ECM showed increases in iNOS immunolabeling and nitric oxide production with aged muscle ECM indicative of a shift to a pro-inflammatory phenotype.

The second objective of this work was to characterize the macrophage response to artificially glycated ECM. Young muscle ECM was artificially glycated with low and high concentrations of glucose, ribose or fructose. The macrophage response to glycated muscle ECM showed an increased nitric oxide production compared to young ECM. ECM glycation caused pro-inflammatory phenotypes from bone marrow-derived macrophages.

The third objective of this work was to characterize the in vivo host response to young, aged and glycated muscle ECM implanted into an abdominal muscle injury. The host response to aged and glycated ECM was characterized by reduced infiltration of host cells including F4/80[+] macrophages and delayed or prevented activation of macrophage polarization markers iNOS and arginase-1. Glycation led to increased collagen staining and reduced fast:slow muscle fiber type ratio by 90 days. *In vivo* results suggest that aged ECM delays inflammatory cascades while glycated ECM inhibits macrophage activation overall.

Aging and glycation of the skeletal muscle ECM microenvironment had direct effects on the macrophage response *in vitro* and *in vivo*. This provides evidence for a cell-extrinsic mechanism of aging which is separate from known changes in stem cell function and population with age.

TABLE OF CONTENTS

LIST OF TABLES

LIST OF FIGURES

PREFACE

The path to completion of this doctoral degree has involved the support and guidance from many people. Firstmost, I would like to thank Professor Bryan Brown for accepting me into his laboratory as one of his first graduate students and supporting me throughout this journey. He has been incredibly supportive throughout my graduate career, allowing me to work on many projects and be involved in many different programs, groups and competitions on campus.

I would also like to thank my dissertation committee, including Dr. Fabrisia Ambrosio, Dr. Stephen Badylak, Dr. Jon Piganelli, Dr. William Wagner, Dr. Cecelia Yates, and again Dr. Bryan Brown, for their support and constructive criticism of my work in order to guide this dissertation to a successful conclusion.

I would like to thank the many former and current members of Dr. Brown's laboratory who have helped me with my graduate work and have become great friends. These include Travis Prest, John Wroblewski, Stephen Canton, Deepa Mani, Daniel Hachim, Michael Buckenmeyer, Elizabeth Stahl, Alexis Nolfi, Aimon Iftikhar, Martin Haschak, Arta Kelmendi-Doko, Tyler Meder, Branimir Popovic and Clint Skillen. I would like the many undergraduate students who I have had the honor of mentoring and who have helped with the completion of this work: Joseph Kennedy, Sameer Patel, Sterling Bowers, Sidd Dash, Tomisin Ojo-Aromokudu,

Clint Skillen, Monica Kiesel, Ali Balubaid, Sharisse Victor, Zach Clemens, Yelnash Vedanaparti, and Edward-James Alexander Gardner.

I am also very appreciative of the many friends I have made before and during graduate school in Pittsburgh. All of my friends from Grand Island, NY, Canisius High School and the University of Rochester have continued to be supportive despite how busy graduate school can be at times. I have also made an extraordinary group of friends here in Pittsburgh both in and out of the Department of Bioengineering who have helped make Pittsburgh home.

I would like to thank my family who have been supportive throughout my educational journey, always supportive and encouraging me to achieve at the highest level possible. My father Mark and my mother Marilee have always emphasized education and pushed me to pursue graduate work to further my career. I would like to thank my brothers Stephen and Vincent for their support and helping me to become the person I am today.

I would lastly like to thank my girlfriend Dongeun who has been my best friend and number one supporter for much of my time in Pittsburgh. I would also like to thank her parents Sung Jin and Meemee and her sister Kyoung who have welcomed me into their home and family.

1.0   INTRODUCTION

1.1   AGING

1.1.1   Aging and Muscle Physiology

Aging is a multifactorial process that all organisms experience through time which eventually results in the loss of normal physiological function [1]. Aging is a major risk factor for many disease pathologies including cancer, obesity, diabetes, as well as cardiovascular and neurological diseases. As we age, our skeletal muscles atrophy and our ability to regenerate injured muscles declines [2]. Many factors have been implicated with the diminished ability of our muscles to regenerate with age including satellite cells (muscle stem cells), vascularization, denervation, hormonal decline, oxidative stress, and the immune system [3-8]. However, the direct effects of changes in the muscle microenvironment with aging has only begun to be investigated [9]. With an increasing percentage of the population living to advanced age, reduced independence due to sarcopenia (weakened muscles) poses a large healthcare burden [10].

1.1.2   Clinical significance of sarcopenia

The world's percentage of people over the age of 65 is expected to double by 2050 [11]. Sarcopenia, the age-related increase in muscle weakness, is estimated to affect 22.6% of women

1

and 26.8% of men over the age of 64 with 31.0% and 52.9% in women and men over the age of 80 [12]. Sarcopenia leads to a 30-50% reduction in muscle mass from age 40 to 80 and up to 3% annual decline in muscle function [13]. Incidence of sarcopenia is associated with increased mortality, functional decline, falls and hospitalization [14]. This has a profound impact on the quality of life of patients with sarcopenia as their independence declines. This is also associated with an estimated $18.5 billion cost in 2000 which is a staggering economic burden on the healthcare system [15].

1.1.3   Healthy muscle regeneration

Muscle fibers consist of hundreds of nuclei shared within one connected cytoplasm, making them syncytial cells formed from the fusion of many individual cells [16]. Satellite cells, also known as muscle stem cells, are the major cell type that contributes to skeletal muscle regeneration following injury [17]. Satellite cells are located in the basal lamina of muscle fibers next to the cell membrane under normal conditions [18]. Quiescent satellite cells are characterized by being $Pax7^+/Myf5^+$ [19]. Upon muscle injury, satellite cells are activated and proliferate, transforming into myogenic progenitor cells or myoblasts [20]. Activated satellite cells express MyoD1 and Myf5 which control commitment to a differentiation fate [21]. Known activators of satellite cells which are produced from damaged cells or infiltrating cells are hepatocyte growth factor (HGF), fibroblast growth factor (FGF), insulin growth factor (IGF), and nitric oxide (NO) [22-25]. Terminal differentiation of myogenic precursor cells (MPCs) to myocytes is regulated through expression of myogenin [26]. Myocytes are then able to fuse together or fuse with damaged muscle fibers to propogate muscle regeneration [27].

Nuclear positioning during muscle injury and regeneration plays an important role in myofiber fusion. During regenerative fusion, new myoblasts are incorporated by adding their nucleus to the center of a damaged myofiber [28, 29]. This provides a histological metric for regeneration of muscle fibers, by quantifying the percent of fibers with centralized nuclei [30]. Once many myoblasts have been added to regenerating myofiber, the myofiber matures and the nuclei migrate from the center to the periphery [31]. Once nuclei relocate to the periphery, they space out to maximize the distance between nuclei [32]. Some myonuclei will also migrate from the periphery to the neuromuscular junction in order to establish synaptic transmission [33, 34]. Interestingly, biopsies of muscle disorders show predominant centralization of nuclei in muscle fibers [35, 36]. In muscle dystrophy, the absence of functional dystrophin leads to destabilization of muscle fiber cellular membranes. This leads to chronic damage and repair, which is observed histologically by a centralized nuclei phenotype [35].

1.1.4 Effect of Aging upon Muscle Regeneration

Muscle regeneration is known to decline with aging [37]. The number of satellite cells per muscle fiber decreases with increased age [38]. The proliferation, response to proliferative signals, and ability to replenish the supply of quiescent stem cells all are responsible for declined muscle stem cell function [39, 40]. Stem cell differentiation is also inhibited with advanced age due to reduced proliferation [38]. Expression of the myogenic regulatory factors (MRFs) MyoD, Myf5, and myogenin are reduced in aged muscle and muscle stem cells [41, 42]. The number of regenerating myofibers as assessed by nuclei centralization also reduces [39, 43]. Furthermore, the number of immune cells, including neutrophils and macrophages, decreases during muscle

regeneration in aged individuals [44]. All of these factors lead to reduced muscle mass and strength with aging.

The immune system aging also has an effect during muscle regeneration. Macrophage dysfunction impairs their normal role in preventing satellite cell apoptosis, contributing to declines in satellite cell population [45, 46]. At steady state, there are reduced numbers of pro-inflammatory macrophages but similar numbers of anti-inflammatory macrophages in aged muscle [47]. Following exercise, the number of pro- and anti-inflammatory macrophages increased in young individuals but not in old [47]. Aged muscles experienced increases in the pro-inflammatory cytokine gene expression of IL-6, IL-8 and MCP-1 following exercise [48]. In additions to alterations in immune cell activation, aged muscle stem cells are less sensitive to immune cell signaling [49].

Macrophage polarization is involved in the normal muscle regeneration process following injury [50]. Pro-inflammatory and anti-inflammatory macrophages are associated with satellite cell proliferation and differentiation, respectively [51]. Macrophage polarization has been shown to be deficient with aging [52]. Macrophages in aging muscle have been shown to skew towards anti-inflammatory phenotypes which was associated with fibrosis [53]. There also have been shown to be reduced numbers of macrophages in diabetic and aged human muscle [54]. These altered macrophage phenotypes in aging muscle have been shown to impair muscle regeneration [55].

1.2   MACROPHAGE POLARIZATION

Sections of this chapter are adapted from:

Macrophages are classified as mononuclear phagocytes that serve as one of the primary components of the innate immune system [56]. Macrophages are known to exist in a spectrum of phenotypes known as macrophage polarization [56]. This spectrum ranges from pro-inflammatory (M1) macrophages tasked with the clearance and uptake of foreign cells or debris to a range of anti-inflammatory (M2) phenotypes associated with immune resolution, wound healing and angiogenesis [57]. The shift in macrophage polarization from pro- to anti-inflammatory is associated with the successful host response to injury or biomaterials [58, 59].

1.2.1   Macrophage origins

Macrophages have both embryonic and bone marrow origins [60]. Embryonic macrophages originate in the yolk sac and then populate many tissues throughout the body, including the liver, lung, heart, spleen and intestine [61-66]. Once hematopoiesis begins in the bone marrow, monocytes are recruited to the blood stream. These monocytes are then recruited to tissues during injury and regeneration where they differentiate to macrophages [67]. Over the course of aging, bone marrow-derived macrophages slowly replace tissue resident macrophages [68-70].

As monocyte-derived and tissue resident macrophages have different functional profiles, this is hypothesized to be a reason for diminished regenerative potential with advanced aging.

The response to abdominal muscle injury can involve peritoneal or monocyte-derived macrophages based on the severity of injury [50]. Peritoneal macrophages are known to exist as two subsets: large peritoneal macrophages (LPMs) and small peritoneal macrophages (SPMs) [71]. Large peritoneal macrophages are thought to originate from the embryonic yolk sac like many tissue-resident macrophages and undergo self-renewal [72]. Small peritoneal macrophages are derived from circulating monocytes [73]. Both populations have been shown to be replaced by bone marrow-derived monocytes as seen by bone marrow chimera experiments [73]. SPMs rapidly proliferate during infection or injury and are known to secrete NO, IL-1, TNFα, and IL-12 [74]. LPMs, however, secrete MCP-1, MIP-1β, and G-CSF [73]. These two distinct macrophage population can heavily influence the host response to abdominal muscle injury.

Macrophages that respond to muscle injury are mainly monocyte-derived [75]. Monocytes derive from hematopoietic stem cells (HSCs) which give rise to monoblasts, which differentiate into promonocytes and then mature monocytes [76]. Monocytes are known to exist in two subsets in the mouse: a $CX_3CR1hi/Ly6c^{lo}$ which infiltrates tissue rapidly during infection and a $CX_3CR1^{lo}/Ly6C^{hi}$ population which does not [77]. There is now known to be a $Ly6C^{med}$ population that has been termed intermediate monocytes while $CX_3CR1^{lo}/CCR2^{hi}$ are termed classical monocytes and $CX_3CR1^{hi}/CCR2^{lo}$ are termed non-classical monocytes [78]. Non-classical monocytes have been shown to be more mature and derived from classical monocytes [78]. Non-classical monocytes have higher expression of TNFα following TLR activation, as well as lower CD14 and higher CD16 expression compared to classical monocytes [79, 80].

Tissue resident macrophages are also known to exist within muscles themselves [81]. These cells are known to secrete cytokine induced neutrophil chemoattractant (CINC) and monocyte chemoattractant protein 1 (MCP-1) [81]. While these tissue-resident macrophages, which expressed Ly6C^{hi}/CX$_3$CR1^{lo}/CD11c^{-}, dominate the early muscle inflammatory response, monocytes recruited from the blood were the predominant type thereafter [81]. All three macrophage populations, tissue-resident, peritoneal and monocyte-derived can play a role in abdominal muscle regeneration, depending on the type of injury.

1.2.2 Macrophage polarization

Macrophages were classically described as immune cells that phagocytosed pathogens and killed invading cells through the production of reactive oxygen and nitrogen species [82]. Following the discovery of the T helper 1 / T helper 2 (Th1/Th2) paradigm in T cells, macrophages were found to exist in a similar spectrum between classically activated (M1) and alternatively activated (M2) macrophages [83-85]. Pro-inflammatory (M1) macrophages are described as being stimulated with interferon-γ and lipo-polysaccharides [86]. They are associated with upregulation of IL-12 and IL-23, increased antigen presentation, and production of nitric oxide and reactive oxygen species [87]. Anti-inflammatory (M2) macrophages were originally described as being activated with interleukin-4 (IL-4) and/or IL-13 [88]. Alternative macrophage activation can also be caused by exposure to IL-10, glucocorticoids or secosteroid hormones [89]. Alternative activation has further been broken down into M2a (exposure to IL-4 or IL-13), M2b (activation with immune complexes (ICs) and TLR-agonists or IL-1R), and M2c (exposure to IL-10 or glucocorticoids) [90]. Due the increasing complexity of macrophage classes and many inconsistencies, new nomenclature has been proposed focused around the specific

7

activators used to stimulate the macrophages being studied [91]. Regardless, macrophages have a complex spectrum of phenotypes based on a large pool of activators that can polarize them anywhere between commonly described extremes of M1 and M2.

1.2.3 Macrophage polarization and muscle regeneration

Macrophage polarization has been implicated in the host response to injury of many tissues. Muscle regeneration is intimately tied in with macrophage activation and resolution [92]. Depletion of macrophages prior to muscle injury prevents muscle regeneration [93]. Pro-inflammatory macrophages are found in the first few days of muscle injury, at the same time of satellite cell activation and proliferation [94]. Alternatively activated macrophages arrive around day 4, co-current with myotube regeneration [94]. M1 macrophages lead to a Pax7$^+$/MyoD$^+$ proliferative satellite cell while M2 macrophages lead to MyoD$^+$/Myogenin$^+$ post-mitotic myocytes [94]. Following immune resolution, myotubes will fuse in order to form new muscle fibers [95]. Chronic inflammation from macrophages can impair skeletal muscle regeneration [51]. The dysfunction of the immune system with aging directly impairs the ability of muscles to heal following injury [96].

1.2.4 Macrophage populations and polarization with aging

The output of immune cells from the bone marrow is weighted towards myeloid lineage with aging, the absolute monocyte number is unchanged between young and aged individuals [97, 98]. However, an increased percentage of non-classical monocytes (CD14$^+$ CD16^{++}), and a reduction in classical monocytes (CD14$^+$ CD16$^-$) has been reported in elderly individuals [97,

98]. Like other innate immune cells, macrophage recruitment is delayed in aging, possibly due to a reduction in expression of the integrin very late antigen-4 (VLA-4) on monocytes, and vascular cell adhesion molecule-1 (VCAM-1) on endothelial cells [99]. Furthermore, a reduction in major histocompatibility complex (MHC-II) expression has been observed in both human and murine macrophages, leading to a reduction in antigen-presentation capacity and cross-talk with the adaptive immune system [100, 101]. An increase in prostaglandin E2 production by macrophages has been postulated as a possible explanation for the reduction in MHC-II expression [102]. Toll-like receptors (TLRs) including TLR-1, TLR-2, and TLR-4, important mediators for PAMPs and DAMPs, are also reported to decrease on aged peritoneal and splenic macrophages, perhaps contributing to the susceptibility of the elderly to bacterial, mycotic, and viral infections [103, 104].

Classically activated "M1" macrophages are very efficient at producing pro-inflammatory cytokines, nitric oxide, and performing phagocytosis. With aging, phagocytosis has been reported to decrease, perhaps associated with a reduction in the cellular receptors or responsiveness to cytokines [97, 105, 106]. Furthermore, macrophage senescence and quiescence induced in vitro has been reported to lead to a reduction in phagocytosis in response to biomaterials [107]. In addition, decreases in nitric oxide and superoxide production by aged macrophages have been reported in rats [108]. Alternatively activated "M2" macrophages are crucial for clearing helminth infections, and have important roles in the resolution of inflammatory reactions, including new matrix deposition and anti-inflammatory cytokine production. Changes in "M2" macrophage function are less well documented in the literature. However, "M2" macrophages have been found to accumulate in aged skeletal muscle and result in the detrimental replacement of muscle fibers with fibrotic tissue over time [53]. Advanced age

9

may also impair the ability of macrophages to polarize to either M1 or M2 phenotypes. The gene signature of macrophages isolated from bone marrow and polarized to M1 or M2 phenotypes was mostly unchanged between young and aged mice, with the exception of increased Fizz-1 (M2 marker) expression on aged cells [52]. However, macrophages isolated from mouse spleen had a reduction in both "M1" and "M2" gene expression patterns when stimulated with polarizing cytokines, suggesting deficits in polarization capacity [52].

While less well documented than the adaptive immune system, changes in innate immune function have a significant impact on the host response to infection, biomaterials and the normal wound healing process. Further studies that systemically examine the effect of aging on the innate immune response to biomaterials are necessary to further the development of biocompatible and bioactive materials.

Several studies have identified that tissue-resident macrophages, but not bone marrow derived macrophages, become impaired with aging [52, 106]. Recent work from our group also demonstrates minimal differences between young and aged bone marrow derived macrophage functions, including nitric oxide production and phagocytosis [109]. Interestingly, when bone marrow derived macrophages are pre-exposed to degradation products from young and aged extracellular matrix or "tissue cues", differences in function arise following polarization with M1-inducing cytokines [110]. Taken together, these studies suggest that tissue micro-environments dictate a large portion of the observed immunosenescence of macrophages.

1.3   EXTRACELLULAR MATRIX

1.3.1   Extracellular matrix physiology

The extracellular matrix comprises the structural components of a tissue outside of the cells [111]. These structural molecules provide not only biomechanical support for the cells it contacts, but also provides biochemical cues that maintain homeostasis or promote regeneration during injury [112, 113]. The main extracellular matrix components include collagens, elastin, fibrillins, laminins, proteoglycans and glycosaminoglycans [114]. Extracellular matrix ligands are also recognized by integrins, cellular membrane receptors that allow cells to attach to and migrate across the ECM [115].

As extracellular matrix is produced by cells and the ECM in turn influences cell behavior, their co-dependent relationship has been termed "dynamic reciprocity" [116]. A variety of cell surface receptors, including integrins, discoidin domain receptors, hyaluronan receptors, and cell surface proteoglycans, provide cell signaling from various extracellular matrix molecules [117-120]. Many extracellular matrix proteins, such as thrombospondins, SPARC, tenascins and periostin, have well characterized signaling effects on cells [121]. Growth factors bind to extracellular matrix proteins and glycosaminoglycans as well as signal through integrins [122]. Cleavage of ECM proteins by MMPs or other proteases creates peptides known as matrikines, which have signaling properties in inflammation and disease [123]. Therefore, intact ECM can maintain tissue homeostasis while its degradation during injury can control inflammation.

1.3.2   Extracellular matrix as a biomaterial

Bioengineering techniques have allowed for the isolation of the extracellular matrix from tissues for use as a biomaterial [124]. A collection of processes called decellularization, using enzymes, detergents, acids or bases, and hyper or hypotonic solutions, allow for the removal of cellular material while preserving the extracellular matrix and associated proteins [125]. The resulting biomaterial can be used as an inductive template to instruct cells toward wound healing phenotypes [126]. Extracellular matrix biomaterials have been used successfully in the functional reconstruction of many tissues, including tendon, meniscus, muscle, heart, esophagus, bladder and skin [127-137]. Functional reconstruction is defined as the remodeling of ECM into new, host-derived site appropriate tissue. Extracellular matrix products have been commercialized by a number of companies for use in a wide variety of surgical, reconstructive and wound healing applications [138-141].

Extracellular matrix scaffolds have been processed into a variety of platforms including sheets, tubes, powders, and gels [142-145]. Single and multi-laminate ECM sheets as well as powders have found use in reconstruction applications such as wound healing, corneal repair, and tumor reconstruction [146-148]. Tubes have been used for valve reconstruction and aorta repair [149, 150]. ECM hydrogels have recently gained interest in applications such as myocardial repair, stroke and meniscus repair [151-153]. The biomechanical and signaling properties of extracellular matrix scaffolds can be adapted to many applications for functional reconstruction.

Recently, extracellular matrix has been investigated for its potential as a scaffold for three-dimensional organ engineering. As the structural component for any tissue, ECM serves as the optimal platform for bioengineering an organ. Decellularization of vascularized organs has

been a major strategy for organ engineering which would then proceed with recellularization of the "ghost" organ with host cells or stem cells [154]. Efficient reperfusion of cells and recreation of tissue-cellular architecture remain problematic with this approach. Solubilized ECM has also been adapted to 3D bioprinting efforts in order synthetically create artificial tissues and organs [155]. Adapting large, insoluble ECM macromolecules to soluble bio-inks has complications for recreating organs found in normal physiology. Spatial resolution and engineering the complexity of both cells and matrix normally found in an organ.

1.3.3   Extracellular matrix biomaterials as model microenvironments

Just as extracellular matrix biomaterials can be used as scaffolds for 3D organ engineering, ECM can also model the microenvironment of an organ to study biological phenomena [156]. The effects of altered ECM microenvironments have been studied in aging, cancer, fibrosis, homeostasis, regeneration and disease [157-161]. Decellularization techniques allow the harvest of ECM for the purpose of modeling its effect upon various cellular functions [162]. Use of ECM peptides in controllable polymer gels offers investigation of specific changes in the ECM, but does not fully recapitulate the reality of ECM changes with disease or age [163]. Understanding how changes in the ECM directly affect cell function proves difficult as there are numerous components, each which can change in concentration, degradation, architecture or modification with oxidation or glycation. The process of decellularization itself can modify extracellular matrix through denaturation, degradation or oxidation. Therefore, the act of ECM extraction, while useful in understanding its effects, clouds the ability to accurately preserve its native properties.

1.3.4 Extracellular matrix changes with aging

Muscle ECM comprises approximately 10% of total muscle weight and is organized into three sections: endomysium (surrounding muscle fibers), perimysium (surrounding muscle fascicles), and epimysium (surrounding the entire muscle) [164]. Muscle connective tissue is primarily composed of collagen I whereas muscle basement membrane is composed of collagens I, III and VI in the outer reticular lamina and collagen IV and laminin in the inner basal lamina [165]. Muscle ECM shows increased collagen deposition with age with an increase in collagen I and decrease in collagen III [166-168]. Collagen IV is increased whereas laminin decreases with age in the basal lamina [169]. Collagen accumulation is assumed to be due to decreased degradation rather than increased synthesis, which is corroborated by decreased levels of MMP-2 [170, 171]. Thickening of the basal lamina has been shown to effect the interaction between satellite cells and myofibers [172]. Reduced collagen turnover leads to accumulation of glycation end-products (AGEs) and accumulation of ECM degradation products within the tissue which can interfere with normal tissue interactions [172, 173]. Aging ECM changes may also lead to satellite cell senescence or induced differentiation through stiffer matrix [166, 174]. A recent study showed that aged muscle extracellular matrix promoted a fibrogenic phenotype in muscle stem cells, which could, in part, explain the fibrosis commonly observed in aged muscles [9].

Few studies tying compositional changes in aging tissue to age related changes in the host response have been performed. However, Tottey, et al. demonstrated that source animal age was linked to changes in both the compositional make up and physical properties of decellularized tissue scaffolds composed of small intestinal submucosa (SIS) [175]. Briefly, small intestinal submucosa was harvested from 3, 12, 26, and 52 week old pigs and decellularized using a peracetic acid washing procedure. The resultant tissue was then tested mechanically and

14

subjected to compositional testing for growth factors, collagen, and glycosaminoglycan content. The results showed a trend toward increasing tissue thickness, reduced tensile modulus, and resistance to collagenase degradation with aging. Compositional analysis showed changes in bFGF and VEGF content with age including increases in both growth factors between 3 and 26 weeks with decreased content thereafter. Analysis of glycosaminoglycan content showed a steady drop in content with aging from the 3 to 52 week old source animals. These changes were associated with changes in the mitogenesis, metabolism and migration of perivascular progenitor cells exposed to the materials [175].

A follow-up study utilized the same decellularized small intestinal extracellular matrix as an implant in a well-described model of partial thickness abdominal wall defect repair [176]. The results of this study demonstrated that scaffolds derived from younger animals (3 and 12 weeks) were associated with significantly improved remodeling (i.e. formation of innervated skeletal muscle bundles) of the abdominal skeletal muscle as compared to 26 or 52-week old source tissues and untreated and autograft treated controls. Investigation of the early host response revealed that the materials derived from younger animals (3 and 12 weeks) were also associated with a decreased ratio of M1:M2 macrophages within the site of implantation as compared to 26 or 52-week old source tissues and untreated and autograft treated controls [176].

1.4   AGING MODIFICATIONS OF EXTRACELLULAR MATRIX

1.4.1   Glycation

Advanced glycation end products, a heterogeneous group of over 20 different molecules, are formed through the non-enzymatic glycation of long-lived proteins, lipids, or nucleic acids [177, 178]. AGE formation *in vivo* tends to be a progressive process that occurs with increasing age or following certain lifestyle choices, such as diets high in glucose or exposure to environmental toxins [177, 179]. AGEs are capable of protein cross-linking, resulting in the reduced ability of cellular machinery to degrade damaged proteins, in turn leading to tissue stiffening and dysfunction [180]. AGEs can also promote formation and accumulation of reactive oxidative species (ROS) through the blockade of the 20S subunit of the intracellular proteasome [179, 181]. Since the 20S subunit is typically responsible for the degradation of oxidized intracellular proteins, blockade of this intracellular machinery by AGEs, coupled with reduced antioxidant to oxidative species ratios in aged individuals, allows for a feed-forward loop of oxidative species formation, subsequently resulting in enhanced AGE formation *in vivo* [177, 181, 182].

Additionally, AGEs have been shown to promote inflammatory processes through several distinct signaling pathways, with the receptor for advanced glycation end products (RAGE) pathway being one the best characterized [177]. RAGE is a pattern recognition receptor of the immunoglobulin receptor family and is widely expressed across a variety of cell types, including macrophages [183], T-lymphocytes [184], B-lymphocytes [185], dendritic cells [186], endothelial cells [187], fibroblasts [188], smooth muscle cells [183], and neuronal cell [177, 189, 190]. Additionally, RAGE is able to bind a variety of ligands in addition to AGEs, such as lipopolysaccharide, calgranulin/S100 family ligands, or high mobility group box protein 1 [177,

16

185]. Since RAGE signaling is dependent on both cell and ligand type, RAGE signaling tends to be complex and studied in a context dependent manner [185].

In macrophage populations, ligand binding to RAGE has been shown to induce M1, pro-inflammatory macrophage states through the upregulation of MHC-II expression on the cell surface and secretion of pro-inflammatory cytokines [191, 192]. While it has not been determined definitively how ligand binding to RAGE impacts M2, pro-remodeling states in macrophages, some data exists that suggests RAGE-ligand binding promotes the down-regulation of M2 genes [193]. However, a recent study has shown that AGE-mediated RAGE activation has no impact on M2 marker expression[194]. Thus, further studies will need to be performed to fully elucidate how RAGE signaling can impact M2 gene and surface marker expression. Additionally, while the effects of RAGE-ligand binding have been fairly well elucidated in macrophage populations, the specific signaling pathways utilized in these cell populations have not. RAGE signaling pathways in monocyte and macrophage populations has been shown to be dependent on both the RAGE-bound ligand as well as the extracellular microenvironment [185]. For example, monocyte RAGE stimulation with AGEs resulted in signaling through PKC, ERK1/2, p38 – but not JNK – to activate master inflammatory regulator gene NF-κB [195]. However, under hypoxic conditions Chang et. al. demonstrated that monocyte RAGE stimulation did not signal through this pathway but rather led to the translocation of PKCβII and subsequent JNK activation, resulting in downstream Egr-1 activation [196]. Additionally, macrophages have been shown to signal through p38, p44/42, JNK, and MAPK pathways [191]. Thus, one can see the importance of ligand and extracellular environment in determining the RAGE signaling propagation pathway.

1.4.2 Oxidation of extracellular matrix

Radical oxygen species (ROS) are naturally produced through normal biological functions and are increasingly produced during inflammation [197]. These elevated levels of ROS, while beneficial for pathogen clearance, can lead to oxidative damage to cells and proteins in affected tissues. Because extracellular matrix proteins are long-lived, modifications from oxidative stress can accumulate leading to altered function, structure or degradation. *In vitro* models of oxidative stress have proven that ECM molecules are modified through oxidation as measured by increases in protein carbonyl content [198]. This increased oxidation led to increased degradation by MMP-2 [198]. Protein oxidation could be a cause for increased collagen degradation with aging or accumulation of ECM fragments within aged tissues. ROS also have impacts on signaling pathways for degradative enzymes, leading to the upregulation of MKK and MAPK which lead to elevated MMP-1 expression [199].

1.4.3 Lysyl oxidase cross-linking

Collagen crosslinking is enzymatically accomplished by the lysyl oxidase family of copper-dependent oxido-deaminases. These enzymes work by modifying the lysyl residues in collagen and elastin resulting in the formation of crosslinks between polypeptides that cannot be reduced [200]. Lack of LOX-mediated crosslinks leads to abnormal collagen fibril formation with increased distribution of fiber diameters and irregular profiles [200]. Allosteric inhibition of LOXL2 led to promotion of a pathologic microenvironment characterized by reduced fibroblast activation, demoplasia and endothelial cell activation, as well as decreases in growth factor and cytokine production including TGF-β [201]. LOX family gene expression has been observed to

decrease with aging which has implications for ECM remodeling and signaling [202-204]. Reduced or altered crosslinking has implications for tissue function and biomechanics as well as the response to tissue injury.

1.5   CHANGES WITH AGING OF ECM BIOMATERIALS

As described previously, the extracellular matrix in known to change with age [9, 161, 205, 206]. When extracellular matrix biomaterials are derived from different aged animals, the resultant material properties are shown to be altered with source animal age [175]. These alterations in small intestine submucosa properties with source animal age affected the host response to these materials when implanted into a partial thickness abdominal muscle injury [176]. This alteration in host response was associated with a promotion of enhanced pro-inflammatory macrophage response with increased ECM source animal age. However, this previous study did not investigate the direct effects of age-related changes in the ECM upon macrophage phenotype and function. The direct effects of ECM source animal age upon macrophages was tested in Chapter 2 where murine bone marrow-derived macrophages were exposed to extracellular matrix degradation products derived from 12, 26 and 52-week old pigs.

As discussed in Chapter 1.4, there are many factors that can cause changes in the extracellular matrix with aging. Among these hypotheses include oxidation and increased cross-linking from non-enzymatic glycation or lysyl oxidase activity [198]. Growth factors, which often interact and are sequestered within the extracellular matrix, change in both secretion and content with aging [207]. Lipids also accumulate in aged tissues which can alter the ability to regenerate following muscle injury [208]. Chapter 3 discusses investigation of the effects of

growth factor or lipid extracts from different source animal age small intestine submucosa materials upon macrophage polarization.

2.0 EFFECT OF SOURCE ANIMAL AGE UPON MACROPHAGE RESPONSE TO SMALL INTESTINE SUBMUCOSA

This chapter is modified from the following published work:

2.1 INTRODUCTION

While ECM and other natural scaffolds possess advantages of inherent bioactivity, they are often criticized for their variability. One potential source of variability is the age of the donor animal or cadaver from which the tissues are harvested. The extracellular matrix has been shown to vary in composition with the age of an organism [175]. For example, muscle ECM shows increased deposition of collagen I and decreased collagen III with age [166-168]. Collagen IV is increased whereas laminin decreases with age in the basal lamina [169], a key component of many ECM-based scaffold materials [209]. Increased deposition and reduced collagen turnover leads to accumulation of glycation end-products (AGEs) and associated crosslinks which can interfere with normal cell-tissue interactions [172, 173]. ECM changes may also lead to stem cell

senescence or induced differentiation through stiffer matrix [166, 174]. These aging-related changes have been suggested to affect the ability to regenerate tissue following injury.

It is logical, therefore, that differences observed in native tissues would persist in ECM scaffolds following decellularization and may have implications for their effectiveness following implantation. A recent study showed that small intestinal submucosa (SIS) derived from 52 week old pigs promoted less constructive remodeling and increased collagen deposition when implanted in to a rat abdominal wall defect model compared to SIS derived from 12 and 26 week old pigs [176]. This response was also associated with increased pro-inflammatory (M1) macrophage polarization with increased source animal age, suggesting these poorer outcomes were due to alteration in macrophage phenotype.

The current study sought to examine the impact of changes in ECM scaffolds with different source animal age upon macrophage polarization responses. In order to accomplish this an *in vitro* primary cell model of macrophage polarization to ECM scaffolds was utilized to understand these age-related changes in ECM. Murine bone marrow-derived macrophages were chosen as a model system to reduce variability in the host immune responses due to genetic and/or environmental factors. As aging is a multifactorial condition, genetically similar mice with similar environments and diets were necessary to eliminate comorbidities associated with aging such as obesity, diabetes, and cardiovascular disorders that could be present in blood drawn from young and aged humans [210-213]. Additional studies can take advantage of murine genetic models in order to understand pathways involved in the macrophage response to biomaterials. Nevertheless, future studies involving human monocyte-derived macrophages will be necessary to assess the response to such materials in humans.

In order to assess the effect of aging upon extracellular matrix biomaterials, small intestine submucosa was chosen as a model scaffold. Small intestine submucosa is commercially available through Cook Medical for a variety of surgical and reconstructive applications [214-217]. A common animal source for the derivation of small intestine submucosa (SIS) biomaterials is the pig [218]. A previous study investigating the effect of source animal age upon the remodeling of extracellular matrix biomaterials also used porcine small intestine submucosa as a source [176]. This study found that when implanted into a rodent model of abdominal wall partial thickness defect repair, that SIS of increasing source animal age caused an increased pro-inflammatory response and increased collagen deposition, indicative of fibrosis.

2.2   METHODS

2.2.1   Scaffold preparation

Jejunum were harvested from 12 week, 26 week, and 52 week-old Landrace pigs immediately following euthanasia (Tissue Source, Lafayette, IN). The animals were of similar genetic heritage, diet and immunization history. Small intestine submucosa (SIS) extracellular matrix biomaterials were prepared from these tissues as previously described [129]. Briefly, the tissues were rinsed with water and the mesenteric tissues were removed. Tissues were cut longitudinally then mechanically delaminated to remove the tunica serosa, tunica muscularis externa, and the luminal tunica mucosa, including most of the lamina propria. After delamination, the tunica submucosa and the basilar layer of the tunica mucosa including the muscularis mucosa and the stratum compactum of the lamina propria remained. The material was

23

further decellularized using mechanical agitation with an orbital shaker at 300 rpm in a solution of 0.1% (v/v) peracetic acid (Rochester Midland Corporation, Rochester, NY). Tissues were then rinsed multiple times with saline and deionized water. Decellularized scaffolds were frozen at -80°C and then lyophilized. The resultant scaffolds were considered "intact ECM scaffolds." Scaffolds were digested at a concentration of 10 mg/mL in an acid-pepsin solution (pH 2) under constant magnetic stir for 48 hours. These digested scaffolds were considered "ECM degradation products."

2.2.2 Scaffold characterization

Hydrated native tissue and decellularized scaffolds were fixed in 10% neutral buffered formalin (NBF) and then embedded in paraffin. Sections of these scaffolds were stained separately with hematoxylin & eosin or DAPI to confirm removal of nuclei. Proteinase K digests of native and decellularized scaffolds underwent phenol: chloroform: isoamyl alcohol (25:24:1) extraction for DNA and were resuspended in 1X TE buffer. DNA extracts were separated using electrophoresis on a 2% agarose gel in 0.5X TBE buffer to confirm reduction of DNA content and fragmentation of remnant DNA in decellularized scaffolds compared to native controls. DNA extracts were also quantified for double-stranded DNA content using a PicoGreen assay (Thermo) according to manufacturer's instructions. Endotoxin content was assayed using the Pierce LAL Chromogenic Endotoxin Quantification kit (Thermo) according to manufacturer instructions.

2.2.3   Growth factor ELISA quantification

Urea heparin extracts were performed on lyophilized native and decellularized SIS samples as previously described [219]. Briefly, 100 mg of lyophilized tissue was extracted using 3 mL urea-heparin extraction buffer (2M urea, 50mM Tris Base, 5 mg/mL heparin, 10mM N-Ethylmaleimide, 5mM benzamidine, 1mM PMSF in DI H_2O). Samples were agitated overnight at 4°C. Samples were centrifuged at 10,000 xg for 10 min at 4°C. Supernatants were collected, volumes recorded, and stored at -80°C until time of assay. Extraction procedure was repeated once more to ensure complete extraction. Growth factor ELISAs were purchased from R&D Biosystems for basic fibroblast growth factor (bFGF), hepatocyte growth factor (HGF), and heparin-binding EGF-like growth factor (HB-EGF). Urea-heparin extracts were assayed for growth factor content using the ELISA assays above according to manufacturing instructions.

2.2.4   Artificial glycation of small intestine submucosa ECM

In order to determine the effect of glycation upon small intestine submucosa, positive controls for glycation were created through *in vitro* glycation protocols previously described [220]. Young (12 week) SIS were artificially glycated by incubating lyophilized scaffolds in 50, 250 or 500 mM ribose with 44mM $NaHCO_3$ and 25mM HEPES in 1XPBS for 5 days. Following glycation scaffolds were washed in 1X PBS, frozen at -80°C and lyophilized.

2.2.5 Assessment of age-related biomarkers in small intestine submucosa

Periodic acid-Schiff stain was performed on paraffin sections of SIS to detect levels of polysaccharides, glycoproteins, glycolipids, and mucins as previously described. Paraffin sections were deparaffinized and rehydrated to water and then oxidized with 0.5% periodic acid solution for 5 mins. Following water washes, slides were incubated in Schiff's reagent for 15 minutes. Slides were washed in warm water then counterstained with hematoxylin for 1 minute. Slides were then dehydrated and mounted with a resinous mounting media and coverslipped. Slides were imaged using brightfield microscopy.

Protein oxidation was tested by staining tissue sections. Paraffin sections were deparaffined and then rehydrated to water. Sections were stained with 1mg/mL 2,4-dinitrophenylhydrazine in 1N HCl for 1 hour. Sections were then washed 3 times for 3 minutes in 1X PBS. Sections were then dehydrated, cleared with xylenes then mounted in resinous mounting media then coverslipped. Slides were imaged using brightfield microscopy.

Advanced glycation end-product content in extracellular matrix was assessed via immunohistochemical staining. Briefly, paraffin sections were deparaffinized and rehydrated to water. Antigen retrieval was performed using 10mM citric acid pH 6 0.05% Tween20 for 20 mins at 95-100 °C. Slides were washed twice with 1X TBST for 5 mins then twice with 1XPBS for 3 mins. Endogenous peroxidase activity was blocked by incubating slides in 0.3% hydrogen peroxide for 30 mins. Slides were washed 3 times in 1X PBS for 3 minutes. Slides were blocked for non-specific antibody binding with a blocking buffer made of 2% donkey serum/1% bovine serum albumin/0.1% Tween-20 for 1 hour at room temperature. Primary antibodies were incubated overnight at 4 °C diluted in blocking buffer. Slides were washed 3 times for 3 minutes with 1XPBS. Slides were then incubated with biotinylated secondary antibodies diluted in

blocking buffer (goat anti-rabbit 1:200 (Vector)). Slides were was again 3 times for 3 minutes with 1XPBS. Slides were incubated with VectaShield ABC Reagent for 30 mins then washed again 3x3mins with 1XPBS. Staining was developed by incubating sections with 4% DAB. Sections were washed then mounted with resinous mounting media and coverslipped. Slides were images on a brightfield microscope at the same settings.

Advanced glycation end-product mass content was quantified using an OxiSelect™ Advanced Glycation End Product (AGE) Competitive ELISA Kit (Cell BioLabs). Papain digested SIS were assayed for AGE content according to manufacturer instructions.

2.2.6 Microarchitecture and biomechanical analysis

Microarchitecture was assessed via scanning electron microscopy. Hydrated decellularized small intestine submucosa was processed for scanning electron microscopy according to standards established by the University of Pittsburgh Center for Biologic Imaging (CBI). Samples were fixed in 2.5% glutaraldehyde in 0.1 M PBS (pH 7.4) for 1 hour. ECM was then washed with 3 changes 0.1 M PBS for 15 minutes each. Lipid fixation was then performed using 1% OsO4 in 0.1 M PBS for 60 minutes. Samples were again washed with 3 changes of 0.1 M PBS for 15 minutes each. Samples were then dehydrated in graded series of alcohol (in PBS) for 15 minutes each: 30% ethanol, 50% ethanol, 70% ethanol, 90% ethanol, 3x 100% ethanol. Samples were then chemically dried using hexamethyldisilazane (HMDS) for 15 minutes and then allowed to dry in a fume hood overnight. Samples were then sputter coated according to CBI protocol. Samples were imaged at 2500X on a JSM 6335F SEM.

Biomechanical properties of decellularized small intestine submucosa using uniaxial tensile mechanical testing under constant strain on an Instron mechanical testing system.

Samples were cut using a dogbone template and then mounted using screw clamps. Hydrated samples underwent 10 loading cycles to 0.5 N of tensile force under a constant strain rate before being stretched to failure

2.2.7 Bone marrow-derived macrophage isolation

Bone marrow-derived macrophages were harvested from 2 month or 18-20 month-old C57/BL6 mice as previously described [221]. Briefly, femurs and tibiae were harvested and separated from muscle and connective tissue. Bones were cut at either end to expose bone marrow. Sterile syringe and needles were used to flush out bone marrow using macrophage differentiation media (DMEM/10% FBS/10% L-929 Supernatant/1% PenStrep/2% MEM non-essential amino acids/1% HEPES/0.1% 55μM β-2 mercaptoethanol). Bone marrow lysate was reconstituted in media and filtered through a sterile cell filter. Cells were cultured for 7 days in media to differentiate them into macrophages, changing differentiation media every 2 days.

2.2.8 Macrophage Treatment

Following 7 days of differentiation culture as described above, macrophages were treated with acute polarizing regimens to distinguish phenotypes over 24 hours. Naïve macrophage (M0) controls were treated with basal media for 24 hours. M1 (20 ng/mL IFN-γ and 100 ng/mL LPS) and M2 (20 ng/mL IL-4) polarizing cytokines were used to create positive controls for classical pro- and anti-inflammatory macrophages. ECM degradation products were neutralized and diluted to 250 μg/mL in macrophage media to isolate biochemical effects of degradation products and prevent structural moieties from forming. Pepsin buffer (1 mg/mL pepsin in 0.01

28

M HCl) diluted in macrophage media was used as a control. Another set of treatment groups involved 24-hour exposure of ECM degradation products followed by 24-hour treatment with either the M1 or M2 treatment regimen, referred to as ECM→M1 or ECM→M2, respectively.

2.2.9   Indirect immunofluorescent antibody labeling

Cells were fixed with 2% paraformaldehyde (PFA) for 30 minutes then washed in 1XPBS. Cells were incubated in blocking buffer (2% donkey serum, 1% bovine serum albumin (BSA), 0.1% Triton X-100, 0.1% Tween-20) for 1 hour at room temperature. Primary antibodies were diluted in this blocking buffer as follows and incubated overnight at 4 °C: F4/80 (1:200, Abcam 6640), iNOS (1:100, Abcam 3523), Arginase-1 (1:200, Abcam 91279), Fizz1 (1:200, Peprotech 500-P214), CCR2 (1:200, Abcam 21667), CX$_3$CR1 (1:200, Abcam 8021), MHC-II (1:100, Abcam). F4/80 is a marker of macrophage differentiation. iNOS and MHC-II are classical M1 macrophage markers whereas Arginase-1 and Fizz1 are classical M2 macrophage markers. CCR2 is a chemokine receptor associated with macrophage migration whereas CX$_3$CR1 is a fractalkine receptor associated with tissue-resident macrophages. Cells were washed in 1XPBS then incubated in the appropriate fluorescently-labeled secondary antibody solution in blocking buffer for 1 hour at room temperature (donkey anti-rat Alexa Fluor 488, Invitrogen, 1:200; donkey anti-rabbit Alexa Fluor 488, Invitrogen, 1:300). Cell nuclei were counterstained with DAPI. Cells from five young (2 month) and aged (18 month) mice were imaged nine times in the center of each well at 10X magnification using automated position capture function to remove bias from subjective image location acquisition. This set of 9 images per well was counted as one biological replicate and was repeated in cells from n=5 mice for a total of 5 sets of 9 images per group. All imaging was performed on an Axio observer T1 microscope. Mean

fluorescence intensity of cells was analyzed using Cell Profiler software (Broad Institute). Briefly, DAPI images were used by the program to identify cell nuclei then FITC images were used to identify cell borders around the identified nuclei. The mean fluorescent intensity was calculated by averaging the pixel intensities (scale of 0 to 1) across the entire cell area. Mean fluorescence intensity values were averaged for all imaged cells in each well.

2.2.10 Phagocytosis assay

Following treatments, cells were assayed for phagocytic ability using Vybrant Phagocytosis Assay Kit (Invitrogen). Cells were incubated in FITC-labeled dead E. Coli particles for 2 hours in the cell culture incubator. Following washing, the cells were fixed with 2% PFA for 30 minutes then washed with 1X PBS. Cells were counterstained with DAPI then imaged and analyzed as described above.

2.2.11 Taqman gene expression assay

Following treatments, macrophages (n=5 biological replicates from 5 young (2 month) and 5 aged (18 month) mice) were harvested for RNA using Qiagen RNEasy MiniPrep RNA Isolation Columns following standard protocol. RNA was quantified using a NanoDrop Lite Spectrophotometer (Thermo). cDNA templates were created from 1 μg of RNA using Invitrogen High Capacity RNA-to-cDNA kits (Thermo). Taqman Gene Expression Assays (Thermo) were performed for the following commonly reported M1 and M2 macrophage markersgenes: Nos2 (Mm00440502_m1), IL1b (Mm00434228_m1), IL12b (Mm01288989_m1), TNFa (Mm00443258_m1), MHC-II (Mm01181326_m1), Arg (Mm00475988_m1), Fizz1 Retlna

(Fizz1) (Mm00445109_m1), Mrc1 (Mm01329362_m1), IL10 (Mm01288386_m1), and PPARg (Mm00440940_m1).

2.2.12 Nitric Oxide Assay

Following treatments, 50 µL of supernatant from macrophages were transferred into a fresh plate. Nitric oxide content was assayed using a Greiss Reagent system. Briefly, 50 µL of sulfanilamide (1% in 5% phosphoric acid) was added to supernatants for 10 minutes. Then, 50 µL of 0.1% N-1-napthylethylenediamine in water was added to the mixture for an additional 10 minutes. The absorbance at 540 nm was measured using a BioTek SYNERGY HTX spectrophotometer.

2.2.13 Seahorse metabolic analysis

XF96 well plates were coated with CellTak (Corning) and then seeded with macrophages as previously described. Following treatments as described above, metabolic stress tests were performed to assay metabolic activity of the cells using a Seahorse XF96 Metabolic Assay System. Basal extracellular acidification and oxygen consumption rates were taken for 30 min. Cells were stimulated with oligomycin (2 µM), FCCP (0.5 µM), 2-deoxyglucose (100mM) and rotenone/antimycin A (100 µM) to obtain maximal respiratory and control values. Spare respiratory capacity is measured as the difference between basal OCR values and maximal OCR values obtained after FCCP uncoupling.

2.2.14 Statistical Analysis

Quantitative results were analyzed using a two-way ANOVA (treatment, age) with Tukey post-hoc analysis using GraphPad PRISM 7 software. Significance was determined at a p-value less than 0.05.

2.3   RESULTS

2.3.1   Confirmation of decellularization

Hematoyxlin & eosin staining of native and decellularized small intestinal submucosa samples confirmed decellularization (Figure 1). Outer intestinal musculature and inner luminal mucosa were removed in decellularized samples as previously described [222].
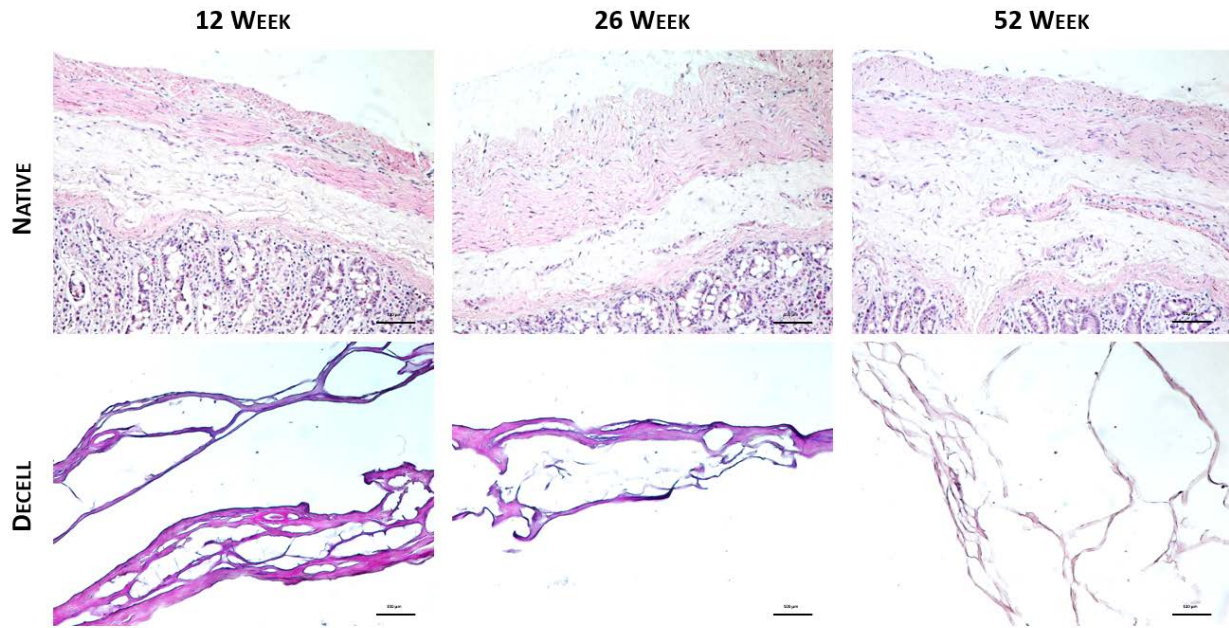
Figure 1: Hematoxylin & eosin staining of native and decellularized small intestine submucosa.
Images taken at 10X magnification. Scale bars indicate 100 µm.

Nuclear removal was confirmed through visual observation in H&E (Figure 1) and DAPI staining (Figure 2).
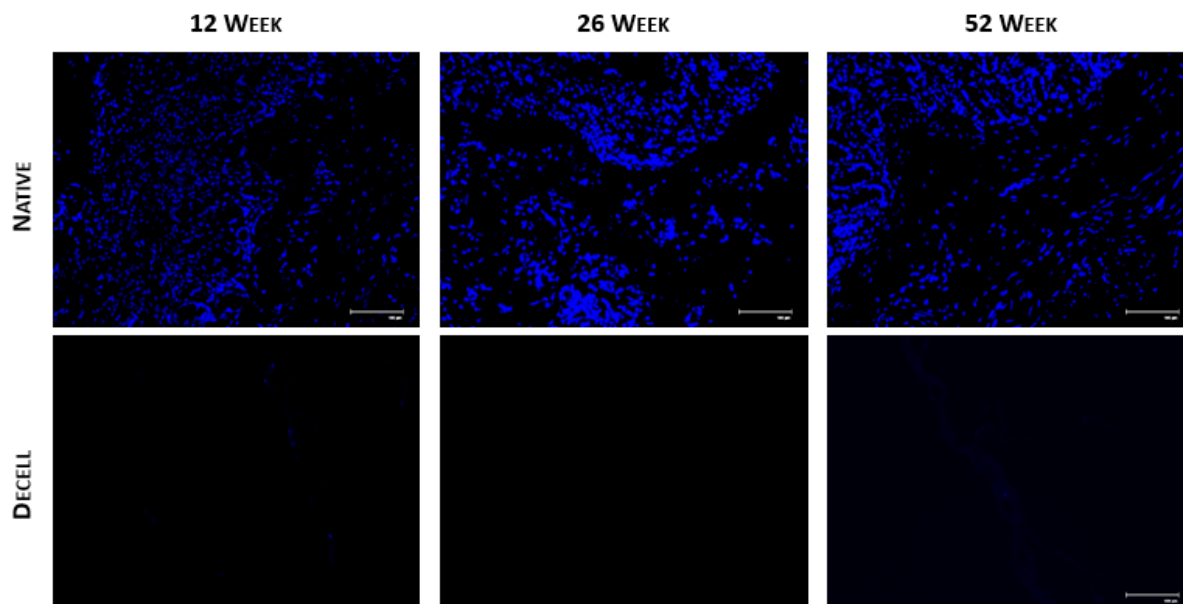
Figure 2: DAPI fluorescence staining of native and decellularized small intestine submucosa.

Images taken at 20X magnification. Scale bars indicate 100 µm.

DNA fragmentation was confirmed through DNA agarose gel electrophoresis (Figure 3A). DNA extracts from native samples show large continuous bands indicative of large DNA fragments. Extracts from decellularized samples show significant removal of DNA material, with remnant DNA existing as lower molecular weight (Figure 3B). This is indicative of effective removal and fragmentation of any remnant DNA. Results from PicoGreen DNA quantification (Figure 3B) showed that scaffolds were effectively decellularized [223]. Effective and similar levels of decellularization confirm that DNA content should not cause differences in immune responses between different source age samples.
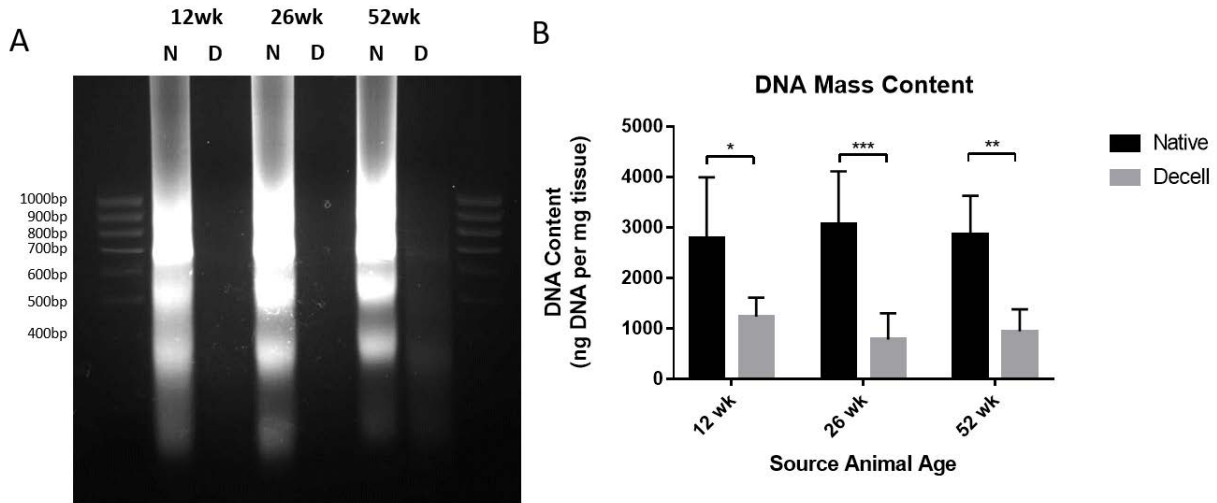
Figure 3: DNA agarose gel electrophoresis (A) and PicoGreen dsDNA quantification (B).

Data shown as mean ± S.D. Statistical significance reported as *p<0.05, **p<0.01, ***p<0.001, ****p<0.0001

2.3.2   Analysis of ECM Composition

SIS scaffolds of different source animal age were analyzed for content of major extracellular matrix structural proteins, specifically collagens and glycosaminoglycans. Hydroxyproline content was assessed to approximate collagen composition in SIS scaffolds (Figure 4A). In native small intestine submucosa, hydroxyproline content significantly increased with source animal age. However, in decellularized scaffolds, there was no significant difference in hydroxyproline content. Glycosaminoglycan content was assessed using dimethylmethylene blue dye (Figure 4B). Native small intestine submucosa showed a significant increase in glycosaminoglycan content with increasing source animal age. However, no trend appeared with glycosaminoglycan content in decellularized scaffolds of different source animal age.
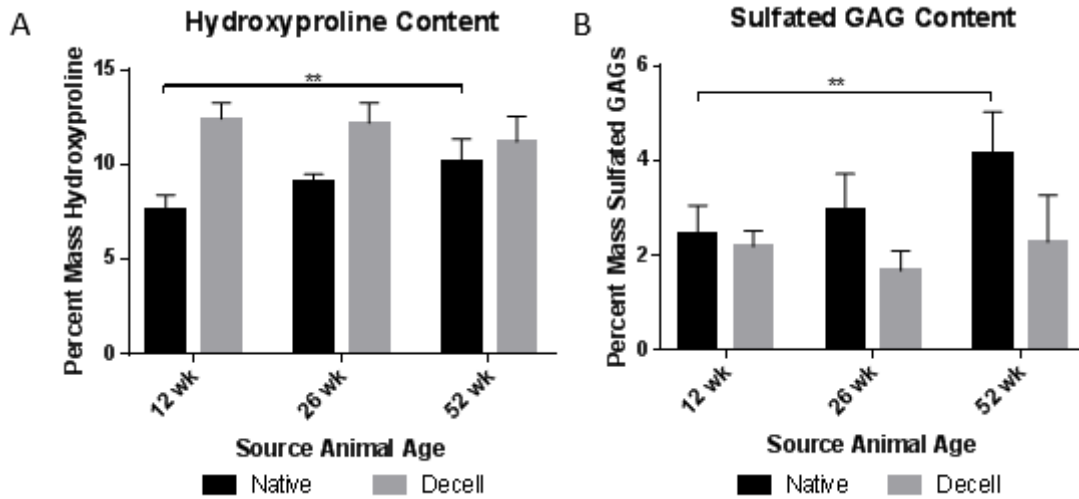
Figure 4: Biochemical assessment of mass content of hydroxyproline and sulfated GAGs.

Data shown as mean ± S.D. Statistical significance reported as *p<0.05, **p<0.01, ***p<0.001, ****p<0.0001.

Endotoxin content was also assessed using an LAL Endotoxin Assay. Pepsin digests of native or decellularized small intestine submucosa were diluted 1:25 and assayed using the LAL Endotoxin kit according to manufacturer instructions. Native tissues were taken from the mechanically delaminated small intestine submucosa as to not include results from the mucosa or muscularis layers. However, our results show that endotoxin content did not differ in ECM degradation products (Figure 5). This suggests that any changes in the immune response to these biomaterials was not due to alterations in endotoxin content.
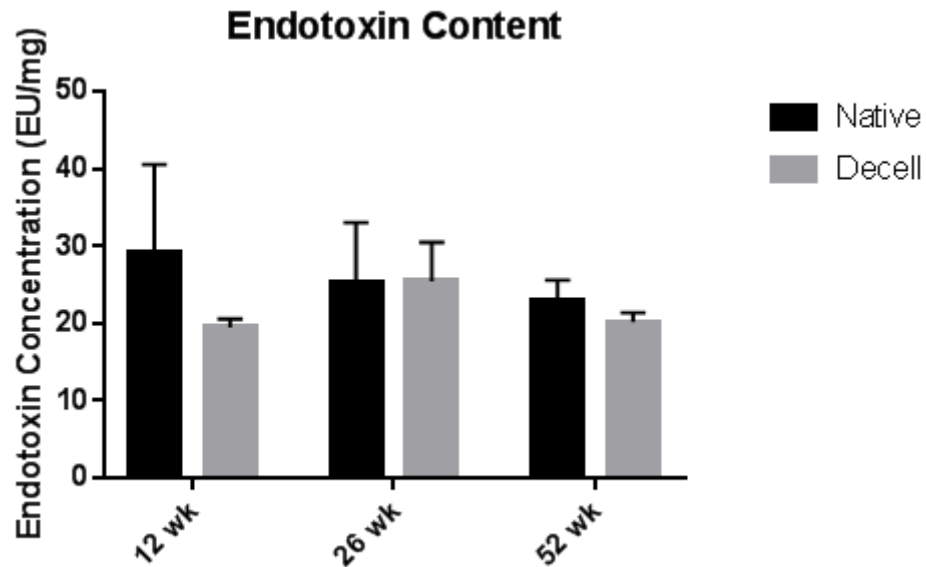
Figure 5: LAL Chromogenic Endotoxin quantification of LPS content in SIS degradation products.

Data shown as mean ± S.D. Statistical significance reported as $*p<0.05$, $**p<0.01$, $***p<0.001$, $****p<0.0001$.

Growth factors laden within extracellular matrix scaffolds can contribute to the overall biochemical microenvironment created by the scaffold. Analysis of growth factor content change with source animal age is important to the overall characterization of ECM's effect on macrophage phenotype. Due to previous work showing ECM scaffolds of different animal source age affected both skeletal muscle regeneration and macrophage phenotype, growth factors were selected that are known to affect both of these phenomena and have also been found in whole small intestine tissue [224-226]. Native small intestine tissue showed significant increases in bFGF and HB-EGF. However, no significant changes in content were observed following decellularization (Figure 6A-C).
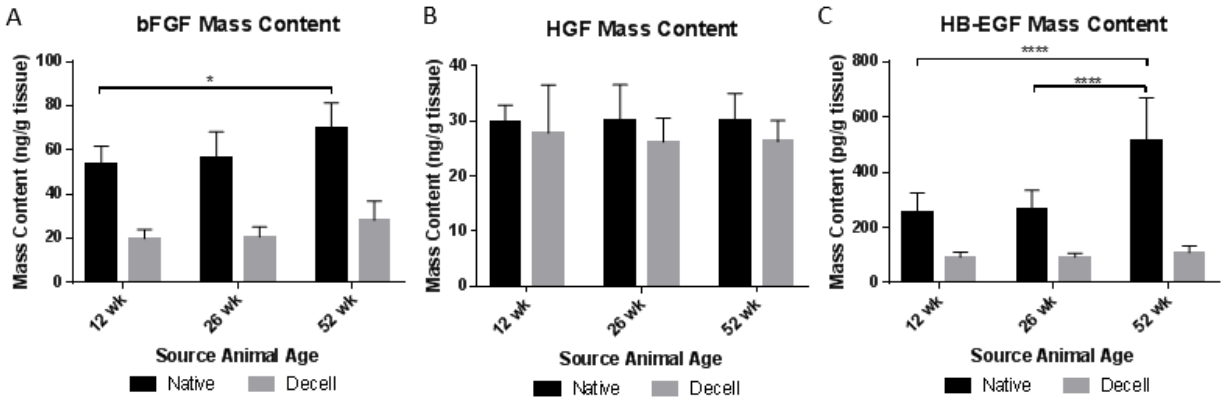
Figure 6: Growth factor ELISA quantification of urea extracts from small intestine submucosa.

Data shown as mean ± S.D. Statistical significance reported as *p<0.05, **p<0.01, ***p<0.001, ****p<0.0001.

2.3.3   Assessment of age-related biomarkers

Paraffin sections of decellularized SIS and SIS artificially glycated with ribose were stained with Periodic Acid Schiff stain in order to determine levels of polysaccharides and mucosubstances such as glycoproteins, glycolipids or mucins. This was performed in order to potentially detect glycation level changes with aging ECM. There were not large changes in Periodic Acid Schiff staining intensity with aging though a brighter section on the inside of 52 week old SIS was detected. Artificial glycation of SIS resulted in progressively brighter periodic acid Schiff staining (Figure 7).
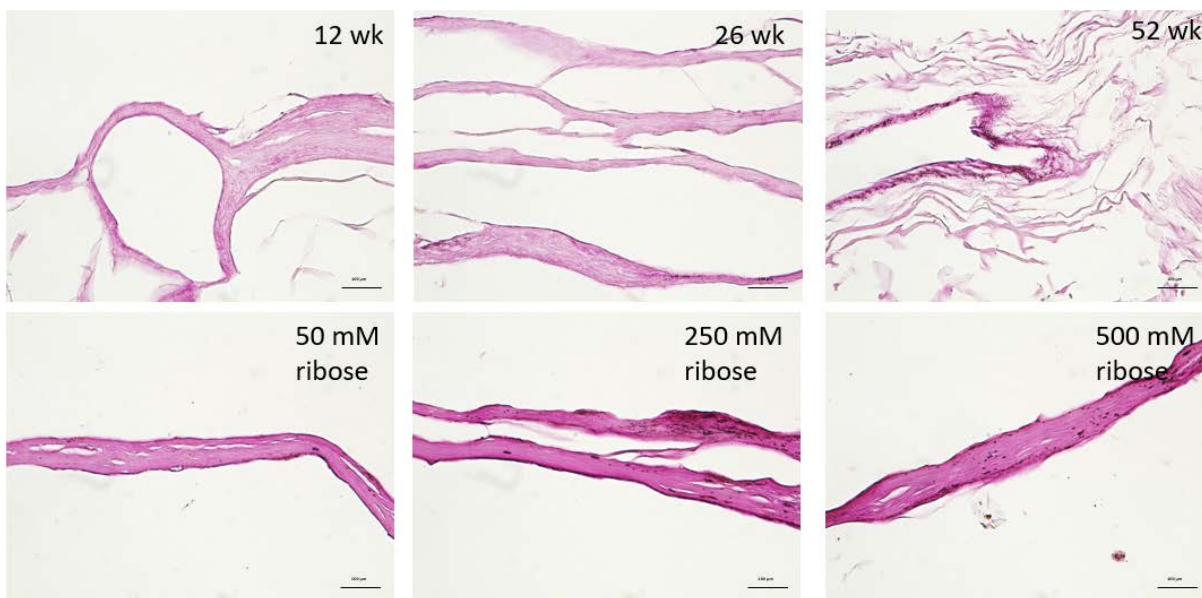
Figure 7: Periodic acid-Schiff stain of different aged SIS and artificially glycated SIS.

Images taken at 10X magnification. Scale bars indicate 100 µm.

Staining of tissue with DNPH did not produce a noticeable signal alone (Figure 8). There was some particulate matter that stained dark in 52 wk SIS but it is unclear the cause of this. Other types of assays for protein carbonyl may be better suited for detection in extracellular matrix scaffolds.

Figure 8: DNPH staining of different aged small intestine submucosa ECM.

Images taken at 10X magnification. Scale bars indicate 100 µm.

Immunohistochemical staining of small intestine submucosa did not reveal large changes in AGE staining (Figure 9).
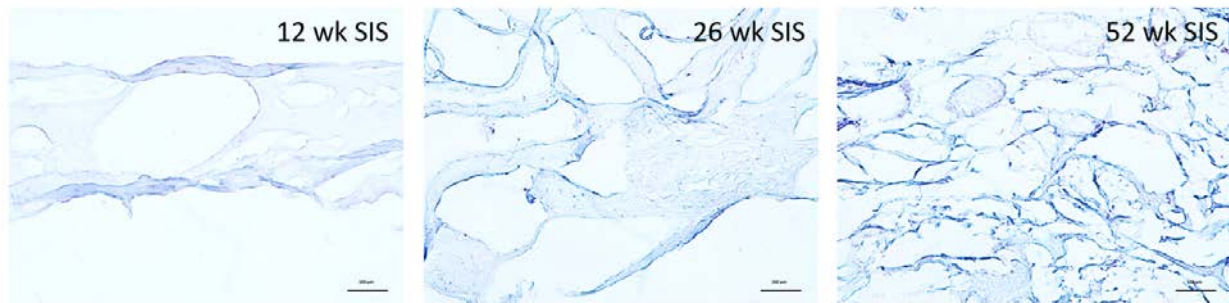
Figure 9: Immunohistochemical staining for advanced glycation end-products.

Images taken at 10X magnification. Scale bars indicate 100 µm.

Assessment of advanced glycation end-product content via ELISA revealed a significant reduction in AGE content from 12 week SIS to 26 and 52 week SIS. Artificial glycation of SIS resulted in numerical increase AGE content with increased concentration of ribose used to glycate the SIS (Figure 10).
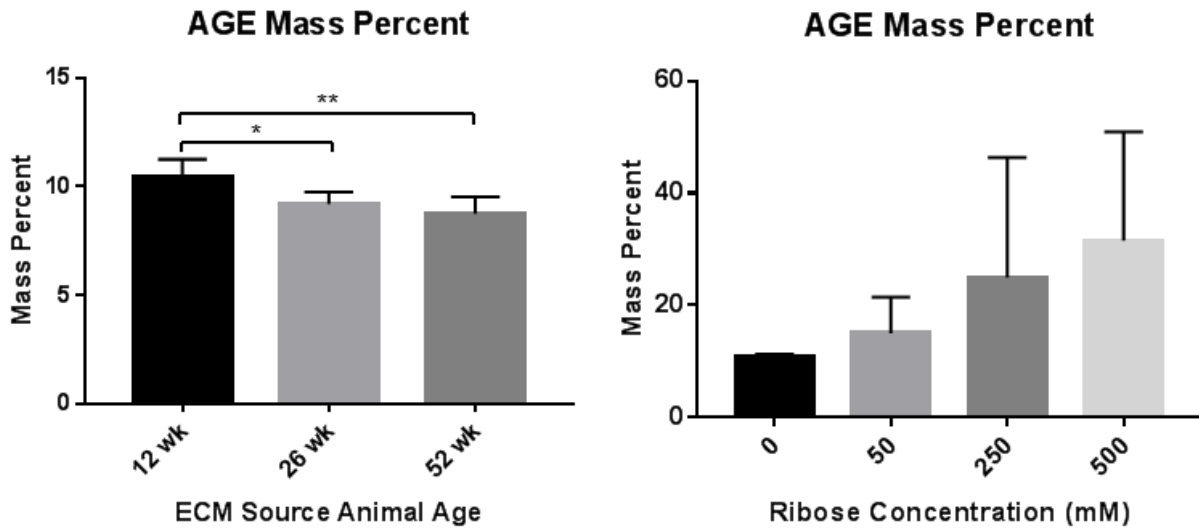
Figure 10: ELISA for advanced glycation end-products.

Data shown as mean ± S.D. Statistical significance reported as *p<0.05, **p<0.01, ***p<0.001, ****p<0.0001.

2.3.4 Biomechanical assessment

Visual assessment of scanning electron microscopy (SEM) images showed there was more fiber alignment in 12 week SIS than in 52 week SIS (Figure 11). Quantitative assessment should be performed in order to confirm this observation.
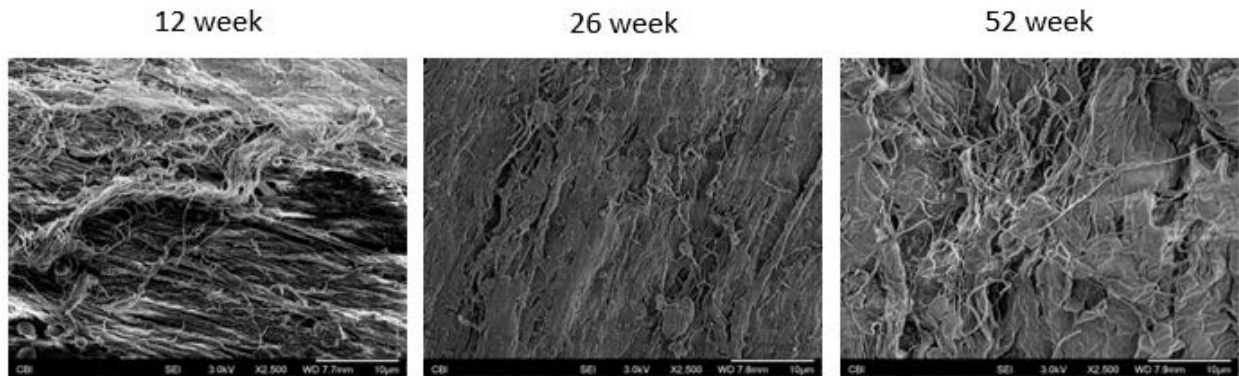
Figure 11: Scanning electron microscopy images of small intestine submucosa at 2500X.
Scale bars indicate 10 µm.

Tensile mechanical testing of small intestine submucosa revealed differences in mechanical properties in both circumferential and longitudinal directions. Fifty two week SIS had significantly lower peak stress in both the longitudinal and circumferential directions. There was no difference in peak strain in either direction. The elastic modulus of 52 week SIS was significantly less than 12 week SIS in both directions. Twenty-six week SIS had significantly higher toughness than 12 or 52 week SIS in the longitudinal direction. In the circumferential direction, 52 week SIS had less toughness than 26 week SIS (Figure 12).
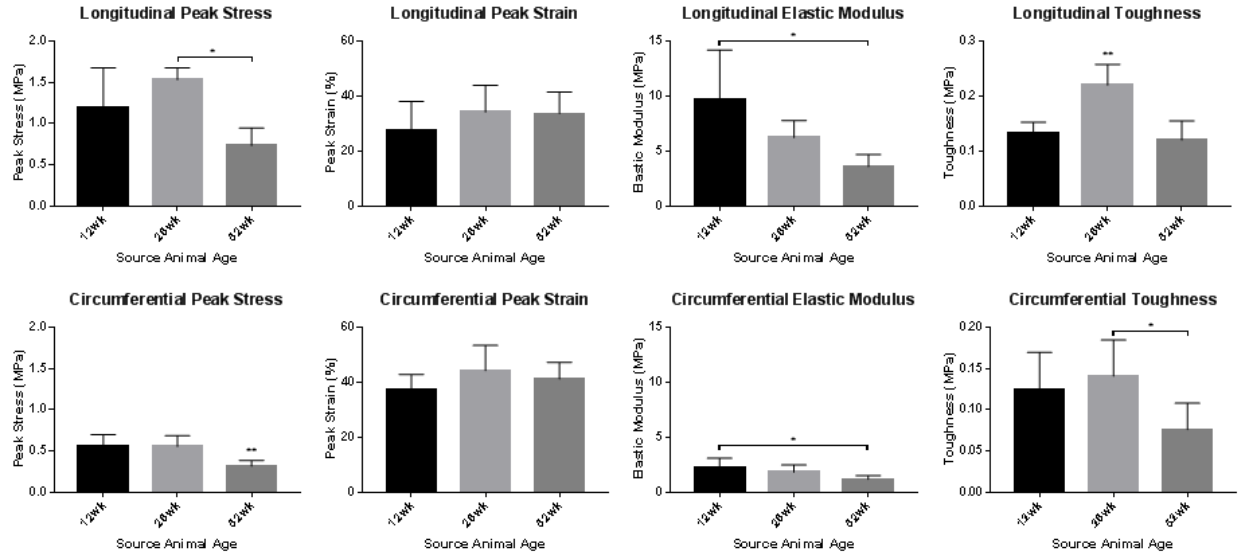
Figure 12: Uniaxial tensile mechanical testing performed under constant strain rate.

Data shown as mean ± S.D. Statistical significance reported as *p<0.05, **p<0.01, ***p<0.001, ****p<0.0001.

2.3.5 Immunofluorescent antibody labeling

Differentiation into a macrophage phenotype was confirmed with antibody immunolabeling for F4/80, a commonly reported macrophage marker in mice. All treatment groups displayed staining for F4/80 with M1 treatment resulting in significant increases in F4/80 labeling (Figure 13A). Macrophages treated with ECM degradation products were stained for classical differentiation markers of macrophage phenotype. Staining for iNOS, a classical M1, pro-inflammatory marker, showed upregulation in M1 controls and downregulation in M2 controls (Figure 13B). Macrophages treated with ECM degradation products showed slight iNOS activation. Increasing source animal age resulted in significantly decreased iNOS surface marker expression with increasing age in macrophages from 2 month mice (Figure 13B). Macrophages derived from 18 month mice did not have a significant decrease in iNOS expression between 12

and 52 week ECM but ECM groups in 18 month macrophages had significantly higher iNOS expression over 2 month macrophages (p<0.0001) (Table 1). Staining for Arginase-1, a marker for M2, alternative activation, showed large upregulation in M2 controls and slight downregulation in M1 controls (Figure 13C). ECM-treated macrophages showed no differences in Arginase-1 surface marker expression compared to M0 controls. There were no significant changes in Arginase-1 immunoexpression with source animal age (Figure 13C).

Fizz1, a marker for alternative macrophage activation, showed increased labeling in M2 controls and decreased labeling in M1 controls (Figure 13D). Fizz1 expression of ECM-treated macrophages was intermediate, neither pro- nor anti-inflammatory. Source animal age significantly decreased Fizz1 expression from 12 week to 52 week SIS. Fizz1 expression was significantly higher in macrophages derived from 18 month mice compared to 2 month old mice (p<0.0001) (Table 1).

CCR2, a chemokine receptor for CCL2, is classically a marker for invading macrophages. CCR2 showed decreased surface marker expression in M1 controls (Figure 13E). There were no significant differences in CCR2 immunolabeling based on source animal age of ECM. However, 18 month macrophages responded to ECM with increased CCR2 immunoexpression compared to 2 month macrophages (p = 0.0463) (Table 1). CX_3CR1, a fractalkine receptor, is a marker for tissue-resident macrophages. There were no significant changes in fractalkine receptor expression in cytokine controls or ECM treatment (Figure 13F).
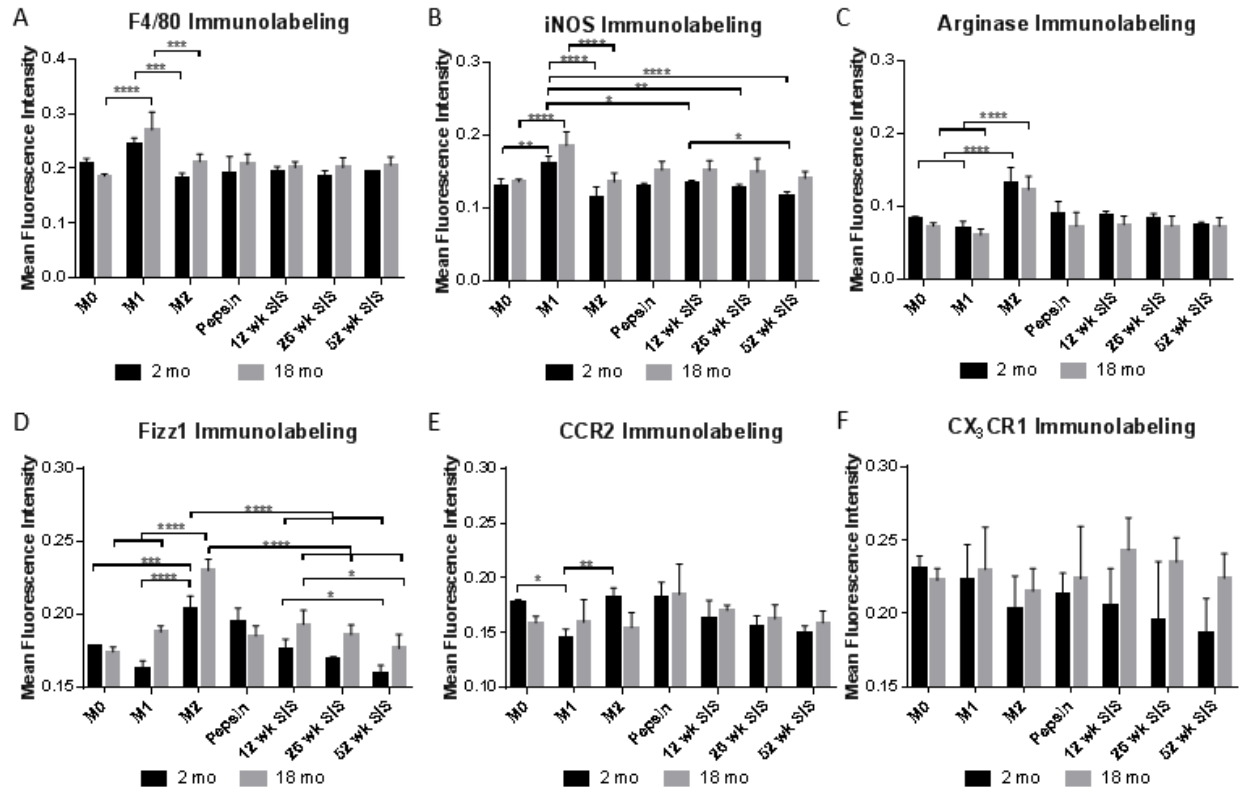
Figure 13: Immunofluorescent antibody labeling of bone marrow macrophages treated with ECM.

Data shown as mean ± S.D. Statistical significance reported as *p<0.05, **p<0.01, ***p<0.001, ****p<0.0001.

Table 1: List of p-values for age of macrophages and age of ECM source animal.

	Mouse Age (p-value)	ECM Source Age (p-value)
iNOS	<0.0001	0.0201
Arginase-1	0.0249	0.2623
Fizz	<0.0001	0.001
CCR2	0.056	0.0463
CX3CR1	0.0003	0.2663

In order to determine whether ECM degradation product exposure altered the ability of macrophages to polarize, macrophages were treated with ECM degradation products for 24 hours then treated with M1 or M2 cytokine regimes for the subsequent 24 hours. 52 week SIS significantly increased iNOS immunoexpression in ECM→M1 groups over IFN-γ/LPS treatments in 2 month old macrophages and 12 week SIS treatments in 18 month old macrophages (Figure 14A). Arginase-1 immunoexpression was significantly upregulated with 12 week pre-treatment with subsequent IL-4 treatment compared to M2 controls (Figure 14B). In 18 month macrophages, 52 week SIS caused a significant increase in Arginase-1 immunoexpression over 12 week SIS with IL-4 post-stimulation. The only significant change in Fizz1 immunoexpression was a significant increase in Fizz1 in all ECM pre-treatments with IFN-γ/LPS post-stimulation over M1 controls in the 2 month macrophage group (Figure 14C). MHC-II immunoexpression was significantly decreased with 26 or 52 week SIS pre-stimulation over M1 and 12 week SIS pretreatment samples in 2 month old macrophages (Figure 14F). SIS from 26

and 52 week SIS only decreased MHC-II expression compared to M1 stimulation in 18 month old macrophages.
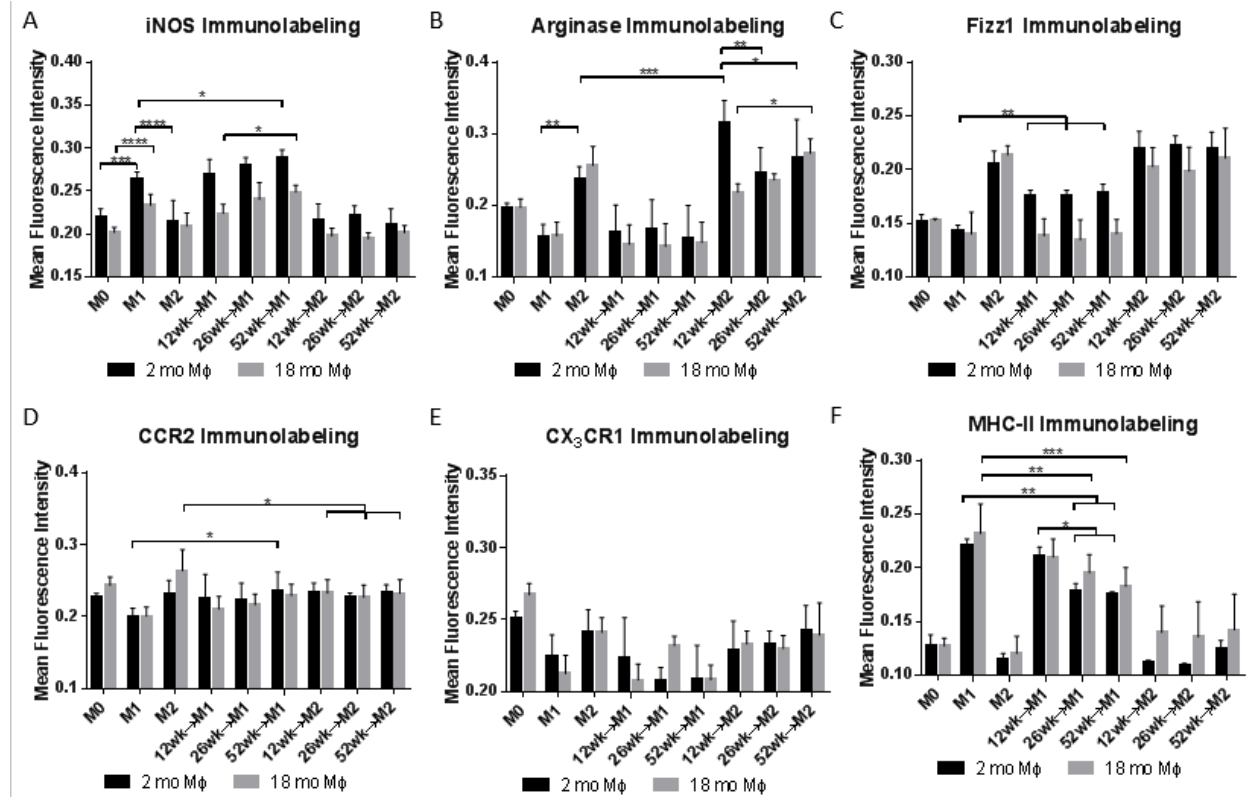
Figure 14: Immunofluorescent antibody labeling of macrophages treated with ECM then cytokines.

Data shown as mean ± S.D. Statistical significance reported as *p<0.05, **p<0.01, ***p<0.001, ****p<0.0001.

2.3.6 Taqman gene expression analysis

Transcriptional levels of classical pro-inflammatory and anti-inflammatory markers and cytokines were assayed in 24 hour macrophage RNA extracts using Taqman gene expression assays (Figure 15). Pro-inflammatory markers *NOS2, IL1b, IL12b,* and *Tnfa* showed large increases in fold expression change in M1 treatment over naïve M0 macrophages. The anti-

inflammatory gene targets *Arg1*, *Fizz1*, *IL10*, and *Mrc1* showed significant increases in IL-4-stimulated M2 macrophages. Fifty two week SIS treatment resulted in significant increases of IL-1ra expression over 12 and 26 week SIS treatment in 2 month old macrophages. Eighteen month old macrophages treated with 52 week SIS resulted in significant increases in Fizz1 expression over 12 week SIS treatment.
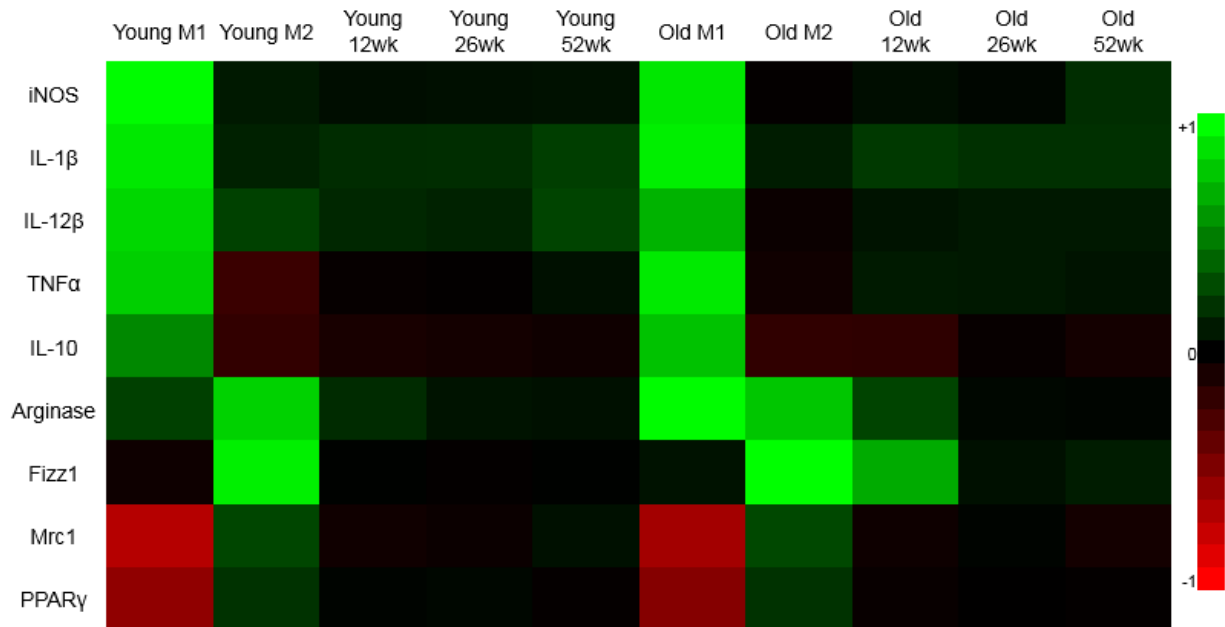
Figure 15: Taqman gene expression analysis of macrophages treated with ECM.

Data shown are $\log_{10}$ of fold expression changes and are plotted on a scale where +1 indicates 10^x where x is the power of the highest fold change for each gene target and -1 indicated 10^{-x}.

Gene expression assays were also conducted in challenge experiments where macrophages were exposed to ECM degradation products for 24 hours then challenged with M1 or M2 polarizing cytokines for an additional 24 hours (Figure 16). Pro-inflammatory (M1) controls showed large fold expression increase in iNOS, IL-12β, IL-1β, MHC-II, TNF-α, and IL-10. Anti-inflammatory

(M2) controls showed large fold expression increase in Arginase-1 and Fizz1 and smaller increases in Mrc1, PPARγ, MHC-II and IL-1β with decreases in TNFα and IL-10. ECM pre-treatment did not alter expression of any genes following M1 or M2 treatment.
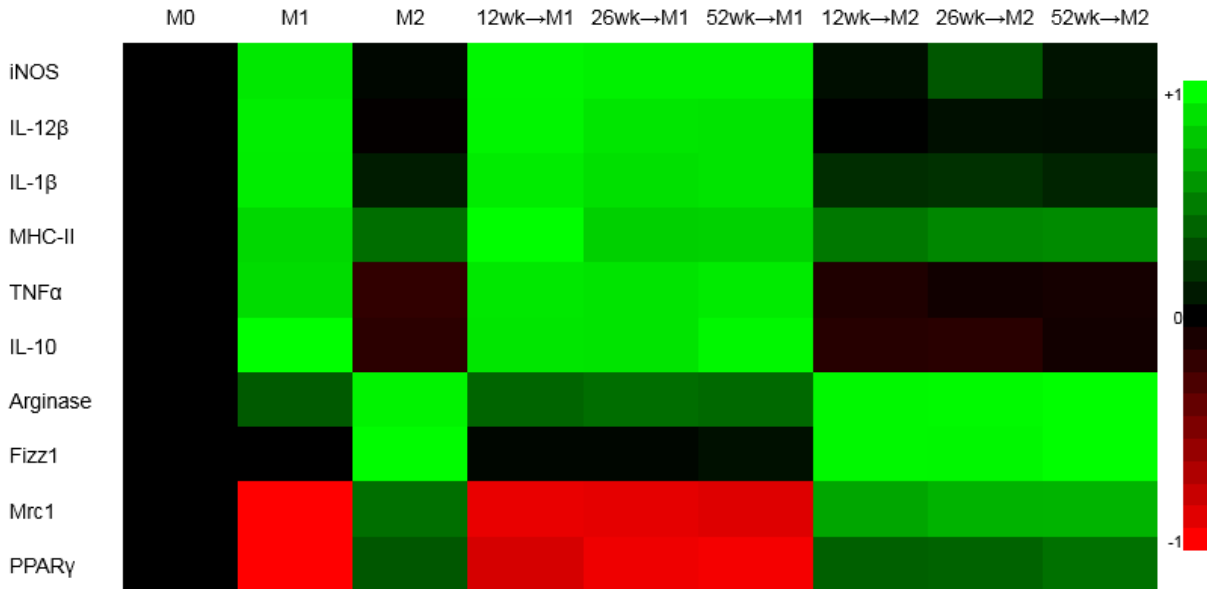
Figure 16: Taqman gene expression of macrophages treated with ECM then cytokines.

Data shown are $\log_{10}$ of fold expression changes and are plotted on a scale where +1 indicates 10^x where x is the power of the highest fold change for each gene target and -1 indicated 10^{-x}.

2.3.7 Nitric oxide production

Nitric oxide was assayed in the supernatants of macrophages treated with ECM degradation products (Figure 17). The stable form of nitric oxide, nitrite, was identified using the Greiss reagent system. Results showed an increase in nitric oxide production in M1 controls but no increase in M2 controls. ECM treatment showed limited levels of nitric oxide production. There were no significant differences in nitric oxide production from macrophages treated with ECM

49

alone. ECM pre-treatment followed by M1 stimulus increased nitric oxide production in 12 week

SIS samples compared to M1 controls and 52 week SIS pre-treatment.

Nitrite Production
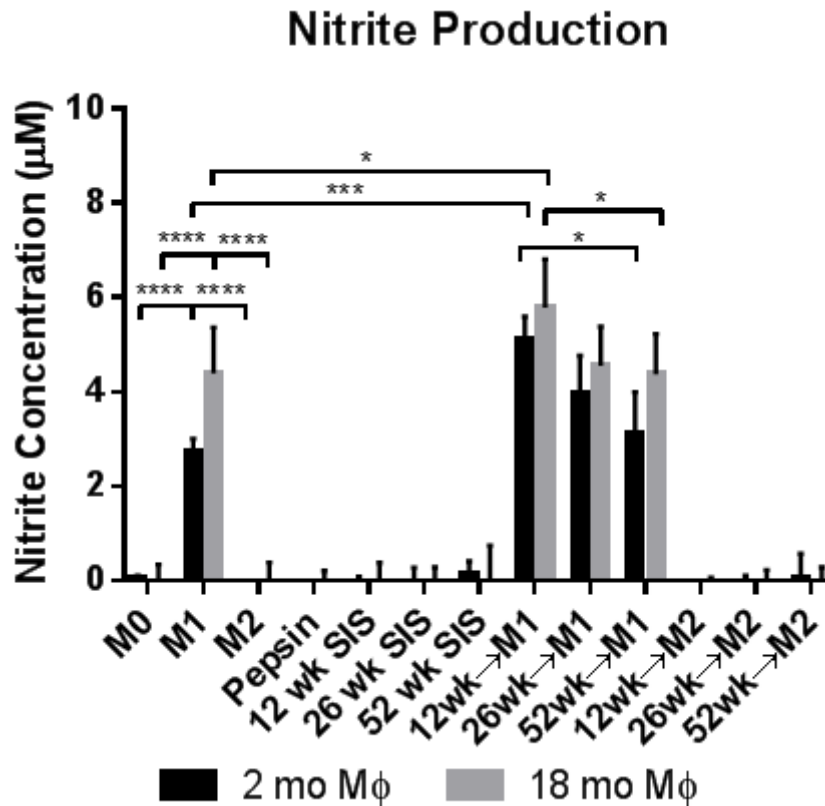
Figure 17: Greiss reagent system assay of nitrite content from macrophage supernatants.

Data shown as mean $\pm$ S.D. Statistical significance reported as *$p<0.05$, **$p<0.01$,

***$p<0.001$, ****$p<0.0001$.

2.3.8   Phagocytosis

To assess phagocytic function, Vybrant Phagocytosis Beads produced from FITC-labeled E. coli

bacteria particles were used. Phagocytic activity increased in pro-inflammatory controls but not

in anti-inflammatory controls (Figure 18). ECM degradation products did not significantly

change baseline phagocytosis or phagocytosis following cytokine regimens.
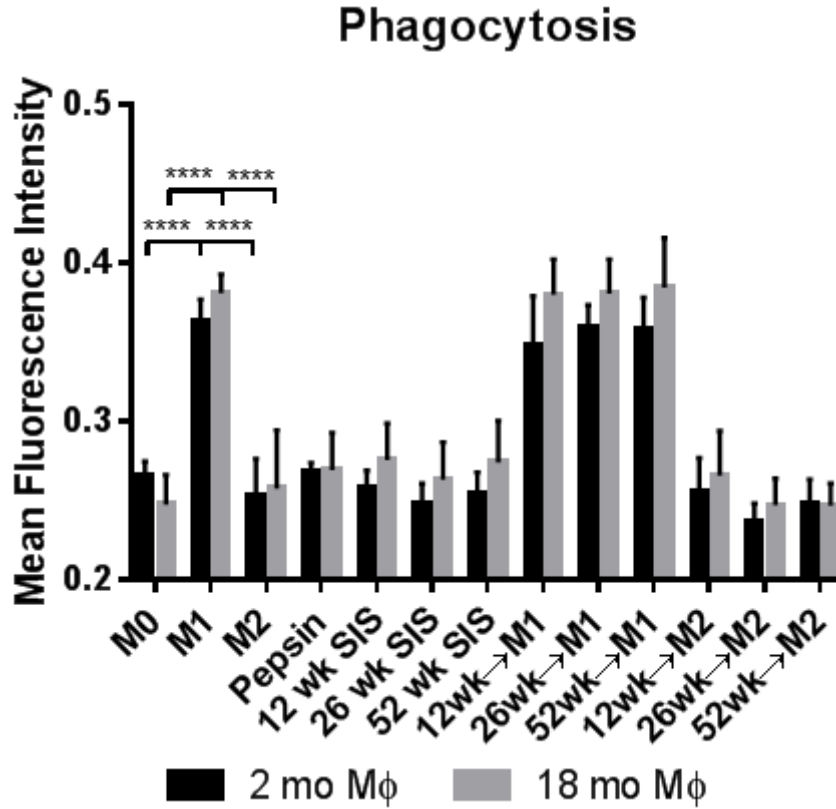
Figure 18: Vybrant FITC-labeled E. Coli phagocytosis assay on macrophages treated with ECM.

Data shown as mean ± S.D. Statistical significance reported as $*p<0.05$, $**p<0.01$, $***p<0.001$, $****p<0.0001$.

2.3.9   Seahorse metabolic analysis

Pro-inflammatory (M1) macrophages exhibited significantly less ATP production and coupling efficiency (Figure 19). There were not significant changes in metabolism due to ECM treatment or ECM source animal age.
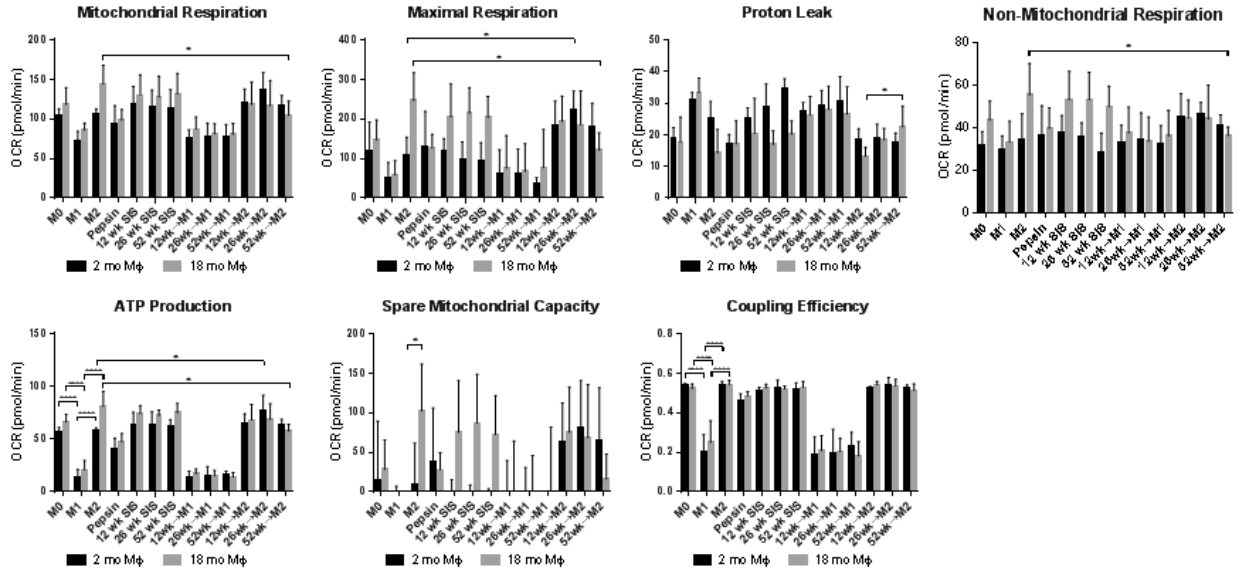
Figure 19: Seahorse metabolic analysis of mitochondrial metabolic parameters.

Data shown as mean ± S.D. Statistical significance reported as *p<0.05, **p<0.01, ***p<0.001, ****p<0.0001.
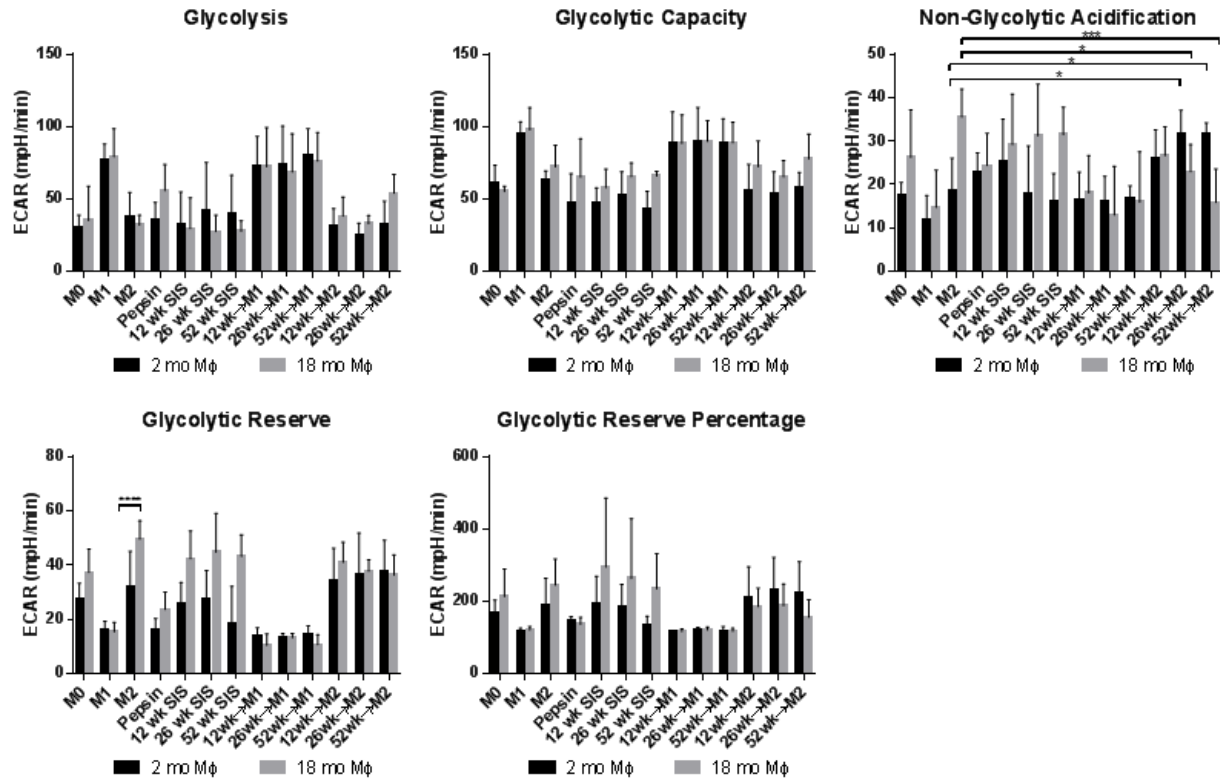
Figure 20: Seahorse metabolic analysis of glycolytic metabolic parameters.

Data shown as mean ± S.D. Statistical significance reported as *p<0.05, **p<0.01, ***p<0.001, ****p<0.0001.

2.4   DISCUSSION

The present study investigated the response of macrophages to extracellular matrix (ECM) degradation products within an aging context. Specifically, this study investigated porcine small intestine submucosa (SIS) scaffolds that differ in only the variable of source animal age (the age of the animal from which it was derived). Previous work has shown that these scaffolds, when implanted into a rat abdominal wall reconstruction model, elicited different potentials for muscle healing [176]. This previous study showed that increasing source animal age resulted in

increased fibrosis and decreased skeletal muscle formation, which was related to increased pro-inflammatory macrophage phenotype at early time-points. In order to identify macrophages as being able to respond to these age-related changes, the present study utilized an *in vitro* model of macrophage response to ECM biomaterials. Results showed that ECM biomaterials caused the greatest shifts in macrophage phenotype when examined in combination with inflammatory cytokine polarization. The lack of robust macrophage response to ECM scaffolds alone is logical as the ECM is naturally occurring and involved in the homeostasis of tissues.

There are currently over 50 extracellular matrix-based products registered with the FDA, many of which are derived from animal sources [227]. Due to known differences in composition of biologic materials due to individual organism variabilities, it is important to understand what characteristics of donor animals have effects on resultant biomaterial properties and their response upon implantation. Quality compliance of source animal facilities (SAFs) is regulated under FDA guidance "Source Animal, Product, Preclinical, and Clinical Issues Concerning the Use of Xenotransplantation Products in Humans" which ensures that animals used for clinical products are infection and disease free. However, factors such as age are not included in this guidance and could potentially have an effect on the performance of medical devices derived from aged animals. Understanding how changes in the extracellular matrix changes with source animal age could lead to reduced variability in xenogeneic biomaterials and improved outcomes.

It is well documented that there are changes with age in extracellular matrix composition of many tissues. Aged colon exhibits increases in collagen content and decreases in strength [228]. Macrophages have been shown to respond differently to different collagen subtypes with collagen I increasing CCL18, IL-1ra, CCL2, CD204 and p-Akt expression whereas collagen III only increased CCL18 and IL-1ra [229]. Therefore, changes in extracellular matrix composition

with age could alter the macrophage response to biomaterials derived from different aged source animals, as shown in this study. This could compromise normally beneficial host responses and remodeling outcomes downstream of implantation. Furthermore, the influence of ECM on responses to inflammatory cytokines suggest the ECM environment may play a role in the nature and progression of the host inflammatory responses to injury and infection. Biochemical analyses for hydroxyproline and glycosaminoglycan content were unable to detect changes in decellularized ECM scaffolds. Therefore, more rigorous analysis including mass spectrometry is needed to understand changes in composition of specific components within aged ECM.

The importance of changes in animal tissue product composition is most important with regard to how these changes affect the host response following implantation. A recent study has shown that aged animals elicited an altered macrophage response to polypropylene mesh implanted subcutaneously compared to young controls [230]. Results in this study show that bone marrow-derived macrophages from young and aged mice have similar abilities to polarize to M1 and M2 profiles *in vitro*. This suggests that changes in the macrophage response to implantable biomaterials cannot be explained by macrophage-intrinsic changes with age alone. It is logical to infer that the aged local microenvironment, consisting of the extracellular matrix and cellular signals, could be responsible for these changes in responses to biomaterials. These *in vivo* results further findings in this paper that aged ECM microenvironments affect macrophage phenotypes which could lead to altered immune responses.

There are documented changes in macrophage populations and phenotypes in aged organisms. Peritoneal macrophage populations increased in the percentage of monocyte-derived and mature macrophages. Aged peritoneal macrophages also exhibited increased pro-inflammatory cytokine IL-1b and IL-6 expression when stimulated with GM-CSF or IL-4. Aged

macrophages also exhibited a decreased nitric oxide/urea ratio [231]. Aged splenic macrophages exhibited decreased expression of IL-6, iNOS, IL-1b and TNFa when stimulated with LPS. Aged splenocytes also had reduced M2 markers when stimulated with IL-4 compared with young controls [52]. Aged macrophages have also been shown to have decreased MHC-II expression following IFN-y treatment, suggesting onset of immunosenescence [100]. Our results showed 52 week ECM reduced MHC-II immunoexpression following IFN-y/LPS suggesting aged ECM may contribute to this immunosenescent phenotype. Further elucidation of these mechanisms is necessary to determine how aged ECM causes changes in macrophage phenotype.

Treatment of macrophages with aged ECM *in vitro* results in similar alterations in phenotype compared to young ECM, reduced iNOS and Fizz1 immunoexpression. Aged ECM treatment with IFN-y/LPS stimulus increased iNOS immunoexpression and reduced nitric oxide production at 24 hours. This could suggest that aged ECM incites a delayed iNOS response as nitric oxide production is a result of the cumulative production in media over 24 hours whereas immunolabeling assays protein level at 24 hours only. This suggests that age-related changes in the ECM may contribute to the altered immune responses observed in aged wound healing.

Previous studies have noted that the aging microenvironment is responsible for alterations in macrophage populations. Aging muscle exhibits an increase in M2a macrophage populations that could be the cause of increased fibrosis [53]. Transplantation of young bone marrow cells into aged muscle reduced the number of M2a macrophages, which could be caused by altered phenotypes in aged macrophages or be a result of the shift toward myeloid lineages in aged bone marrow [53]. These changes in aged muscle are also corrected by transfection of nNOS, suggesting that reduced nitric oxide in aged muscle could be a factor in this macrophage phenotype shift. Blau et al. also suggest that the aging microenvironment impacts the function of

muscle stem cells [232]. Some changes were attributed to intrinsic changes in MuSCs with age but others have been attributed to the local microenvironment. Age-related changes in the ECM microenvironment thus represents a cell-extrinsic mechanism of altered wound healing and regeneration in aged individuals.

Aging has an effect not only on macrophage phenotypes and populations, but also macrophage function. Linehan et al. showed that the aged peritoneal microenvironment significantly impaired phagocytic function of macrophages independent of intrinsic changes in bone marrow macrophage populations [106]. Some of these changes were attributed to changes in T and B cell populations and levels of IL-10. Reduced phagocytic function could lead to impaired responses to pathogens or delayed debris removal in wound environments. However, our results did not show any change in phagocytic function due to aged ECM exposure. Aged alveolar macrophages were also shown to have reduced production of nitric oxide [233]. This matches our findings that macrophages exposed to aged ECM produced less nitric oxide upon IFN-y/LPS exposure. This reduction in macrophage function could impair pathogen immunity and alter angiogenic responses.

The effects of aging have also been well documented in the area of wound healing. Wound healing in aged individuals is associated with delayed monocyte infiltration, increases in mature macrophages, and impaired macrophage function including reduced phagocytic capacity and increased secretion of pro-inflammatory mediators [99, 234, 235]. There are also delays in angiogenesis, collagen production and re-epithelialization, all of which are functions that are orchestrated by macrophages and their interaction with other cells of the injury response [236, 237]. In spinal cord injury, macrophages have been shown to have reduced IL-10 expression in aged individuals [238]. Macrophages in aged vascular injury exhibited increased IL-18

expression which was associated with higher fibrinogen deposition [239]. All these examples show the impact of shifts in aged macrophage populations and phenotypes upon normal wound healing. Aged microenvironments may be responsible for these shifts in maintained or recruited macrophage populations or alterations from expected phenotypic responses.

There were several limitations to the present study. This study only analyzed the effects of aging on porcine small intestine submucosa over the ages of 12 to 52 weeks. Not only does the extracellular matrix from different organs have different compositions but there are also organ-specific changes in this ECM makeup with age. Therefore, these results may not apply to ECM biomaterials derived from different sources. Furthermore, an in-depth assessment of what changed in these SIS scaffolds was not performed. More work would need to be done to understand, at a detailed level, the specific compositional changes and the signaling pathways which dictate changes in ECM-treated macrophage phenotype, which are currently unknown. Assessment of the presence and change in composition of matrix bound nanovesicles was also not completed. Changes in MBV content with age could be a potential mechanism for altered responses to these biomaterials [240]. This study also focused on the effects of extracellular matrix biomaterials on the phenotypes of macrophages alone. Many other cells participate during, before and after the involvement of macrophages during wound healing and biomaterial remodeling, including neutrophils, fibroblasts, adaptive immune cells, endothelial cells and stem cells. Little investigation has been performed on the synergistic roles of these cells during regenerative processes and further work is warranted in order to understand how these cells function together.

2.5   CONCLUSION

Extracellular matrix scaffolds vary significantly due to their biological origin, and age effects their properties significantly. These changes in ECM structure are recognized by macrophages which change both their expression and function in response. Aged ECM degradation products alter macrophage phenotype and function both alone and in the presence of polarizing cytokines. These findings suggest that age-related changes in the ECM microenvironment have direct effects on the immune system. This suggests that age-related changes in wound healing and regeneration could be a result, in part, due to alterations in the extracellular matrix. This suggests further investigation into the ECM from aged individuals and its direct effect on immune and host response cells could help to elucidate mechanisms of altered healing responses in elderly populations.

3.0 EFFECT OF LIPID AND UREA EXTRACTS FROM AGED SMALL INTESTINE SUBMUCOSA UPON MACROPHAGE POLARIZATION

3.1 INTRODUCTION

The composition of the extracellular matrix is known to change with age [241-243]. Therefore, it is logical to conclude that extracellular matrix biomaterials derived from different aged animals will be different. Previous work has shown that small intestine submucosa (SIS) derived from 3-, 12-, 26-, and 52-week old pigs showed differences in ECM and growth factor composition [175]. The *in vivo* host response to these different source animal age ECM showed increased pro-inflammatory macrophage responses with increased ECM source animal age [176]. Extracellular matrix degradation products from aged small intestine submucosa were shown to directly alter the bone marrow macrophage response [110].

Changes in growth factor composition is suggested to be one potential mechanism for the altered host response to aged extracellular matrix but has yet to be tested directly [244]. There are a number of growth factors naturally found in the intestine, including epidermal growth factor (EGF), heparin-binding epidermal-like growth factor (HB-EGF), glucagon—like peptide 2 (GLP2), growth hormone (GH), insulin-like growth factor 1 (IGF-1), granulocyte colony stimulating factor (G-CSF), erythropoietin (Epo), intestinal trefoil factor (ITF), keratinocyte growth factor (KGF), and hepatocyte growth factor (HGF) [245]. Some reports have shown that

certain growth factor levels change with aging and affect lifespan, including IGF-1 [207, 246]. Insulin-like growth factor 1 has been shown to be both produced and to maintain M2 macrophage polarization [247]. Granulocyte-colony stimulating factor (G-CSF) is also known to polarize macrophages to an anti-inflammatory phenotype [248]. Production of HB-EGF by IL-4-stimulated macrophages leads to transactivation of epidermal growth factor receptor (EGFR) [249]. Growth factors have previously been extracted from extracellular matrix bioscaffolds using urea solubilization [219, 244]. Therefore, a direct effect of ECM-laden growth factors upon macrophage polarization can be tested.

Lipid content in aged porcine extracellular matrix biomaterials is another potential factor as pigs rapidly gain mass and fat content as they mature [250]. Fatty acid oxidation has been shown to be necessary for an M2 macrophage polarization and is also involved in the progression of many diseases including obesity and diabetes [251]. Exposure of macrophages to several types of fatty acids has been shown to induce M2 macrophage polarization [252-254].

3.2   METHODS

3.2.1   Extracellular Matrix Scaffold Preparation

Jejunum were harvested from 12 week, 26 week, and 52 week-old Landrace pigs immediately following euthanasia (Tissue Source, Lafayette, IN). The animals were of similar genetic heritage, diet and immunization history. Small intestine submucosa (SIS) extracellular matrix biomaterials were prepared from these tissues as previously described [129]. Briefly, the tissues were rinsed with water and the mesenteric tissues were removed. Tissues were cut

longitudinally then mechanically delaminated to remove the tunica serosa, tunica muscularis externa, and the luminal tunica mucosa, including most of the lamina propria. After delamination, the tunica submucosa and the basilar layer of the tunica mucosa including the muscularis mucosa and the stratum compactum of the lamina propria remained. The material was further decellularized using mechanical agitation with an orbital shaker at 300 rpm in a solution of 0.1% (v/v) peracetic acid (Rochester Midland Corporation, Rochester, NY). Tissues were then rinsed multiple times with saline and deionized water. Decellularized scaffolds were frozen at -80°C and then lyophilized. The resultant scaffolds were considered "whole ECM scaffolds." A Wiley mill with a #60 mesh was used to grind ECM scaffolds into powder.

3.2.2 Lipid Extraction

Lipids were extracted from lyophilized ECM scaffolds using a 2:1:1 chloroform:methanol:water mixture. Twenty milligrams of lyophilized ECM were added to 2 mL of 2:1:1 chloroform:methanol:water in a scintillation vial and then agitated on a tube vortexer for 2 hours. Scintillation vials were then centrifuged at 3000 rpm for 10 minutes. The organic phase was removed and placed in a clean scintillation vial. The organic solvents were then allowed to evaporate in a fume hood overnight. Once dry, the scintillation vials were lyophilized to remove residual organic solvent. Two milliliters of macrophage media was added to each scintillation vial and mixed on a vortexer for 48 hours.

3.2.3 Urea Extraction

Growth factors and soluble proteins were extracted using a urea extraction protocol. Fifty milligrams of powdered ECM was added to microcentrifuge tubes and then 1 mL of 2M urea / 1M Tris-HCl was added to each tube. The tubes were allowed to incubate on a rocker overnight at 4 °C. The tubes were centrifuged at 10,000xg for 30 mins and then the supernatant was saved. Another 1mL of urea extraction buffer was added to each tube and the tubes were incubated on the rocker for another 2 hours. The tubes were centrifuged as before and the supernatant combined from the two tubes. Urea soluble fractions were placed into 3kDa dialysis tubing and dialyzed against type 1 water for 3 days. Urea insoluble fractions were washed with type 1 water 3 times via vortexing and then centrifuged to remove the water. Urea soluble fractions were adjusted to 10 mg/mL based on original ECM mass added. The urea insoluble fractions were frozen at -80 °C and then lyophilized.

3.2.4 Pepsin digestion of ECM

Whole ECM powder or urea extracted ECM powder was digested at a concentration of 10 mg/mL in an acid-pepsin solution (pH 2) under constant magnetic stir for 48 hours. These digested scaffolds were considered "ECM degradation products."

3.2.5 Fatty acid quantification

Lipid extracts were analyzed for free fatty acid content using the Free Fatty Acid Quantification Kit (Sigma) according to manufacturer instructions. Twenty milligrams of lyophilized ECM was

lipid extracted using 2 mL of 2:1:1 chloroform:methanol:water for 2 hours as described above. The organic phase was removed and allowed to evaporate overnight. The dried lipids were then lyophilized to remove any residual organic solvent. Samples were then diluted in 200 µL Fatty Acid Buffer and agitated until dissolved. Fifty microliters of sample or palmitic acid standards (0, 2, 4, 6, 8, 10 nmol) were added to a 96 well plate. Two microliters of ACS reagent was added to each well and the samples were incubated for 30 mins at 37ºC. Then, fifty microliters of the master reaction mix was added to each well and the samples were again incubated for 30 mins at 37ºC. The absorbance of each well was measured at 570 nm using a spectrophotometer plate reader. Concentrations were calculated based on measurements from the palmitic acid standard curve.

3.2.6   Bone marrow-derived macrophage isolation

Bone marrow-derived macrophages were harvested from 2 month or 18-20 month-old C57/BL6 mice as previously described [221]. Briefly, femurs and tibiae were harvested and separated from muscle and connective tissue. Bones were cut at either end to expose bone marrow. Sterile syringe and needles were used to flush out bone marrow using macrophage differentiation media (DMEM/10% FBS/10% L-929 Supernatant/1% PenStrep/2% MEM non-essential amino acids/1% HEPES/0.1% 55µM β-2 mercaptoethanol). Bone marrow lysate was reconstituted in media and filtered through a sterile cell filter. Cells were cultured for 7 days in media to differentiate them into macrophages, changing differentiation media every 2 days.

3.2.7 Macrophage Treatment

Following 7 days of differentiation culture as described above, macrophages were treated with acute polarizing regimens to distinguish phenotypes over 24 hours. Naïve macrophage (M0) controls were treated with basal media for 24 hours. M1 (20 ng/mL IFN-γ and 100 ng/mL LPS) and M2 (20 ng/mL IL-4) polarizing cytokines were used to create positive controls for classical pro- and anti-inflammatory macrophages. ECM degradation products were neutralized and diluted to 1 mg/mL in macrophage media to isolate biochemical effects of degradation products and prevent structural moieties from forming. Pepsin buffer (1 mg/mL pepsin in 0.01 M HCl) diluted in macrophage media was used as a control. Another set of treatment groups involved 24-hour exposure of ECM degradation products followed by 24-hour treatment with either the M1 or M2 treatment regimen.

3.2.8 Indirect immunofluorescent antibody labeling

Cells were fixed with 2% paraformaldehyde (PFA) for 30 minutes then washed in 1XPBS. Cells were incubated in blocking buffer (2% donkey serum, 1% bovine serum albumin (BSA), 0.1% Triton X-100, 0.1% Tween-20) for 1 hour at room temperature. Primary antibodies were diluted in this blocking buffer as follows and incubated overnight at 4 °C: F4/80 (1:200, Abcam 6640), iNOS (1:100, Abcam 3523), Arginase-1 (1:200, Abcam 91279), Fizz1 (1:200, Peprotech 500-P214), CCR2 (1:200, Abcam 21667), CX$_3$CR1 (1:200, Abcam 8021), MHC-II (1:100, Abcam). F4/80 is a marker of macrophage differentiation. iNOS and MHC-II are classical M1 macrophage markers whereas Arginase-1 and Fizz1 are classical M2 macrophage markers. CCR2 is a chemokine receptor associated with macrophage migration whereas CX$_3$CR1 is a

fractalkine receptor associated with tissue-resident macrophages. Cells were washed in 1XPBS then incubated in the appropriate fluorescently-labeled secondary antibody solution in blocking buffer for 1 hour at room temperature (donkey anti-rat Alexa Fluor 488, Invitrogen, 1:200; donkey anti-rabbit Alexa Fluor 488, Invitrogen, 1:300). Cell nuclei were counterstained with DAPI. Cells from six young mice were imaged nine times in the center of each well at 10X magnification using automated position capture function to remove bias from subjective image location acquisition. This set of 9 images per well was counted as one biological replicate and was repeated in cells from n=6 mice for a total of 5 sets of 9 images per group. All imaging was performed on an Axio observer T1 microscope. Mean fluorescence intensity of cells was analyzed using Cell Profiler software (Broad Institute). Briefly, DAPI images were used by the program to identify cell nuclei then FITC images were used to identify cell borders around the identified nuclei. The mean fluorescent intensity was calculated by averaging the pixel intensities (scale of 0 to 1) across the entire cell area. Mean fluorescence intensity values were averaged for all imaged cells in each well.

3.2.9   Phagocytosis assay

Following treatments, cells were assayed for phagocytic ability using Vybrant Phagocytosis Assay Kit (Invitrogen). Cells were incubated in FITC-labeled dead E. Coli particles for 2 hours in the cell culture incubator. Following washing, the cells were fixed with 2% PFA for 30 minutes then washed with 1X PBS. Cells were counterstained with DAPI then imaged and analyzed as described above.

3.2.10 Nitric Oxide Assay

Following treatments, 50 µL of supernatant from macrophages were transferred into a fresh plate. Nitric oxide content was assayed using a Greiss Reagent system. Briefly, 50 µL of sulfanilamide (1% in 5% phosphoric acid) was added to supernatants for 10 minutes. Then, 50 µL of 0.1% N-1-napthylethylenediamine in water was added to the mixture for an additional 10 minutes. The absorbance at 540 nm was measured using a BioTek SYNERGY HTX spectrophotometer.

3.3   RESULTS

3.3.1   Fatty acid content in ECM lipid extracts

Quantification of free fatty acid content within lipid extracts of small intestine submucosa ECM bioscaffolds showed that a significant portion of SIS composition is fatty acids (3-10%) (Figure 21). Small intestine submucosa from 26 week old pigs had significantly higher free fatty acid content than SIS from 12 week old pigs. Fifty two week old SIS had significantly higher free fatty acid content than both 12 and 26 week old SIS.
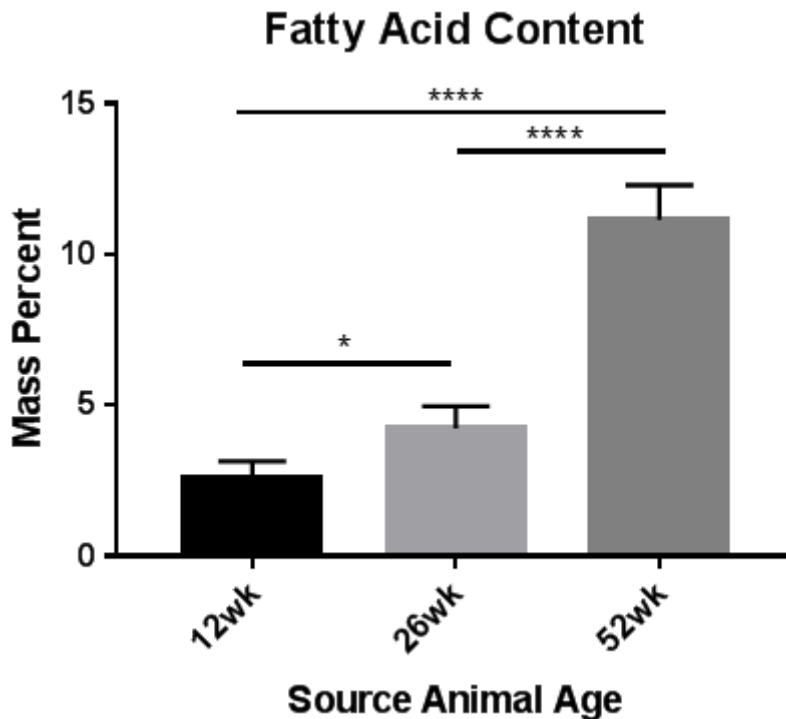
Figure 21: Free fatty acid quantification of lipid extracts from small intestine submucosa ECM.

Data shown as mean ± S.D. Statistical significance reported as *p<0.05, **p<0.01, ***p<0.001, ****p<0.0001.

3.3.2 Immunofluorescent antibody labeling

Macrophages treated with IFN-y and LPS showed an increase in iNOS immunoexpression as expected. Extracellular matrix degradation products from 12 and 26 week old pigs had significantly less iNOS immunolabeling compared to M1 and M2 controls. Fifty two week old SIS was not significantly different than M1 and M2 controls (Figure 22A). Both whole ECM degradation products and urea soluble factors from 52 week old SIS promoted significantly higher iNOS immunoexpression than their respective fractions from 12 week old SIS (Figure 22B). Lipid fractions from 52 week old SIS promoted significantly higher iNOS

immunoexpression than 12 week SIS lipid extracts with IFN-y/LPS stimulus. Urea insoluble fractions from 52 week old SIS promoted significantly more iNOS immunoexpression than 12 and 26 week old SIS with IFN-y/LPS stimulus (Figure 22C). Whole ECM degradation products from 52 week old pigs promoted a significantly decreased iNOS immunoexpression than 12 week SIS with M2 stimulus (Figure 22D).
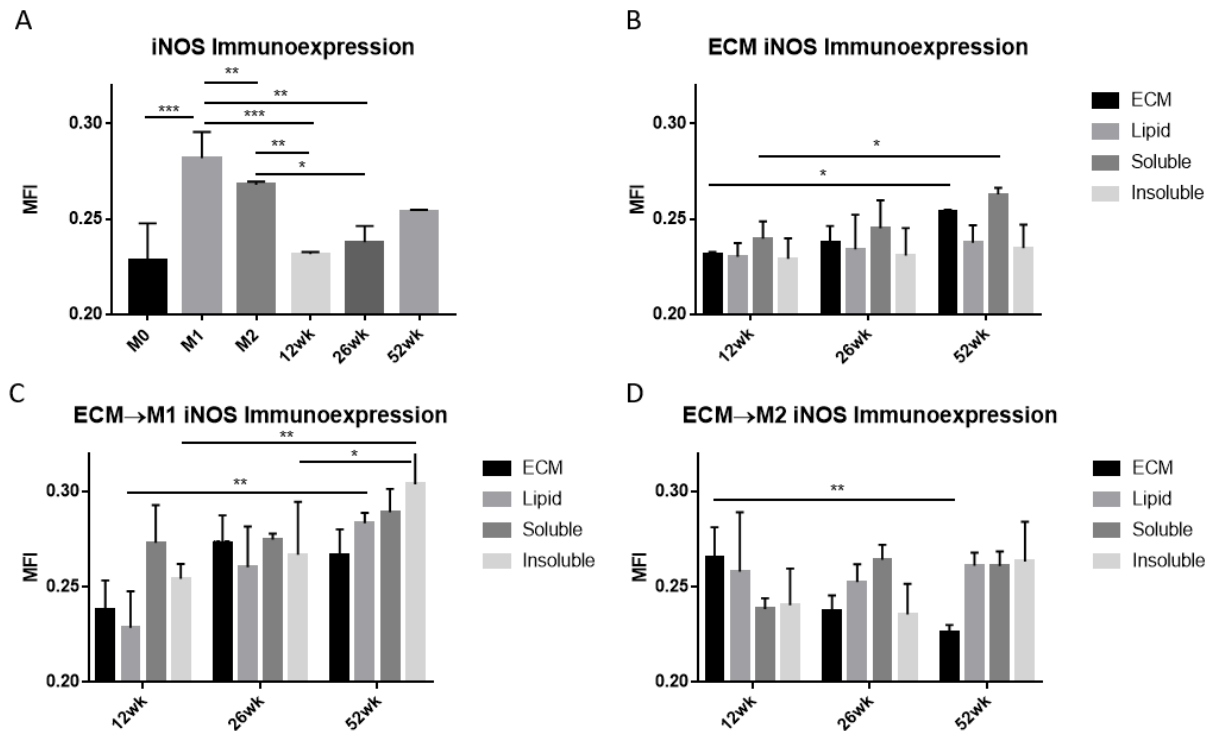
Figure 22: Antibody labeling of macrophages treated with ECM extracts for iNOS.

Macrophages were treated with polarizing cytokines (A), ECM alone (B), ECM then M1 cytokines (C), or ECM then M2 cytokines (D). Macrophages were then fixed and stained for iNOS immunoexpression using indirect fluorescent antibody labeling and mean fluorescence intensity was calculated. Data shown as mean ± S.D. Statistical significance reported as *p<0.05, **p<0.01, ***p<0.001, ****p<0.0001.

Interleukin-4 stimulation of macrophages resulted in significantly increased arginase-1 immunolabeling, as expected (Figure 23A). Treatment of macrophages with ECM degradation products alone did not result in significant changes in arginase immunolabeling compared to M0 controls. Whole ECM degradation products from 52 week old SIS did promote significantly more arginase-1 immunoexpression than 26 week SIS. Lipid extracts from 52 week old SIS promoted significantly less arginase immunoexpression than 26 week old lipid extracts (Figure 23B). With pro-inflammatory stimulus, there was not significant changes in arginase immunoexpression compared to M0 controls. However, soluble and insoluble fractions from 52 week old SIS did promoted significantly more arginase immunoexpression with M1 cytokine treatment (Figure 23C). With IL-4 stimulation, whole and lipid fractions from 52 week old SIS promoted more arginase immunoexpression while soluble and insoluble fractions promoted a reduction (Figure 23D).
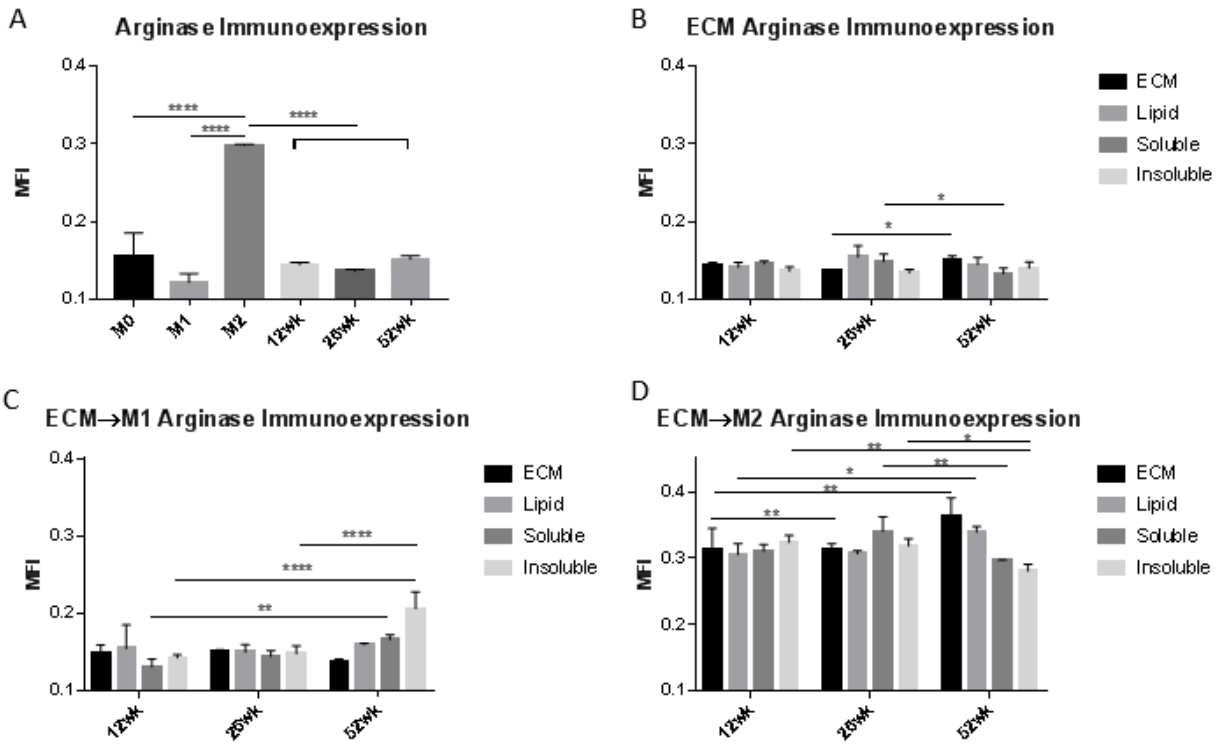
Figure 23: Antibody labeling of macrophages treated with ECM extracts for arginase.

Macrophages were treated with polarizing cytokines (A), ECM alone (B), ECM then M1 cytokines (C), or ECM then M2 cytokines (D). Macrophages were then fixed and stained for arginase immunoexpression using indirect fluorescent antibody labeling and mean fluorescence intensity was calculated. Data shown as mean ± S.D. Statistical significance reported as $*p<0.05$, $**p<0.01$, $***p<0.001$, $****p<0.0001$.

3.3.3 Phagocytosis

Interleukin-4 stimulation of macrophages promoted a reduction in phagocytosis as expected (Figure 24A). ECM degradation products from 12 and 26 week SIS also promoted a significant decrease in phagocytosis from M0 and M1 controls to similar levels as M2 controls. Fifty two week SIS further reduced phagocytosis from 12 and 26 week SIS (Figure 24A). With basal ECM

extract treatment, whole and insoluble 52 week SIS extracts promoted less phagocytosis while soluble extracts promoted more (Figure 24B). With pro-inflammatory stimulus, both whole and urea insoluble fractions from 52 week SIS reduced phagocytosis compared to 12 week SIS. Soluble fraction with M1 cytokines promoted higher phagocytosis with 52 week SIS over 26 week SIS (Figure 24C). With IL-4 stimulation, whole and insoluble fractions from 52 week SIS again reduced phagocytosis while soluble fractions increased it (Figure 24D).
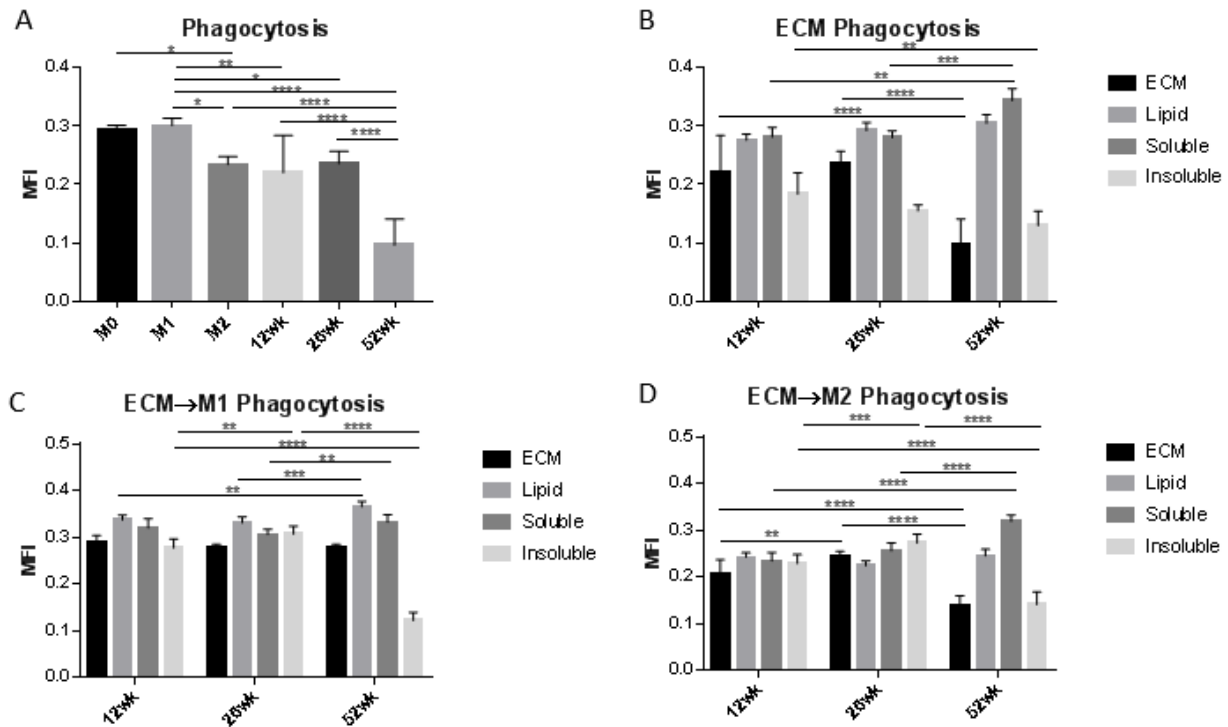
Figure 24: Phagocytic function of macrophages treated with ECM extracts.

Macrophages were treated with polarizing cytokines (A), ECM alone (B), ECM then M1 cytokines (C), or ECM then M2 cytokines (D). Macrophages were then incubated with FITC-labeled E. Coli beads and then fixed and counterstained with DAPI and mean fluorescence intensity was calculated. Data shown as mean ± S.D. Statistical significance reported as *p<0.05, **p<0.01, ***p<0.001, ****p<0.0001.

3.3.4 Nitric oxide production

Pro-inflammatory (M1) macrophages produced significantly higher levels of nitric oxide than M0 and M1 controls. ECM degradation products from 52 week old SIS promoted higher levels of nitric oxide production than 12 week SIS (Figure 25A). With basal ECM extract treatment, there was no substantial nitric oxide production from any 12 or 26 week old SIS. Whole, soluble and insoluble SIS from 52 week old pigs all promoted higher levels of nitric oxide (Figure 25B). With pro-inflammatory cytokine stimulus, 52 week old whole, soluble and insoluble fractions promoted less nitric oxide production (Figure 25C). With IL-4 stimulation, soluble and insoluble fractions from 52 week SIS promoted more nitric oxide production (Figure 25D).
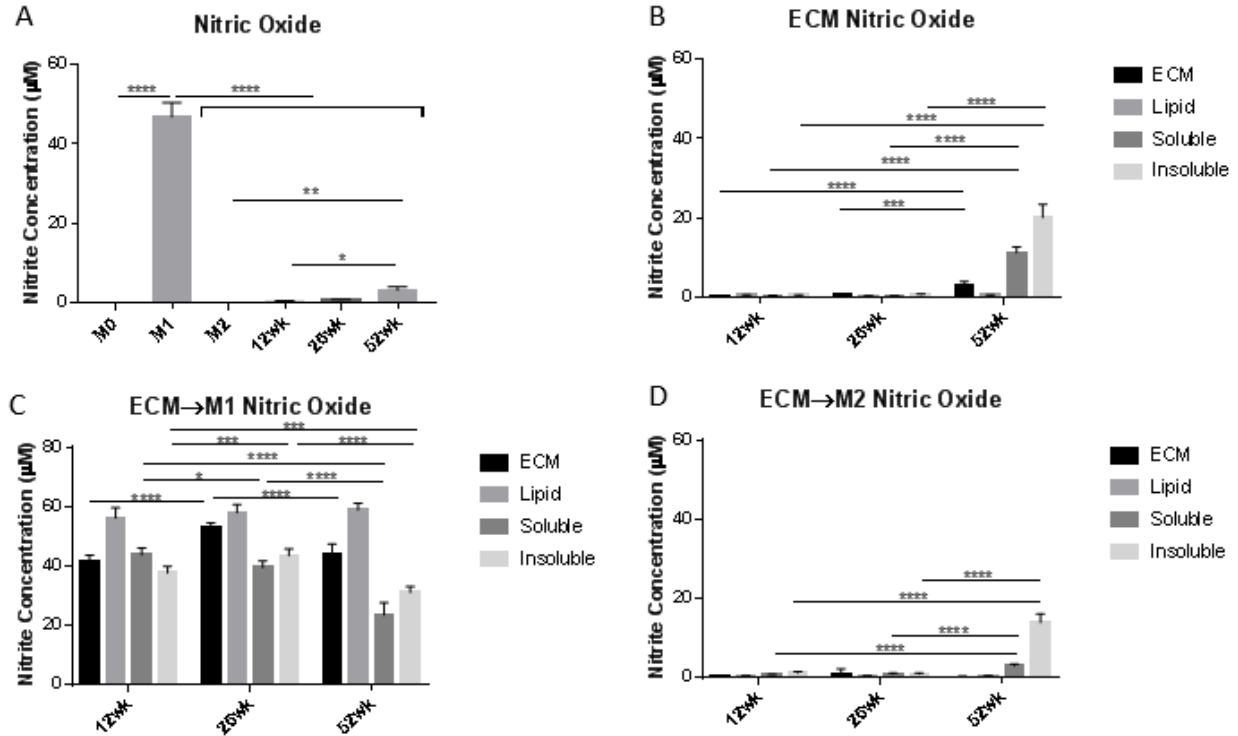
Figure 25: Nitric oxide production from macrophages treated with ECM extracts.

Macrophages were treated with polarizing cytokines (A), ECM alone (B), ECM then M1 cytokines (C), or ECM then M2 cytokines (D). Macrophage supernatant was then removed and assayed for nitrite content using the Greiss reagent system. Data shown as mean $\pm$ S.D. Statistical significance reported as $*p<0.05$, $**p<0.01$, $***p<0.001$, $****p<0.0001$.

3.4   DISCUSSION

Analysis of different extracts within small intestine submucosa shows that ECM scaffolds are more than just insoluble matrix proteins. Small intestine submucosa has a substantial lipid content which increases significantly from 26 to 52 weeks. Further analysis of different types of lipids present within SIS and how they change with age would be beneficial to understand how

this composition is contributing to the host response to ECM biomaterials. While our current analysis of the growth factor content in decellularized small intestine submucosa found no significant differences, mass spectrometry analysis has shown significant differences in not only extracellular matrix proteins but also soluble cellular proteins as well [255]. Proteomic and lipidomic analysis of these matrix fractions could reveal more accurately changes in composition and help to understand what pathways may be activated because of them.

3.5   CONCLUSION

There are many different types of biomolecules within extracellular matrix scaffolds despite adequate decellularization. These different classes of biomolecules each affect macrophage polarization and function differently. Further investigation into the composition of these different components will help to understand extracellular matrix scaffolds and how they influence the host response to them. Most dramatic changes were in insoluble fractions of the ECM, suggesting that changes to the structural molecules dictate changes in the macrophage response. Investigation of modification of structural ECM molecules with glycation or oxidation is the most logical explanation for these differences.

3.6   FUTURE DIRECTIONS

The results from Chapter 2 and 3 illustrate how extracellular matrix derived from different aged animals directly affects macrophage polarization and function. These results have important

implication for sourcing of tissues to produce extracellular matrix biomaterials. Because of these implications, previous work was performed using a tissue non-specific and xenogeneic approach, which models clinical use of extracellular matrix biomaterials. The direct effects of source animal age upon macrophage polarization and function have implications for aging biology. In order to test similar questions with aging biology relevance, our approach changed to using extracellular matrix in a tissue-specific and allogeneic experimental design. In this way, we would be able to investigate whether the natural changes in the extracellular matrix with aging would be sufficient to alter the regenerative capacity of an otherwise healthy, young tissue. This forms the central basis for the hypotheses formed for this dissertation work.

4.0   HYPOTHESIS AND SPECIFIC AIMS

The central hypothesis for the following work is that aged muscle extracellular matrix (1) directly impacts the host response through altered macrophage activation and polarization and (2) that these changes are due to accumulation of advanced glycation end-products within the aged extracellular matrix.

4.1   SPECIFIC AIM 1: TO DETERMINE THE EFFECT OF AGED SKELETAL MUSCLE EXTRACELLULAR MATRIX UPON MACROPHAGE POLARIZATION AND FUNCTION

Hypothesis: Aged muscle extracellular matrix induces an increased pro-inflammatory macrophage response.

Rationale: Previous studies have shown that aged muscle experiences increased pro-inflammatory responses during injury [47]. Chronic inflammation has been well characterized in elderly individuals [256]. This chronic inflammation has also been associated with the declining muscle mass and strength in sarcopenia [257].

4.2   SPECIFIC AIM 2: TO DETERMINE THE EFFECT OF GLYCATION UPON THE MACROPHAGE RESPONSE TO MUSCLE ECM

Hypothesis: Glycation of muscle ECM promotes an enhanced pro-inflammatory macrophage phenotype.

Rationale: Advanced glycation end-products are known to signal through RAGE [177]. This receptor signals through the NF-κB transcription factor which mediates pro-inflammatory cytokine expression [258]. Macrophages express the RAGE receptor and have been shown to respond to AGEs with increased pro-inflammatory responses [194].

4.3   SPECIFIC AIM 3: TO DETERMINE THE EFFECT OF AGED AND GLYCATED ECM UPON THE HOST RESPONSE FOLLOWING MUSCLE INJURY

Hypothesis: Aging and glycation of muscle ECM enhances pro-inflammatory macrophage response and impairs healing in a model of muscle injury.

Rationale: Muscle regeneration is impaired in aged individuals [37]. Following exercise, the number of pro- and anti-inflammatory macrophages increased in young individuals but not in old [47]. Previous studies have shown aged small intestine submucosa created an increased pro-inflammatory response and increased collagen deposition [176].

5.0 EFFECT OF AGED SKELETAL MUSCLE ECM UPON MACROPHAGE POLARIZATION AND FUNCTION

5.1 INTRODUCTION

Extracellular matrix acts as the supporting structure of a tissue and dynamically changes in a reciprocal relationship with cells of that tissue. ECM changes with aging and disease and can affect the responses of cells in these altered states. Therefore, ECM can be used as a model for aged microenvironments to more fully understand their effect on cellular function. Skeletal muscle strength and healing potential are known to decrease with aging [232]. The immune response, which is integral to muscle regeneration, is also dysfunctional with age [259]. Macrophage polarization in particular has been shown to be necessary for appropriate skeletal muscle healing [51]. There has been no direct investigation to determine whether age-related changes in skeletal muscle extracellular matrix influence macrophage polarization and contribute to altered host responses observed in aged individuals during skeletal muscle injury.

Decellularization techniques have been used for decades now to develop biomaterials for a variety of surgical and tissue engineering strategies [260]. These same methodologies can be used to harvest the extracellular matrix from skeletal muscle of animals differing in age or disease state in order to understand how these factors contribute to altered physiology [261]. Previous investigations into changes in aging's effect on skeletal muscle ECM has relied on

histologic analysis of intact muscle tissue only [262]. Therefore, in order to isolate the role of extracellular matrix in altered host responses during injury, bioengineering techniques must be utilized to separate the ECM from the rest of the skeletal muscle tissue.

The present study seeks to combine several bioengineering strategies to study the isolated effects of aging and glycation of the extracellular matrix upon the macrophage response *in vitro*. While many studies focus on cellular dysfunction during aging, this study seeks to understand the isolated role of alterations in the extracellular microenvironment.

5.2   METHODS

5.2.1   Skeletal muscle extracellular matrix preparation

Skeletal muscle extracellular matrix was prepared using modified methods previously developed [261]. Briefly, abdominal muscle was harvested from 4 month and 18 month old C57BL6/J mice (NIA). Muscle was washed in water. Samples were enzymatically digested in 0.2% trypsin/0.2% EDTA for 2 hrs at 37 °C with agitation. All subsequent steps were performed on a mechanical shaker at 300 rpm. Samples were washed once in water and twice in 1XPBS, 30 mins each. Samples were decellularized using 2% sodium deoxycholate for 5 hrs, washed in water and twice in 1XPBS for 30 mins each and then decellularized with 2% sodium deoxycholate for 14-16 hrs and 1% Triton X-100 for 1 hr. Samples were washed with type 1 water until no bubbles were detectable, suggesting detergents had been removed. Samples were either treated with 0.1% peracetic acid/4% ethanol for 2 hours. Samples were then washed twice with 1XPBS then twice

with water for 30 mins each. Samples used for implantation were terminally sterilized with ethylene oxide. ECM degradation products were produced using a 1mg/mL pepsin solution in 0.01N HCl under constant stir for 48 hrs to create a 10mg/mL ECM digest.

5.2.2   Skeletal Muscle ECM Characterization

Hydrated native tissue and decellularized scaffolds were fixed in 10% neutral buffered formalin (NBF) and then embedded in paraffin. Sections of these scaffolds were stained separately with hematoxylin & eosin or DAPI to confirm removal of nuclei. Proteinase K digests of native and decellularized scaffolds underwent phenol: chloroform: isoamyl alcohol (25:24:1) extraction for DNA and were resuspended in 1X TE buffer.   DNA extracts were separated using electrophoresis on a 2% agarose gel in 0.5X TBE buffer to confirm reduction of DNA content and fragmentation of remnant DNA in decellularized scaffolds compared to native controls. DNA extracts were also quantified for double-stranded DNA content using a PicoGreen assay (Thermo) according to manufacturer's instructions.

5.2.3   Biochemical Assessment

ECM scaffold biochemistry was performed to assess hydroxyproline and sulfated glycosaminoglycan content. ECM scaffolds were digested at 10mg/mL in a papain solution. Sulfate glycosaminoglycan content was assessed using a dimethylmethylene blue (DMMB) reagent. Hydroxyproline content was assessed by adding 50 μL 2N NaOH to 50 μL papain digests then hydrolyzing at 110 °C for 18 hrs. Samples were neutralized with 5N HCl. One hundred microliters of 0.01M copper sulfate, 2.5N NaOH and 6% H_2O_2 were added. Samples

were incubated at 80 °C for 5 minutes then cooled. Four hundred microliters of 3N sulfuric acid was added followed by 200 µL of 5% DMAB in propanol. Samples were incubated at 70 °C for 15 minutes then the absorbance was read at 540 nm. Advanced glycation end-product (AGE) fluorescence levels were determined by reading the fluorescence intensity of pepsin-digested ECM at excitation of 370nm and emission of 440nm. Protein carbonyl content was quantified using a protein carbonyl quantification kit (Cayman Chemical) according to manufacturer instructions.

Paraffin sections were stained with PicroSirius Red as an indicator of collagen content. Briefly, slides were deparaffinized and rehydrated to water. Slides were stained in PicroSirius Red solution for 1 hour then differentiated in 35% acetic acid for 10 seconds. Slides were quickly dehydrated and cleared in xylenes then mounted with resinous mounting media.

Paraffin sections were stained with Masson's trichrome as an indicator of collagen content. Briefly, slides were deparaffinized and rehydrated to water. Slides were re-fixed in Bouin's solution for 1 hour at 56 °C to improve staining quality. Slides were rinsed in running tap water for 10 minutes to remove the yellow color. Slides were then stained in Weigert's iron hematoxylin working solution for 10 minutes then rinsed in running warm tap water for 10 minutes then washed in distilled water. Slides were stained in Biebrich scarlet-acid fuchsin solution for 10 minutes then washed in distilled water. The stain was differentiated in phosphomolybdic-phosphotungstic acid solution for 10 minutes. Slides were transfered directly to aniline blue solution and stained for 10 minutes then rinsed briefly in distilled water and differentiate in 1% acetic acid solution for 5 minutes then washed in distilled water. Slides were dehydrated very quickly and cleared in xylene then mounted with resinous mounting medium.

5.2.4   Assessment of advanced glycation end product content

Fluorescence AGE levels were assessed by pipetting papain digested ECM into 96 well plates. Fluorescence intensity levels were assessed on a spectrophotometer (BioTek) for several signature AGE wavelengths: excitation = 295 nm emission = 395 nm, excitation = 335 nm emission = 385 nm, excitation = 370 nm emission = 440 nm.

5.2.5   Immunohistochemical staining

Native and decellularized muscle ECM was fixed in 10% NBF then embedded in paraffin wax. Sections were stained using DAB immunohistochemistry for collagen type I, advanced glycation end-products, cysteine sulfonate, S-nitro-cysteine, or 3-nitro-tyrosine. Briefly, paraffin sections were deparaffinized to water then antigen was retrieved using 10mM citric acid pH 6 0.05% Tween20 for 20 mins at 95-100 °C. Slides were washed twice with 1X TBST for 5 mins then twice with 1XPBS for 3 mins. Endogenous peroxidase activity was blocked by incubating slides in 0.3% hydrogen peroxide for 30 mins. Slides were washed 3 times in 1X PBS for 3 minutes. Slides were blocked for non-specific antibody binding with a blocking buffer made of 2% donkey serum/1% bovine serum albumin/0.1% Tween-20 for 1 hour at room temperature. Primary antibodies were incubated overnight at 4 °C diluted in blocking buffer. Slides were washed 3 times for 3 minutes with 1XPBS. Slides were then incubated with biotinylated secondary antibodies diluted in blocking buffer (goat anti-rabbit 1:200 (Vector)). Slides were was again 3 times for 3 minutes with 1XPBS. Slides were incubated with VectaShield ABC Reagent for 30 mins then washed again 3x3mins with 1XPBS. Staining was developed by

incubating sections with 4% DAB. Sections were washed then mounted with resinous mounting media and coverslipped. Slides were images on a brightfield microscope at the same settings.

5.2.6 Bone marrow-derived macrophage isolation

Bone marrow-derived macrophages were harvested from 2 month or 18-20 month-old C57/BL6 mice as previously described [221]. Briefly, femurs and tibiae were harvested and separated from muscle and connective tissue. Bones were cut at either end to expose bone marrow. Sterile syringe and needles were used to flush out bone marrow using macrophage differentiation media (DMEM/10% FBS/10% L-929 Supernatant/1% PenStrep/2% MEM non-essential amino acids/1% HEPES/0.1% 55μM β-2 mercaptoethanol). Bone marrow lysate was reconstituted in media and filtered through a sterile cell filter. Cells were cultured for 7 days in media to differentiate them into macrophages, changing differentiation media every 2 days.

5.2.7 Macrophage Treatment

Following 7 days of differentiation culture as described above, macrophages were treated with acute polarizing regimens to distinguish phenotypes over 24 hours. Naïve macrophage (M0) controls were treated with basal media for 24 hours. M1 (20 ng/mL IFN-γ and 100 ng/mL LPS) and M2 (20 ng/mL IL-4) polarizing cytokines were used to create positive controls for classical pro- and anti-inflammatory macrophages. ECM degradation products were neutralized and diluted to 1000 μg/mL in macrophage media to isolate biochemical effects of degradation products and prevent structural moieties from forming. Pepsin buffer (1 mg/mL pepsin in 0.01 M HCl) diluted in macrophage media was used as a control. Another set of treatment groups

involved 24-hour exposure of ECM degradation products followed by 24-hour treatment with either the M1 or M2 treatment regimen.

5.2.8   Indirect Immunofluorescent Antibody Labeling

Cells were fixed with 2% paraformaldehyde (PFA) for 30 minutes then washed in 1XPBS. Cells were incubated in blocking buffer (2% donkey serum, 1% bovine serum albumin (BSA), 0.1% Triton X-100, 0.1% Tween-20) for 1 hour at room temperature. Primary antibodies were diluted in this blocking buffer as follows and incubated overnight at 4 °C: iNOS (1:100, Abcam 3523) or Arginase-1 (1:200, Abcam 91279).   iNOS is a classical M1 macrophage marker whereas Arginase-1 is a classical M2 macrophage marker. Cells were washed in 1XPBS then incubated in the appropriate fluorescently-labeled secondary antibody solution in blocking buffer for 1 hour at room temperature (donkey anti-rat Alexa Fluor 488, Invitrogen, 1:200; donkey anti-rabbit Alexa Fluor 488, Invitrogen, 1:300). Cell nuclei were counterstained with DAPI. Cells from 2 month old mice were imaged nine times in the center of each well at 10X magnification using automated position capture function to remove bias from subjective image location acquisition. All imaging was performed on an Axio observer T1 microscope. Mean fluorescence intensity of cells was analyzed using Cell Profiler software (Broad Institute). Briefly, DAPI images were used by the program to identify cell nuclei then FITC images were used to identify cell borders around the identified nuclei. The mean fluorescent intensity was calculated by averaging the pixel intensities (scale of 0 to 1) across the entire cell area. Mean fluorescence intensity values were averaged for all imaged cells in each well.

5.2.9   Taqman gene expression assay

Following treatments, macrophages (n=5 biological replicates from 5 young (2 month) and 5 aged (18 month) mice) were harvested for RNA using Qiagen RNEasy MiniPrep RNA Isolation Columns following standard protocol.   RNA was quantified using a NanoDrop Lite Spectrophotometer (Thermo). cDNA templates were created from 1 µg of RNA using Invitrogen High Capacity RNA-to-cDNA kits (Thermo). Taqman Gene Expression Assays (Thermo) were performed for the following commonly reported M1 and M2 macrophage genes: Nos2 (Mm00440502_m1), IL1b (Mm00434228_m1), IL12b (Mm01288989_m1), TNFa (Mm00443258_m1), MHC-II (Mm01181326_m1), Arg (Mm00475988_m1), Retlna (Fizz1) (Mm00445109_m1), Mrc1 (Mm01329362_m1), IL10 (Mm01288386_m1), and PPARg (Mm00440940_m1).

5.2.10 Phagocytosis Assay

Following treatments, 50 µL of supernatant from macrophages were transferred into a fresh plate.   Nitrite content was assayed using a Greiss Reagent system.   Briefly, 50 µL of sulfanilamide (1% in 5% phosphoric acid) was added to supernatants for 10 minutes. Then, 50 µL of 0.1% N-1-napthylethylenediamine in water was added to the mixture for an additional 10 minutes.   The absorbance at 540 nm was measured using a BioTek SYNERGY HTX spectrophotometer.

5.2.11 Nitric oxide assay

Following treatments, 50 µL of supernatant from macrophages were transferred into a fresh plate. Nitrite content was assayed using a Greiss Reagent system. Briefly, 50 µL of sulfanilamide (1% in 5% phosphoric acid) was added to supernatants for 10 minutes. Then, 50 µL of 0.1% N-1-napthylethylenediamine in water was added to the mixture for an additional 10 minutes. The absorbance at 540 nm was measured using a BioTek SYNERGY HTX spectrophotometer.

5.2.12 Arginase Activity Assay

Following treatments, media was removed and macrophages were lysed in 50µL 0.001% Triton X-100 in type 1 H_2O with 1X Halt Protease Inhibitors (Thermo). Twenty five microliters of lysate was added to 25 µL of arginase activation solution (10mM $MnCl_2$/50mM Tris-HCl, pH7.5) and incubated at 55°C for 10 minutes. Samples were allowed to cool and then 50 µL of arginine substrate solution (0.5M L-arginine pH 9.7) was added to each well. Samples were incubated at 37°C for 2 hours. A urea standard curve was created via 2 fold serial dilution from 100 mg/mL to 1.5625 mg/mL with a 0 mg/mL blank in lysis buffer. Five microliters of samples or standards were added to a new 96-well plate and 200 µL of urea detection solution (513 mg/L primaquine, 100 mg/L phthalaldehyde, 2.5 mol/L sulfuric acid, 2.5 g/L boric acid, 0.03% Brij35) was added to each well. Absorbance of samples was analyzed using a plate spectrophotometer at 430 nm between 5-20 minutes following addition of detection solution.

5.3   RESULTS

5.3.1   Muscle ECM Decellularization Characterization

Native and decellularized muscle ECM were characterized using hematoxylin & eosin staining (Figure 26). Histological assessment showed that skeletal muscle ECM had no presence of cellular constituents from muscle fibers and that nuclei were removed.
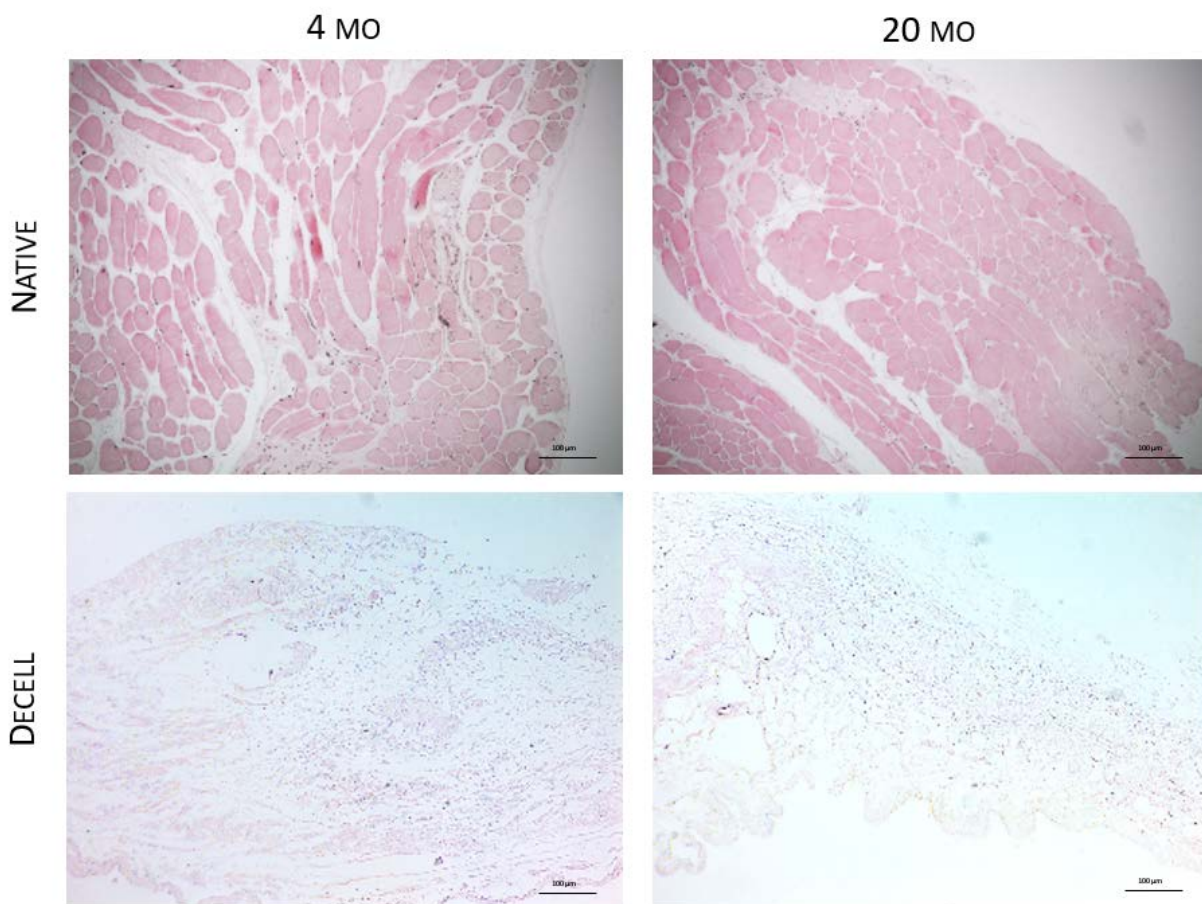
Figure 26: Hematoxylin & eosin staining of young and aged skeletal muscle and muscle ECM.
Images taken at 10X magnification. Scale bars indicate 100 µm.

Nuclear removal was confirmed with fluorescent DAPI staining of nuclei showing that skeletal muscle decellularization was effective (Figure 27).
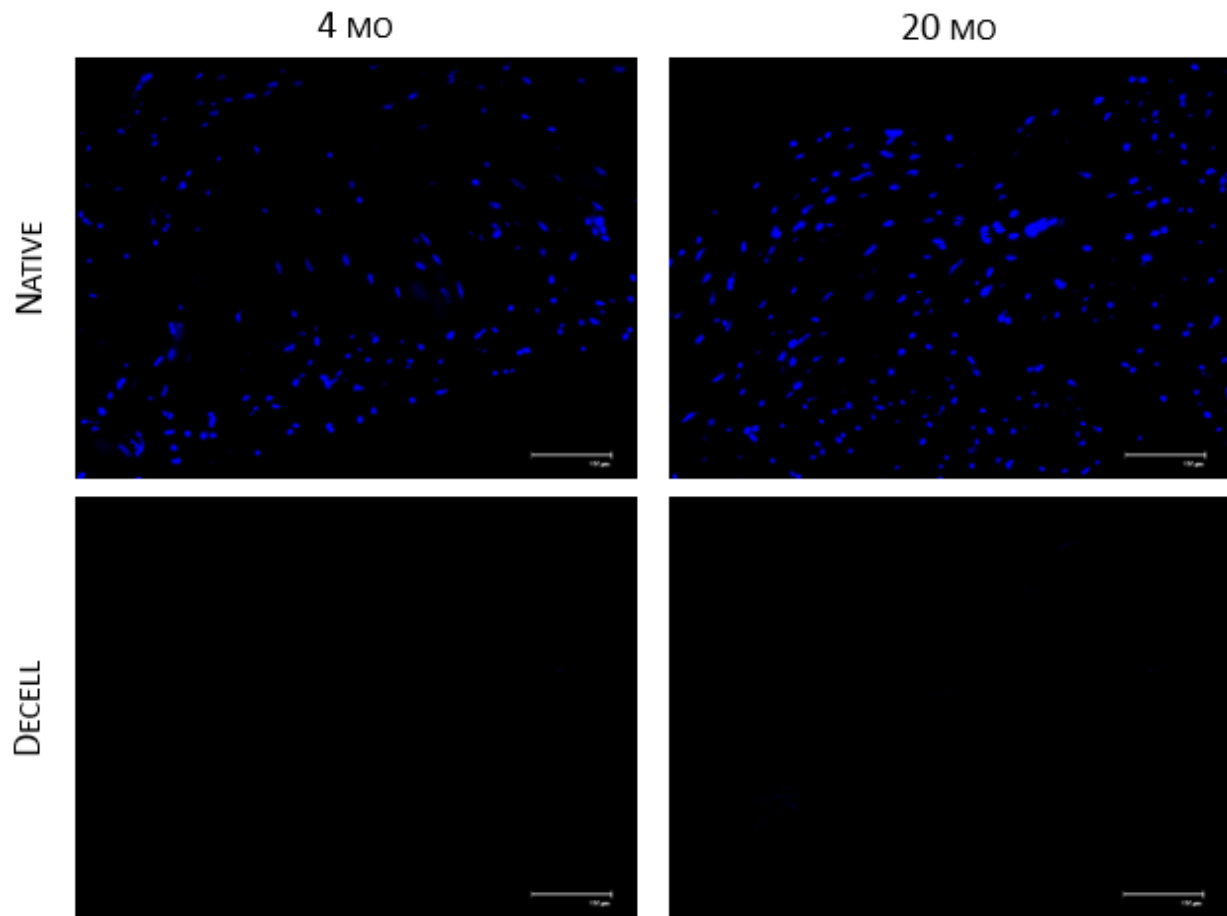
Figure 27: DAPI fluorescent imaging of native and decellularized skeletal muscle.

Images taken at 20X magnification. Scale bars indicate 100 µm.

DNA agarose gel electrophoresis confirmed that there was minimal remnant DNA and that any DNA was largely fragmented (Figure 28A). PicoGreen quantification of double stranded DNA confirmed a significant portion of DNA was removed from decellularized tissues (Figure 28B).
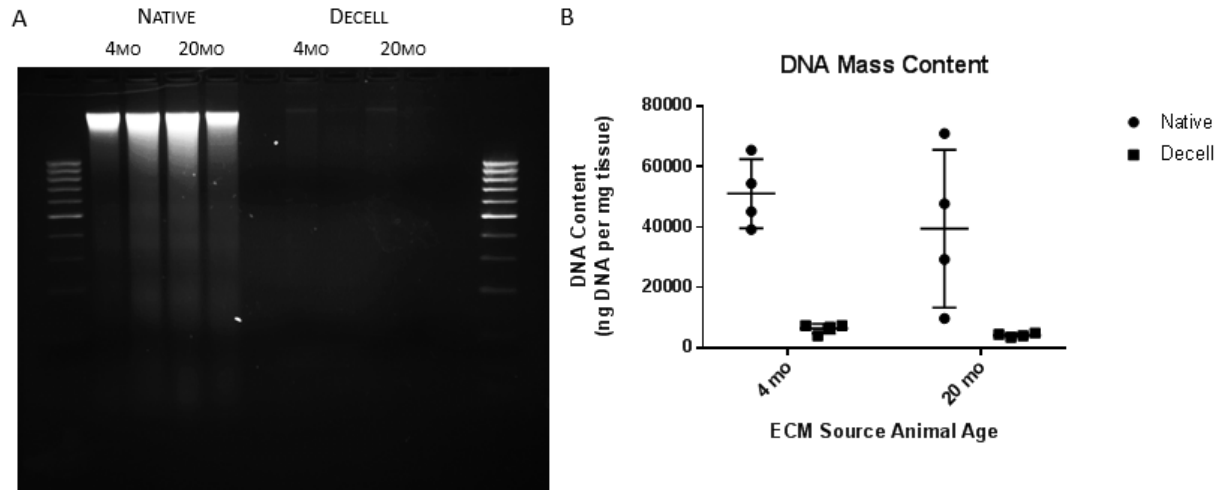
Figure 28: DNA gel electrophoresis (A) and PicoGreen dsDNA quantification (B) of muscle ECM.

Data shown as mean ± S.D. Statistical significance reported as *p<0.05, **p<0.01, ***p<0.001, ****p<0.0001.

5.3.2 Muscle ECM Biochemical Characterization

Sulfated glycosaminoglycan content was assessed via DMMB assay. Results showed there were no significant differences in sulfated glycosaminoglycan content in either native or decellularized skeletal muscle (Figure 29A). Assessment of hydroxyproline content suggested there were no significant differences in hydroxyproline content in native skeletal muscle. Following decellularization, young skeletal muscle ECM was assessed to have more hydroxyproline content than old skeletal muscle ECM (Figure 29B).
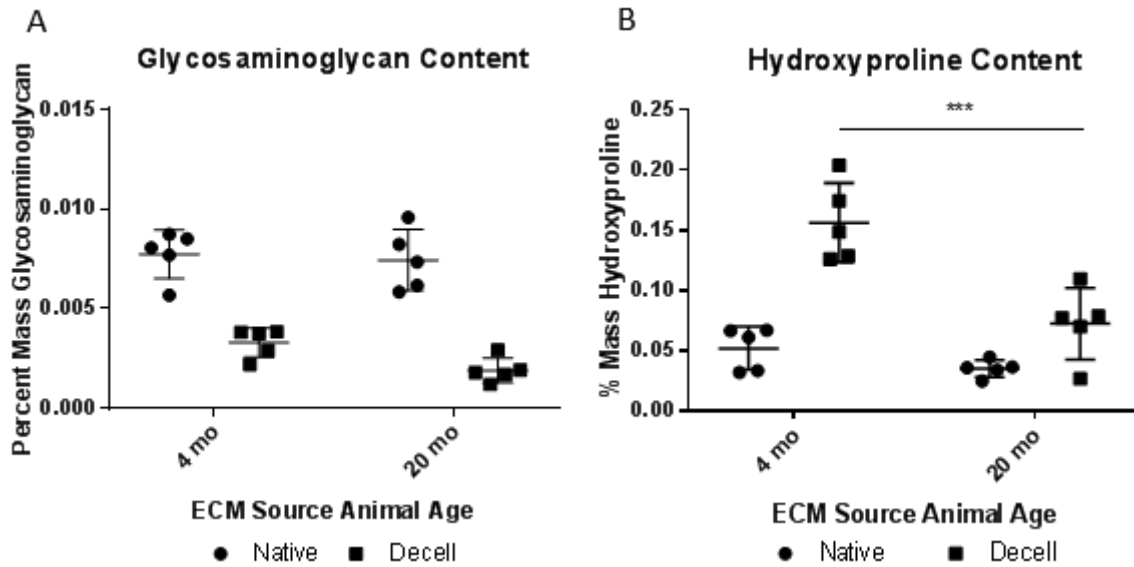
Figure 29: DMMB sulfated GAG (A) and hydroxyproline quantification (B) of muscle ECM.

Data shown as mean ± S.D. Statistical significance reported as *p<0.05, **p<0.01, ***p<0.001, ****p<0.0001.

Assessment of free fatty acid content showed there was significantly less free fatty acid content in aged skeletal muscle. This is counterintuitive to reports which have shown that there is increased fatty acid content in the plasma of aged mice [263]. This reduction in fatty acid content may be explained by greater incorporation into triglycerides due to reduced levels of hormone-sensitive lipase which degrades triglycerides into free fatty acids [264]. Upon decellularization, there was a significant reduction in free fatty acid content. There was also no significant difference in free fatty acid content between young and aged skeletal muscle ECM (Figure 30).
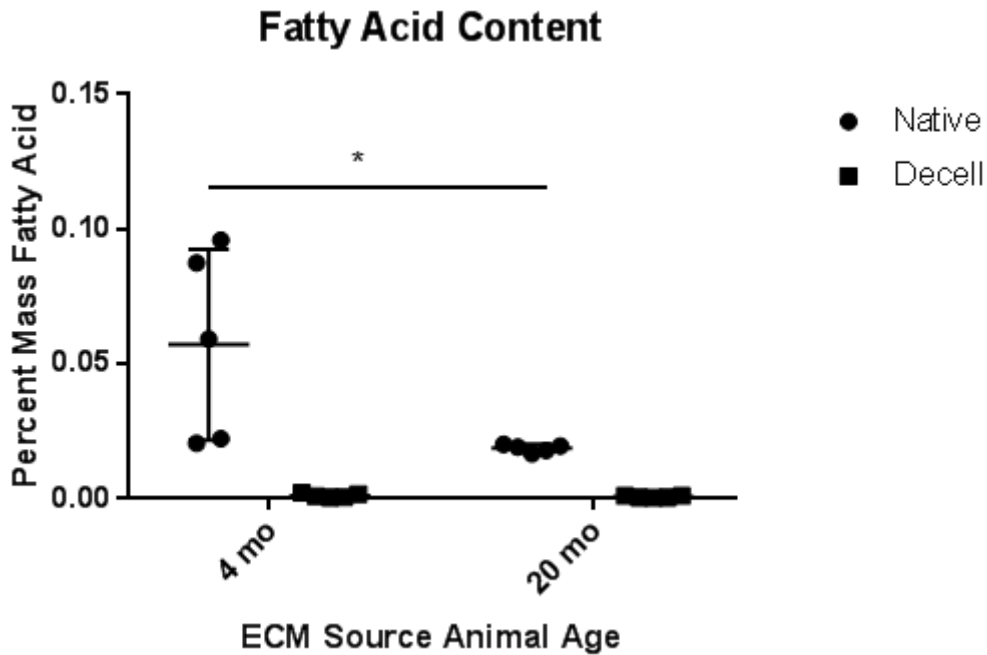
Figure 30: Free fatty acid quantification from lipid extracts of skeletal muscle ECM.

Data shown as mean ± S.D. Statistical significance reported as *p<0.05, **p<0.01, ***p<0.001, ****p<0.0001.

Advanced glycation end-product (AGE) content was assessed by measuring characteristic fluorescence signatures for AGEs in pepsin-digested ECM (ex 370nm em 440nm). Fluorescence levels were similar in native samples but reduced in decellularized ECM (Figure 31A). Fluorescent AGEs are a subset of AGEs and further work is necessary to determine if they are affected by decellularization processes. Quantification of AGE content by ELISA did not reveal any differences in AGE content in muscle ECM with age (Figure 31B).
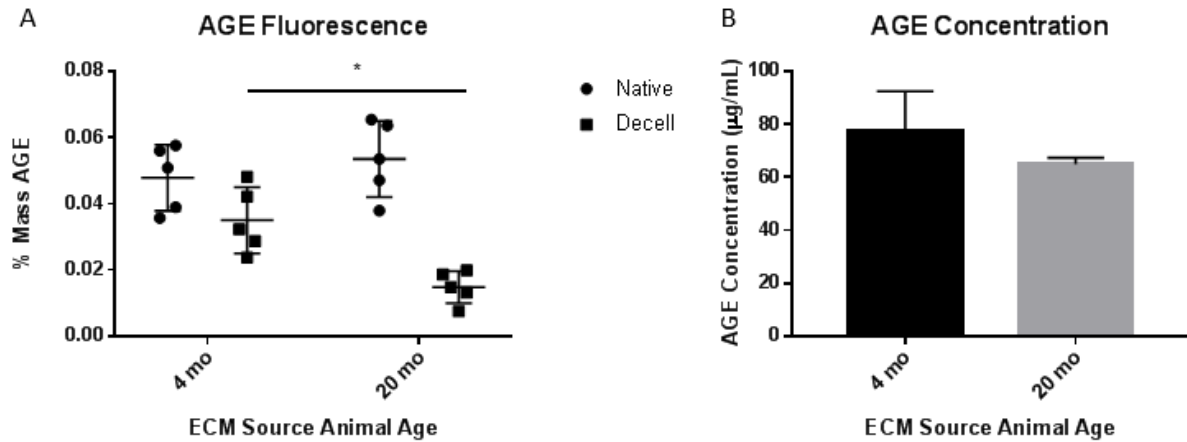
Figure 31: Fluorescence level for AGEs in skeletal muscle and muscle ECM.

Data shown as mean ± S.D. Statistical significance reported as *p<0.05, **p<0.01, ***p<0.001, ****p<0.0001.

In order to determine the level of protein oxidation in young and aged skeletal muscle ECM, a DNPH protein carbonyl quantification was performed. There was no difference in protein carbonyl content in native skeletal muscle. Upon decellularization, it was determined that there was significantly higher protein carbonyl content in young skeletal muscle ECM than in aged (Figure 32). This suggests there is not an accumulation of protein oxidation with aging in skeletal muscle ECM. It could be possible that decellularization procedures affect this biological phenomenon but that has yet to be tested.
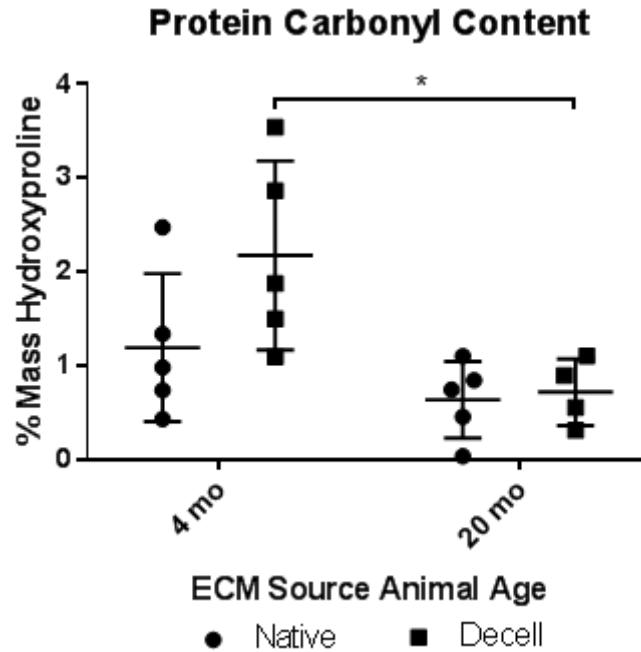
Figure 32: DNPH protein carbonyl quantification on skeletal muscle and muscle ECM.

Data shown as mean ± S.D. Statistical significance reported as *p<0.05, **p<0.01, ***p<0.001, ****p<0.0001.

To confirm differences in hydroxyproline content, paraffin sections were stained with PicroSirius Red and Masson's trichrome. PicroSirius Red staining showed increased staining levels in young skeletal muscle ECM compared to old (Figure 33). This suggests there is reduced collagen content in aged skeletal muscle ECM.
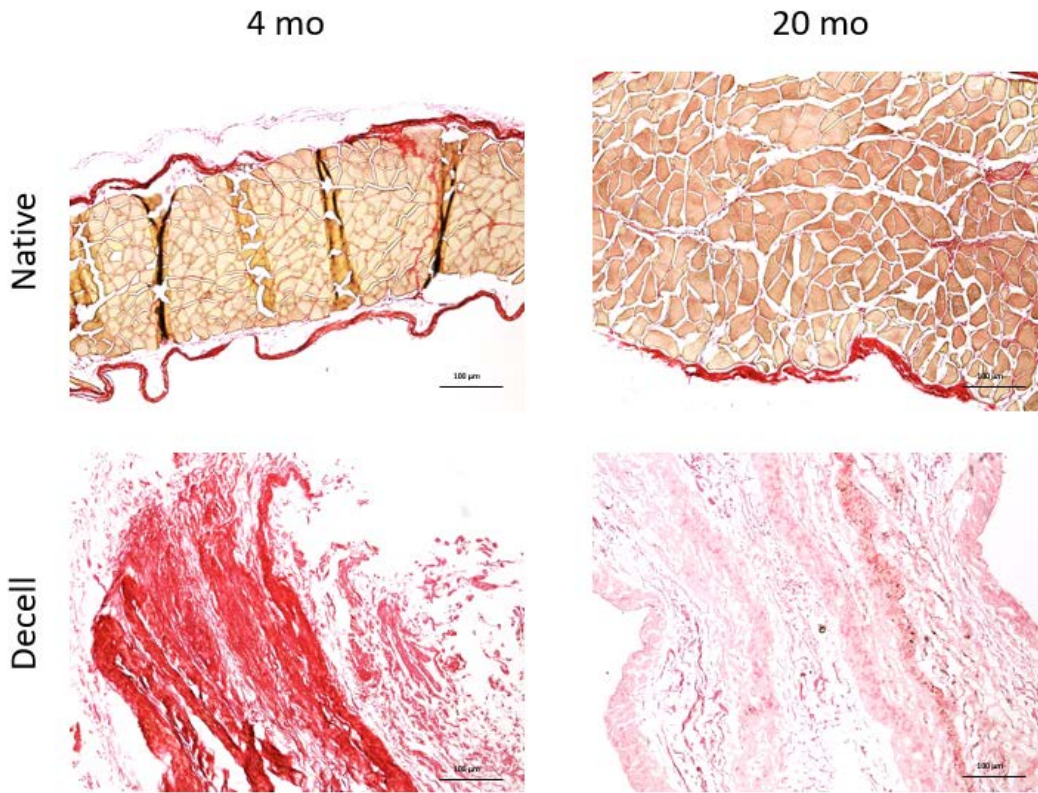
Figure 33: PicroSirius Red staining of young and old native and decellularized skeletal muscle.
Images taken at 10X magnification. Scale bars indicate 100 µm.

Masson's trichrome staining also showed elevated levels of collagen staining in young skeletal muscle ECM (Figure 34). In native sections, collagen staining localized to the external regions surrounding the abdominal muscle.
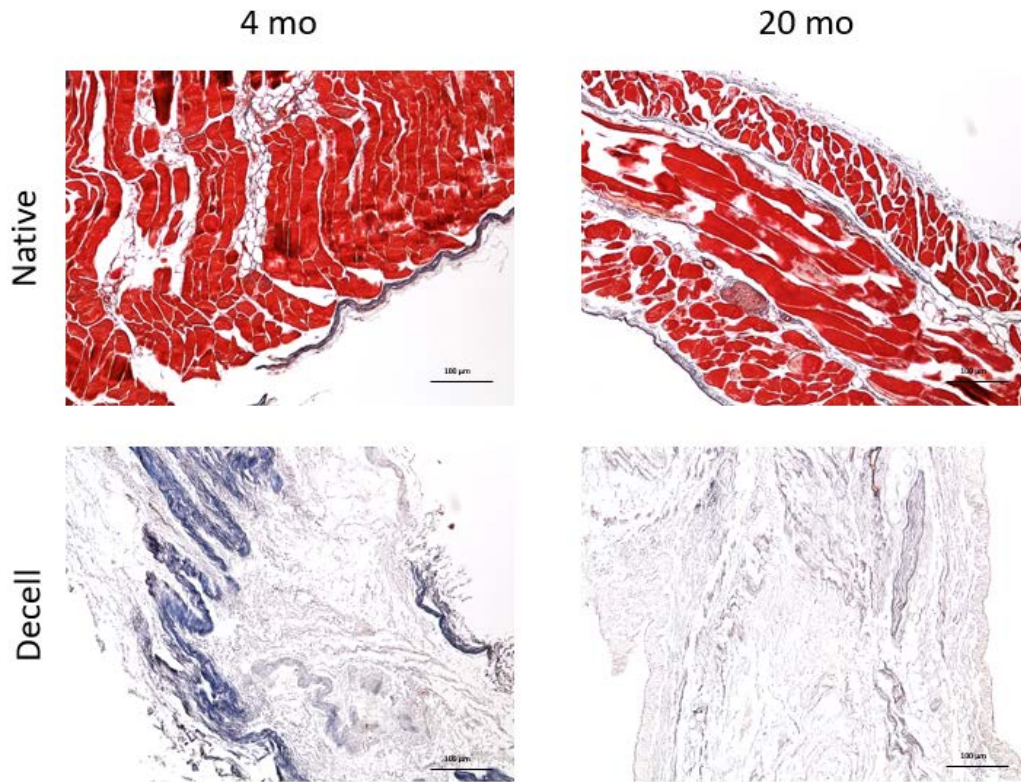
Figure 34: Masson's trichrome stains of young and old native and decellularized skeletal muscle. Images taken at 10X magnification. Scale bars indicate 100 µm.

Collagen content was confirmed further through immunohistochemical staining for collagen type I. Collagen I IHC also showed reduced levels of collagen in skeletal muscle ECM (Figure 35). No differences in collagen I immunohistochemical staining was detected in native skeletal muscle by visual inspection.
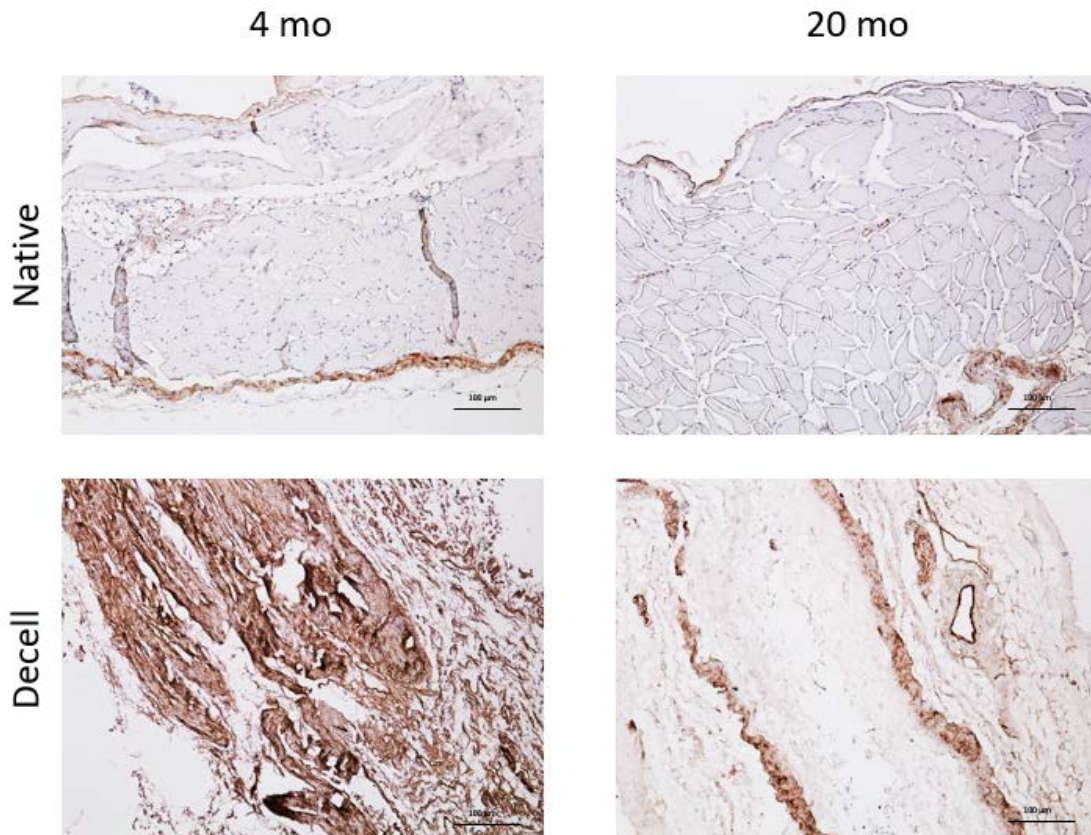
Figure 35: Collagen I immunohistochemistry staining of native and decellularized skeletal muscle.
Images taken at 10X magnification. Scale bars indicate 100 µm.

Advanced glycation end-product content was further assessed via immunohistochemistry staining for AGEs. The antibody used for immunohistochemistry was raised against bovine serum albumin (BSA) artificially glycated with glyoxal (Abcam). Immunohistochemical staining for AGEs revealed an increase in staining in aged skeletal muscle (Figure 36). Upon decellularization, skeletal muscle ECM did not show any substantial staining for AGEs.
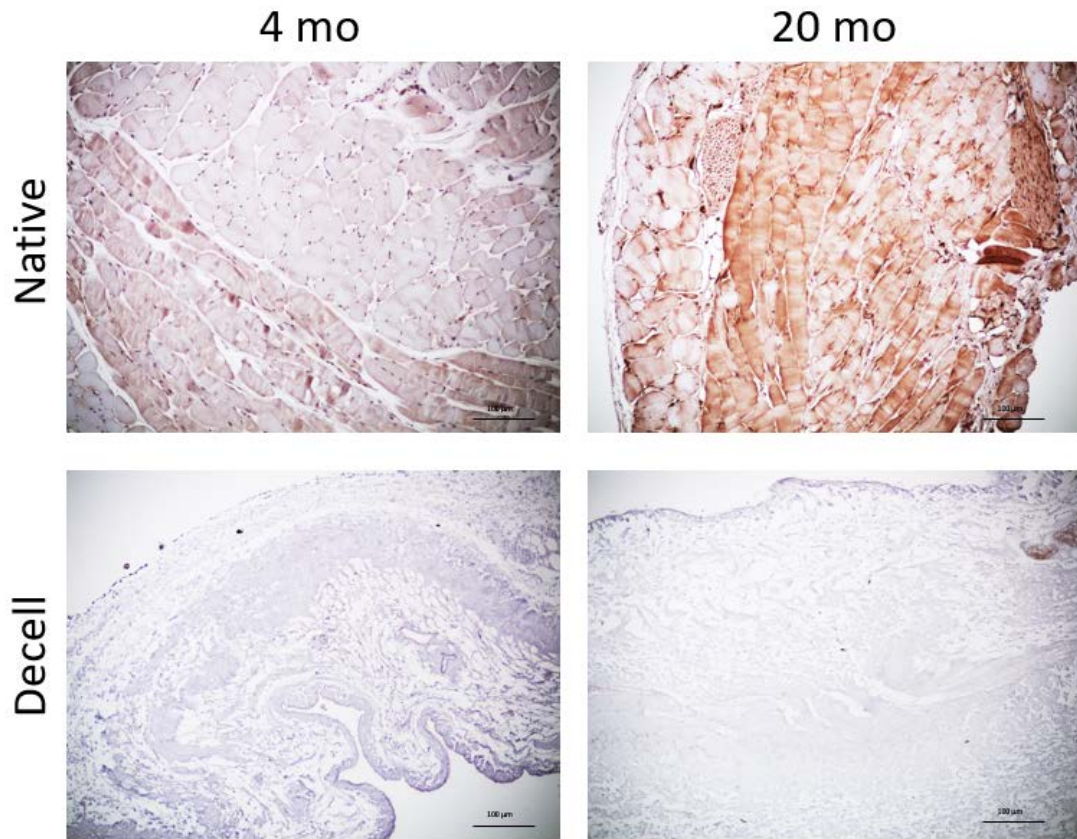
Figure 36: Immunohistochemical staining for advanced glycation end-products.

Images taken at 10X magnification. Scale bars indicate 100 µm.

Paraffin sections were also stained for a specific advanced glycation end product, carboxymethyl lysine (CML), via immunohistochemistry. There may have been slightly more CML staining in young skeletal muscle. Young muscle ECM had higher levels of staining for CML than old ECM (Figure 37). However, further quantitative assessment via ELISA would be necessary to be conclusive.
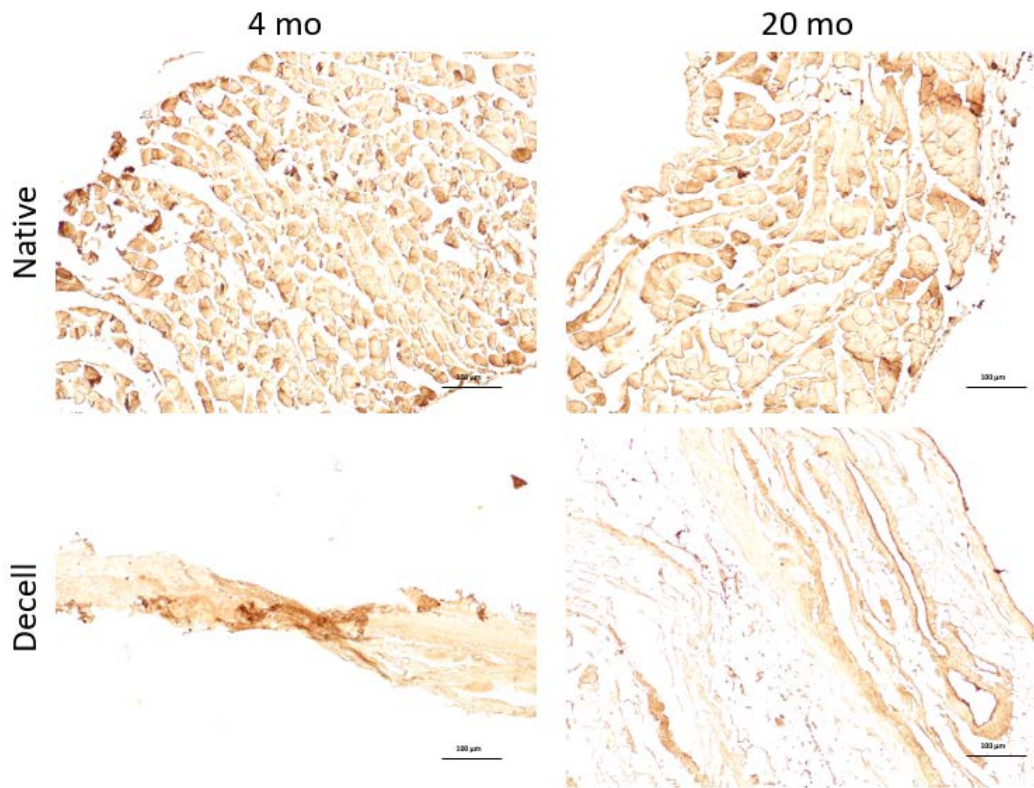
Figure 37: Immunohistochemical staining for carboxymethyllysine of skeletal muscle ECM.

Images taken at 10X magnification. Scale bars indicate 100 µm.

Levels of protein oxidation were assessed by immunohistochemistry staining for cysteine sulfonate. Aged muscle fibers had higher levels of IHC staining for cysteine sulfonate than young muscle fibers, suggesting more protein oxidation (Figure 38). Skeletal muscle ECM did not exhibit noticeable changes in cysteine sulfonate IHC staining.
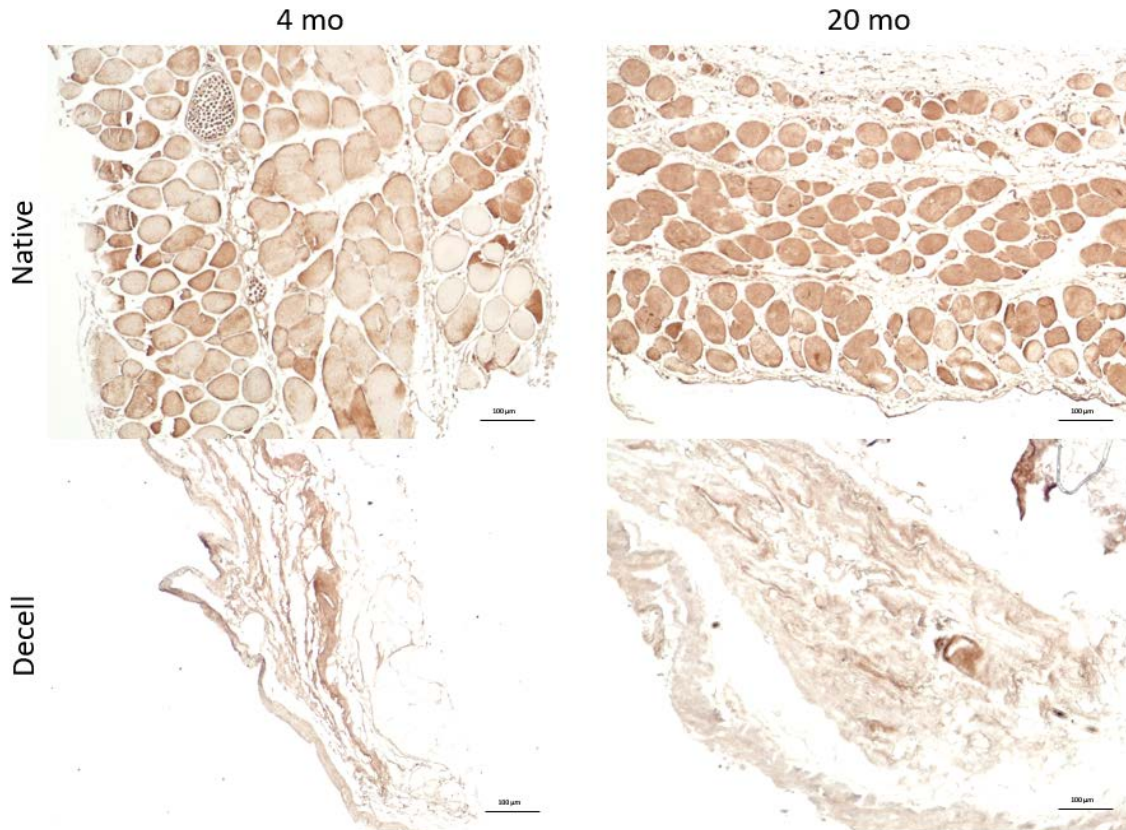
Figure 38: Cysteine sulfonate IHC staining of native and decellularized skeletal muscle.

Images taken at 10X magnification. Scale bars indicate 100 µm.

To assess levels of protein nitration, immunohistochemical staining for S-nitro-cysteine was performed. There were no observable differences in S-nitro-cysteine staining in native skeletal muscle with aging (Figure 39). There appeared to be higher levels of S-nitro-cysteine IHC staining in aged skeletal muscle ECM. Quantification via ELISA would be necessary to confirm.
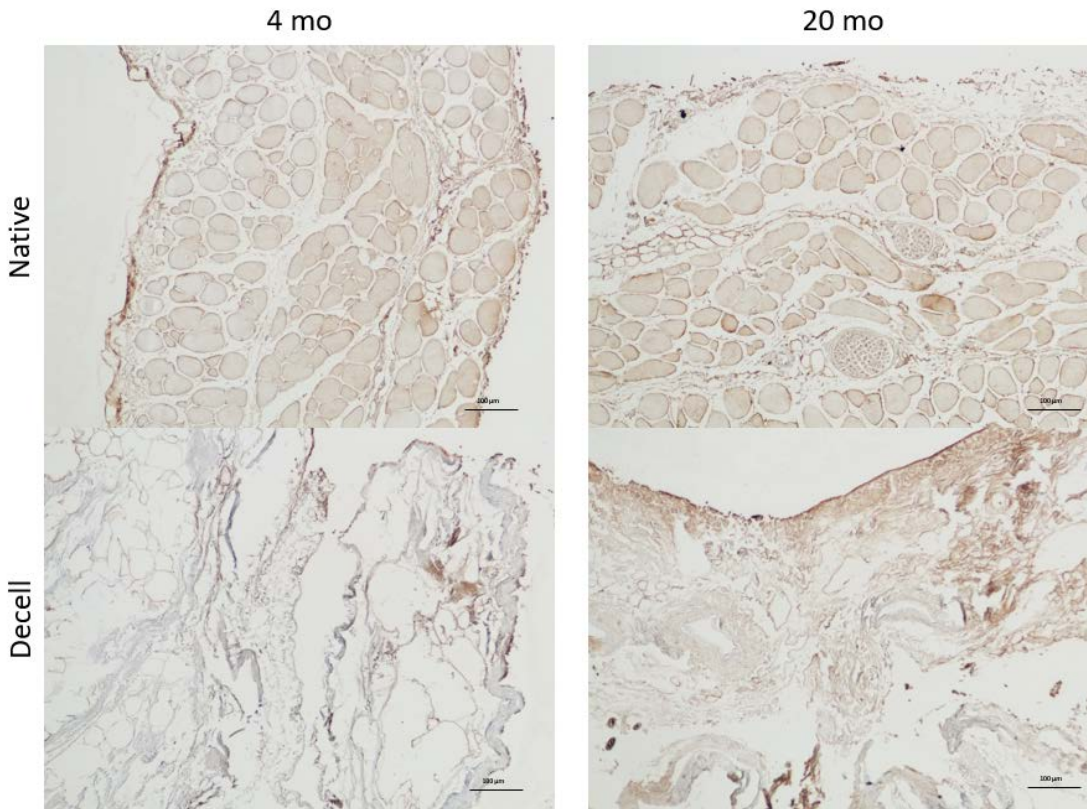
Figure 39: S-nitrocysteine IHC staining of native and decellularized skeletal muscle.

Images taken at 10X magnification. Scale bars indicate 100 µm.

Another marker of protein nitration, 3-nitro-tyrosine (3-NT), was assessed via immunohistochemical staining. Native skeletal muscle stained positive for 3-NT. However, there was no substantial difference in staining for 3-NT with aging. Decellularized skeletal muscle ECM did not have substantial staining for 3-NT; however, aged skeletal muscle ECM stained positive around blood vessels (Figure 40).
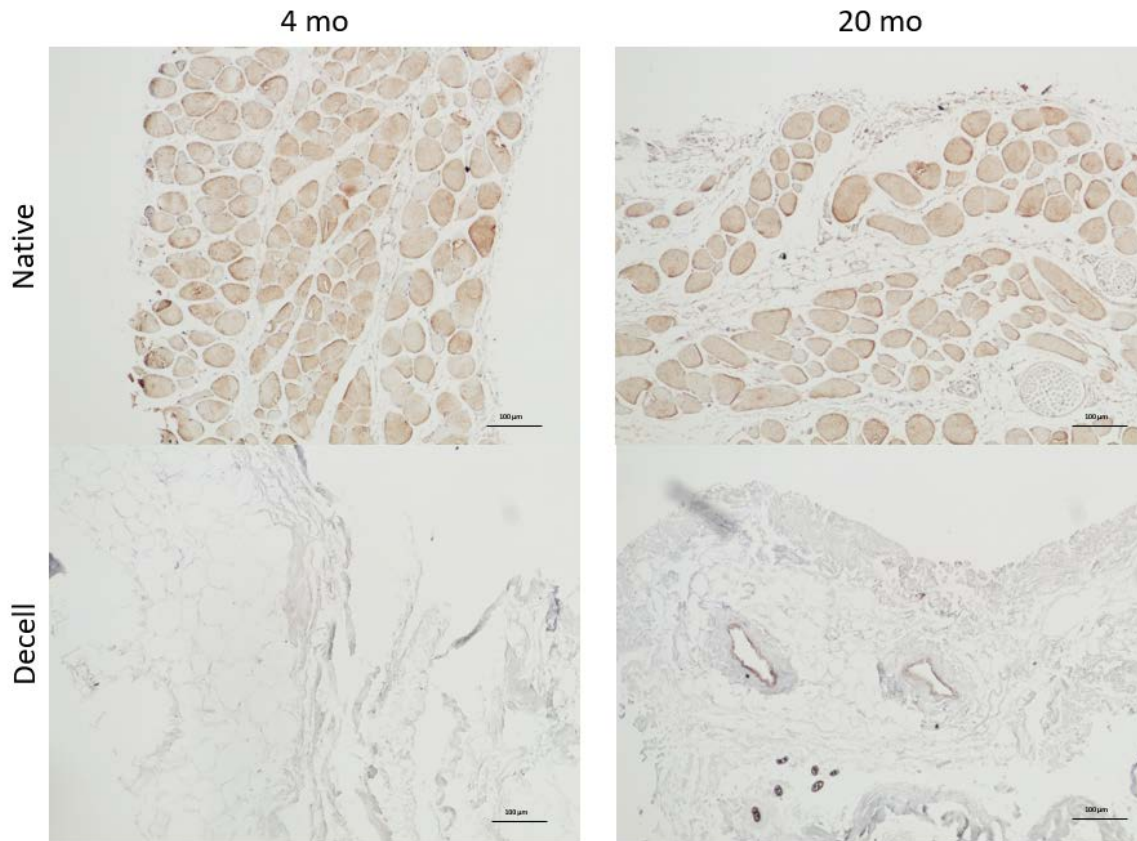
Figure 40: 3-nitro-tyrosine IHC staining of native and decellularized skeletal muscle.

Images taken at 10X magnification. Scale bars indicate 100 µm.

5.3.3 Bone marrow macrophage treatment with skeletal muscle ECM

To assess the effects of skeletal muscle ECM aging upon macrophage polarization, murine bone marrow derived macrophages were treated with pepsin-digested skeletal muscle extracellular matrix. Pro-inflammatory (M1) macrophage phenotype was assessed via immunofluorescence antibody labeling for iNOS. Aged skeletal muscle ECM promoted a higher iNOS immunolabeling than young muscle ECM (Figure 41). Both young and aged skeletal muscle ECM promoted enhanced iNOS immunolabeling with IFN-γ/LPS stimulus over M1 controls

(IFN-γ/LPS alone). However, there were no differences between young and aged skeletal muscle ECM with either M1 or M2 stimulus.
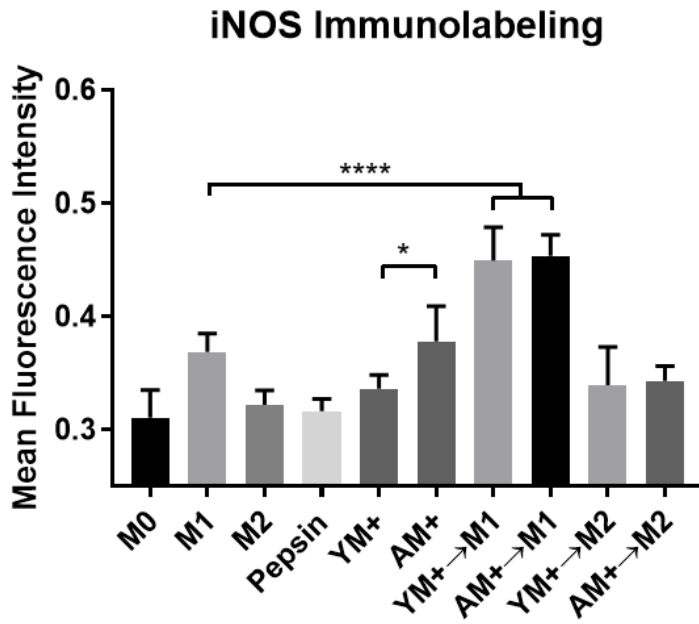
Figure 41: Immunofluorescence staining of macrophages treated with muscle ECM for iNOS.

Data shown as mean ± S.D. Statistical significance reported as *p<0.05, **p<0.01, ***p<0.001, ****p<0.0001.

To assess anti-inflammatory (M2) macrophage phenotype, immunofluorescent antibody labeling for arginase was performed. Interleukin-4 stimulation resulted in increased immunolabeling for arginase-1 as expected (Figure 42). Skeletal muscle ECM did not promote any changes in arginase-1 immunolabeling nor was there any difference with aging. Both young and aged skeletal muscle ECM with IFN-γ/LPS stimulus promoted more arginase-1 immunolabeling over M1 controls. There were no differences in arginase-1 immunolabeling between young and aged skeletal muscle ECM with M1 or M2 cytokine stimulus.
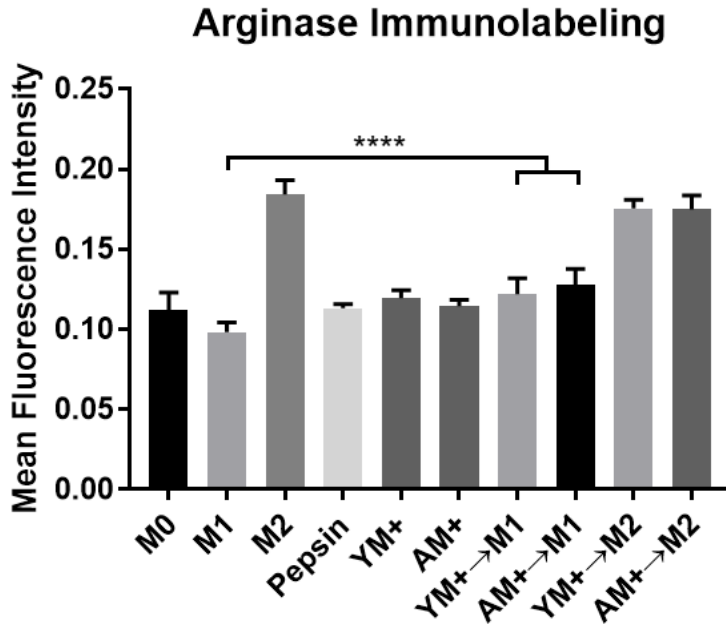
Figure 42: Immunofluorescent staining of macrophages treated with muscle ECM for arginase.

Data shown as mean ± S.D. Statistical significance reported as *p<0.05, **p<0.01, ***p<0.001, ****p<0.0001.

To assess the effect of skeletal muscle ECM upon macrophage gene expression, Taqman gene expression assays were performed for classical M1 and M2 gene transcripts (Figure 43). Interferon-γ and LPS stimulation (M1) promoted increased gene expression of *Nos2*, *Arg1*, *H2A-a* (MHC-II), *Il1b*, *Ccl2*, *Il6*, *Tnfa*, and *Il10* while downregulating *Retlna* (Fizz1), *Pparg*, and *Tgfb*. Interleukin-4 stimulation promoted upregulation of *Arg1*, *Retlna*, *H2-Aa*, *Pparg* and *Ccl2* while downregulating *Tnfa* and *Il10*. Skeletal muscle ECM promoted upregulation of *Nos2*, *Arg1*, *H2-Aa*, *Il1b*, *Ccl2*, *Il6* and *Tnfa* while downregulating *Pparg* and *Il10*. Aged skeletal muscle ECM enhanced upregulation of *Nos2*, *H2-Aa*, *Il1b*, *Ccl2*, *Il6* and *Tnfa* while promoting reduced downregulation of *Pparg* and *Il10*.
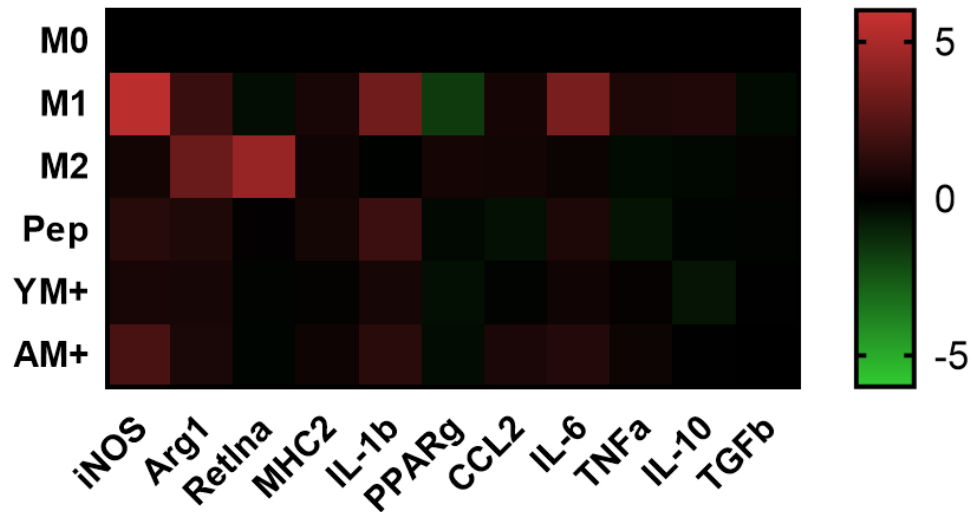
Figure 43: Taqman gene expression assays on macrophages treated with muscle ECM.

Gene expression represented as $\log_{10}$ of fold expression change where 5 indicates 10^5 fold expression change compared to M0.

To assess macrophage function, macrophage supernatants were assessed for nitric oxide production via the Greiss reagent system. Interferon-γ and LPS stimulation (M1) promoted increased nitric oxide production as expected (Figure 44). Skeletal muscle extracellular matrix treatment alone did not promote significant nitric oxide production. Extracellular matrix treatment with IFN-γ/LPS stimulus significantly enhanced nitric oxide production over M1 controls. Aged skeletal muscle ECM promoted reduced nitric oxide production compared to young with IFN-γ/LPS stimulus.

Nitric Oxide Production
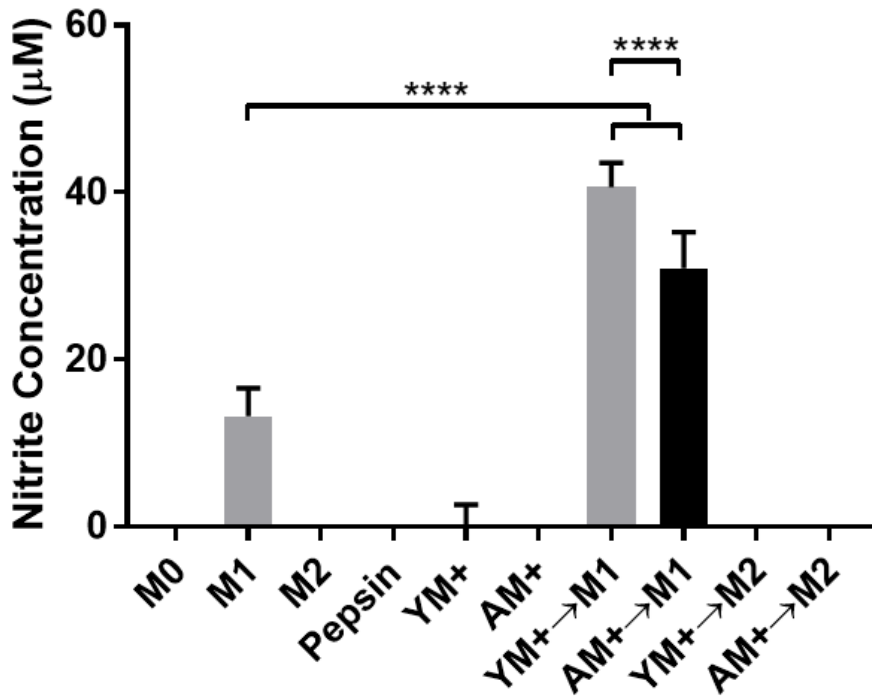
Figure 44: Nitric oxide production from macrophages treated with muscle ECM.

Data shown as mean ± S.D. Statistical significance reported as *p<0.05, **p<0.01, ***p<0.001, ****p<0.0001.

To assess macrophage phagocytic function, Vybrant FITC-labeled E. Coli particles (Thermo) were incubated with macrophages following treatment. M2 macrophages had reduced phagocytosis compared to M1 macrophages as expected (Figure 45). Skeletal muscle ECM treatment did not alter macrophage phagocytosis in basal conditions or with M1 or M2 cytokine stimulus.
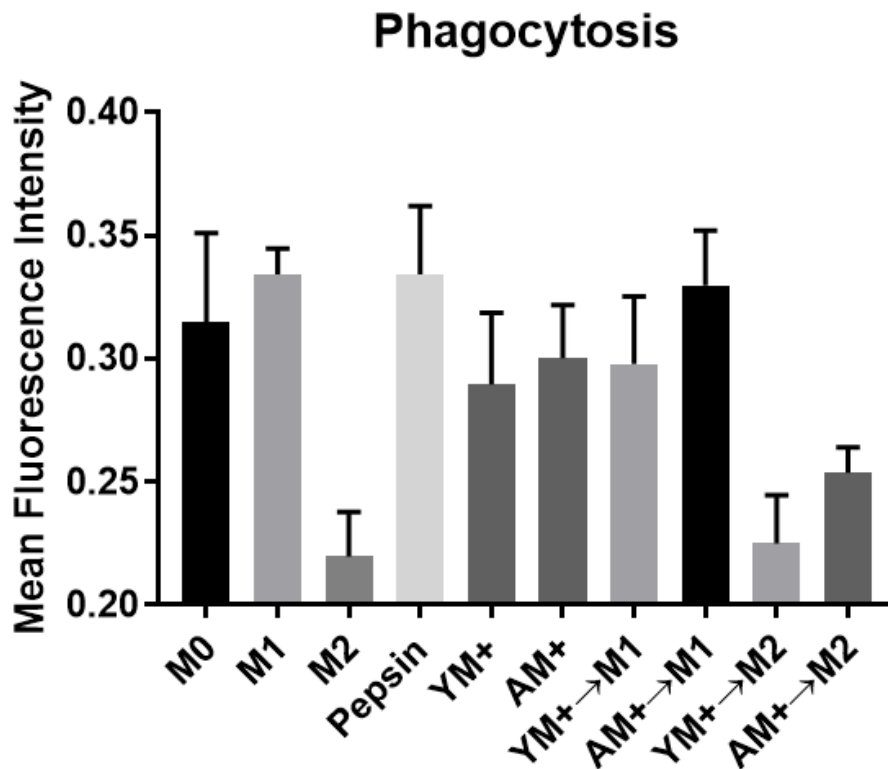
Phagocytosis

Figure 45: Vybrant E. Coli phagocytosis of macrophages treated with muscle ECM.

Data shown as mean ± S.D. Statistical significance reported as *p<0.05, **p<0.01, ***p<0.001, ****p<0.0001.

5.4   DISCUSSION

It is well documented that the response to muscle injury in aged individuals is compromised [265]. However, the mechanisms governing impairment of elderly repair following muscle injury are not fully understood. The regenerative properties of satellite cells (muscle stem cells) is known to decline with aging [266]. Some reports suggest this is due to intrinsic changes in satellite cell function or number [267-269]. Other studies suggest that there are extrinsic or

environmental factors that cause this decline in regenerative potential [39, 270, 271]. Impaired immune function with aging, including immunosenescence, has been correlated to aged sarcopenia and deficient muscle healing [272]. Macrophages, in particular, are known to be important for muscle regeneration and are impacted by inflamm-aging and immunosenescence [51, 273]. This paper investigated the effect of age-related changes in muscle ECM microenvironments upon the macrophage and host response following muscle injury.

Characterization of decellularized muscle tissue showed sufficient removal of cells as determined by reduction of nuclei, fragmentation of DNA and reduction in levels of double-stranded DNA. This quality control is necessary to ensure that remnant cellular material is not contributing to differences in the macrophage or host response [223]. The main detectable changes in the muscle ECM was a reduction in hydroxyproline content and Collagen I immunohistochemical staining. This suggests either an alteration in collagen content or modification of hydroxyproline residues and collagen fibers. Integrins and other receptors used by cells to migrate into the site of injury recognize specific matrix ligands [274]. Altered matrix composition or modification could impair interactions between integrins on infiltrating cells and the matrix from old tissues. Proteomic analysis would be necessary to fully understand how this muscle ECM is changing with age, however.

Macrophage response to muscle ECM was altered when the ECM was derived from young or aged sources. These changes with a basal ECM treatment resulted in enhanced pro-inflammatory responses seen by enhanced iNOS immunolabeling, nitrite production and gene expression of pro-inflammatory cytokines. This result suggests in a basal state, old ECM could contribute to the low-grade chronic inflammation observed in aged tissues [275]. With pro-inflammatory cytokine stimulus, muscle ECM promoted enhanced iNOS immunolabeling. ECM

also promoted increased immunolabeling of arginase with pro-inflammatory cytokine treatment. Skeletal muscle ECM did not have any effects on anti-inflammatory protein levels and function did not change with anti-inflammatory cytokine stimulus. The enhanced nitrite production from skeletal muscle ECM suggests that the ECM degradation products may promote a pro-inflammatory response.

5.5   CONCLUSION

Aged muscle ECM degradation products promote an enhanced pro-inflammatory response in macrophages during basal conditions. This could potentially be from NF-κB signaling but further testing would be needed to confirmed with further experiments. Both young and aged skeletal muscle ECM promoted enhanced iNOS immunolabeling with IFN-γ/LPS stimulation. This suggests degraded muscle ECM can increase pro-inflammatory responses during injury. Muscle ECM also increased nitric oxide production following IFN-γ/LPS exposure suggesting enhanced pro-inflammatory function as well as protein expression. Overall, muscle ECM acted through pro-inflammatory macrophage phenotypes with an enhancement with aged ECM.

6.0   EFFECT OF OXIDATION UPON MACROPHAGE RESPONSE TO AGED SKELETAL MUSCLE EXTRACELLULAR MATRIX

6.1   INTRODUCTION

Radical oxygen species (ROS) are naturally produced through normal biological functions and are increasingly produced during inflammation [197]. These elevated levels of ROS, while beneficial for pathogen clearance, can lead to oxidative damage to cells and proteins in affected tissues. Because extracellular matrix proteins are long-lived, modifications from oxidative stress can accumulate leading to altered function, structure or degradation. *In vitro* models of oxidative stress have proven that ECM molecules are modified through oxidation as measured by increases in protein carbonyl content [198]. This increased oxidation led to increased degradation by MMP-2 [198]. Protein oxidation could be a cause for increased collagen degradation with aging or accumulation of ECM fragments within aged tissues. ROS also have impacts on signaling pathways for degradative enzymes, leading to the upregulation of MKK and MAPK which lead to elevated MMP-1 expression [199].

Oxidative reagents have been used for the decellularization and sanitation of extracellular matrix biomaterials, especially peracetic acid (PAA) [276-278]. Peracetic acid is a form of stabilized hydrogen peroxide using as a disinfectant and anti-microbial agent [279]. Hydrogen peroxide can act as an alarmin to recruit inflammatory cells to the site of injury [280]. Prolonged

or enhanced hydrogen peroxide levels, like other ROS, can be responsible for tissue damage [197]. Hydrogen peroxide is produced by neutrophils and macrophage during inflammation [281, 282]. Muscle stem cell proliferation is known to be triggered by ROS such as hydrogen peroxide [283]. Hydrogen peroxide can also influence muscle stem cell differentiation [284]. Therefore, decellularization of extracellular matrix with hydrogen peroxide could mediate some of these effects in macrophage polarization or muscle regeneration.

6.2   METHODS

6.2.1   Skeletal muscle extracellular matrix preparation

Skeletal muscle extracellular matrix was prepared using modified methods previously developed [261]. Briefly, abdominal muscle was harvested from 4 month and 18 month old C57BL6/J mice (NIA). Muscle was washed in water. Samples were enzymatically digested in 0.2% trypsin/0.2% EDTA for 2 hrs at 37 °C with agitation. All subsequent steps were performed on a mechanical shaker at 300 rpm. Samples were washed once in water and twice in 1XPBS, 30 mins each. Samples were decellularized using 2% sodium deoxycholate for 5 hrs, washed in water and twice in 1XPBS for 30 mins each and then decellularized with 2% sodium deoxycholate for 14-16 hrs and 1% Triton X-100 for 1 hr. Samples were washed with type 1 water until no bubbles were detectable, indicating detergents had been removed. Samples were either treated with 0.1% peracetic acid/4% ethanol (+PAA) or with type 1 water (-PAA) for 2 hours. Samples were then washed twice with 1XPBS then twice with water for 30 mins each. Samples used for implantation were terminally sterilized with ethylene oxide. ECM degradation products were

111

produced using a 1mg/mL pepsin solution in 0.01N HCl under constant stir for 48 hrs to create a 10mg/mL ECM digest.

6.2.2 Biochemical Assessment

ECM scaffold biochemistry was performed to assess hydroxyproline and sulfated glycosaminoglycan content. ECM scaffolds were digested at 10mg/mL in a papain solution. Sulfate glycosaminoglycan content was assessed using a dimethylmethylene blue (DMMB) reagent. Hydroxyproline content was assessed by adding 50 μL 2N NaOH to 50 μL papain digests then hydrolyzing at 110 °C for 18 hrs. Samples were neutralized with 5N HCl. One hundred microliters of 0.01M copper sulfate, 2.5N NaOH and 6% H_2O_2 were added. Samples were incubated at 80 °C for 5 minutes then cooled. Four hundred microliters of 3N sulfuric acid was added followed by 200 μL of 5% DMAB in propanol. Samples were incubated at 70 °C for 15 minutes then the absorbance was read at 540 nm.

Paraffin sections were stained with PicroSirius Red as an indicator of collagen content. Briefly, slides were deparaffinized and rehydrated to water. Slides were stained in PicroSirius Red solution for 1 hour then differentiated in 35% acetic acid for 10 seconds. Slides were quickly dehydrated and cleared in xylenes then mounted with resinous mounting media.

Paraffin sections were stained with Masson's trichrome as an indicator of collagen content. Briefly, slides were deparaffinized and rehydrated to water. Slides were re-fixed in Bouin's solution for 1 hour at 56 °C to improve staining quality. Slides were rinsed in running tap water for 10 minutes to remove the yellow color. Slides were then stained in Weigert's iron hematoxylin working solution for 10 minutes then rinsed in running warm tap water for 10 minutes then washed in distilled water. Slides were stained in Biebrich scarlet-acid fuchsin

solution for 10 minutes then washed in distilled water. The stain was differentiated in phosphomolybdic-phosphotungstic acid solution for 10 minutes. Slides were transfered directly to aniline blue solution and stained for 10 minutes then rinsed briefly in distilled water and differentiate in 1% acetic acid solution for 5 minutes then washed in distilled water. Slides were dehydrated very quickly and cleared in xylene then mounted with resinous mounting medium.

6.2.3   Assessment of advanced glycation end product content

Fluorescence AGE levels were assessed by pipetting papain digested ECM into 96 well plates. Fluorescence intensity levels were assessed on a spectrophotometer (BioTek) for several signature AGE wavelengths: excitation = 295 nm emission = 395 nm, excitation = 335 nm emission = 385 nm, excitation = 370 nm emission = 440 nm.

6.2.4   Immunohistochemical staining

Native and decellularized muscle ECM was fixed in 10% NBF then embedded in paraffin wax. Sections were stained using DAB immunohistochemistry for collagen type I, advanced glycation end-products, cysteine sulfonate, S-nitro-cysteine, or 3-nitro-tyrosine. Briefly, paraffin sections were deparaffinized to water then antigen was retrieved using 10mM citric acid pH 6 0.05% Tween20 for 20 mins at 95-100 °C. Slides were washed twice with 1X TBST for 5 mins then twice with 1XPBS for 3 mins. Endogenous peroxidase activity was blocked by incubating slides in 0.3% hydrogen peroxide for 30 mins. Slides were washed 3 times in 1X PBS for 3 minutes. Slides were blocked for non-specific antibody binding with a blocking buffer made of 2% donkey serum/1% bovine serum albumin/0.1% Tween-20 for 1 hour at room temperature.

Primary antibodies were incubated overnight at 4 °C diluted in blocking buffer. Slides were washed 3 times for 3 minutes with 1XPBS. Slides were then incubated with biotinylated secondary antibodies diluted in blocking buffer (goat anti-rabbit 1:200 (Vector)). Slides were was again 3 times for 3 minutes with 1XPBS. Slides were incubated with VectaShield ABC Reagent for 30 mins then washed again 3x3mins with 1XPBS. Staining was developed by incubating sections with 4% DAB. Sections were washed then mounted with resinous mounting media and coverslipped. Slides were images on a brightfield microscope at the same settings.

6.2.5   Bone marrow-derived macrophage isolation

Bone marrow-derived macrophages were harvested from 2 month or 18-20 month-old C57/BL6 mice as previously described [221]. Briefly, femurs and tibiae were harvested and separated from muscle and connective tissue. Bones were cut at either end to expose bone marrow. Sterile syringe and needles were used to flush out bone marrow using macrophage differentiation media (DMEM/10% FBS/10% L-929 Supernatant/1% PenStrep/2% MEM non-essential amino acids/1% HEPES/0.1% 55μM β-2 mercaptoethanol). Bone marrow lysate was reconstituted in media and filtered through a sterile cell filter. Cells were cultured for 7 days in media to differentiate them into macrophages, changing differentiation media every 2 days.

6.2.6   Macrophage Treatment

Following 7 days of differentiation culture as described above, macrophages were treated with acute polarizing regimens to distinguish phenotypes over 24 hours. Naïve macrophage (M0) controls were treated with basal media for 24 hours. M1 (20 ng/mL IFN-γ and 100 ng/mL LPS)

and M2 (20 ng/mL IL-4) polarizing cytokines were used to create positive controls for classical pro- and anti-inflammatory macrophages. ECM degradation products were neutralized and diluted to 1000 μg/mL in macrophage media to isolate biochemical effects of degradation products and prevent structural moieties from forming. Pepsin buffer (1 mg/mL pepsin in 0.01 M HCl) diluted in macrophage media was used as a control. Another set of treatment groups involved 24-hour exposure of ECM degradation products followed by 24-hour treatment with either the M1 or M2 treatment regimen.

6.2.7 Indirect Immunofluorescent Antibody Labeling

Cells were fixed with 2% paraformaldehyde (PFA) for 30 minutes then washed in 1XPBS. Cells were incubated in blocking buffer (2% donkey serum, 1% bovine serum albumin (BSA), 0.1% Triton X-100, 0.1% Tween-20) for 1 hour at room temperature. Primary antibodies were diluted in this blocking buffer as follows and incubated overnight at 4 °C: iNOS (1:100, Abcam 3523) or Arginase-1 (1:200, Abcam 91279). iNOS is a classical M1 macrophage marker whereas Arginase-1 is a classical M2 macrophage marker. Cells were washed in 1XPBS then incubated in the appropriate fluorescently-labeled secondary antibody solution in blocking buffer for 1 hour at room temperature (donkey anti-rat Alexa Fluor 488, Invitrogen, 1:200; donkey anti-rabbit Alexa Fluor 488, Invitrogen, 1:300). Cell nuclei were counterstained with DAPI. Cells from 2 month old mice were imaged nine times in the center of each well at 10X magnification using automated position capture function to remove bias from subjective image location acquisition. All imaging was performed on an Axio observer T1 microscope. Mean fluorescence intensity of cells was analyzed using Cell Profiler software (Broad Institute). Briefly, DAPI images were used by the program to identify cell nuclei then FITC images were used to identify cell borders

around the identified nuclei. The mean fluorescent intensity was calculated by averaging the pixel intensities (scale of 0 to 1) across the entire cell area. Mean fluorescence intensity values were averaged for all imaged cells in each well.

6.2.8   Taqman gene expression assay

Following treatments, macrophages (n=5 biological replicates from 5 young (2 month) and 5 aged (18 month) mice) were harvested for RNA using Qiagen RNEasy MiniPrep RNA Isolation Columns following standard protocol.   RNA was quantified using a NanoDrop Lite Spectrophotometer (Thermo). cDNA templates were created from 1 µg of RNA using Invitrogen High Capacity RNA-to-cDNA kits (Thermo). Taqman Gene Expression Assays (Thermo) were performed for the following commonly reported M1 and M2 macrophage genes: Nos2 (Mm00440502_m1), IL1b (Mm00434228_m1), IL12b (Mm01288989_m1), TNFa (Mm00443258_m1), MHC-II (Mm01181326_m1), Arg (Mm00475988_m1), Retlna (Fizz1) (Mm00445109_m1), Mrc1 (Mm01329362_m1), IL10 (Mm01288386_m1), and PPARg (Mm00440940_m1).

6.2.9   Phagocytosis Assay

Following treatments, 50 µL of supernatant from macrophages were transferred into a fresh plate.   Nitrite content was assayed using a Greiss Reagent system.   Briefly, 50 µL of sulfanilamide (1% in 5% phosphoric acid) was added to supernatants for 10 minutes. Then, 50 µL of 0.1% N-1-napthylethylenediamine in water was added to the mixture for an additional 10

minutes. The absorbance at 540 nm was measured using a BioTek SYNERGY HTX spectrophotometer.

6.2.10 Nitric oxide assay

Following treatments, 50 µL of supernatant from macrophages were transferred into a fresh plate. Nitrite content was assayed using a Greiss Reagent system. Briefly, 50 µL of sulfanilamide (1% in 5% phosphoric acid) was added to supernatants for 10 minutes. Then, 50 µL of 0.1% N-1-napthylethylenediamine in water was added to the mixture for an additional 10 minutes. The absorbance at 540 nm was measured using a BioTek SYNERGY HTX spectrophotometer.

6.3   RESULTS

6.3.1   Biochemical characterization

In order to understand the effect of peracetic acid upon biochemical content of muscle ECM, DMMB sulfated glycosaminoglycan and hydroxyproline assays were repeated. There were no significant differences in sulfated glycosaminoglycan content in native skeletal muscle or decellularized skeletal muscle ECM treated with PAA (Figure 46A). Removal of PAA from the decellularization procedure resulted in significantly more sGAG content in young skeletal muscle ECM and a significant reduction in sGAG content in old skeletal muscle ECM (Figure 46A). Hydroxyproline content was found to be higher in aged skeletal muscle over young. Aged

skeletal muscle ECM had reduced hydroxyproline content with or without peracetic acid treatment. However, peracetic acid treatment reduced hydroxyproline content levels in young skeletal muscle ECM (Figure 46B).
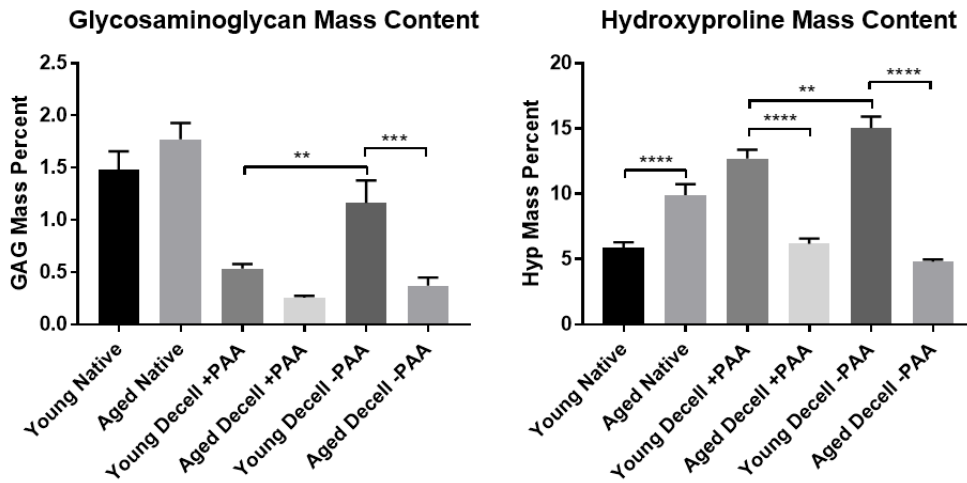
Figure 46: Glycosaminoglycan and hydroxyproline content of muscle ECM with or without PAA.

Data shown as mean ± S.D. Statistical significance reported as *p<0.05, **p<0.01, ***p<0.001, ****p<0.0001

Confirmation of collagen content with PicroSirius Red staining revealed a reduction in staining with peracetic acid treatment. Without peracetic acid treatment, there appeared to be more equal staining though still more in young skeletal muscle ECM (Figure 47).
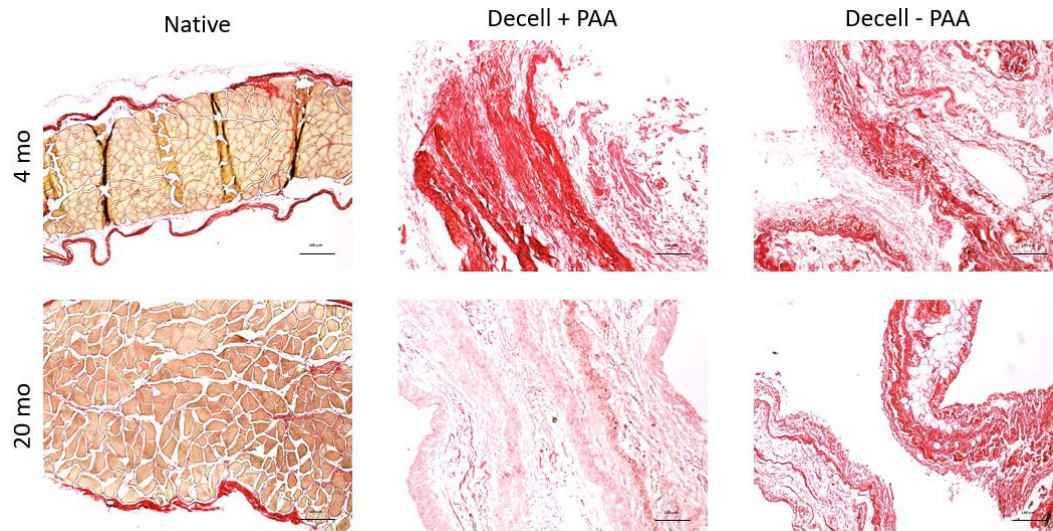
Figure 47: PicroSirius Red staining of muscle ECM with or without PAA treatment.

Images taken at 10X magnification. Scale bars indicate 100 µm.

(Compare to Figure 33)

Masson's trichrome staining showed similar trends where young skeletal muscle ECM had higher levels of collagen staining, but this effect was more extreme with peracetic acid treatment (Figure 48). These observations appear to differ from biochemical quantification assays so further investigation would be necessary to reach a conclusive determination.
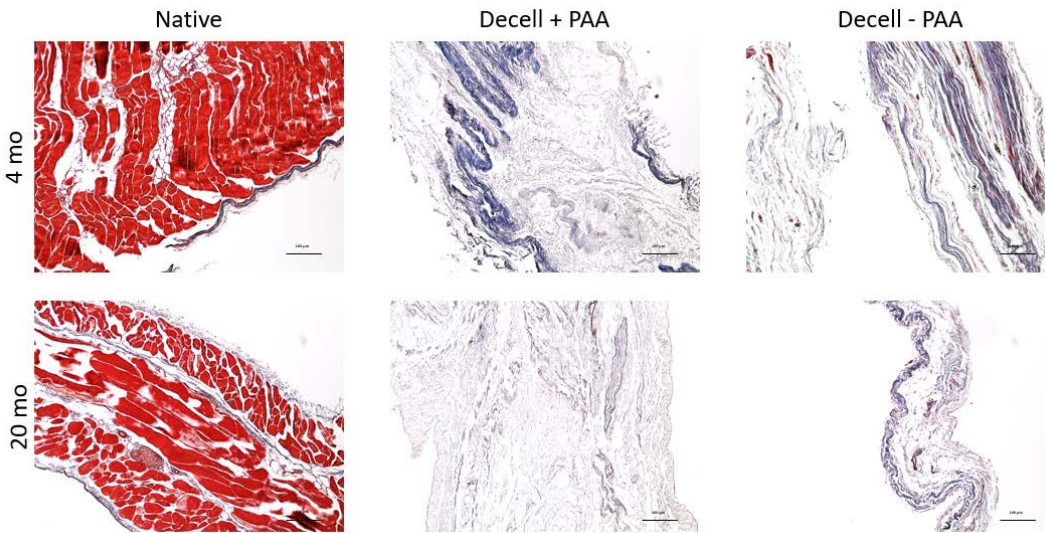
Figure 48: Masson's trichrome staining of muscle ECM with or without PAA treatment.

Images taken at 10X magnification. Scale bars indicate 100 µm.

(Compare to Figure 34)

Immunohistochemical staining for collagen type I showed similar results to PicroSirius Red and Masson's trichrome staining, suggesting the results of those staining methods were indicative of true changes in collagen content (Figure 49).
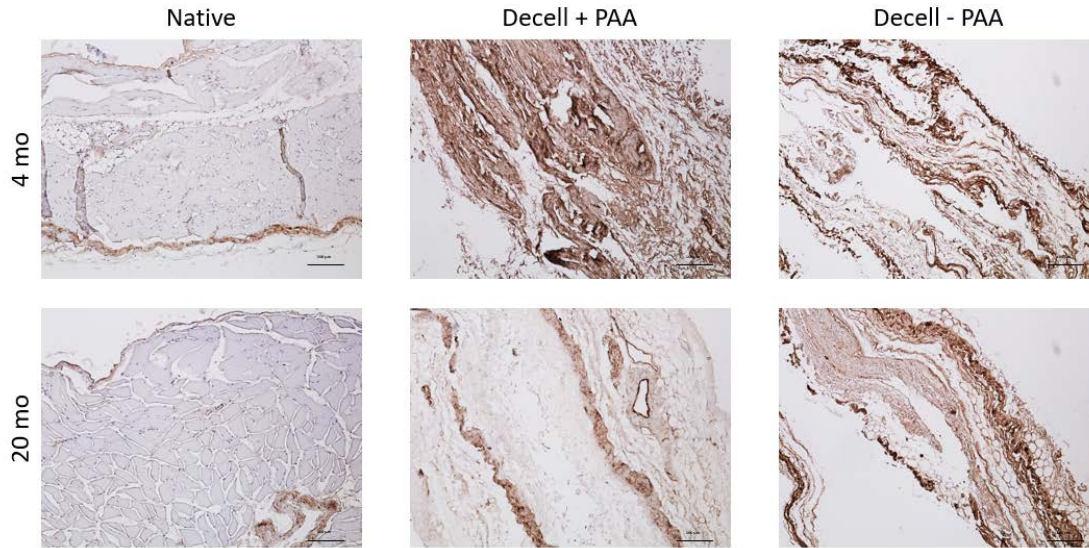
Figure 49: Collagen I IHC on muscle ECM with or without PAA treatment.

Images taken at 10X magnification. Scale bars indicate 100 µm.

(Compare to Figure 35)

Extracellular matrix content was also assessed via Western blotting in order to determine banding and fractionation of matrix proteins. Collagen I, collagen IV and laminin were all detected via Western blotting (Figure 50). Collagen I and IV stained brightly on Western blots but laminin was dim. Banding patterns for all three proteins were similar with old muscle with PAA and young muscle without PAA having strong bands around 40 kDa. Old muscle with PAA treatment lost the four distinct bands between 90-200 kDa.
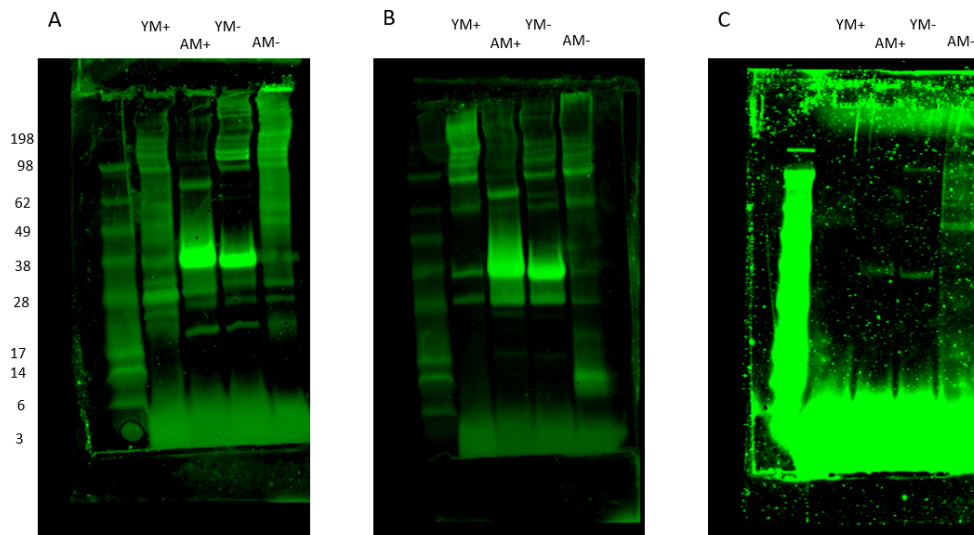
Figure 50: Western blotting for collagen I (A), collagen IV (B) and laminin (C) on muscle ECM.

6.3.2 Assessment of advanced glycation end product content

To assess advanced glycation end product content, fluorescent signatures for known AGE moieties were assessed in papain digested ECM. There was a reduction in fluorescent AGE intensity in all three signatures in aged skeletal muscle (Figure 51). Without peracetic acid treatment, there was a reduction in fluorescent AGE levels at all three signatures. With peracetic acid treatment, there was only a reduction in fluorescent AGEs with an excitation of 370 nm and emission of 440 nm. Peracetic acid treatment reduced the fluorescent AGE levels in young muscle ECM at all three signatures. Old ECM fluorescent AGE levels were enhanced with an excitation of 370 nm and emission of 440 nm and reduced with an excitation of 335 nm and emission of 385 nm with peracetic acid treatment.
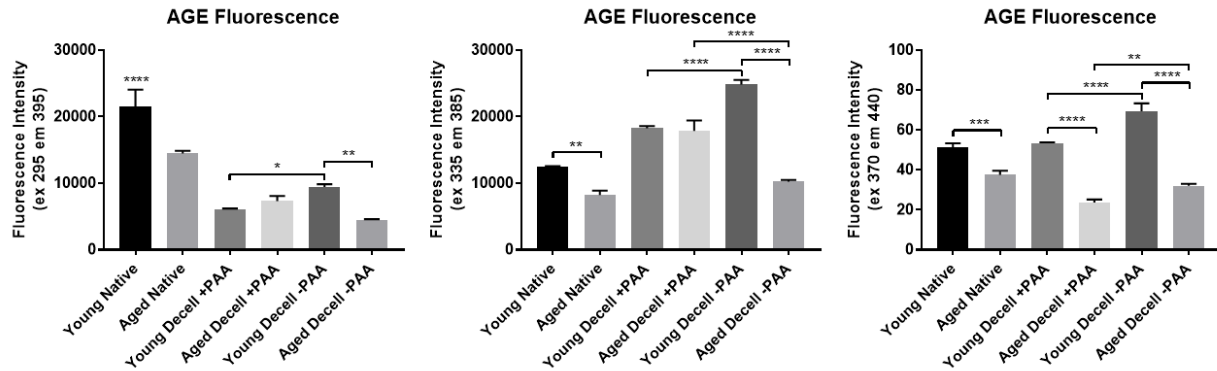
Figure 51: Fluorescence signatures for AGEs in muscle ECM with or without PAA treatment.

Data shown as mean ± S.D. Statistical significance reported as *p<0.05, **p<0.01, ***p<0.001, ****p<0.0001

Confirmation of AGE levels with immunohistochemistry showed reduction in AGE staining in aged skeletal muscle ECM with peracetic acid treatment (Figure 52). Without peracetic acid treatment, AGE IHC staining was localized to border regions in aged ECM while it was stained throughout in young ECM.
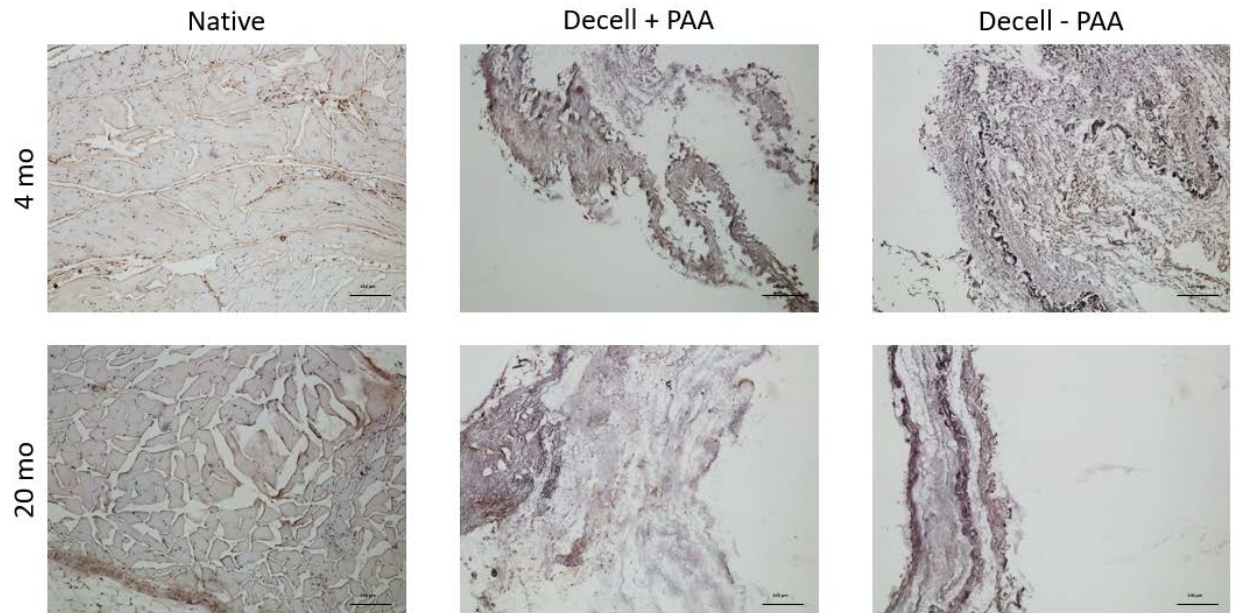
Figure 52: IHC for advanced glycation end products on muscle ECM with or without PAA.

Images taken at 10X magnification. Scale bars indicate 100 µm.

Immunohistochemistry staining for CML showed more intense staining with peracetic acid treatment. There were not large changes in CML IHC staining between young and old skeletal muscle ECM so further quantitative analysis would be necessary (Figure 53).
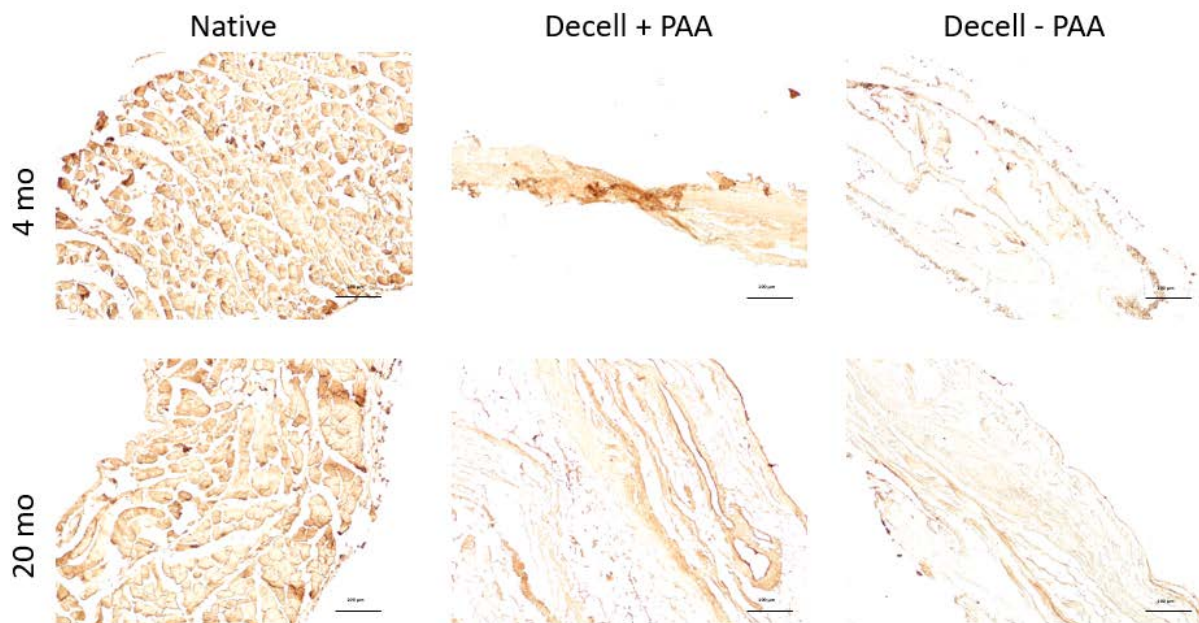
Figure 53: IHC for carboxymethyllysine on muscle ECM with or without PAA.

Images taken at 10X magnification. Scale bars indicate 100 µm.

Advanced glycation end-product (AGE) content was also assessed via Western blotting (Figure 54). The staining for AGEs via Western blotting, however, was weak.
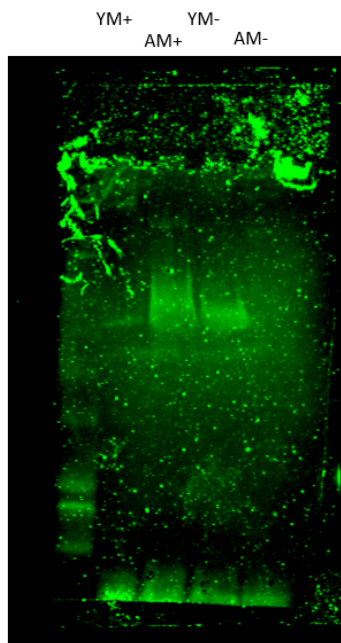
Figure 54: Western blotting for AGEs on young and aged muscle ECM ± PAA treatment.

6.3.3 Assessment of oxidative markers

Immunohistochemical staining for cysteine sulfonate, a marker of protein oxidation, showed staining in both native skeletal muscle and decellularized skeletal muscle ECM (Figure 55). There were higher levels of cysteine sulfonate staining in young skeletal muscle. There appeared to be more cysteine sulfonate staining in young ECM with peracetic acid but not without peracetic acid.
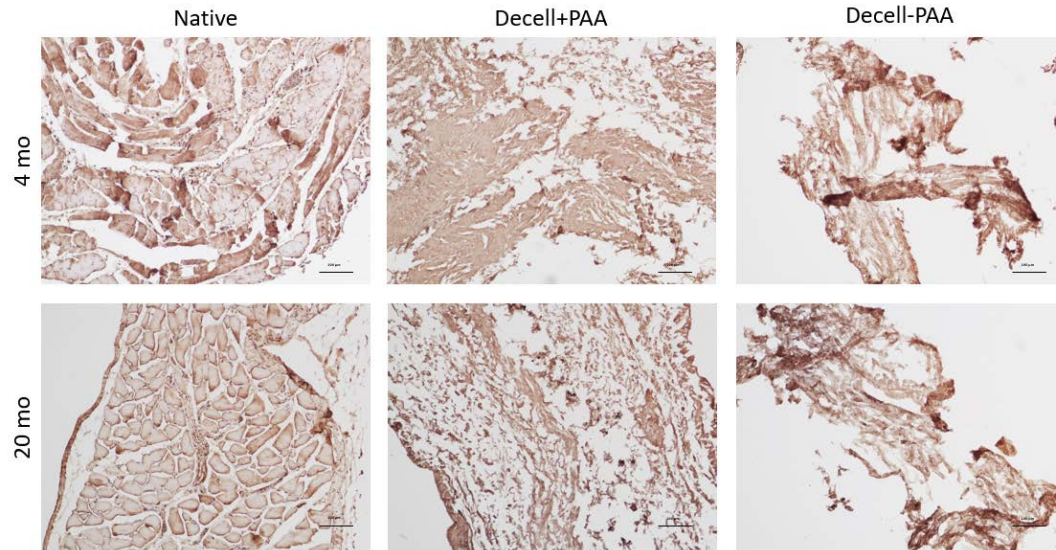
Figure 55: IHC for cysteine sulfonate on muscle ECM with or without PAA.

Images taken at 10X magnification. Scale bars indicate 100 µm.

Immunohistochemistry staining for S-nitro-cysteine showed increased staining in young skeletal muscle (Figure 56). There appeared to be reduced S-nitro-cysteine staining with peracetic acid treatment compared to without. There was more intense staining for S-nitro-cysteine in the border regions of old muscle ECM without PAA treatment.
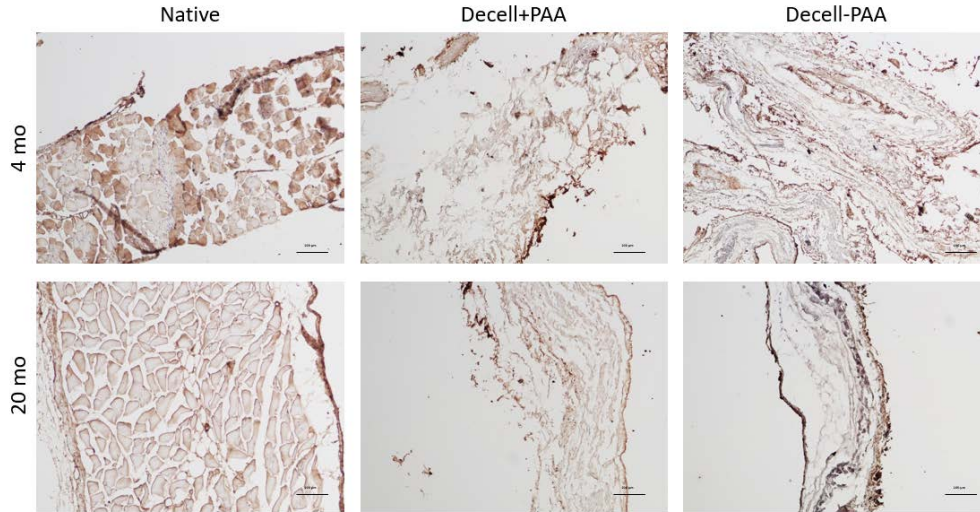
Figure 56: IHC for S-nitro-cysteine on muscle ECM with or without PAA.

Images taken at 10X magnification. Scale bars indicate 100 µm.

Immunohistochemical staining for 3-nitro-tyrosine stained skeletal muscle positive (Figure 57). There was not substantial staining for 3-nitro-tyrosine in any decellularized ECM. Peracetic acid treatment did not seem to affect levels of 3-nitro-tyrosine staining.
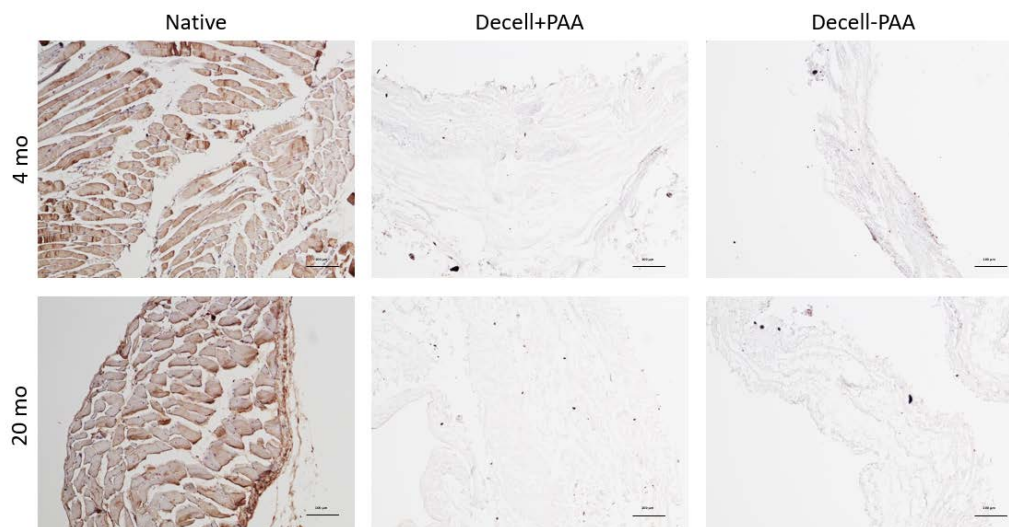
Figure 57: IHC for 3-nitro-tyrosine on muscle ECM with or without PAA.

Images taken at 10X magnification. Scale bars indicate 100 µm.

6.3.4   Bone marrow macrophage phenotype and function

To assess the effect of peracetic acid treatment of muscle ECM upon macrophage phenotype, murine bone marrow macrophages were treated with the ECM degradation products from young or old muscle ECM with or without peracetic acid treatment. iNOS immunolabeling revealed increased iNOS protein levels in aged skeletal muscle ECM with or without peracetic acid treatment (Figure 58). With peracetic acid treatment, there was no difference in iNOS immunolabeling with cytokine treatment (Figure 58A). Without peracetic acid treatment, aged skeletal muscle ECM resulted in increased iNOS immunolabeling with either M1 or M2 cytokine stimulation (Figure 58B).
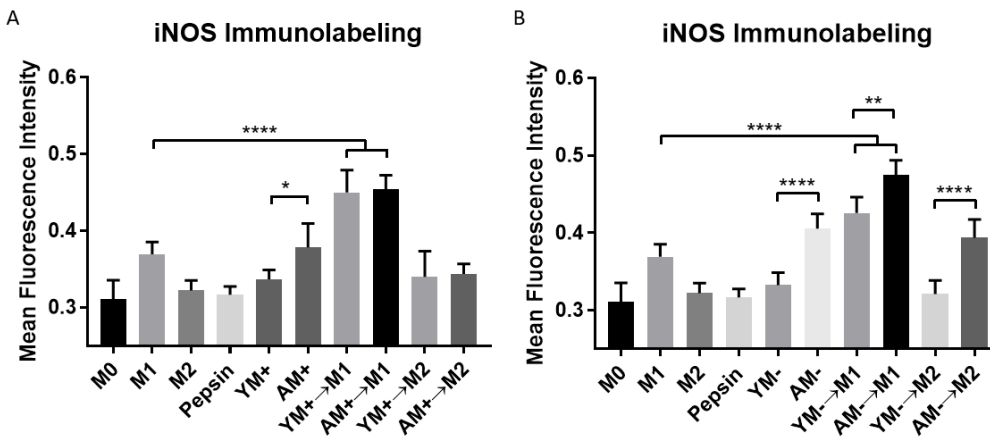
Figure 58: Immunofluorescence for iNOS on macrophages treated with mECM ± PAA treatment.

Data shown as mean ± S.D. Statistical significance reported as *p<0.05, **p<0.01, ***p<0.001, ****p<0.0001

Immunolabeling for arginase-1 resulted in no differences between young and aged skeletal muscle ECM in neither basal treatments nor with M1 or M2 cytokine stimulus (Figure 59A).

Without peracetic acid treatment, aged skeletal muscle ECM treatment promoted enhanced arginase-1 immunolabeling with M1 or M2 stimulus (Figure 59B).
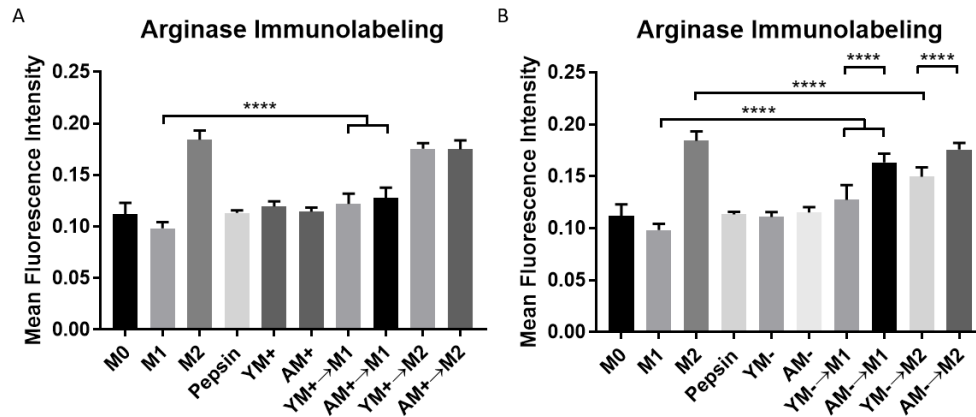
Figure 59: Immunofluorescence for arginase on macrophages treated with mECM ± PAA treatment.

Data shown as mean ± S.D. Statistical significance reported as $*p<0.05$, $**p<0.01$, $***p<0.001$, $****p<0.0001$

To understand the effects of peracetic acid treatment of skeletal muscle ECM, Taqman gene expression assays were performed on RNA extracts from bone marrow-derived macrophages treated with young or aged muscle ECM degradation products with or without PAA treatment. With peracetic acid treatment, aged skeletal muscle ECM enhanced upregulation of *Nos2*, *H2-Aa*, *Il1b*, *Ccl2*, *Il6* and *Tnfa* while promoting reduced downregulation of *Pparg* and *Il10* (Figure 60). Without peracetic acid, these trends reversed in most markers. Aged muscle ECM reduced expression of *Nos2*, *Arg1*, *H2-Aa*, *Il1b*, *Ccl2*, *Il6* and *Tnfa* while further downregulating *Pparg* and *Il10* compared to young muscle ECM without peracetic acid (Figure 60).
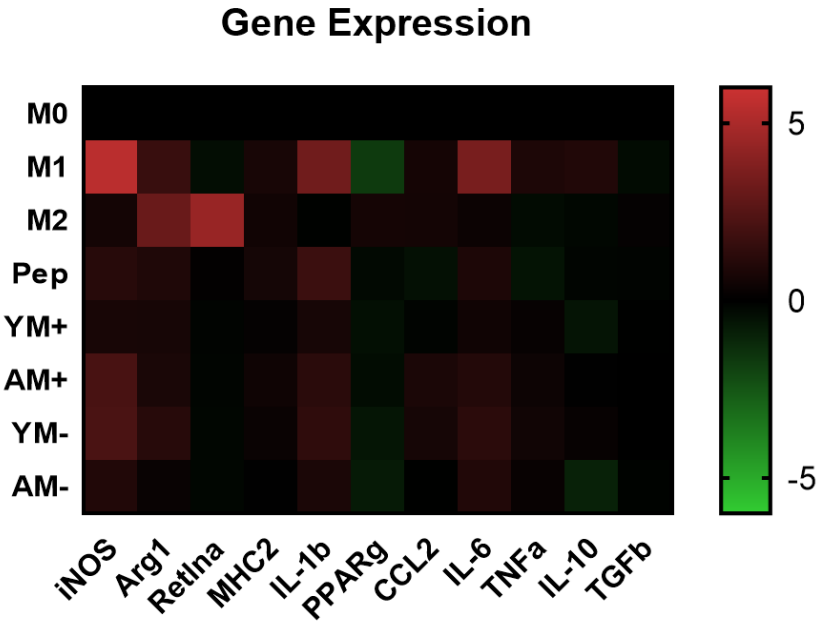
Gene Expression

Figure 60: Taqman gene expression on macrophages treated with mECM ± PAA treatment.

Gene expression represented as $\log_{10}$ of fold expression change where 5 indicates 10^5 fold expression change compared to M0.

Macrophage function for nitric oxide production was tested using the Greiss reagent system (Figure 61). With or without peracetic acid treatment, skeletal muscle ECM enhanced nitric oxide production with IFN-γ/LPS stimulus. Aged skeletal muscle ECM reduced nitric oxide production with IFN-γ/LPS compared to young regardless of peracetic acid treatment. However, peracetic acid treatment increased the nitric oxide production from skeletal muscle ECM with IFN-γ/LPS stimulus compared to without PAA.
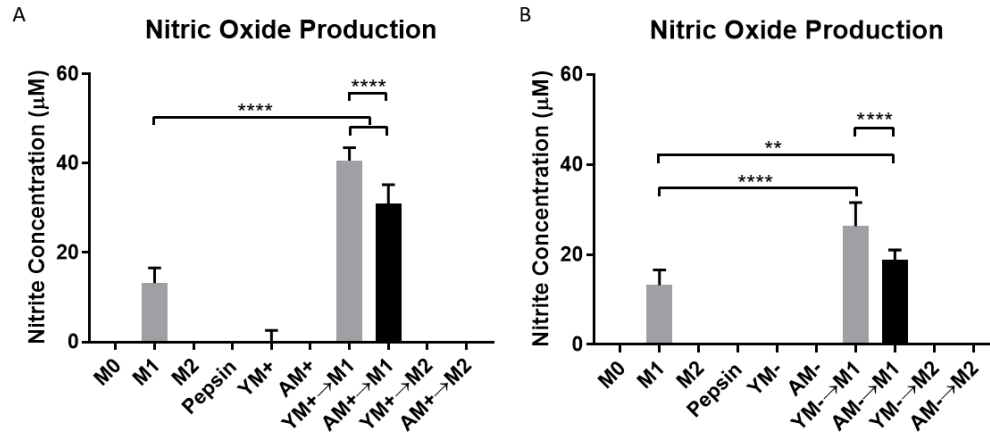
Figure 61: Nitric oxide production on macrophages treated with mECM ± PAA treatment.

Data shown as mean ± S.D. Statistical significance reported as *p<0.05, **p<0.01, ***p<0.001, ****p<0.0001

The effect of peracetic acid treatment of skeletal muscle ECM upon macrophage phagocytosis was assessed using Vybrant FITC-labeled E. Coli particles (Figure 62). With peracetic acid treatment, ECM treatment with basal conditions or with cytokine treatment did not change phagocytosis from appropriate controls (Figure 62A). Without peracetic acid treatment, ECM treatment enhanced phagocytosis with IL-4 stimulation compared to M2 controls (Figure 62B). There was no difference in phagocytosis between young and aged skeletal muscle ECM in any treatment regimen or with or without peracetic acid treatment.
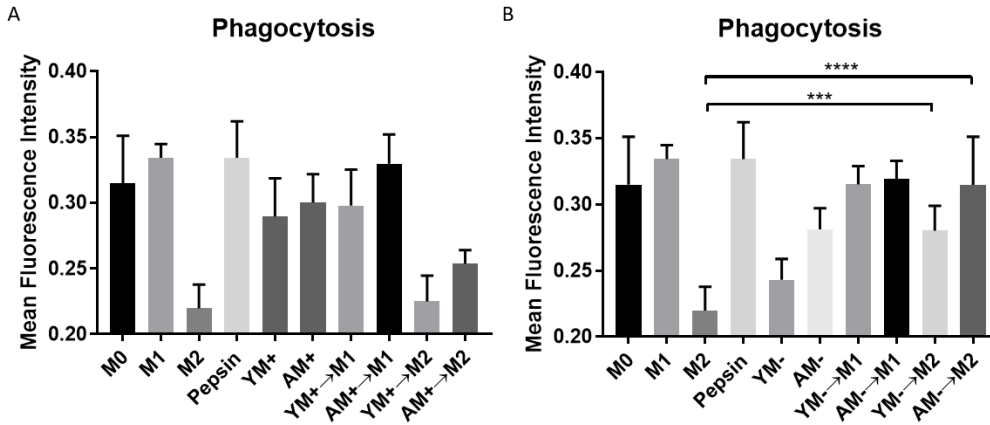
Figure 62: E. coli phagocytosis on macrophages treated with mECM ± PAA treatment.

Data shown as mean ± S.D. Statistical significance reported as $*p<0.05$, $**p<0.01$, $***p<0.001$, $****p<0.0001$

6.4   DISCUSSION

Peracetic acid treatment of extracellular matrix scaffolds normalized the biochemistry and the macrophage response to aged muscle ECM. This action could be through the creation of similar modifications in both young and aged muscle ECM. Peracetic acid is essentially a stabilized form of hydrogen peroxide, which is known to be a potent redox regulator in inflammation, regeneration and disease through the modification of biomolecules [285]. These could include protein oxidation or lipid peroxidation, both of which can affect the immune response [286, 287]. Inflammatory signaling is affected by redox regulation, including NF-KB and Nrf2 transcription factors, which control pro-inflammatory and anti-oxidant gene transcription respectively [288, 289].

Peroxidation of the extracellular matrix while potentially immunomodulatory and beneficial for bioengineering applications could change the native ECM of the aging muscle. This would mask the true effect of aged skeletal muscle ECM upon macrophage polarization. The extracellular matrix is known to accumulate oxidative modifications with aging [290]. Oxidation of ECM is also known to affect the function and phenotype of macrophages [198]. Treatment of both young and aged ECM with oxidizing agents could create similar levels of oxidation in these materials, removing the differences present before treatment.

Analysis of young and aged muscle has previously shown changes in the redox state of these tissues. Analysis of muscles from elderly subjects has shown an increase in oxidative stress [291-293]. This included reduced levels of superoxide dismutase (SOD), an antioxidant enzyme, and increased levels of lipid peroxidation [292]. Mass spectroscopy analysis has shown a reduction in the content of redox sensitive proteins in aged muscle, indicating a shift in redox states of the tissue [294]. Oxidative stress has also been suggested to be a cause for age-related muscle mass loss [295]. Therefore, artificial oxidation through peracetic acid treatment may induce similar levels of this phenomena that would otherwise have increased presence in aged skeletal muscle ECM.

6.5   CONCLUSION

Peracetic acid treatment altered the biochemistry of extracellular matrix scaffolds, reducing differences in several metrics of matrix content. Peracetic acid treatment had a noticeable effect on the macrophage response to muscle ECM, including enhancement of nitric oxide production and reduction in iNOS and arginase immunolabeling. These findings suggest peracetic acid

treatment of extracellular matrix biomaterials can alter the macrophage response which could be beneficial for therapeutic treatment. However, these modifications can complicate the investigation of natural changes in the extracellular matrix with physiological events such as aging or disease. Further investigation in the effects of aged skeletal muscle ECM will exclude peracetic acid treatment to preserve natural changes in ECM biochemistry.

7.0   EFFECT OF GLYCATION UPON MACROPHAGE RESPONSE TO SKELETAL

MUSCLE EXTRACELLULAR MATRIX

7.1   INTRODUCTION

Advanced glycation end-products (AGEs) have been implicated in the pathogenesis of tissues during aging and diabetes [177]. AGEs result from the non-enzymatic glycation of biomolecules including proteins, lipids and nucleic acids [296]. They can produce crosslinks which cause increased stiffness and altered degradation [297-299]. AGEs are known to be recognized by the receptor for advanced glycation end-products (RAGE) which signals through the NF-κB pathway [300]. AGEs have been shown to directly activate pro-inflammatory macrophage responses through this pathway [194]. AGEs have also been shown to increase in aged muscle tissue [262]. However, glycation of aged muscle ECM itself has not been investigated.

In order to investigate the mechanism of advanced glycation end-products, *in vitro* glycation of young muscle ECM can be performed [220]. Previous investigation of artificial glycation has shown that these modifications increase the stiffness of extracellular matrix scaffolds and alter their viscoelastic properties [220]. The stiffness of muscles have been shown to increase with aging, which reduces the ability to regenerate following injury [166]. Aged muscle extracellular matrix as well has been shown to increase in stiffness due to altered anisotropy of ECM fibers [9]. This increase in stiffness could result from glycation of muscle

fibers and extracellular matrix. Artificial glycation of extracellular matrix provides a potential mechanism for the alterations in the host response following muscle injury in aged individuals. This comprises a more physiologically relevant investigation of the role of glycation than current studies involving glycated bovine serum albumin, which are limited to blood applications.

Furthermore, artificial glycation of collagen has been shown to impair enzymatic degradation from collagenase [301]. If similar phenomena occur *in vivo,* glycation would prevent the degradation of extracellular matrix in aged tissues. Extracellular matrix deposition and crosslinking is known to increase with aging [241]. MMP activity also increases with age, which could be a response to the increased matrix accumulation and crosslinking in aged tissues [241]. This increased MMP activity could be responsible for the accumulation of ECM degradation products in aged tissues [302]. Aged muscles are known to have increased collagen content, which may be due to reduced degradation of the ECM [53]. Collagen accumulation could also be due to increased TGF-β signaling promoted by glycation through NF-κB [303]. Glycation could be responsible for the many alterations in the extracellular matrix with aging.

The present study seeks to investigate the direct mechanism of glycation of extracellular matrix upon macrophage phenotype and function. As a proposed mechanism in the altered responses in aging and diabetes, both aged and diabetic ECM will be used as a control of the natural accumulation of these glycation products. Direct evidence of the role of glycation in pro-inflammatory macrophage phenotype is necessary to fully understand how these aging biomarkers affect the ability of aged or diabetic individuals to heal from injury.

7.2   METHODS

7.2.1   Skeletal muscle extracellular matrix preparation

Skeletal muscle extracellular matrix was prepared using modified methods previously developed [261]. Briefly, abdominal muscle was harvested from 4 month and 18 month old C57BL6/J mice (NIA). Muscle was washed in water. Samples were enzymatically digested in 0.2% trypsin/0.2% EDTA for 2 hrs at 37 °C with agitation. All subsequent steps were performed on a mechanical shaker at 300 rpm. Samples were washed once in water and twice in 1XPBS, 30 mins each. Samples were decellularized using 2% sodium deoxycholate for 5 hrs, washed in water and twice in 1XPBS for 30 mins each and then decellularized with 2% sodium deoxycholate for 14-16 hrs and 1% Triton X-100 for 1 hr. Samples were washed with type 1 water until no bubbles were detectable, suggesting detergents had been removed. Samples were either treated with 0.1% peracetic acid/4% ethanol for 2 hours. Samples were then washed twice with 1XPBS then twice with water for 30 mins each. Samples used for implantation were terminally sterilized with ethylene oxide. ECM degradation products were produced using a 1mg/mL pepsin solution in 0.01N HCl under constant stir for 48 hrs to create a 10mg/mL ECM digest.

7.2.2   *In Vitro* Glycation

Young muscle ECM was incubated in 50mM or 250mM solutions of glucose, fructose, or ribose with 44mM NaHCO$_3$ and 25mM HEPES in 1XPBS at 37°C for 1 week and then washed extensively in 1XPBS and water.

7.2.3 High performance liquid chromatography

High performance liquid chromatography (HPLC) was used to assess advanced glycation end product content. Size exclusion chromatography was performed using

7.2.4 Fourier-transform infrared spectroscopy

Fourier-transform infrared spectroscopy was performed at the University of Pittsburgh Swanson School of Engineering Nanofabrication and Characterization Facility (NFCF).

7.2.5 Protein carbonyl assay

Protein carbonyl content was quantified using a protein carbonyl quantification kit (Cayman Chemical) according to manufacturer instructions. Pepsin-solubilized ECM was used for determination of protein carbonyl content.

7.2.6 Bone marrow-derived macrophage isolation

Bone marrow-derived macrophages were harvested from 2 month or 18-20 month-old C57/BL6 mice as previously described [221]. Briefly, femurs and tibiae were harvested and separated from muscle and connective tissue. Bones were cut at either end to expose bone marrow. Sterile syringe and needles were used to flush out bone marrow using macrophage differentiation media (DMEM/10% FBS/10% L-929 Supernatant/1% PenStrep/2% MEM non-essential amino acids/1% HEPES/0.1% 55μM β-2 mercaptoethanol). Bone marrow lysate was reconstituted in

media and filtered through a sterile cell filter. Cells were cultured for 7 days in media to differentiate them into macrophages, changing differentiation media every 2 days.

7.2.7   Macrophage Treatment

Following 7 days of differentiation culture as described above, macrophages were treated with acute polarizing regimens to distinguish phenotypes over 24 hours. Naïve macrophage (M0) controls were treated with basal media for 24 hours. M1 (20 ng/mL IFN-γ and 100 ng/mL LPS) and M2 (20 ng/mL IL-4) polarizing cytokines were used to create positive controls for classical pro- and anti-inflammatory macrophages. ECM degradation products were neutralized and diluted to 1000 μg/mL in macrophage media to isolate biochemical effects of degradation products and prevent structural moieties from forming. Pepsin buffer (1 mg/mL pepsin in 0.01 M HCl) diluted in macrophage media was used as a control. Another set of treatment groups involved 24-hour exposure of ECM degradation products followed by 24-hour treatment with either the M1 or M2 treatment regimen.

7.2.8   Indirect Immunofluorescent Antibody Labeling

Cells were fixed with 2% paraformaldehyde (PFA) for 30 minutes then washed in 1XPBS. Cells were incubated in blocking buffer (2% donkey serum, 1% bovine serum albumin (BSA), 0.1% Triton X-100, 0.1% Tween-20) for 1 hour at room temperature. Primary antibodies were diluted in this blocking buffer as follows and incubated overnight at 4 °C: iNOS (1:100, Abcam 3523) or Arginase-1 (1:200, Abcam 91279). iNOS is a classical M1 macrophage marker whereas Arginase-1 is a classical M2 macrophage marker. Cells were washed in 1XPBS then incubated in

the appropriate fluorescently-labeled secondary antibody solution in blocking buffer for 1 hour at room temperature (donkey anti-rat Alexa Fluor 488, Invitrogen, 1:200; donkey anti-rabbit Alexa Fluor 488, Invitrogen, 1:300). Cell nuclei were counterstained with DAPI. Cells from 2 month old mice were imaged nine times in the center of each well at 10X magnification using automated position capture function to remove bias from subjective image location acquisition. All imaging was performed on an Axio observer T1 microscope. Mean fluorescence intensity of cells was analyzed using Cell Profiler software (Broad Institute). Briefly, DAPI images were used by the program to identify cell nuclei then FITC images were used to identify cell borders around the identified nuclei. The mean fluorescent intensity was calculated by averaging the pixel intensities (scale of 0 to 1) across the entire cell area. Mean fluorescence intensity values were averaged for all imaged cells in each well.

7.2.9   Taqman gene expression assay

Following treatments, macrophages (n=5 biological replicates from 5 young (2 month) and 5 aged (18 month) mice) were harvested for RNA using Qiagen RNEasy MiniPrep RNA Isolation Columns following standard protocol. RNA was quantified using a NanoDrop Lite Spectrophotometer (Thermo). cDNA templates were created from 1 µg of RNA using Invitrogen High Capacity RNA-to-cDNA kits (Thermo). Taqman Gene Expression Assays (Thermo) were performed for the following commonly reported M1 and M2 macrophage genes: Nos2 (Mm00440502_m1), IL1b (Mm00434228_m1), IL12b (Mm01288989_m1), TNFa (Mm00443258_m1), MHC-II (Mm01181326_m1), Arg (Mm00475988_m1), Retlna (Fizz1) (Mm00445109_m1), Mrc1 (Mm01329362_m1), IL10 (Mm01288386_m1), and PPARg (Mm00440940_m1).

7.2.10 Phagocytosis Assay

Following treatments, 50 µL of supernatant from macrophages were transferred into a fresh plate. Nitrite content was assayed using a Greiss Reagent system. Briefly, 50 µL of sulfanilamide (1% in 5% phosphoric acid) was added to supernatants for 10 minutes. Then, 50 µL of 0.1% N-1-napthylethylenediamine in water was added to the mixture for an additional 10 minutes. The absorbance at 540 nm was measured using a BioTek SYNERGY HTX spectrophotometer.

7.2.11 Nitric oxide assay

Following treatments, 50 µL of supernatant from macrophages were transferred into a fresh plate. Nitrite content was assayed using a Greiss Reagent system. Briefly, 50 µL of sulfanilamide (1% in 5% phosphoric acid) was added to supernatants for 10 minutes. Then, 50 µL of 0.1% N-1-napthylethylenediamine in water was added to the mixture for an additional 10 minutes. The absorbance at 540 nm was measured using a BioTek SYNERGY HTX spectrophotometer.

7.3   RESULTS

7.3.1   Characterization of glycated ECM

Glycated ECM were pepsin digested for treatment of macrophages. Visual inspection showed that high concentration (250 mM) of glycation prevented pepsin digestion of glycated ECM (Figure 63). Old muscle ECM degradation products appeared more opaque than young muscle ECM while diabetic ECM appeared more translucent. All glycated ECM increased in opaqueness compared to young muscle ECM.
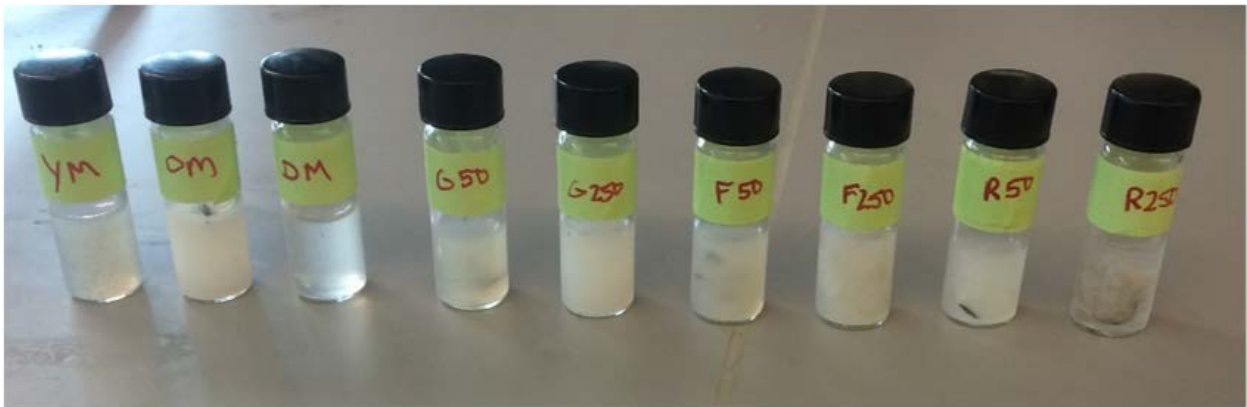
Figure 63: Pepsin digests of young, old, diabetic and glycated muscle ECM.

The presence of fluorescent AGEs were detected using size exclusion chromatography (SEC) on UV-Visible light (UV-Vis) high performance liquid chromatography (HPLC). Three emission spectra were observed for fluorescent AGEs: 335nm, 385nm and 440nm. A standard signal for protein, 280nm, was used as a marker for elution of ECM degradation products. HPLC analysis of ECM degradation products found positive fluorescence signals at the 280nm and 335nm wavelengths (Figure 64).
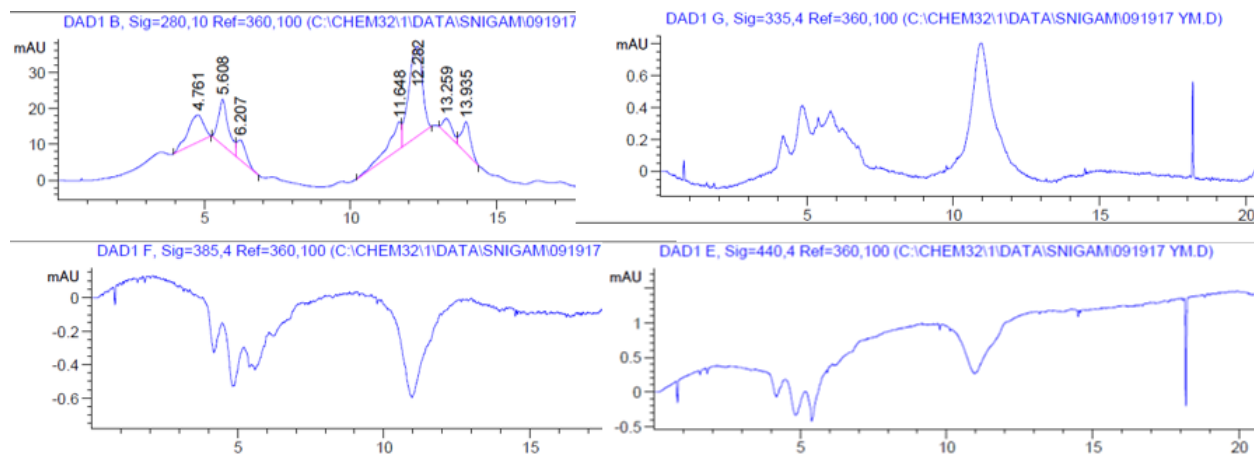
Figure 64: Size exclusion HPLC analysis of muscle ECM for fluorescent AGE signatures.

All extracellular matrix degradation products analyzed had peaks around 5 minutes and another set between 10-15 minutes. Young muscle ECM had several peaks at both elution times in the 280nm emission spectra while having several peaks at 5 minutes and 1 peak at 11 minutes in the 335nm emission spectra (Figure 65). Old muscle ECM had similar peaks in the 10-15 minute range of both emission spectra but lost the peaks at 5 minutes seen in young (Figure 66). Diabetic muscle ECM lost the peak at 5 minutes in the 280nm emission spectra but this peak was retained at 335nm (Figure 67). Ribosylated, glucosylated and fructosylated ECM all had similar peaks to diabetic muscle ECM (Figure 68-Figure 70).

144
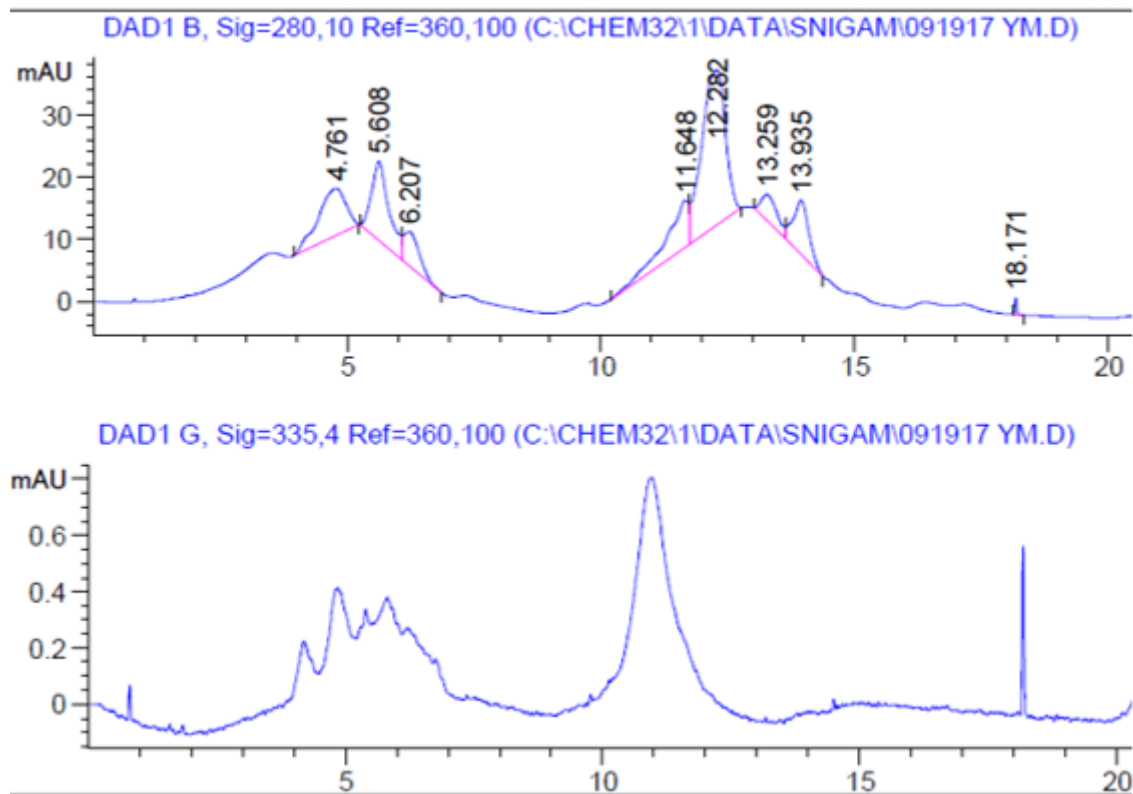
Figure 65: Size exclusion HPLC of young muscle ECM degradation products.
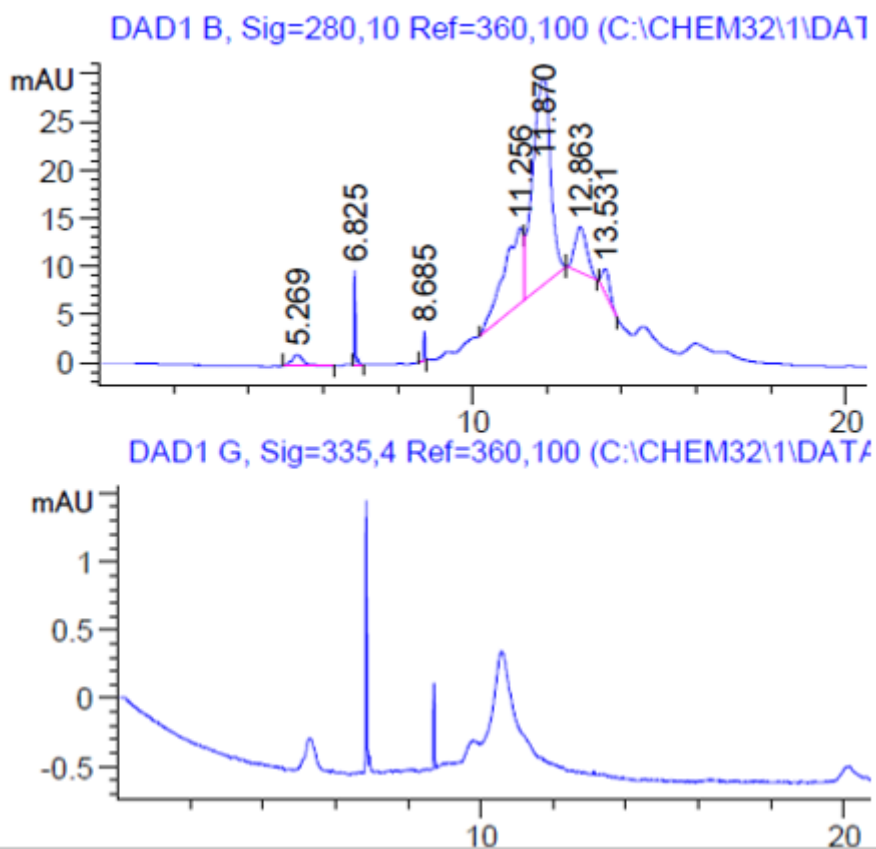
Figure 66: Size exclusion HPLC of old muscle ECM degradation products.
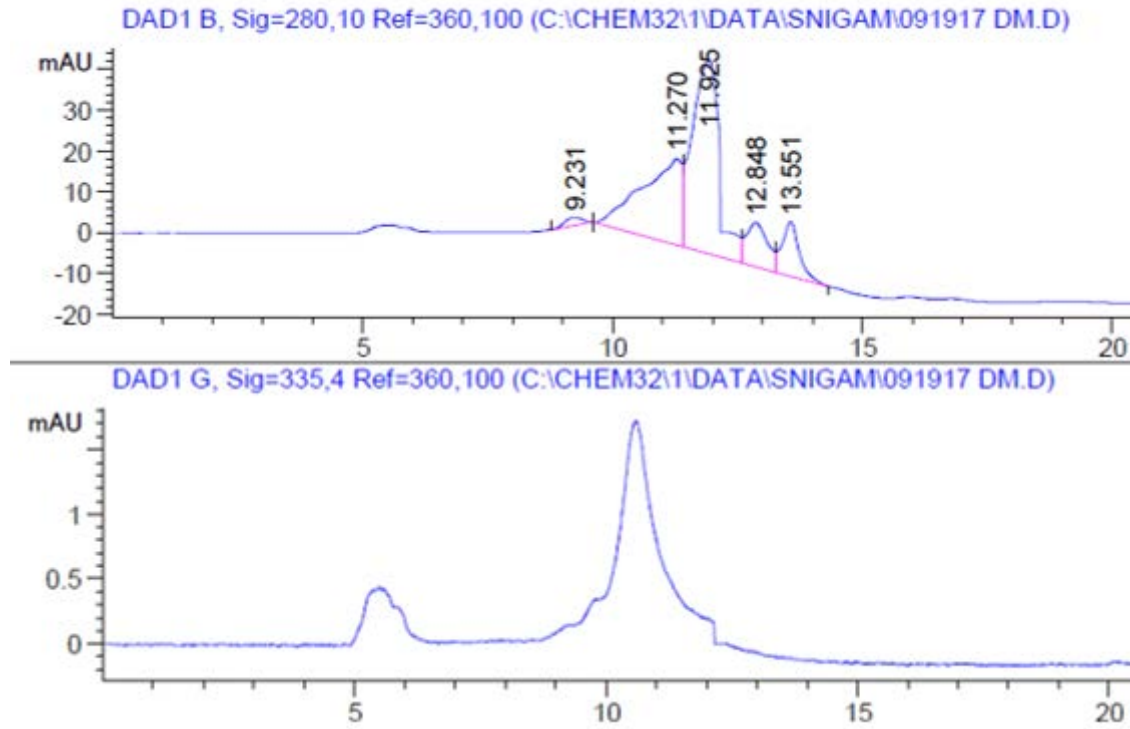
Figure 67: Size exclusion HPLC for diabetic muscle ECM degradation products.
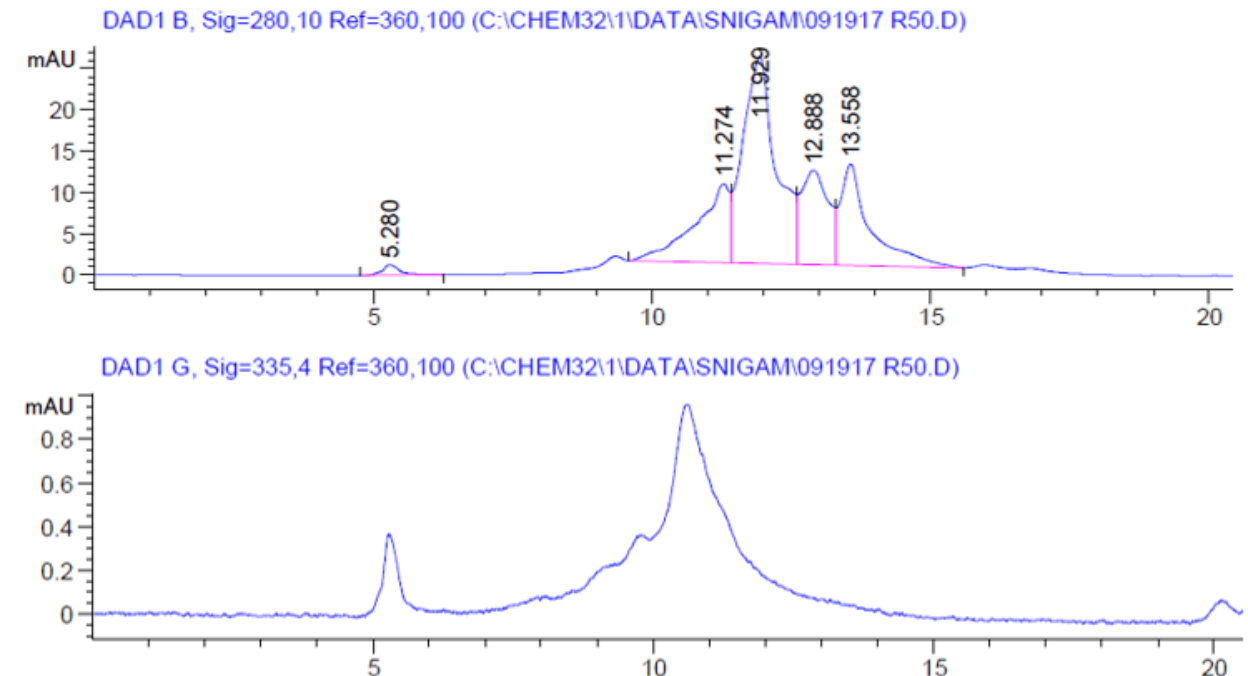
Figure 68: Size exclusion HPLC for ribosylated young muscle ECM degradation products.
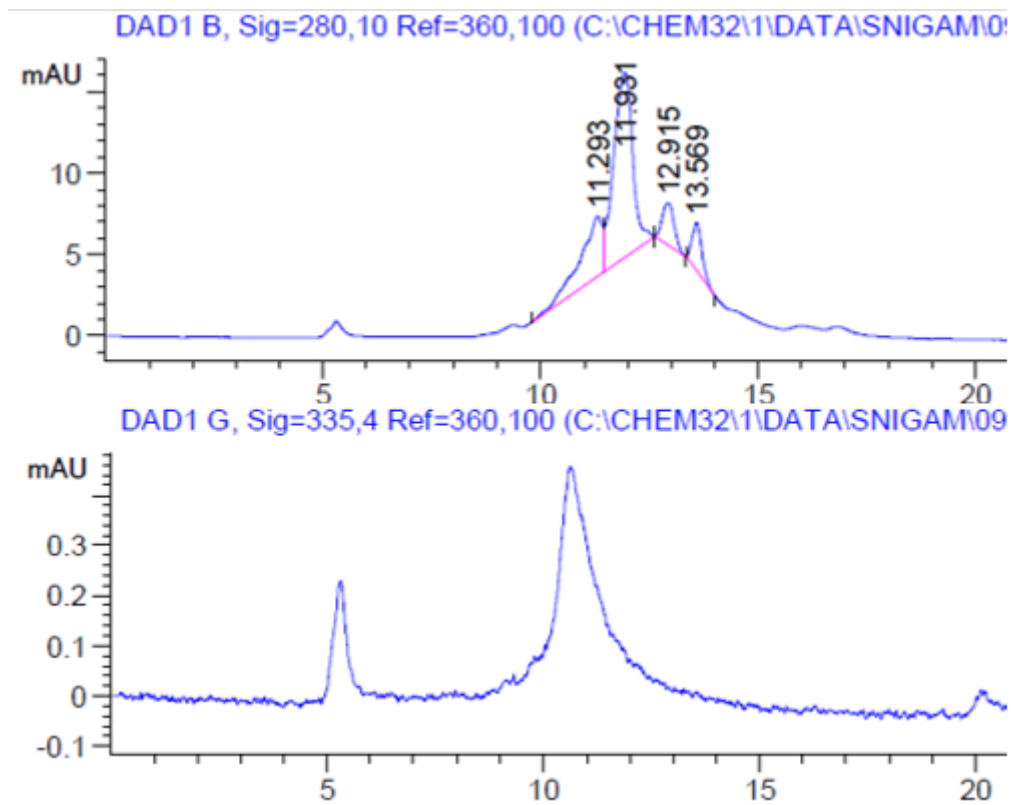
Figure 69: Size exclusion HPLC of glucosylated young muscle ECM degradation products.
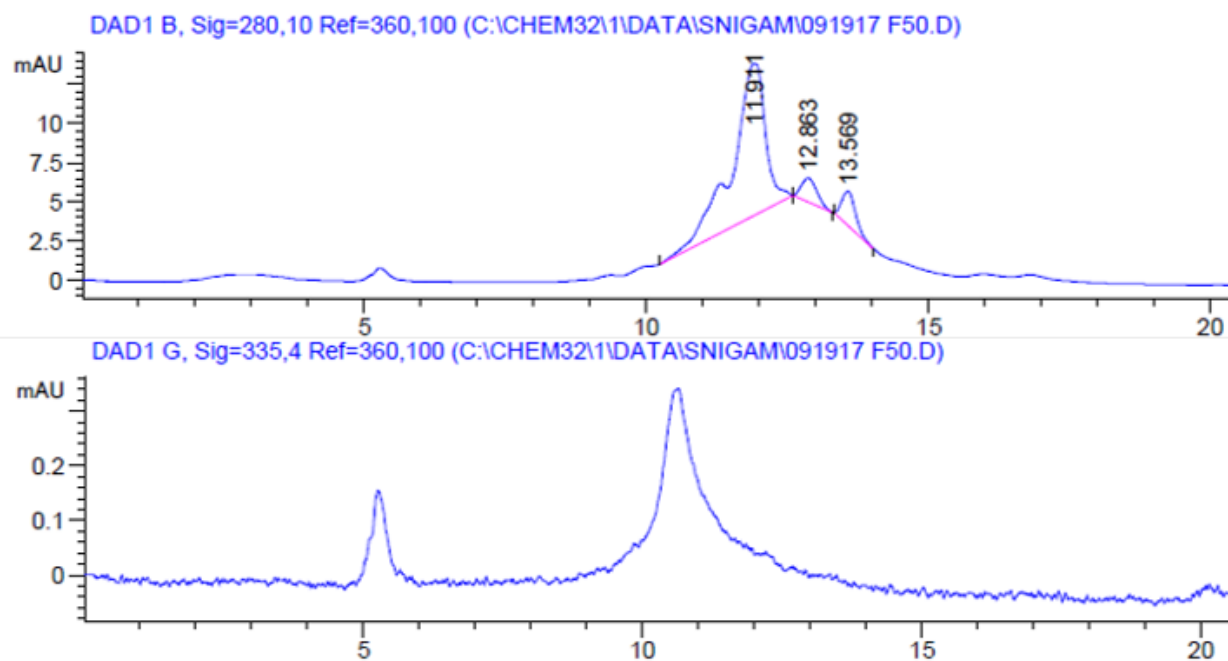
Figure 70: Size exclusion HPLC of fructosylated young muscle ECM degradation products.

In order to evaluate presence of functional groups in extracellular matrix, fourier-transform infrared spectroscopy (FTIR) was performed on whole decellularized ECM scaffolds (Figure 71). Young, old and glycated muscle ECM all had similar FTIR spectra expected from a protein-rich material. Old muscle ECM had two large peaks around 2800-3000 cm^{-1}, which is characteristic for –C-H stretch and –C-H aldehydic. Peaks in this range in biological materials is typical for presence of lipids [304]. Glycated muscle ECM had a slight reduction in the level of peaks in the 2800-3000 cm^{-1} range compared to young. All samples had two peaks around 1550-1650 cm^{-1} indicative of amide bonds from protein. Old muscle ECM had another peak to the left of these peaks, which could be a peak associated with the ester bonds in triglycerides which is typically found around 1740 cm^{-1}. Old muscle ECM also has a higher peak just right of the two amide bond peaks, which could be the peak associated with the –CH$_2$ bending in lipids normally found around 1452-56 cm^{-1}. The other two peaks elevated in old muscle ECM between 1200-1000 cm^{-1} could be the CO-O-C anti-symmetric stretching found between 1171-1160 cm^{-1} associated with phospholipids, triglycerides, and cholesterol esters. The other possibility is the PO$_2^-$ symmetric stretching associated with nucleic acids and phospholipids found at 1083-1078 cm^{-1} which is also associated with the C-O stretch from glycogen, polysaccharides and glycolipids [304]. All of these data suggest there could be an increased triglyceride or other lipid content in old muscle ECM. Glycation of young ECM did not appear to alter the FTIR spectra in a significant way.
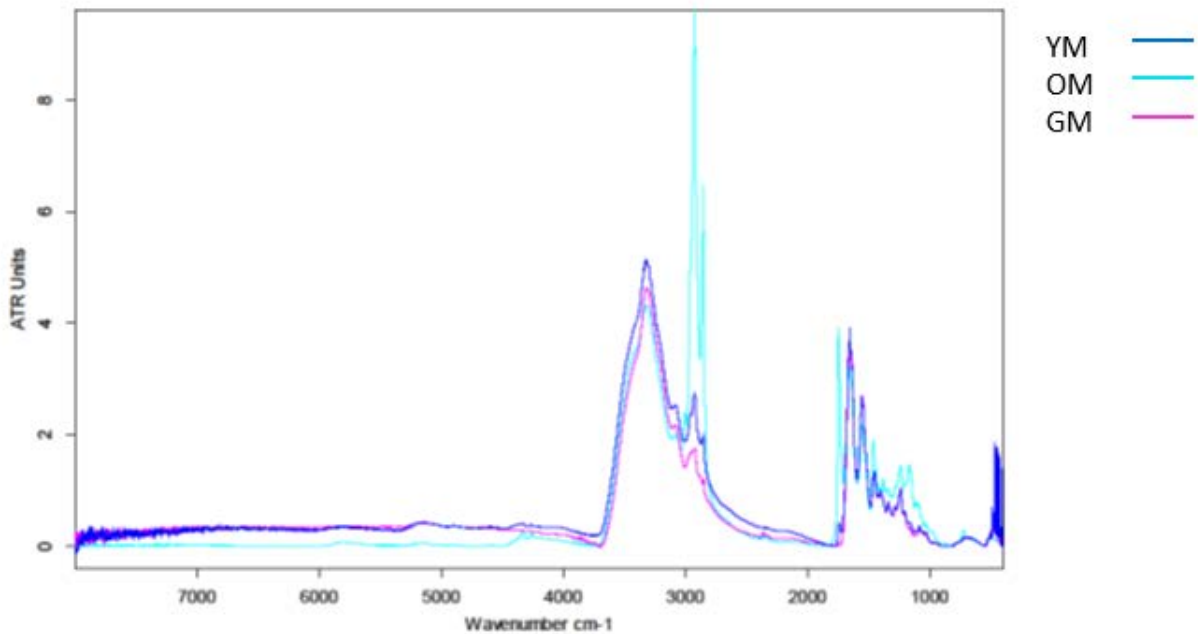
Figure 71: Fourier-transform infrared spectroscopy of decellularized muscle ECM.

In order to assess the levels of protein oxidation in young, old, diabetic or glycated muscle ECM, a protein carbonyl assay was performed on ECM pepsin digests. When normalized to protein content as assessed by BCA assay, old muscle ECM had a reduction in protein carbonyl content while diabetic muscle ECM had an increased content (Figure 72). Artificial glycation of muscle ECM with glucose or fructose led to increase in protein carbonyl content to levels similar to diabetic muscle ECM. Ribosylated muscle ECM led to higher level of protein oxidation than other forms of glycation.

Protein Carbonyl Content
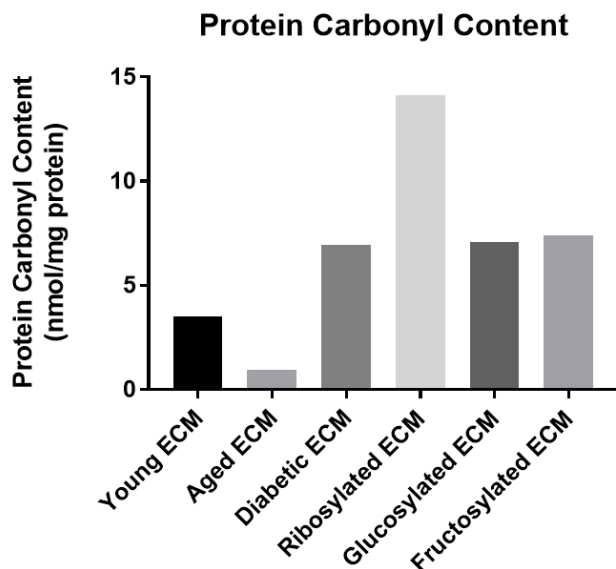
Figure 72: Protein carbonyl content of muscle ECM glycated with different reducing sugars. Mean values shown.

Assessment of protein carbonyl content in native and decellularized muscle showed that glycation significantly increased protein oxidation compared to all other samples. Old and diabetic muscle and muscle ECM had lower quantitative levels of protein oxidation compared to young muscle or muscle ECM, respectively (Figure 73).
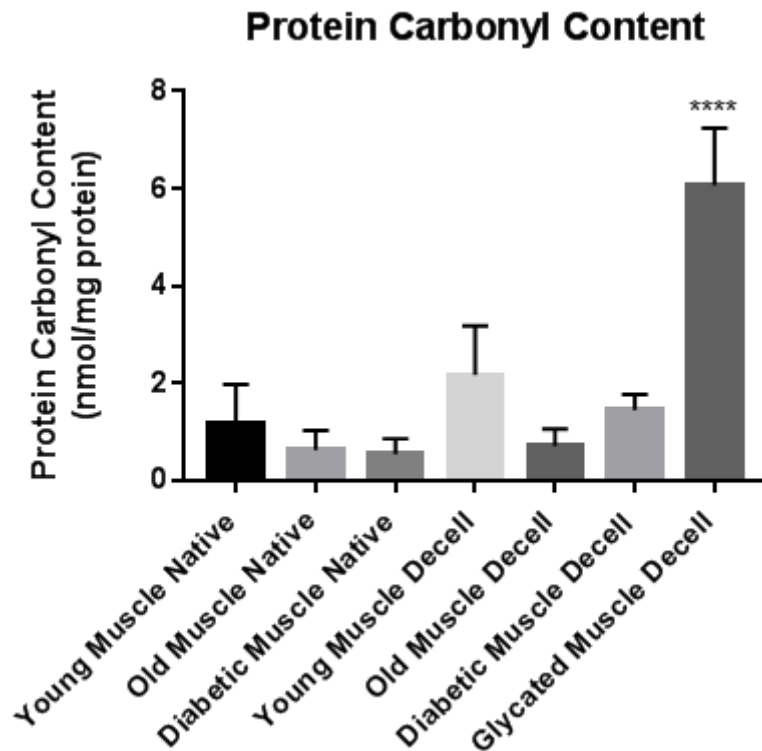
Figure 73: Protein carbonyl content of native and decellularized young, old and glycated ECM.

Data shown as mean ± S.D. Statistical significance reported as *p<0.05, **p<0.01, ***p<0.001, ****p<0.0001

7.3.2 Macrophage phenotype and function

Murine bone marrow-derived macrophages were treated with ECM degradation products to determine the effect of ECM glycation upon macrophage phenotype and function. To assess pro-inflammatory (M1) macrophage polarization, macrophages were immunofluorescently labeled for iNOS following fixation. Interferon-γ/LPS treatment resulted in significantly higher iNOS immunoexpression, as expected (Figure 74A). Old muscle ECM had significantly higher iNOS immunolabeling than diabetic muscle ECM (Figure 74A). Ribosylated ECM elicited significantly higher iNOS immunoexpression than both young and old ECM while glucosylated

ECM reduced iNOS immunolabeling (Figure 74A). With pro-inflammatory cytokine stimulus, young muscle ECM significantly reduced iNOS immunolabeling compared to M1 controls, diabetic ECM and ribosylated and fructosylated ECM (Figure 74B). High concentrations of glycation significantly increased iNOS immunoexpression over all other groups with pro-inflammatory or anti-inflammatory stimulus (Figure 74B-C). With IL-4 stimulus, young muscle ECM significantly increased iNOS immunoexpression over M2 controls and all other ECM groups (Figure 74C).
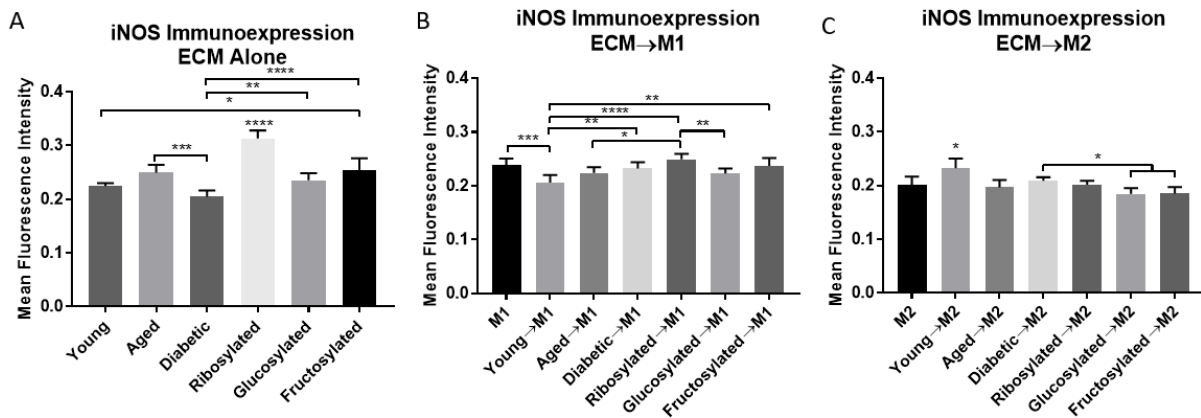
Figure 74: Immunolabeling for iNOS on macrophages treated with glycated muscle ECM.

Data shown as mean ± S.D. Statistical significance reported as *p<0.05, **p<0.01, ***p<0.001, ****p<0.0001

Anti-inflammatory (M2) macrophages phenotype was assessed via immunolabeling for arginase-1. Interleukin-4 stimulation induced significantly increased arginase-1 immunoexpression as expected (Figure 75A). There were no differences in arginase-1 immunolabeling in any of the non-glycated ECM groups. However, high concentrations of ribose and fructose glycation resulted in significantly higher arginase-1 immunoexpression (Figure 75A). With pro-inflammatory stimulus, young, old and diabetic ECM all significantly increased arginase-1

immunolabeling over M2 controls (Figure 75B). Diabetic muscle ECM with M1 cytokines induced lower arginase-1 immunoexpression than old muscle ECM (Figure 75B). Glucosylated ECM and fructosylated ECM at high concentrations significantly increased arginase-1 immunoexpression over young ECM with M1 stimulus (Figure 75B). With IL-4 stimulus, there was no difference between any ECM groups or with M2 controls (Figure 75C).
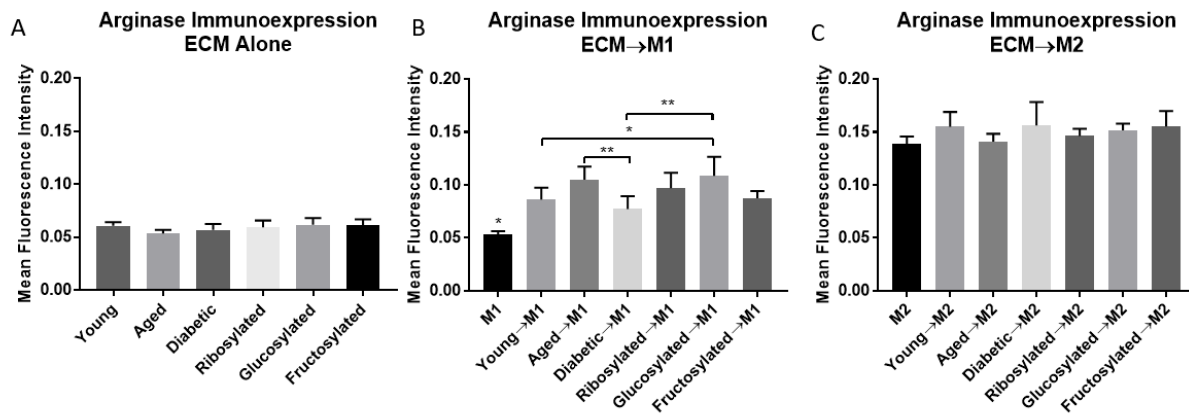
Figure 75: Immunolabeling for arginase on macrophages treated with glycated ECM.

Data shown as mean ± S.D. Statistical significance reported as *p<0.05, **p<0.01, ***p<0.001, ****p<0.0001

To assess the effect of ECM glycation upon macrophage function, macrophages were incubated with FITC-labeled E. Coli particles to assess phagocytic uptake. Interferon-γ/LPS treatment resulted in significantly higher phagocytosis than macrophages treated with IL-4 as expected (Figure 76A). Diabetic ECM as well as high concentration glucosylated ECM significantly reduced phagocytosis compared to young and old muscle ECM (Figure 76A). Fructosylated ECM and high concentration ribosylated ECM both reduced phagocytosis compared to old ECM (Figure 76A). With pro-inflammatory cytokine treatment, old and diabetic ECM induced higher phagocytosis than M1 controls and young muscle ECM (Figure 76B). Low concentration

ribosylation and fructosylation also increased phagocytosis over young ECM with pro-inflammatory cytokine stimulus. All high concentration glycated ECM reduced phagocytosis compared to old muscle ECM with pro-inflammatory cytokine stimulus. With anti-inflammatory cytokine stimulus, old and diabetic muscle ECM increased phagocytosis over M2 controls and young muscle ECM (Figure 76C). Low concentration glycated ECM all increased phagocytosis compared to young ECM with IL-4 stimulus. All types of glycated ECM except low concentrations of glucose significantly decreased phagocytosis with M2 stimulus compared to old muscle ECM (Figure 76C).
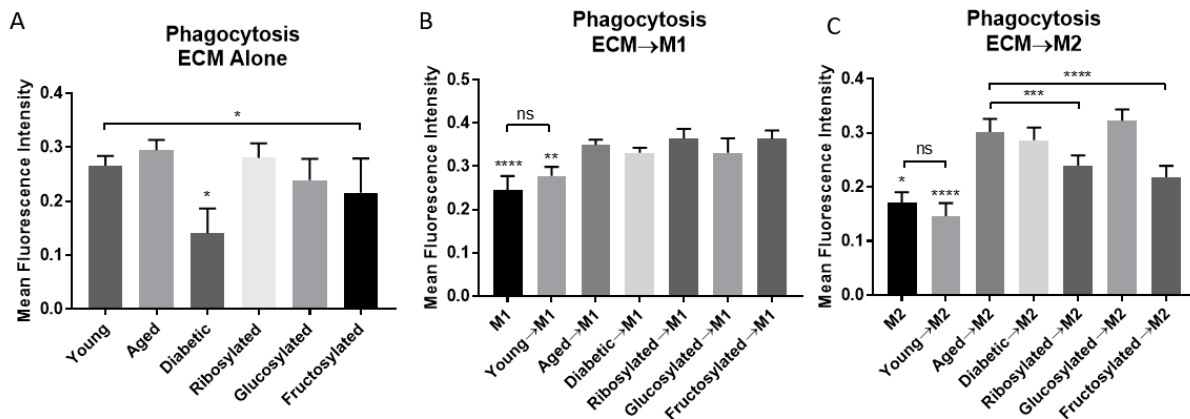
Figure 76: E. coli phagocytosis in macrophages treated with glycated ECM.

Data shown as mean ± S.D. Statistical significance reported as *p<0.05, **p<0.01, ***p<0.001, ****p<0.0001

To further assess the effect of ECM glycation upon macrophage function, nitric oxide production was assessed in the supernatants of macrophages following treatment using the Greiss reagent system. Pro-inflammatory cytokine stimulus resulted in significantly increased nitric oxide production as expected (Figure 77A). Old muscle ECM produced significantly higher nitric

155

oxide than young or diabetic ECM (Figure 77A). Low concentration glycated ECM all increased nitric oxide production compared to young ECM while low concentration ribosylation and glucosylation increased nitric oxide compared to old ECM (Figure 77A). With pro-inflammatory stimulus, neither young, old nor diabetic ECM changed nitric oxide production from M1 controls (Figure 77B). Low concentration ribosylation and glucosylation of ECM resulted in higher nitric oxide production compared to young muscle ECM with pro-inflammatory stimulus (Figure 77B). With anti-inflammatory cytokine stimulus, young muscle ECM increased nitric oxide production over M2 controls as well as old and diabetic muscle ECM (Figure 77C). Low concentration glycation increased nitric oxide production over young, old and diabetic ECM with anti-inflammatory cytokine stimulus (Figure 77C).
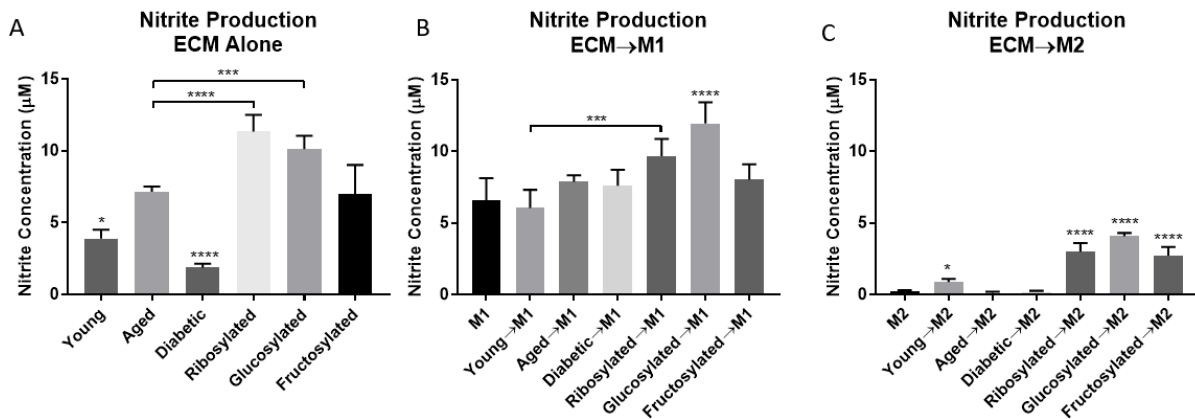
Figure 77: Nitric oxide production in supernatants of macrophages treated with glycated ECM.

Data shown as mean ± S.D. Statistical significance reported as *$p<0.05$, **$p<0.01$, ***$p<0.001$, ****$p<0.0001$

7.4   DISCUSSION

Advanced glycation end-products (AGEs) are associated with many disease states including aging and diabetes [305, 306]. Through RAGE signaling, AGEs can cause pro-inflammatory responses, cellular dysfunction and tissue damage [307]. While the formation of AGEs has been studied extensively in cellular and blood proteins such as albumin, the effect of glycation on structural proteins of the extracellular matrix has not been investigated [308]. This study showed the direct effects of glycation upon the macrophage response to extracellular matrix. Of the two concentrations of reducing sugars tested, the higher concentration of 250mM inhibited the degradation of ECM via pepsin. This confirms previous hypotheses that AGEs can inhibit ECM turnover [309]. However, due to the fact that aged muscle ECM will solubilize with pepsin degradation, these high levels of reducing sugars probably glycated the ECM far beyond physiologic levels of normal aging in mice. It is worth noting that the production and accumulation of AGEs is a slow process which takes years [310] .

There were also differences in glycation and macrophage response to the different type of reducing sugar used for these experiments. Fructose has previously been shown to glycated more rapidly than glucose, while ribose is much stronger than both [311]. Glucose and fructose are naturally occurring sugars that are a part of glycolysis as well as being commonly found in the diet [312]. Glucose is mainly found in skeletal muscle as glycogen but is rapidly absorbed from the bloodstream following exercise [313]. Ribose is a naturally sugar used for the synthesis of riboflavin (vitamin B2), RNA, and ATP [314-316]. As muscle uses ATP as an energy source for contractility, ribose is freely available for glycation in muscle as well [317]. Therefore, artificial glycation by any of these sugars is relevant to normal muscle aging.

The effects of ECM glycation upon macrophage polarization was most noticeable in the upregulation of iNOS protein levels and nitric oxide production. This response is expected due to AGE signaling through the RAGE receptor to trigger an NF-κB transcription profile [318]. iNOS is one of many proteins whose transcription is upregulated by NF-κB [319]. High concentrations of glycation resulted in high levels of iNOS in both pro- and anti-inflammatory conditions, suggesting the dysfunctional macrophage response AGEs can create. Lower levels of glycation interestingly elevated nitric oxide production in all cases while higher levels did not. Higher levels may create such a dysfunctional environment that prevents normal macrophage function while lower levels create a truly pro-inflammatory macrophage environment.

7.5   CONCLUSION

This study showed that skeletal muscle extracellular matrix was successfully glycated with multiple sugar types. These glycated ECM had a direct effect on macrophage polarization, creating a pro-inflammatory or dysfunctional phenotype. This suggests that glycated ECM can be used to observe the direct effects of glycated microenvironments upon the regeneration of muscle following injury.

8.0 EFFECT OF AGED AND GLYCATED MUSCLE ECM UPON HOST RESPONSE FOLLOWING MUSCLE INJURY

8.1 INTRODUCTION

Extracellular matrix acts as the supporting structure of a tissue and dynamically changes in a reciprocal relationship with cells of that tissue. ECM changes with aging and disease and can affect the responses of cells in these altered states. Therefore, ECM can be used as a model for aged microenvironments to more fully understand their effect on cellular function. Skeletal muscle strength and healing potential are known to decrease with aging [232]. The immune response, which is integral to muscle regeneration, is also dysfunctional with age [259]. Macrophage polarization in particular has been shown to be necessary for appropriate skeletal muscle healing [51]. There has been no direct investigation to determine whether age-related changes in skeletal muscle extracellular matrix influence macrophage polarization and contribute to altered host responses observed in aged individuals during skeletal muscle injury.

Decellularization techniques have been used for decades now to develop biomaterials for a variety of surgical and tissue engineering strategies [260]. These same methodologies can be used to harvest the extracellular matrix from skeletal muscle of animals differing in age or disease state in order to understand how these factors contribute to altered physiology [261]. Previous investigations into changes in aging's effect on skeletal muscle ECM has relied on

histologic analysis of intact muscle tissue only [262]. Therefore, in order to isolate the role of extracellular matrix in altered host responses during injury, bioengineering techniques must be utilized to separate the ECM from the rest of the skeletal muscle tissue.

Advanced glycation end-products (AGEs) have been implicated in the pathogenesis of tissues during aging and diabetes [177]. AGEs result from the non-enzymatic glycation of biomolecules including proteins, lipids and nucleic acids [296]. They can produce crosslinks which cause increased stiffness and altered degradation [297-299]. AGEs are known to be recognized by the receptor for advanced glycation end-products (RAGE) which signals through the NF-κB pathway [300]. AGEs have been shown to directly activate pro-inflammatory macrophage responses through this pathway [194]. AGEs have also been shown to increase in aged muscle tissue [262]. However, glycation of aged muscle ECM itself has not been investigated. In order to investigate the mechanism of advanced glycation end-products, *in vitro* glycation of young muscle ECM can be performed [220]. This comprises a more physiologically relevant investigation of the role of glycation than current studies involving glycated bovine serum albumin.

The present study seeks to combine several bioengineering strategies to study the isolated effects of aging and glycation of the extracellular matrix upon the macrophage response during skeletal muscle injury *in vivo*. While many studies focus on cellular dysfunction during aging, this study seeks to understand the isolated role of alterations in the extracellular microenvironment.

8.2 METHODS

8.2.1 Scaffold Preparation

Skeletal muscle extracellular matrix was prepared using modified methods previously developed [261]. Briefly, abdominal muscle was harvested from 4 month and 18 month old C57BL6/J mice (NIA). Muscle was washed in water. Samples were enzymatically digested in 0.2% trypsin/0.2% EDTA for 2 hrs at 37 °C with agitation. All subsequent steps were performed on a mechanical shaker at 300 rpm. Samples were washed once in water and twice in 1XPBS, 30 mins each. Samples were decellularized using 2% sodium deoxycholate for 5 hrs, washed in water and twice in 1XPBS for 30 mins each and then decellularized with 2% sodium deoxycholate for 14-16 hrs and 1% Triton X-100 for 1 hr. Samples were then washed twice with 1XPBS then twice with water for 30 mins each. Samples used for implantation were terminally sterilized with ethylene oxide.

8.2.2 Abdominal Wall Partial Thickness Defect Implantation

Four month old C57BL6/J mice (Jackson) were anesthetized using isofluorane and analgesized using Buprenex prior to surgical manipulation. Abdominal skin was incised and abdominal muscle exposed. Partial thickness defects (1 cm^2 were created in the abdominal muscle by removing 2 of the 3 muscle layers. Rehydrated 1 cm^2 muscle ECM scaffolds (n=5 per treatment) were sutured over the defect using polypropylene sutures. Skin incisions were sutured close using PGCL suture. Animals were maintained on Buprenex and Baytril for 3 days post-operation. ECM was explanted following 3, 7, 14 and 90 days post-implantation. Sections were

fixed in 10% NBF for histologic analysis or *RNALater* Stabilization Solution (Thermo) for gene expression analysis.

8.2.3   Histologic Analysis

Paraffin sections were stained for hematoxylin & eosin as an evaluation of cellularity and remodeling. Briefly, slides were deparaffinized and rehydrated to water. Slides were stained in Harris hematoxylin for 8 minutes then washed twice for 30 seconds in type 1 water. Hematoxylin was differentiated in 5% glacial acetic acid for 1 minute then washed twice for 30 seconds in type 1 water. Hematoxylin was blued using Scott's water for 15 seconds then washed twice for 1 minute each. Slides were stained with alcoholic eosin for 2 minutes then washed twice in 95% ethanol and twice in 100% ethanol for 30 seconds each. Slides were washed twice in xylenes for 1 minute then mounted with a resinous mounting media.

Paraffin sections were stained with Alcian blue as an indicator of glycosaminoglycan content. Briefly, slides were deparaffinized and rehydrated to water. Slides were stained in 1% (w/v) alcian blue/3% acetic acid (v/v) pH 2.5 solution for 30 minutes then washed in running tap water for 2 minutes. Slides were counterstained in nuclear fast red solution for 5 minutes then washed in running tap water for 1 minute. Slides were dehydrated in 1 change of 95% ethanol and 2 changes of 100% ethanol for 3 minutes each. Slides were then cleared in xylenes and mounted with a resinous mounting media.

Paraffin sections were stained with Masson's trichrome as an indicator of collagen content. Briefly, slides were deparaffinized and rehydrated to water. Slides were re-fixed in Bouin's solution for 1 hour at 56 °C to improve staining quality. Slides were rinsed in running

tap water for 10 minutes to remove the yellow color. Slides were then stained in Weigert's iron hematoxylin working solution for 10 minutes then rinsed in running warm tap water for 10 minutes then washed in distilled water. Slides were stained in Biebrich scarlet-acid fuchsin solution for 10 minutes then washed in distilled water. The stain was differentiated in phosphomolybdic-phosphotungstic acid solution for 10 minutes. Slides were transfered directly to aniline blue solution and stained for 10 minutes then rinsed briefly in distilled water and differentiate in 1% acetic acid solution for 5 minutes then washed in distilled water. Slides were dehydrated very quickly and cleared in xylene then mounted with resinous mounting medium.

Paraffin sections were stained with PicroSirius Red as an indicator of collagen content. Briefly, slides were deparaffinized and rehydrated to water. Slides were stained in PicroSirius Red solution for 1 hour then differentiated in 35% acetic acid for 10 seconds. Slides were quickly dehydrated and cleared in xylenes then mounted with resinous mounting media.

Five images were taken per slide at 20X for quantitation using brightfield microscopy or circularly polarized light microscopy for PicroSirius Red. Muscle was quantified for percent regenerating muscle fibers by manually counting number of muscle fibers with centralized nuclei divided by total number of muscle fibers. Acute timepoints (3, 7, 14d) were stained using immunofluorescent antibody labeling. Briefly, slides were deparaffinized then antigen retrieved using 10mM citric acid at 95-100°C for 20 mins. Autofluorescence was quenched using a 10mM copper sulfate/50mM ammonium acetate (pH5) solution for 20 mins at 37 °C. Sections were blocked using 2% donkey serum/1% BSA/0.1% Tween-20 for 1 hour then incubated overnight at 4 °C with primary antibodies for F4/80 (1:100 BioRad MCA497), iNOS (1:100 Abcam 3523), Arginase-1 (1:200 Abcam 92179) or MyoD1 (1:100 Abcam 203383). Sections were washed in PBS then incubated for 1 hour with the appropriate Alexa Fluor 488 donkey antibody at 1:200

(Abcam). Sections were washed, counterstained with DAPI then mounted with FluoroGel mounting solution. Ninety day explants were stained immunohistochemically for fast & slow myosin heavy chain using alkaline phosphatase and DAB solutions, respectively [261].

8.2.4   Gene Expression Analysis

Explants were placed in RNALater Stabilization Solution (Thermo) at 4 °C for 2 days then solution was aspirated and samples were stored at -80 °C. Samples were thawed and RNA was extracted from remodeled ECM using the Fibrous Tissue RNA Extraction Kit according to manufacturer protocol (Qiagen). cDNA templates were created from extracted RNA using the High Capacity RNA-to-cDNA Kit (Applied Biosystems). Taqman gene expression assays were performed for primers described above in the *in vitro* methods section.

8.2.5   Statistical Analysis

Quantitative results were analyzed using a two-way ANOVA (treatment, age) with Tukey post-hoc analysis using GraphPad PRISM 7 software. Significance was determined at a p-value less than 0.05.

8.3   RESULTS

8.3.1   Histological evaluation

The host response to the implanted muscle ECM was observed with hematoxylin & eosin staining (Figure 78). The extracellular matrix scaffold is easily detectable in histologic sections as the grouping of protein fibers above the muscle injury. At 3 days post implantation, the scaffolds appear completely intact and loosely associated with surrounding tissues. There is already some cellular infiltration at 3 days but mostly on the border of the implanted ECM. At 7 days, the bioscaffolds appear to be integrated more with the surrounding tissues as cellular infiltration increases. However, remodeling of ECM scaffolds appears minimal at 7 days. By 14 days, remodeling of ECM is underway as the scaffold appears to be degraded in areas and fully infiltrated with host cells. Ninety days post-implantation, the extracellular matrix has been fully remodeled into a section of fibrous tissue with cellularity being restored to normal levels. Quantification of cellularity shows low levels of cellular infiltration at 3 days. Cellularity peaks at 7 days with young muscle ECM promoting significantly more than old or glycated ECM (Figure 78A). There was a reduction in cellularity at 14 days; however, young muscle ECM still had higher cellularity than old or glycated. By 90 days, cellularity was similar across ECM types and had returned to levels below that seen at 3 days. This suggests that old and glycated ECM impair the ability of host cells to infiltrate the site of a muscle injury.
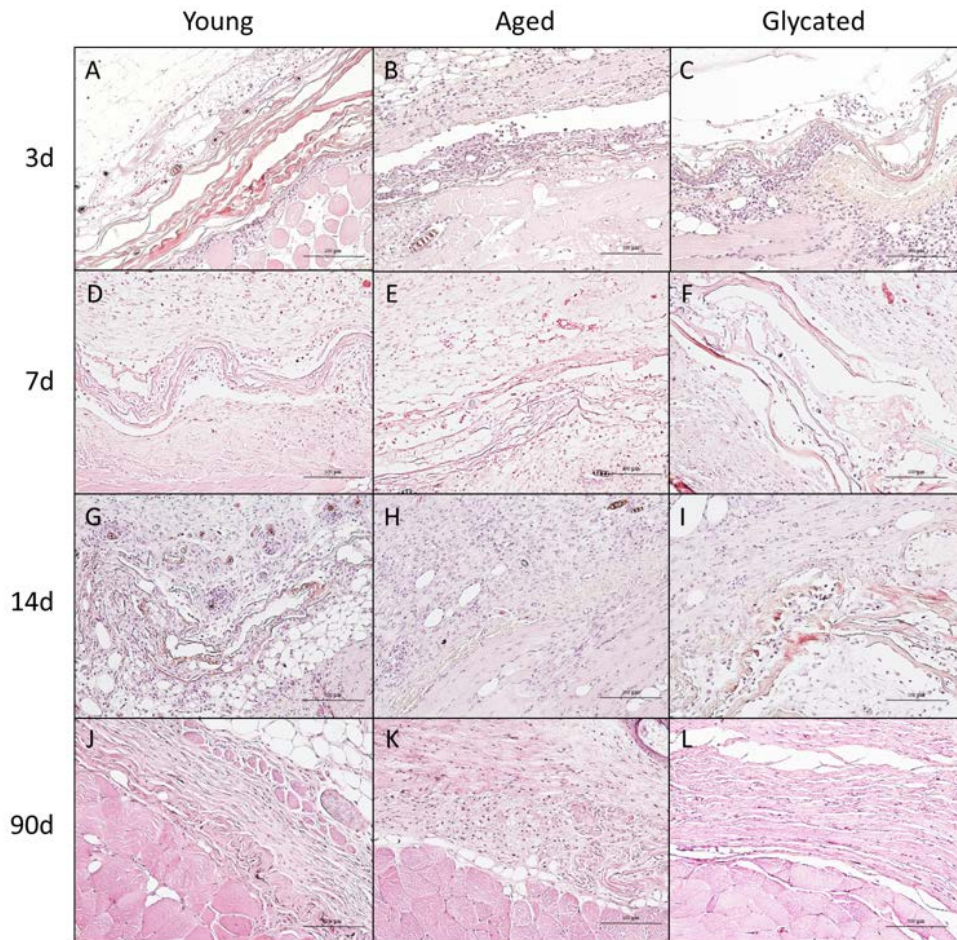
Figure 78: Hematoxylin & eosin staining of muscle ECM implanted into abdominal muscle injury.
Images taken at 20X. Scale bars indicate 100 µm.

Glycosaminoglycan production following implantation was assessed via Alcian blue staining (Figure 79). There were no differences in GAG content at 3 days. Glycosaminoglycan content increased from 3 to 7 days as well as 7 to 14 days then reduced to basal levels by 90 days (Figure 83C). There was significantly higher glycosaminoglycan production in young muscle ECM implants at 7 days over old and glycated ECM (Figure 83C). Young muscle ECM also elicited higher glycosaminoglycan production at 14 days over old muscle ECM (Figure 83C). By 90 days, young muscle ECM had lower glycosaminoglycan content than glycated muscle ECM.

Changes in glycosaminoglycan production mirrored changes in cellularity which suggests the two are related. However, further investigation would be necessary to understand if one phenomena causes the other.
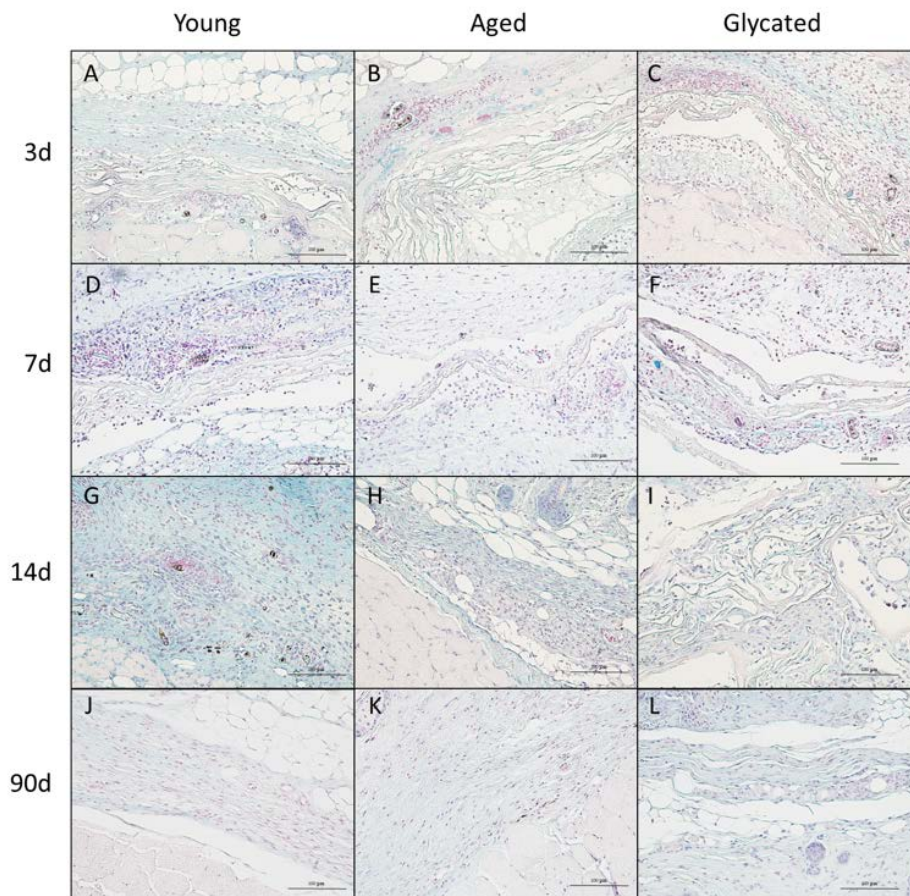
Figure 79: Alcian blue staining for muscle ECM implanted over abdominal muscle injury.

Images taken at 20X. Scale bars indicate 100 µm.

To assess collagen production, explants were stained with Masson's trichrome (Figure 80). There were no differences in any groups in 3 and 7 days post-implantation (Figure 83B). However, all groups followed the trend of increasing from 3 to 7 days, decreasing from 7 to 14 days and then increasing sharply by 90 days. Glycated muscle ECM groups resulted in significantly higher

Masson's trichrome staining at 14 and 90 days over young and old muscle ECM (Figure 83B). This suggests that glycated muscle ECM elicits increased fibrosis.
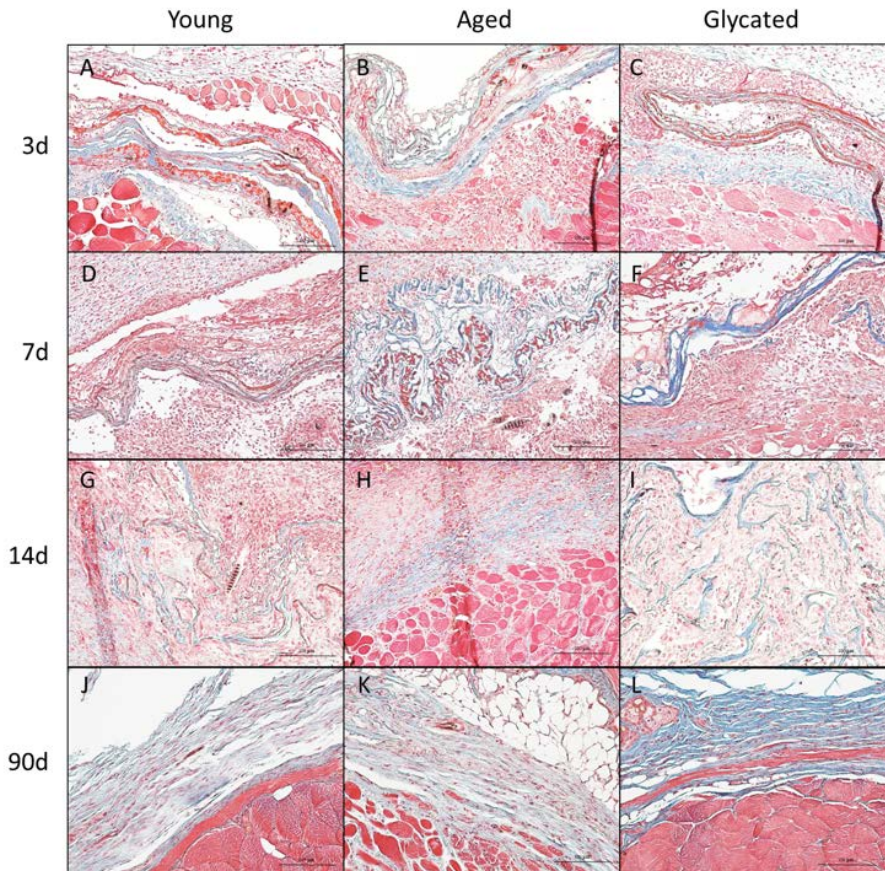
Figure 80: Masson's trichrome staining of muscle ECM implanted in abdominal muscle injury. Images taken at 20X. Scale bars indicate 100 µm.

In order to analyze collagen fiber alignment, PicroSirius red staining was performed on paraffin sections (Figure 81). Staining appeared to decrease from 3 to 7 days as the collagen was slowly remodeled by host cells. Staining was much brighter at 90 days, similar to Masson's trichrome staining, indicative of increased collagen content and fiber alignment.
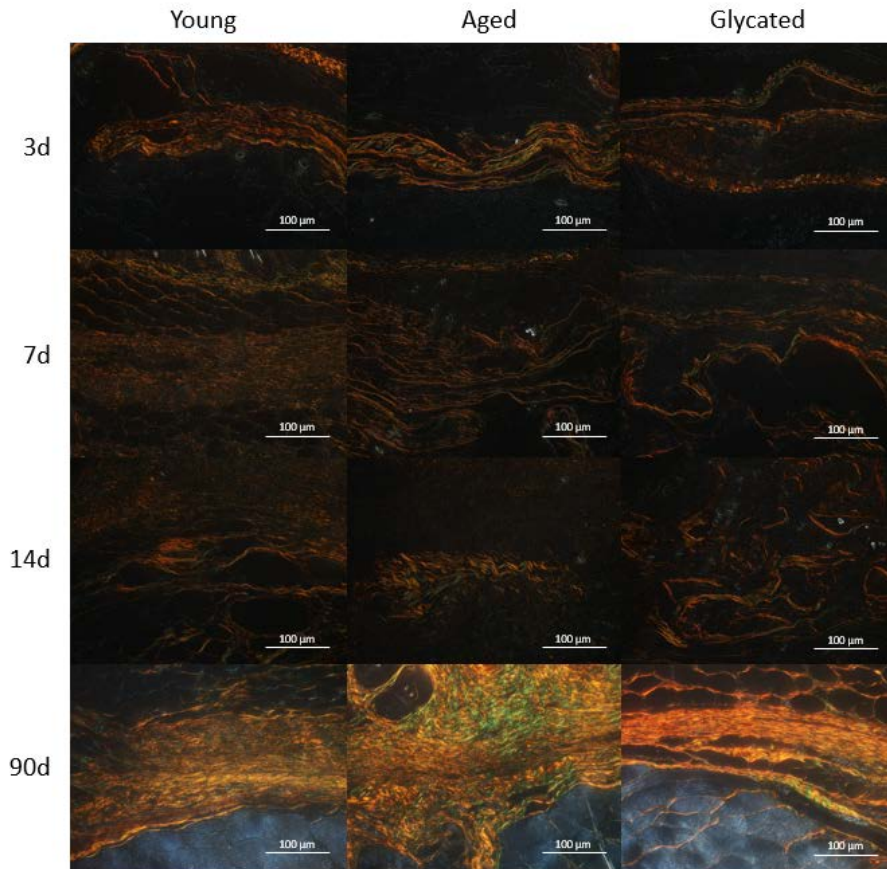
Figure 81: PicroSirius Red staining of muscle ECM implanted into abdominal muscle injury.

Images taken at 20X. Scale bars indicate 100 µm.

Muscle regeneration was quantified by counting the number of muscle fibers with centralized nuclei versus the number with peripheral nuclei (Figure 82). Quantification of regenerating muscle fibers via nuclei centralization showed that there was no substantial muscle fiber regeneration occurring 3 days post-injury (Figure 83D). By 7 days, significant muscle regeneration was underway as young and aged ECM samples had 50-60% muscle fiber nuclei centralization. However, glycated ECM elicited significantly less muscle regeneration at 7 days compared to young and old ECM, showing that glycation has an inhibitory effect on both inflammation and stem cell activation. Aged muscle ECM did not seem to inhibit muscle

regeneration even if there were signs of chronic inflammation. This is counter to reports of reduced numbers of regenerating myofibers in aged mice [43].
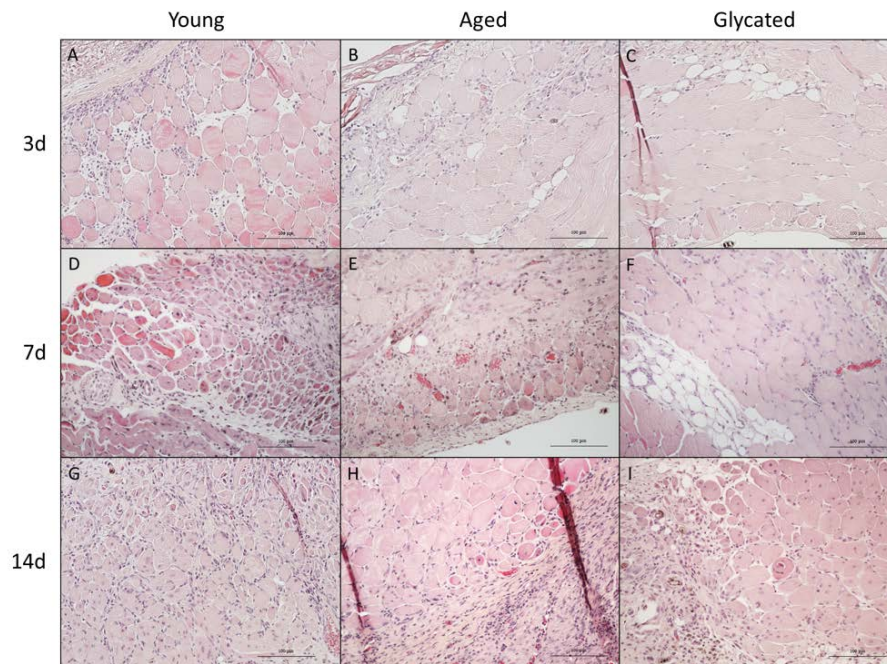
Figure 82: Hematoxylin & eosin staining of muscles injured and repaired with muscle ECM.

Images taken at 20X. Scale bars indicate 100 µm.
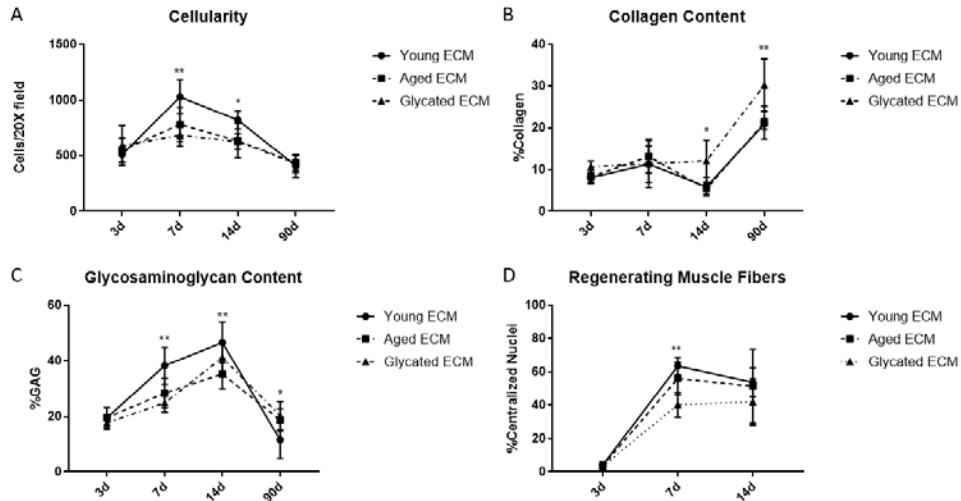
Figure 83: Quantification of histological stains for muscle ECM reconstruction.

Data shown as mean ± S.D. Statistical significance reported as $*p<0.05$, $**p<0.01$, $***p<0.001$, $****p<0.0001$

8.3.2 Immunofluorescent staining for macrophage markers

To understand changes in macrophage infiltration and phenotype during the acute host response following injury, immunofluorescent antibody staining was utilized. Presence of macrophages was assessed via staining for F4/80, a classical murine macrophage marker (Figure 84). At 7 days, there was a significantly higher level of F4/80$^+$ macrophages in young muscle ECM over glycated muscle ECM (Figure 88A). This suggests that ECM glycation inhibits the infiltration of macrophages into the site of muscle injury. By 14 days, F4/80$^+$ macrophage numbers decreased in young muscle ECM but remained high in aged muscle ECM groups (Figure 88A). This result suggests that aged ECM promotes chronic inflammation through pro-longed macrophage

171

presence. Ninety days post-implantation all groups exhibited reduction in macrophage presence to normal levels.
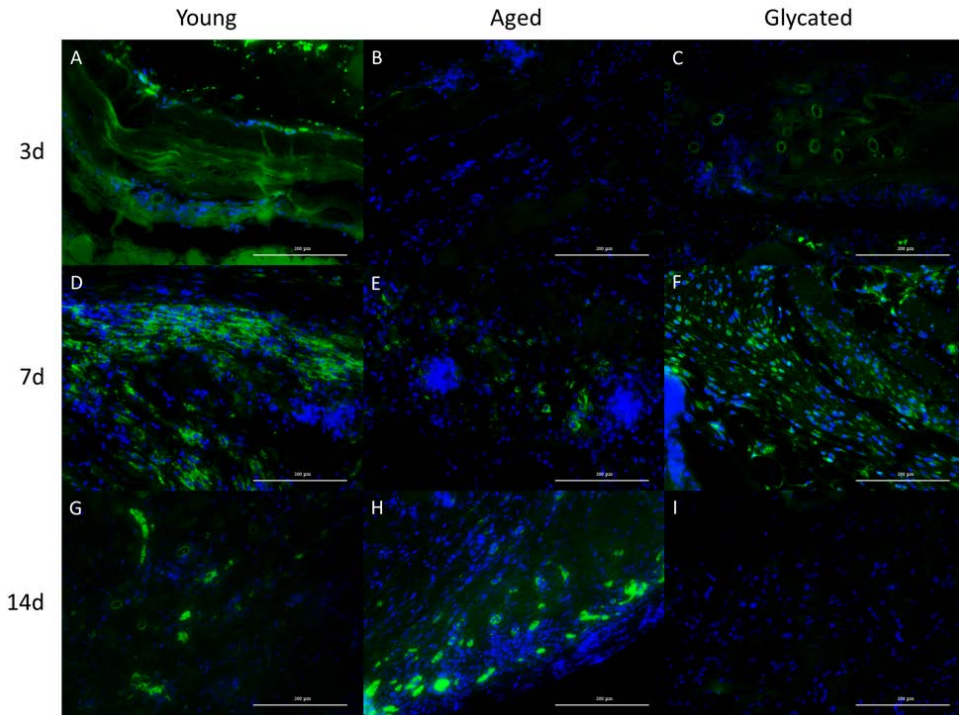
Figure 84: Immunofluorescent F4/80 labeling of muscle ECM reconstruction of muscle injury. Images taken at 20X. Scale bars indicate 100 µm.

Pro-inflammatory macrophage presence was determined via staining for induced nitric oxide synthase (iNOS), a classical M1 macrophage marker (Figure 85). There were no differences in the number of iNOS⁺ cells at 3 days. At 7 days post-implantation, the number of iNOS⁺ cells increased in the young muscle ECM group over aged and glycated muscle ECM, which remained at levels similar to 3 days (Figure 88B). By 14 days, young and aged muscle ECM reached similar levels of iNOS⁺ cells while glycated muscle ECM continued to remain at low levels. This suggests that aged muscle ECM delays macrophage polarization while glycated

muscle ECM completely inhibits it in acute inflammation. By 90 days, all groups exhibited a return to levels of iNOS$^+$ cells seen at 3 days.
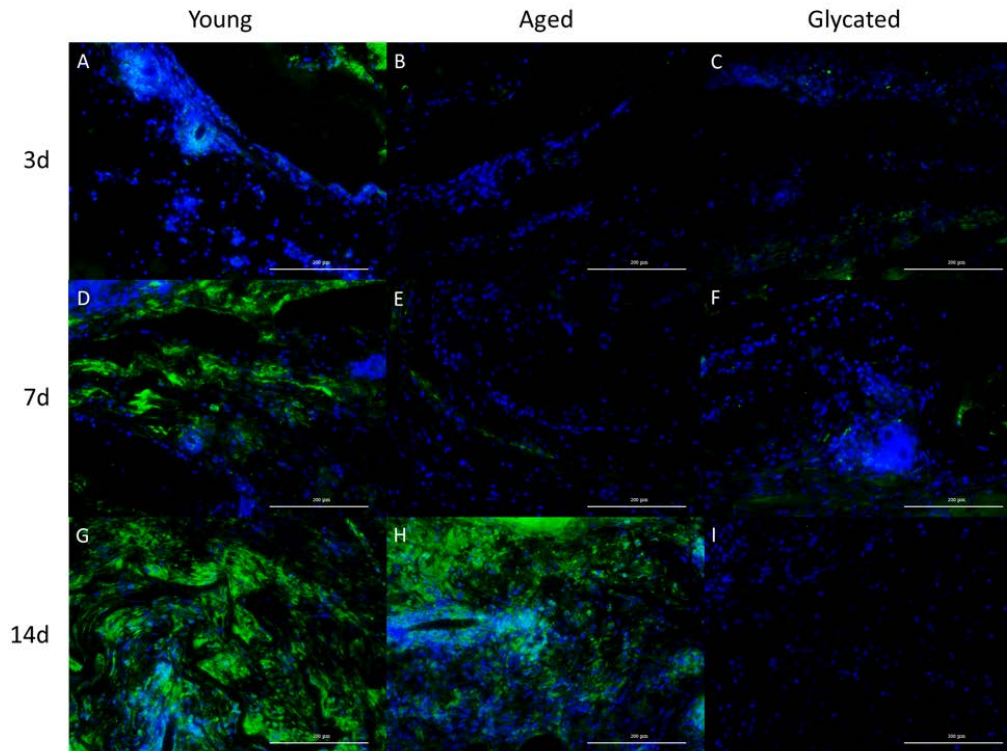
Figure 85: Immunofluorescence staining for iNOS in muscle ECM reconstruction of muscle injury.
Images taken at 20X. Scale bars indicate 100 µm.

Anti-inflammatory macrophage presence was determined via Arginase-1 immunofluorescent staining (Figure 86). Arginase-1 is a classical murine anti-inflammatory macrophage marker. At 3 days, there was significantly more Arginase-1$^+$ cells in young muscle ECM over aged and glycated ECM (Figure 88C). The number of Arginase-1$^+$ cells continued to increase in the young muscle ECM group over the aged and glycated groups, which stayed constant from 3 days. By 14 days, arginase-1$^+$ cells in young muscle ECM reduced to levels seen in aged and glycated muscle ECM groups which continued to stay constant. While young muscle ECM seemed to

elicit a normal temporal anti-inflammatory response expected during injury, aged and glycated

muscle ECM promoted a deficiency in anti-inflammatory macrophage activation.
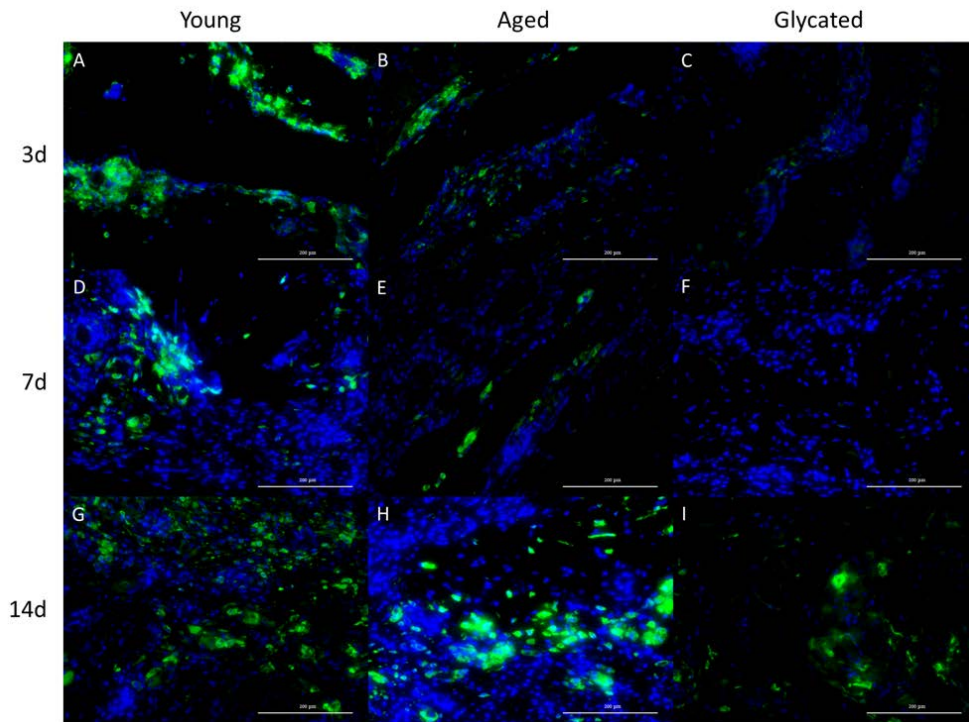
Figure 86: Immunofluorescent arginase staining on muscle ECM reconstruction of muscle injury.

Images taken at 20X. Scale bars indicate 100 µm.

8.3.3 Immunofluorescent staining for satellite cell activation

MyoD staining was performed at acute timepoints to understand how these ECM

microenvironments and the resulting inflammatory response affected satellite cell differentiation

(Figure 87). There was no substantial MyoD positive cells at 3 days (Figure 88D). By 7 days,

aged ECM elicited significantly more MyoD staining while glycated had a reduced staining

level. This suggests that aged ECM enhances stem cell differentiation while glycation inhibits it.

All groups reduced in levels of MyoD$^+$ cells by 14 days.
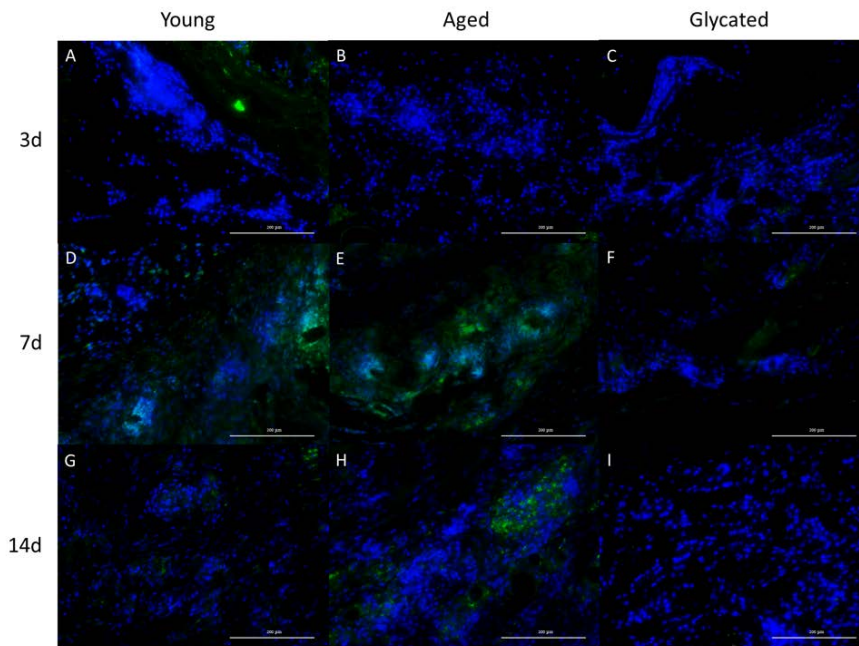
Figure 87: Immunofluroescent MyoD staining for muscle ECM reconstruction of muscle injury.

Images taken at 20X. Scale bars indicate 100 µm.
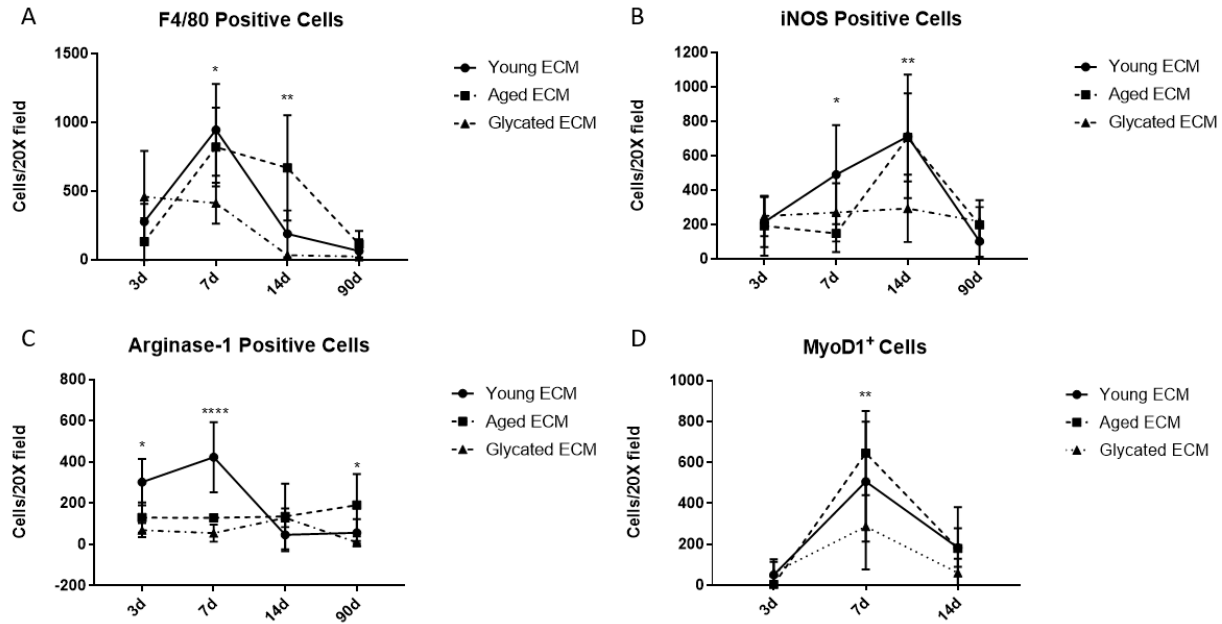
Figure 88: Quantification of immunofluorescence staining of ECM reconstruction of muscle injury.

Data shown as mean ± S.D. Statistical significance reported as *p<0.05, **p<0.01, ***p<0.001, ****p<0.0001

8.3.4 Gene expression analysis

To understand changes in gene expression during the inflammatory phase following muscle reconstruction, RNA was extracted from remodeling ECM at 7 and 14 days then analyzed via Taqman gene expression assays (Figure 89). Fold expression change normalized to young muscle ECM showed that largely inflammatory gene expression was reduced in aged and glycated ECM at 7 days. Aged ECM elicited higher IL-6 and Ccl2 gene expression at 7 days suggesting some promotion of increased inflammation (Figure 89A). At 14 days, aged ECM elicited a large increase in Fizz1 gene expression and slight increases in Tnfa, Hgf and Igf1.

Glycated ECM promoted increases in Ccl2 and Hgf suggesting early promotion of chronic inflammation (Figure 89B). Largely, the reduced gene expression seen at 7 days was gone by 14 days with aged and glycated ECM having similar or higher levels of transcripts at this timepoint.
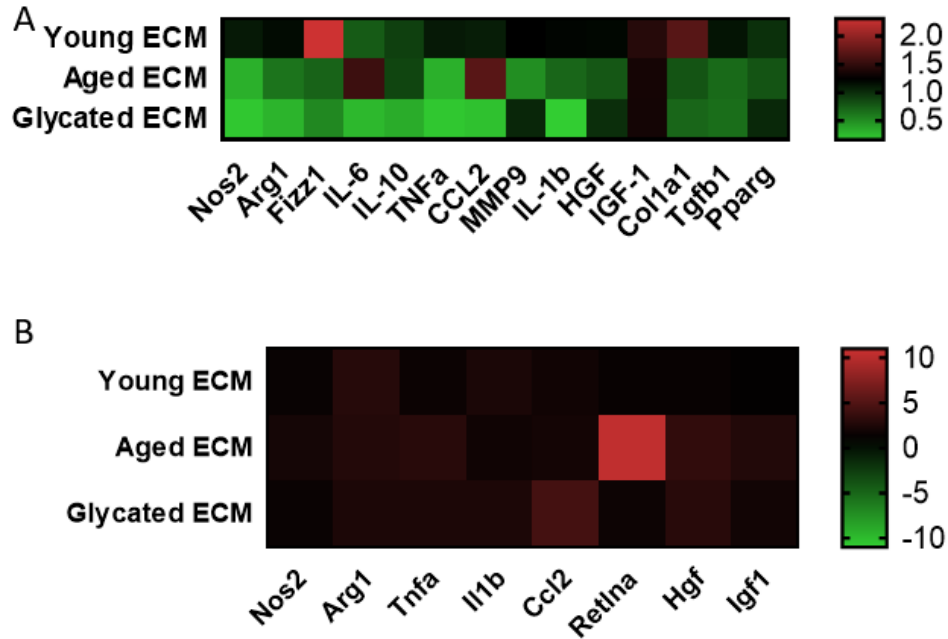
Figure 89: Taqman gene expression of remodeling ECM in muscle injury at 7 (A) and 14 days (B).

Gene expression represented as fold expression change where 2 indicates 2 fold expression change compared to young ECM.

8.3.5   Evaluation of chronic remodeling

To understand how muscle ECM affected the repair of abdominal muscle downstream of injury, immunohistochemical staining for fast and slow myosin heavy chain was performed (Figure 90). Acute muscle injury results in increased slow muscle fiber type and resolution of muscle injury results in a return to normal ratios of fast to slow muscle fibers. By 90 days, young and aged

muscle ECM groups had similar ratios of fast to slow muscle fibers while glycated muscle ECM had a reduced ratio. This suggests that glycated muscle ECM has an unresolved muscle injury response at 90 days or has permanently increased the presence of slow muscle fibers.
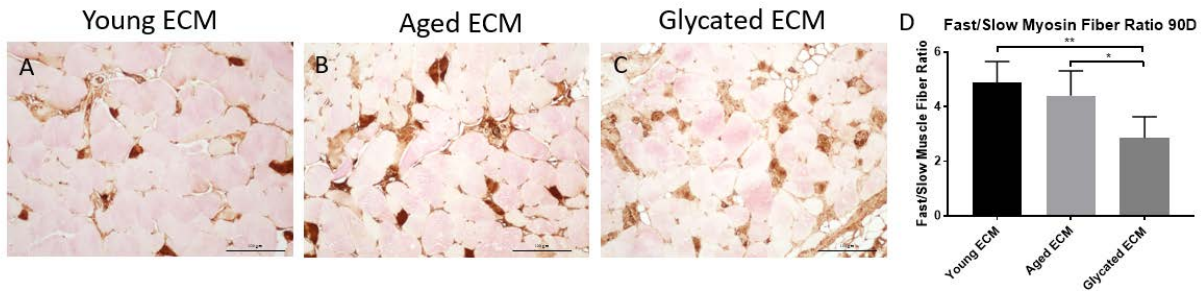
Figure 90: Fast/slow myosin IHC on 90d explants from ECM reconstruction of muscle injury.

Images taken at 20X. Scale bars indicate 100 µm. Data shown as mean ± S.D. Statistical significance reported as *p<0.05, **p<0.01, ***p<0.001, ****p<0.0001

To understand remodeling of the extracellular matrix at 90 days, picrosirius red staining was performed (Figure 91). Using imaging under polarized light and a previously described algorithm, the presence of red, orange, yellow and green fibers was determined. At 90 days, glycated muscle ECM groups had higher levels of red fibers than young and aged groups, which is indicative of more thick fibers associated with fibrosis. This result is similar to the increased Masson's trichrome staining found in glycated groups at 90 days. There were no differences in the intermediate thickness orange and yellow fibers in any groups. Aged and glycated muscle ECM elicited higher levels of green fibers, which are the thinnest detected by picrosirius staining. These fibers have low collagen fiber alignment which could indicate more unorganized matrix produced in an aged or glycated muscle ECM microenvironment.
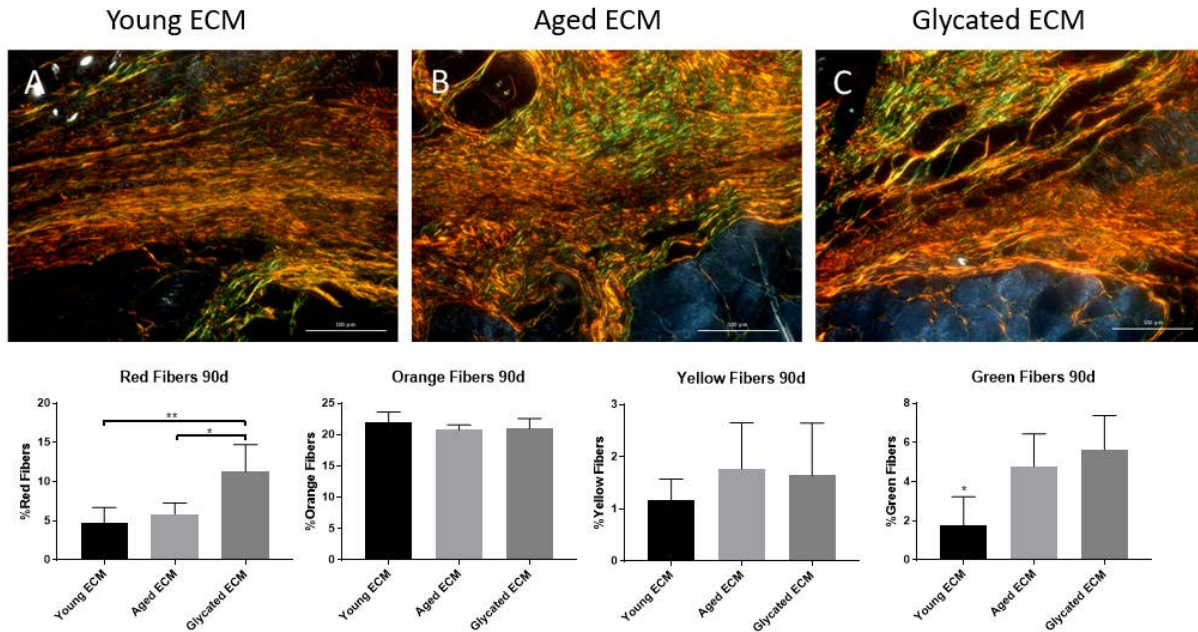
Figure 91: PicroSirius Red staining and analysis of 90d explants from muscle ECM implant.

Images taken at 20X. Scale bars indicate 100 µm. Data shown as mean ± S.D. Statistical significance reported as *p<0.05, **p<0.01, ***p<0.001, ****p<0.0001

Macrophage polarization in chronic 90 day explants was evaluated using immunofluorescent antibody labeling (Figure 92). Aged ECM had higher levels of F4/80 positive macrophages, suggesting chronic inflammation is promoted with aging ECM (Figure 92A). Aged and glycated ECM had higher levels of iNOS positive cells which suggests they are promoted pro-inflammatory signals chronically following injury while young ECM has more resolved inflammation (Figure 92B). Aged muscle ECM also promoted higher levels of arginase positive cells over glycated muscle ECM (Figure 92C). This suggests that glycated ECM promotes a more pro-inflammatory chronic environment while aged muscle ECM elicits a broader range of macrophage activation.
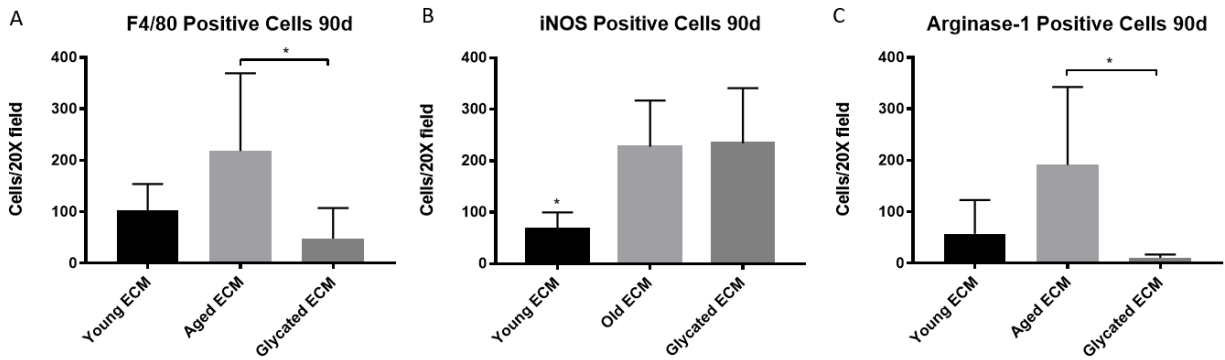
Figure 92: Analysis of immunofluorescent staining on 90d explants from muscle ECM implants.

Data shown as mean ± S.D. Statistical significance reported as *p<0.05, **p<0.01, ***p<0.001, ****p<0.0001

8.4   DISCUSSION

Explants from acute time-points following muscle injury showed impaired cellular infiltration and matrix production within aged and glycated muscle ECM microenvironments. There are many reports of impaired neutrophil migration with aging [47, 320, 321], as well as impaired macrophage infiltration [47, 322]. Investigation into the cause of impaired immune cell infiltration has focused on changes in cellular populations and levels of inflammatory cytokines and chemokines. Results from this paper suggest that the aged extracellular matrix microenvironment contributes to this altered immune cell infiltration. In addition, aged and glycated ECM promoted reductions in glycosaminoglycan content during the acute response following injury. GAGs are important orchestrators of the host response as they assist with collagen reorganization, growth factor activity, and angiogenesis [323]. Reduced GAG production during muscle injury may cause poorer healing downstream.

Macrophage infiltration and activation was also impaired in aged and glycated muscle environments. Macrophage polarization is known to be important to healthy muscle regeneration [51]. Reduction in macrophage response have been shown to impair muscle healing [324]. Aged wound healing has been associated with impairments in chemokine signaling and leukocyte infiltration [234]. While young microenvironments promoted temporal activation of pro- and anti-inflammatory macrophage phenotypes, aged and glycated groups experienced delayed or diminished immune activation. This impairment could directly impact the regenerative cascade necessary for proper muscle healing. Previous work from our lab has shown the host response to biomaterials in aged animals is delayed, which is similar to the results seen here with a delayed peak in F4/80+ cells [230].

Aging and glycation of muscle ECM also affected metrics of muscle regeneration. Aging of ECM seemed to enhance MyoD positive cells while glycation reduced them. Glycation reduced both metrics of muscle regeneration. Several studies have shown that aging and senescence reduces expression of satellite cell differentiation markers such as MyoD [41, 42]. However, there are other reports that aged muscle has increased number of MyoD+ cells following injury, as well as increased apoptosis of these activated stem cells [45]. Our data suggest this could be due to the effects of glycation but not aging of the ECM. Reports have also shown reduced percentages of centralized nuclei in aged muscles following injury [39, 43]. Both aged and glycated ECM reduced the percent centralized nuclei in muscle fibers, suggesting they could be promoting this reduction in muscle regeneration.

Chronic remodeling outcomes were impaired by glycated extracellular matrix but not aged. This included increased fibrosis as seen by Masson's trichrome and PicroSirius Red staining, as well as increased presence of slow-twitch muscle fibers. Aged muscle experiences

181

fibrosis so glycation of the extracellular matrix with aging could be a cause for this phenotype [53]. Intravenous administration of AGEs has previously been shown to increase cardiac fibrosis [325]. Previous reports have shown that methylglyoxal modified ECM enhanced myofibroblast differentiation, which could lead to fibrosis [326]. Further investigation into the effect of aged or glycated ECM upon fibroblast activation would need to be performed.

Increased presence of slow type muscle fibers has been shown to be an indication of injury [327]. Therefore, glycated extracellular matrix may promote an ongoing or unresolved inflammatory process at 90 days following injury. Previous reports have shown that diabetic patients have increased proportion of slow-twitch muscle fibers, which corroborates the effects seen in this study [328].

There were several limitations to the study. A comprehensive analysis of the compositional changes in the aged muscle extracellular matrix was not conducted. Mass spectrometry analysis for composition of extracellular matrix components as well as for the presence of glycation crosslinks is necessary to fully understand how muscle ECM changes with age. The in vitro glycated ECM was also fabricated using one sugar type and in saline conditions, which may not replicate what is happening in vivo. Further the artificial glycation was conducted on decellularized ECM which is not exposed during the in vivo setting. Therefore, the glycated matrix may not completely mimic the alterations experienced by muscle ECM in aged individuals.

8.5   CONCLUSION

Overall, this work provides evidence for a cell-extrinsic mechanism for alterations in the immune response and resultant regeneration following muscle injury in aged individuals. This study adds further evidence that the extracellular microenvironment, specifically the matrix, directly contributes to the aging phenotype in muscle regeneration. This adds another facet to the understanding of the causes of muscle dysfunction in aged populations. As sarcopenia and poor muscle healing is a symptom experienced by the majority of aged people, this is an important issue to fully understand. Furthermore, the cellular changes with aging in both immune and stem cell populations may be acquired incrementally over time through dynamic reciprocity. Therefore, many facets of muscle tissue could all accumulate aging changes over time while each imbuing more aging phenotypes upon each other.

9.0   DISCUSSION

The results presented in this dissertation work have broad applications to both biomaterials and aging biology fields. In the biomaterials field, the sourcing of extracellular matrix from mammalian tissues is dependent upon the characteristics of the species, organ, aging, health and nutrition of the source animal, among other characteristics [176, 329-331]. However, current standards for biomaterial sourcing only consider documentation, general health, nutrition and transmission of infectious agents [332]. Tissues harvested from abattoirs are commonly of "market-weight" which normalizes age [333]. Results from this study as well as others suggests that inclusion of animals beyond market-weight age could remove beneficial properties of extracellular matrix biomaterials while animals younger than market weight could improve regeneration [110, 176]. More rigorous standards concerning the age of animals used for the harvest of tissues for biomaterial production could reduce the well-known variability associated with biologically-derived materials.

This dissertation has also provided preliminary evidence for several factors which may directly impact the immune cell response to extracellular matrix scaffolds derived from different aged animals. The composition of extracellular matrix proteins and modifications of them, as well as content of lipids and growth factors are known to change with age [122, 208, 243, 334-338]. Extraction of these lipid, growth factor or structural components of the extracellular allows for investigation of the compositional changes in these different fractions. Our results indicate

that these different components have different effects on the host response and these effects change with the age of the animal from which the materials are harvested. The relative solubility of the growth factors and lipids versus the slower degrading structural matrix molecules could be relevant to the different immune cell phenotypes observed inside and at extracellular matrix surfaces versus those observed in the periphery of the remodeling zone [109].

The skeletal muscle extracellular matrix was found to change with aging; however, many of these results were counter to previous investigations of whole tissue. Our results showed there were reductions in collagen content, oxidation and glycation in decellularized aged muscle, which is opposite of whole tissue analyses [198, 309, 339]. Decellularization of aged tissues may remove components of the extracellular matrix which contribute to these aging changes seen in whole tissue. Aged tissue has been shown to have increased degraded ECM and oxidized or glycated ECM may also lead to more matrix degradation [198, 335, 337]. Further evidence is necessary to understand why decellularized and whole tissue analyses of aged skeletal muscle ECM differ.

The investigation of skeletal muscle extracellular matrix aging upon macrophage phenotype relates to many studies showing changes in muscle macrophage populations with aging. Aged skeletal matrix promoted increased iNOS and arginase immunoexpression as well as reduced nitric oxide production with polarizing cytokines. These results correlate to other findings showing increased in both M1 and M2 macrophage population in aged muscle [53, 340]. Our investigations *in vitro* involved degraded extracellular matrix, which applies mostly to advanced inflammation or chronic responses following inflammation. Further investigation of intact matrix *in vitro* would relate more to physiology during aging without injury.

The investigation of the effects of oxidation and glycation upon skeletal muscle extracellular matrix reveals distinct effects on their roles in aging and disease. Oxidation of extracellular matrix resulted in increased nitric oxide production and reduce iNOS immunoexpression. Considering extracellular matrix is known to acquire oxidative changes with aging, these studies may suggest a direct effect of ECM oxidation upon macrophage polarization [290]. Glycation of extracellular matrix resulted in increased pro-inflammatory macrophage responses. This correlates with previous reports that glycation leads to pro-inflammatory responses. Further experimentation is needed to confirm the signaling pathways involved in these responses. These studies show that the age-related changes in oxidation and glycation of the extracellular matrix can directly affect the macrophage response. Previous studies of glycation have mainly focused on glycated bovine serum albumin which is less relevant than using extracellular matrix materials [341].

Implantation of aged or glycated ECM into a muscle injury showed distinct changes in muscle regeneration compared to young ECM. The delays or inhibition in macrophage accumulation with aged or glycated ECM correlate to observations in aged or diabetic animals [44, 342]. Reduction in iNOS levels *in vivo* is similar to other studies showing reduced nitric oxide activity in aged and diabetic muscle regeneration [343, 344]. The inhibition of arginase activation in acute timepoints with aged or glycated ECM could be a cause for the chronic inflammation observed in aged or diabetic muscle injury due to delayed immune resolution [345]. The direct effects of ECM aging and glycation upon the host response to muscle injury *in vivo* suggests ECM may play a larger role in regenerative decline than previously hypothesized.

Implantation of aged or glycated extracellular matrix also affected the processes associated with healthy muscle regeneration. Extracellular matrix glycation resulted in reduced

muscle fiber nuclei centralization at 7 days. This correlates to reports of impaired stem cell accretion with aging or diabetes [232, 346]. The enhancement of MyoD levels at 7 days with aged muscle ECM correlates to reports of satellite cell entrapment in an activated phenotype without progression to differentiation [347]. The downregulation of most inflammatory targets investigated shows aged and glycated ECM replicates the dysfunctional inflammatory gene expression observed in aged rodents and humans [340]. Overall, age-related changes in the muscle extracellular matrix may be, in part, responsible for aberrant satellite cell activation *in vivo*.

The chronic response to implantation of aged or glycated ECM also mirrors the remodeling alterations observed with aging and diabetes. The increases in collagen staining at chronic time points with glycated muscle ECM shows similarities to the increases in collagen accumulation in aged and diabetic individuals [348]. The reduced ratio of fast:slow muscle fibers at chronic time points following glycated ECM implantation correlates to shifts in the muscle fiber type with sarcopenia and diabetes [349]. Aging and glycation both led to increased presence of macrophages and macrophage activation at chronic timepoints. This could explain the increased presence of macrophage subtypes in uninjured aged muscles [47, 53]. Aging and glycation of ECM affects not only acute inflammation but chronic remodeling and inflammation as well.

The results presented in this dissertation show that the age-related or glycation modifications of muscle extracellular matrix have direct effects upon the inflammatory and muscle regeneration processes following injury. Aging of the extracellular matrix alone resulted in a partial aging phenotype when implanted into a healthy host. This suggests that extracellular matrix aging contributes to the deficiencies observed in aged individuals; however, age-related

cellular changes still have a large role in this response. Further work is necessary to understand how age-related changes in the extracellular matrix affect the ability to regenerate within an aged or diabetic organism. Regardless, these studies lend further evidence towards hypotheses centered around a cell-extrinsic mechanism of regenerative declines with aging.

10.0   CONCLUSION

The work presented herein provides concrete evidence that the aging of the extracellular matrix has a profound effect upon its properties and upon the resultant host response elicited upon implantation. These results have implications for both biomaterial sourcing and aging biology. Biomaterial scientists and companies should use source animal age as a quality control criterion in order to achieve better, more consistent outcomes from their products. In aging biology, the role of extracellular matrix must be considered as an equal contributor to the aging phenotype in addition to the aging of stem cells and immune cells. Overall, this work shows that aging of the extracellular matrix alone has profound implications for regenerative outcomes.

APPENDIX A: FREE RADICAL-DELLULARIZATION OF TISSUES PROMOTES ENHANCED ANTI-INFLAMMATORY AND ANTI-OXIDANT HOST RESPONSE

A.1   INTRODUCTION

Extracellular matrix biomaterials have been used clinically and pre-clinically in a wide variety of applications, including hernia repair, breast reconstruction, skin grafts and wound healing [138-141]. Typically, extracellular matrix materials are prepared through the decellularization of mammalian tissues using detergents, enzymes and/or oxidants [350]. When decellularized and prepared properly, extracellular matrix (ECM) biomaterials have been shown to promote constructive remodeling, defined as the formation of new site-appropriate host tissue [124]. This positive outcome has been correlated with a shift during the acute immune response from a pro-(M1) to anti-inflammatory (M2) phenotype (macrophage polarization) [59, 221].

Oxidative reagents used in decellularization have an interesting correlation with macrophage phenotype as reactive oxygen species (ROS) and reactive nitrogen species (RNS) are produced by macrophages during inflammation [351]. A common oxidant used in extracellular matrix decellularization is peracetic acid, a stabilized form of hydrogen peroxide [223, 352-354]. Hydrogen peroxide itself is an important inflammatory mediator and damage signal which can modify proteins via cysteine oxidation and lipids via lipid peroxidation [355-357]. The oxidative modification of extracellular matrix biomaterials by peracetic acid used during decellularization may be responsible, in part, for the beneficial host responses observed following implantation [251, 358]. In addition, peracetic acid serves as a sterilization step

through protein denaturation, cell wall permeabilization, and sulfur oxidation in proteins and enzymes which can inactivate bacteria, viruses and spores [359-361].

Decellularization of extracellular matrix biomaterials with more potent RNS and ROS mediators may further enhance the promotion of an anti-inflammatory phenotype. ROS have been shown to promote the polarization of macrophages to an anti-inflammatory phenotype [362]. Nitric oxide signaling, which is important in angiogenesis and oxidative burst, also signals macrophages to polarize to an anti-inflammatory state via VASP signaling [363-365]. Reactive nitrogen species themselves and modification of fatty acids has been shown to reduce pro-inflammatory macrophage phenotype [366]. Reactive oxygen species have also been shown to induce an anti-oxidant oxidative stress pathway via the Nrf2 transcription factor which could be beneficial for the treatment of ischemic injuries [367]. Therefore, ROS or RNS decellularization methods pose a novel, potential alternative which can enhance or modify the beneficial effects of extracellular matrix biomaterials.

This study investigates the macrophage response to extracellular matrix biomaterials decellularized with nitric oxide, hydroxyl radical or both in comparison to a standard method using peracetic acid. Bone marrow-derived macrophages were used as an *in vitro* model of macrophage response to assess the direct effect of these scaffolds upon macrophage polarization [110]. Degradation products of extracellular matrix were used for *in vitro* experiments as degradation has been shown to be important for constructive remodeling [59]. ECM degradation products have also been shown to promote anti-inflammatory macrophage phenotypes *in vitro* [368]. Muscle injury was used as an *in vivo* model for the assessment of the host response to sheets of these materials decellularized using free radical reagents [59, 369, 370]. We

191

hypothesized that decellularization of ECM would promote enhanced anti-inflammatory and anti-oxidant macrophage polarization which would enhance healing following muscle injury.

A.2   METHODS

A.2.1   Scaffold Preparation

Porcine small intestine was purchased from local slaughterhouse (Thoma Meat Market, Saxonburg, PA). Porcine small intestine submucosa was harvested through mechanical delamination of the external muscularis and internal mucosa layers. Native submucosa was cut into 1 foot lengths and then washed in DI H_2O until water was no longer discolored by the tissue. Samples were decellularized using standard peracetic acid wash or nitric oxide, hydroxyl radical or both at washes for 2 hours [176]. As nitric oxide and hydroxyl radicals will quickly react into other reactive nitrogen and oxygen species, decellularization methods will be described as RNS, ROS or RNS+ROS as the full range of species present was not characterized. Samples were then washed twice with 1XPBS then twice with water for 30 mins each. Decellularized scaffolds were frozen at -80 °C and then lyophilized. Samples used for implantation were terminally sterilized with ethylene oxide. ECM degradation products were produced using a 1mg/mL pepsin solution in 0.01N HCl under constant stir for 48 hrs to create a 10mg/mL ECM digest.

A.2.2 Scaffold Characterization

Hydrated native tissue and decellularized scaffolds were fixed in 10% neutral buffered formalin (NBF) and then embedded in paraffin. Sections of these scaffolds were stained separately with hematoxylin & eosin or DAPI to confirm removal of nuclei. Proteinase K digests of native whole small intestine, native submucosa and decellularized scaffolds underwent phenol: chloroform: isoamyl alcohol (25:24:1) extraction for DNA and were resuspended in 1X TE buffer. Native submucosa was used as a control in addition to whole small intestine as the submucosa is the layer used for biomaterial preparation. DNA extracts were separated using electrophoresis on a 2% agarose gel in 0.5X TBE buffer to confirm reduction of DNA content and fragmentation of remnant DNA in decellularized scaffolds compared to native controls. DNA extracts were also quantified for double-stranded DNA content using a PicoGreen assay (Thermo) according to manufacturer's instructions.

A.2.3 Biochemical Analysis

ECM scaffold biochemistry was performed to assess hydroxyproline and sulfated glycosaminoglycan content. Native small intestine, native small intestine submucosa, and decellularized ECM scaffolds were digested at 10mg/mL in a papain solution. Sulfate glycosaminoglycan content was assessed using a dimethylmethylene blue (DMMB) reagent. Hydroxyproline content was assessed by adding 50 µL 2N NaOH to 50 µL papain digests then hydrolyzing at 110 °C for 18 hrs. Samples were neutralized with 5N HCl. One hundred microliters of 0.01M copper sulfate, 2.5N NaOH and 6% H_2O_2 were added. Samples were

193

incubated at 80 °C for 5 minutes then cooled. Four hundred microliters of 3N sulfuric acid was added followed by 200 µL of 5% DMAB in propanol. Samples were incubated at 70 °C for 15 minutes then the absorbance was read at 540 nm. Protein carbonyl content, a marker of oxidation, was determined using a kit from Cayman Chemical as per manufacturer instructions.

A.2.4 Immunohistochemical Analysis

Native and decellularized SIS was fixed in 10% NBF then embedded in paraffin wax. Sections were stained using DAB immunohistochemistry for markers of nitrosylation or oxidation, including S-nitro-cysteine, 3-nitro-tyrosine and cysteine sulfonate. Briefly, paraffin sections were deparaffinized to water then antigen was retrieved using 10mM citric acid pH6 0.05% Tween20 for 20 mins at 95-100 °C. Slides were washed twice with 1X TBST for 5 mins then twice with 1XPBS for 3 mins. Endogenous peroxidase activity was blocked by incubating slides in 0.3% hydrogen peroxide for 30 mins. Slides were washed 3 times in 1X PBS for 3 minutes. Slides were blocked for non-specific antibody binding with a blocking buffer made of 2% donkey serum/1% bovine serum albumin/0.1% Tween-20 for 1 hour at room temperature. Primary antibodies (1:500 S-nitrocysteine (abcam 94930), 1:200 nitrotyrosine (abcam 7048), or 1:100 cysteine sulfonate (Enzo ADI-OSA-820-D) were incubated overnight at 4 °C diluted in blocking buffer. Slides were washed 3 times for 3 minutes with 1XPBS. Slides were then incubated with biotinylated secondary antibodies diluted in blocking buffer (goat anti-mouse or goat anti-rabbit 1:200 (Vector)). Slides were was again 3 times for 3 minutes with 1XPBS. Slides were incubated with VectaShield ABC Reagent for 30 mins then washed again 3x3mins with 1XPBS. Staining was developed by incubating sections with 4% DAB (Vector). Sections were washed then

194

mounted with resinous mounting media and coverslipped. Slides were images on a brightfield microscope at the same settings.

A.2.5 Macrophage Isolation

Bone marrow-derived macrophages were harvested from 2 month or 18-20 month-old C57/BL6 mice as previously described [221]. Briefly, femurs and tibiae were harvested and separated from muscle and connective tissue. Bones were cut at either end to expose bone marrow. Sterile syringe and needles were used to flush out bone marrow using macrophage differentiation media (DMEM/10% FBS/10% L-929 Supernatant/1% PenStrep/2% MEM non-essential amino acids/1% HEPES/0.1% 55μM β-2 mercaptoethanol). Bone marrow lysate was reconstituted in media and filtered through a sterile cell filter. Cells were cultured for 7 days in media to differentiate them into macrophages, changing differentiation media every 2 days.

A.2.6 Macrophage Treatment

Following 7 days of differentiation culture as described above, macrophages were treated with acute polarizing regimens to distinguish phenotypes over 24 hours. Naïve macrophage (M0) controls were treated with basal media for 24 hours. M1 (20 ng/mL IFN-γ and 100 ng/mL LPS) and M2 (20 ng/mL IL-4) (Peprotech) polarizing cytokines were used to create positive controls for classical pro- and anti-inflammatory macrophages. ECM degradation products were neutralized and diluted to 1000 μg/mL in macrophage media to isolate biochemical effects of degradation products and prevent structural moieties from forming. Pepsin buffer (1 mg/mL pepsin in 0.01 M HCl) diluted in macrophage media was used as a control. Another set of

195

treatment groups involved 24-hour exposure of ECM degradation products followed by 24-hour treatment with either the M1 or M2 treatment regimen. These experiments were performed to assess the effect of ECM exposure upon the ability of macrophages to polarize to classical M1 and M2 phenotypes.

A.2.7 Indirect Immunofluorescent Antibody Staining

Cells were fixed with 2% paraformaldehyde (PFA) for 30 minutes then washed in 1XPBS. Cells were incubated in blocking buffer (2% donkey serum (Lampire), 1% bovine serum albumin (BSA) (Sigma), 0.1% Tween-20 (Fisher)) for 1 hour at room temperature. Primary antibodies were diluted in this blocking buffer as follows and incubated overnight at 4 °C: iNOS (1:100, Abcam 3523), Arginase-1 (1:200, Abcam 91279), or heme oxygenase-1 (1:200, Abcam ab13243). iNOS is a classical M1 macrophage marker whereas Arginase-1 is a classical M2 macrophage marker [371]. Heme oxygenase-1 is an anti-oxidant marker upregulated by macrophages during oxidative stress [372]. Cells were washed in 1XPBS then incubated in the appropriate fluorescently-labeled secondary antibody solution in blocking buffer for 1 hour at room temperature (donkey anti-rat Alexa Fluor 488, Invitrogen, 1:200; donkey anti-rabbit Alexa Fluor 488, Invitrogen, 1:300). Cell nuclei were counterstained with 500 nM DAPI (Ebioscience) for 10 minutes. Cells from 2 month old mice were imaged nine times in the center of each well at 10X magnification using automated position capture function to remove bias from subjective image location acquisition. All imaging was performed on an Axio observer T1 microscope. Mean fluorescence intensity of cells was analyzed using Cell Profiler software (Broad Institute). Briefly, DAPI images were used by the program to identify cell nuclei then FITC images were used to identify cell borders around the identified nuclei. The mean fluorescent intensity was

calculated by averaging the pixel intensities (scale of 0 to 1) across the entire cell area. Mean fluorescence intensity values were averaged for all imaged cells in each well.

A.2.8 Phagocytosis Assay

Following treatments, cells were assayed for phagocytic ability using Vybrant Phagocytosis Assay Kit (Invitrogen). Cells were incubated in FITC-labeled dead E. Coli particles for 2 hours in the cell culture incubator. Following washing, the cells were fixed with 2% PFA for 30 minutes then washed with 1X PBS. Cells were counterstained with DAPI then imaged and analyzed as described above.

A.2.9 Nitrite Assay

Following treatments, 50 µL of supernatant from macrophages were transferred into a fresh plate. Nitrite content was assayed using a Greiss Reagent system. Briefly, 50 µL of sulfanilamide (1% in 5% phosphoric acid) was added to supernatants for 10 minutes. Then, 50 µL of 0.1% N-1-napthylethylenediamine in water was added to the mixture for an additional 10 minutes. The absorbance at 540 nm was measured using a BioTek SYNERGY HTX spectrophotometer.

A.2.10 Arginase Activity Assay

Following treatments, media was removed and macrophages were lysed in 50μL 0.001% Triton X-100 in type 1 H_2O with 1X Halt Protease Inhibitors (Thermo). Twenty five microliters of lysate was added to 25 μL of arginase activation solution (10mM $MnCl_2$/50mM Tris-HCl, pH7.5) and incubated at 55°C for 10 minutes. Samples were allowed to cool and then 50 μL of arginine substrate solution (0.5M L-arginine pH 9.7) was added to each well. Samples were incubated at 37°C for 2 hours. A urea standard curve was created via 2 fold serial dilution from 100 mg/mL to 1.5625 mg/mL with a 0 mg/mL blank in lysis buffer. Five microliters of samples or standards were added to a new 96-well plate and 200 μL of urea detection solution (513 mg/L primaquine, 100 mg/L phthalaldehyde, 2.5 mol/L sulfuric acid, 2.5 g/L boric acid, 0.03% Brij35) was added to each well. Absorbance of samples was analyzed using a plate spectrophotometer at 430 nm between 5-20 minutes following addition of detection solution.

A.2.11 Abdominal Wall Partial Thickness Defect Implantation

Four month old C57BL6/J mice (Jackson) were anesthetized using isofluorane and analgesized using Buprenex prior to surgical manipulation. Abdominal skin was incised and abdominal muscle exposed. Partial thickness defects (1 cm^2 were created in the abdominal muscle by removing the external 2 of the 3 muscle layers. Rehydrated 1 cm^2 muscle ECM scaffolds (n=5 per treatment) were sutured over the defect using 4-0 polypropylene sutures. Skin incisions were sutured close using 3-0 PGCL suture. This is a modification of an existing animal model for biomaterial host response evaluation [369]. Animals were maintained on Buprenex and Baytril

for 3 days post-operation. ECM was explanted following 7 and 90 days post-implantation. Sections were fixed in 10% NBF for histologic analysis.

A.2.12 Histologic Analysis

Paraffin sections at 5μm were stained for hematoxylin & eosin, Masson's trichrome, Alcian blue, Herovici's polychrome, and PicroSirius Red. Five images were taken per slide at 20X for quantitation using brightfield microscopy or circularly polarized light microscopy for PicroSirius Red. Acute time-points (7 days) were stained using immunofluorescent antibody labeling. Briefly, slides were deparaffinized then antigen retrieved using 10mM citric acid at 95-100°C for 20 mins. Autofluorescence was quenched using a 10mM copper sulfate/50mM ammonium acetate (pH5) solution for 20 mins at 37 °C. Sections were blocked using 2% donkey serum/1% BSA/0.1% Tween-20 for 1 hour then incubated overnight at 4 °C with primary antibodies for F4/80 (1:100 BioRad MCA497), iNOS (1:100 Abcam 3523), Arginase-1 (1:200 Abcam 92179), or Heme oxygenase-1 (1:100, Abcam 13243). Sections were washed in PBS then incubated for 1 hour with the appropriate Alexa Fluor 488 donkey antibody at 1:200 (Abcam). Sections were washed, counterstained with DAPI then mounted with FluoroGel mounting solution. Immunofluorescent stained slides were imaged 5 times per slide at 20X on a Nikon Eclipse TI-U and analyzed on Nikon Elements software. Mean fluorescence intensity of cells were analyzed using Cell Profiler software as described above. Ninety day explants were stained immunohistochemically for fast & slow myosin heavy chain using alkaline phosphatase and DAB solutions, respectively [261].

A.2.13 Statistical Analysis

Quantitative results were analyzed using a two-way ANOVA (treatment, age) with Tukey post-hoc analysis using GraphPad PRISM 7 software. Significance was determined at a p-value less than 0.05.

A.3   RESULTS

A.3.1   Assessment of decellularization

Histologic assessment of decellularization showed that all methods resulted in significant removal of nuclei (Figure 93A-E). Morphologically, ECM decellularized with PAA seemed to be more similar to native morphology whereas FR-decellularized ECM seemed to organize into thicker, irregular fiber bundles. Masson's trichrome staining appeared similar across decellularized ECM, suggesting similar levels of collagen content (Figure 93F-J). Alcian blue staining was also consistent, suggesting similar glycosaminoglycan content across decellularization methods (Figure 93K-O). Cysteine sulfonate staining, a marker of oxidation, only appeared to be weaker in the ROS decellularization method (Figure 93P-T). S-nitrocysteine immunohistochemistry showed higher staining with RNS and RNS+ROS decellularization methods, as expected (Figure 93U-Y). 3-nitrotyrosine immunohistochemistry also showed higher staining in RNS and RNS+ROS decellularization methods (Figure 93Z-AD). This suggests a

higher presence of nitroxidative protein modifications within RNS and RNS+ROS decellularization protocols.
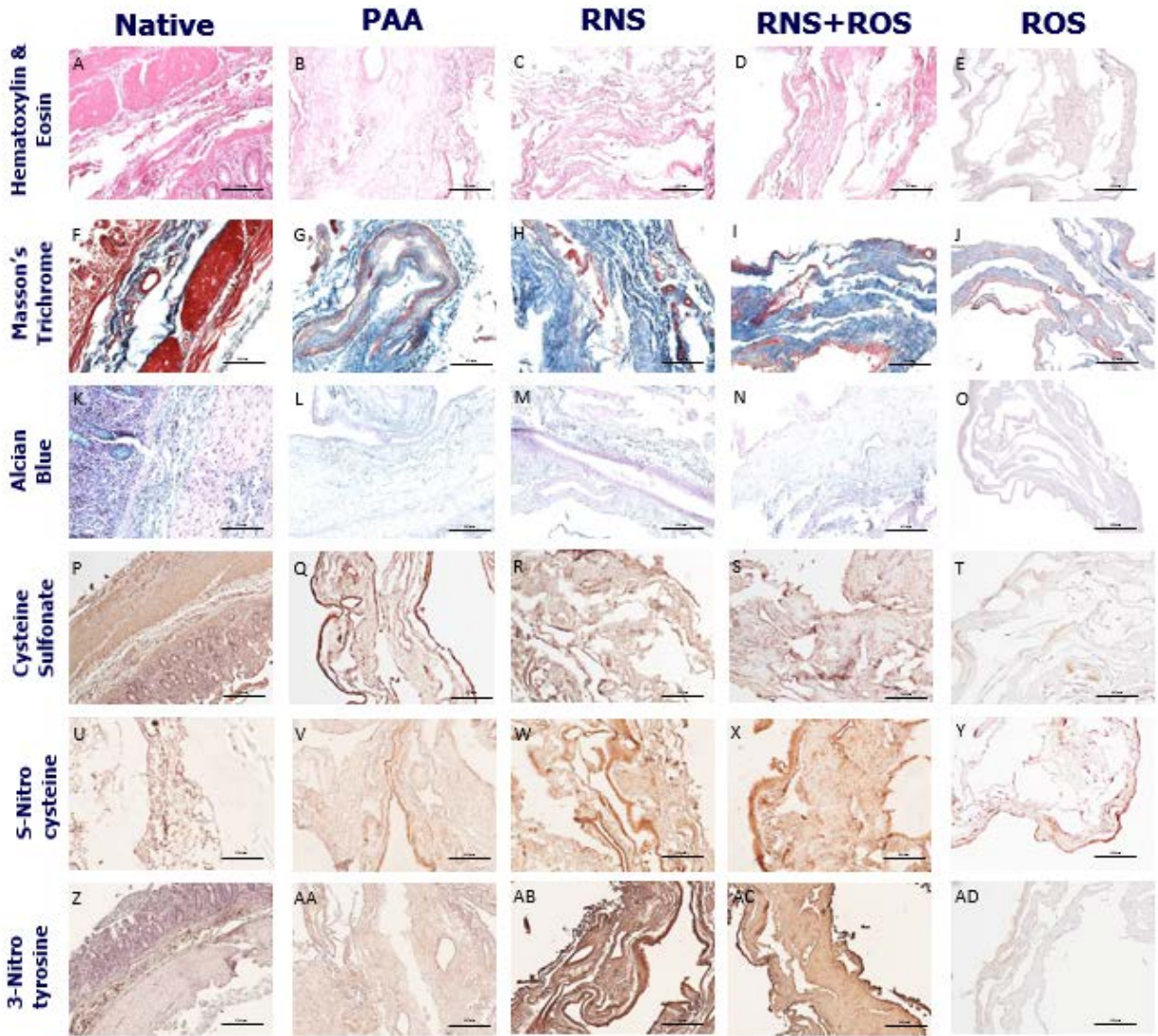
Figure 93: Histologic assessment of decellularized extracellular matrix biomaterials.

Images taken at 10X. Scale bars indicate 100 µm.

Hematoxylin & eosin (A-E), Masson's trichrome (F-J) and Alcian blue (K-O) staining of histologic sections. Immunohistochemical staining for cysteine sulfonate (P-T), S-nitro-cysteine (U-Y), and 3-nitro-tyrosine Z-AD). All images at 10X (Scale bar = 100 µm).

201

A.3.2 Biochemical Analysis

Biochemical assessment of native and decellularized scaffolds confirmed sufficient removal of cellular DNA content. Agarose gel electrophoresis showed significant fragmentation and removal of DNA from all decellularization methods (Figure 94A). However, there seemed to be higher levels of small DNA fragments in the RNS and RNS+ROS decellularized samples. Despite this finding, double stranded DNA quantification showed no significant difference in the amount of DNA between any decellularization method (Figure 94B). The dsDNA content in decellularization methods was reduced 90-95% from native small intestine and 86-93% from native submucosa. All methods resulted in dsDNA content less than 2000 ng/mg dry tissue.

All decellularization methods resulted in an enrichment in hydroxyproline content. However, all FR methods resulted in a significant reduction in hydroxyproline content compared to PAA controls (Figure 94C). Similarly, glycosaminoglycan content was enriched with decellularization but reduced from PAA to RNS+ROS and ROS scaffolds (Figure 94E). RNS+ROS decellularization resulted in significantly higher protein carbonyl content compared to PAA controls while ROS scaffolds had higher protein carbonyl content than all other methods (Figure 94D). This confirms that FR decellularization methods induced protein oxidation in all groups.
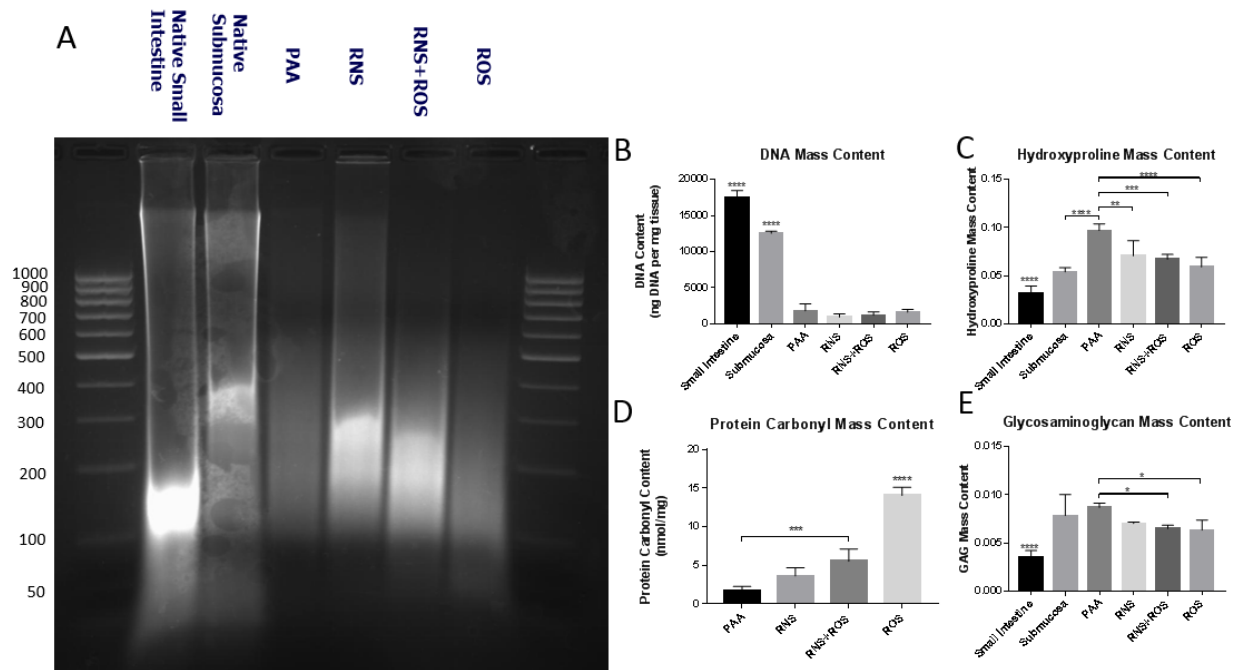
Figure 94: Biochemical assessment of DNA, hydroxyproline, glycosaminoglycan and protein carbonyl content.

DNA agarose gel electrophoresis of DNA extracts from ECM (A). PicoGreen quantification of ds DNA content in ECM (B). Hydroxyproline (C), protein carbonyl (D) and DMMB glycosaminoglycan (E) assays for biochemical content. Results presented as mean ± S.D. (* represents $p < 0.05$, ** $p < 0.01$, *** $p < 0.001$, **** $p < 0.0001$)

A.3.3 *In vitro* macrophage response

Murine bone marrow-derived macrophages were exposed to ECM degradation products in order to determine if radical inflammatory species decellularization altered the macrophage response to ECM. M1 controls which were exposed to IFN-γ and LPS had higher levels of iNOS immunoexpression and nitric oxide production, as well as reduced levels of heme oxygenase-1

203

immunoexpression (Figure 95A, G, J). M2 controls treated with IL-4 had increased levels of arginase-1 immunoexpression and increased urea production (Figure 95D, M). ECM controls treated with PAA had baseline levels of iNOS, arginase and HO-1 immunoexpression as well as no nitric oxide or urea production (Figure 95A, D, G, J, M). All FR-decellularized ECM resulted in increased immunoexpression of iNOS, arginase-1 and heme oxygenase-1 compared to PAA controls (Figure 95A, D, G). RNS ECM had higher levels of iNOS immunoexpression than RNS+ROS ECM (Figure 95A). ROS ECM had lower levels of heme oxygenase-1 than RNS and RNS+ROS ECM but was not different than PAA ECM (Figure 95G).

The effect of ECM exposure upon the ability of macrophages to polarize to extremes is important in understanding the mechanism of biomaterial promotion of altered host responses. Previous studies have shown that macrophage exposure to different types of extracellular matrix biomaterials have altered their phenotype and function following established cytokine polarization schemes [110]. Macrophages were exposed to ECM degradation products for 24 hours then exposed to M1 or M2 cytokines for the subsequent 24 hours. PAA ECM had no effect on iNOS immunoexpression with M1 stimulus but all FR ECM resulted in an increased iNOS immunoexpression level over M1 controls (Figure 95B). All ECM exposure resulted in significant increases in iNOS immunoexpression with IL-4 stimulus over M2 controls (Figure 95C). FR ECM with IL-4 post-stimulation resulted in a significant increase over PAA controls as well (Figure 95C). Arginase immunoexpression was significantly increased with IFN-γ/LPS stimulation over M1 controls (Figure 95E). ROS ECM also had significantly less arginase-1 immunoexpression compared to PAA ECM with M1 stimulation (E). In the M2 stimulation group, no ECM treatment had different arginase immunoexpression than M2 controls (Figure 95F). ROS ECM elicited decreased arginase immunoexpression from PAA and RNS+ROS ECM

while RNS ECM was lower than PAA ECM with IL-4 stimulus (Figure 95F). With M1 stimulus, all ECM groups resulted in increases in heme oxygenase-1 immunoexpression (Figure 95H). RNS and RNS+ROS ECM with M1 stimulus were higher than PAA and ROS ECM (Figure 95H). With IL-4 stimulus, PAA, RNS and RNS+ROS ECM resulted in significantly higher heme oxygenase-1 immunoexpression than M2 controls (Figure 95I). Nitric oxide production with M1 post-stimulus was higher with PAA, RNS and RNS+ROS ECM (Figure 95K). PAA ECM resulted in the highest nitric oxide production with IFN-γ/LPS while RNS and RNS+ROS was higher than ROS ECM (Figure 95K). There was not substantial nitric oxide production with any IL-4 stimulation condition (Figure 95L). With IFN-γ/LPS stimulus, PAA-treated ECM increased urea production over M2 controls and FR-ECM (Figure 95N). With IL-4 stimulus, PAA ECM also increased urea production over M2 controls as well as RNS+ROS and ROS ECM (Figure 95O).
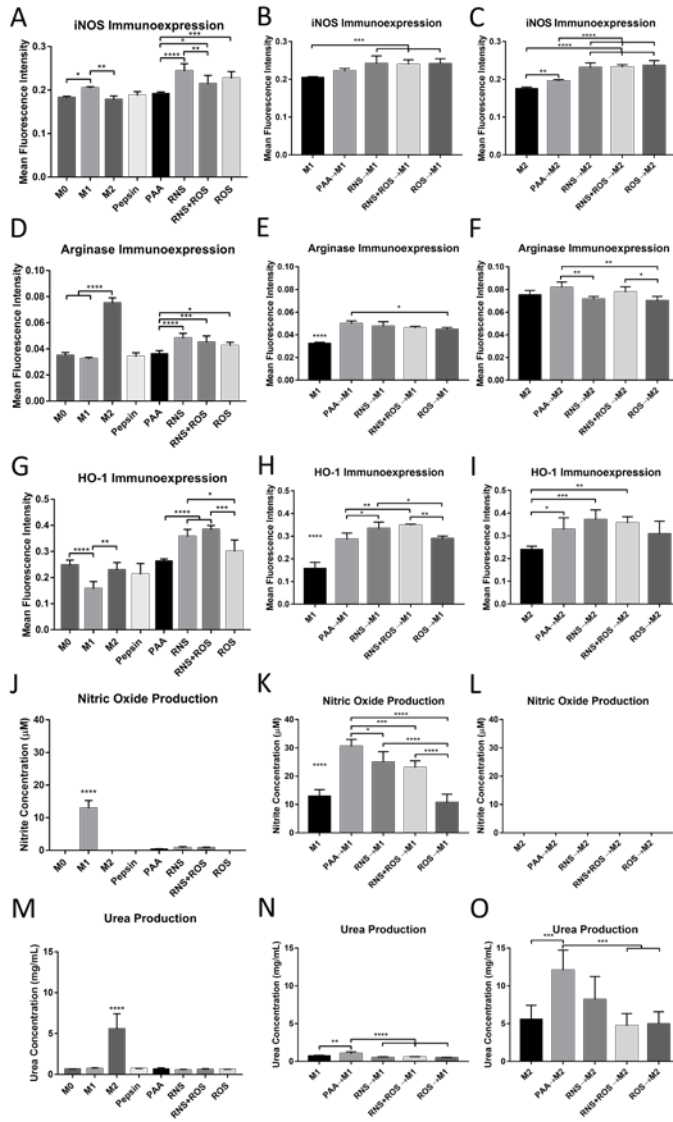
Figure 95: Bone marrow macrophage cultures with ECM pepsin digests.

Immunofluorescence staining for iNOS (A-C), arginase (D-F) and HO-1 (G-I). Greiss reagent system assessment of nitric oxide production in macrophage supernatants (J-L). Urea production from arginase activity assay (M-O). Results presented as mean ± S.D. (* represents $p < 0.05$, ** $p < 0.01$, *** $p < 0.001$, **** $P < 0.0001$).

A.3.4   Histological evaluation of in vivo host response

ECM scaffolds were used to repair a partial thickness defect of the abdominal wall in order to assess the host response to FR-decellularized ECM *in vivo*. This is a standard model which has been used extensively to assess the host response and remodeling of ECM scaffolds [59, 369, 370, 373]. Cellularity was assessed using hematoxylin & eosin staining (Figure 96A-D). RNS and ROS ECM exhibited an enhanced cellular infiltration at 7 days compared to PAA controls (Figure 96Q). This suggests the RNS and ROS modifications elicit higher levels of cellular migration to the wound site. Collagen content as assessed by Masson's trichrome staining did not show large changes at 7 days (Figure 96E-H). There was a significant decrease in Masson's trichrome staining with RNS+ROS ECM from RNS ECM (Figure 96R). Glycosaminoglycan content, as assessed by Alcian blue staining, was similar in magnitude across groups (Figure 96I-L). ROS ECM explants at 7 days did result in significantly higher Alcian blue staining at 7 days compared to RNS+ROS ECM (Figure 96S). There was no difference in the percentage of centralized nuclei in muscle fibers, indicating there was no difference in the regeneration of muscle fibers at 7 days (Figure 96T). Overall, histologic assessment showed a more robust cellular infiltration from RNS and ROS ECM without substantial changes in broad ECM production.

Figure 96: Histological assessment of explants from 7 day ECM repair of abdominal wall defect.

Representative 20X images of hematoxylin & eosin (A-D), Masson's trichrome (E-H) and Alcian blue (I-L) staining of 7 day explants of remodeling ECM. Masson's trichrome staining of regenerating muscle fibers (M-P). Quantification of cellularity (Q), collagen staining (R), glycosaminoglycan staining (S) and percent centralized muscle fiber nuclei (T). Scale bar = 100 μm) Results presented as mean ± S.D. (* represents $p<0.05$, ** $p<0.01$, *** $p<0.001$, **** $p<0.0001$)

A.3.5 Evaluation of In Vivo Macrophage Response

As macrophage phenotype at acute time-points following injury has been shown to predict positive remodeling outcomes downstream, explant sections were immunolabeled with

antibodies detecting macrophage polarization markers [59]. F4/80 was used as a marker for overall macrophage presence within the implant zone at 7 days (Figure 97A-D) [374]. F4/80 immunolabeling showed an increased presence of F4/80$^+$ cells in FR-ECM repaired mice (Figure 97Q). This suggests that FR-ECM elicits a more robust macrophage response at acute time-points. iNOS immunolabeling was performed to detect presence of pro-inflammatory macrophages at 7 days post-implant (Figure 97E-H). There were no significant increases in iNOS immunolabeling at 7 days (Figure 97R). Arginase-1 immunofluorescent labeling was performed to assess presence of anti-inflammatory macrophages at 7 days (Figure 97I-L). ROS ECM repair resulted in significantly increased arginase-1$^+$ response over PAA and RNS ECM, suggesting an increased anti-inflammatory response (Figure 97S). Heme oxygenase immunofluorescent staining was used to assess the presence of anti-oxidant macrophages at 7 days (Figure 97M-P). All FR-ECM resulted in significantly higher percentage of HO-1$^+$ cells at 7 days, indicating a robust anti-oxidant response over PAA ECM (Figure 97T). The results from macrophage phenotyping indicate that free radical decellularization of ECM results in increased macrophage infiltration and increased anti-oxidant macrophage polarization. This response could be beneficial to a variety of regenerative and ischemic injury applications.
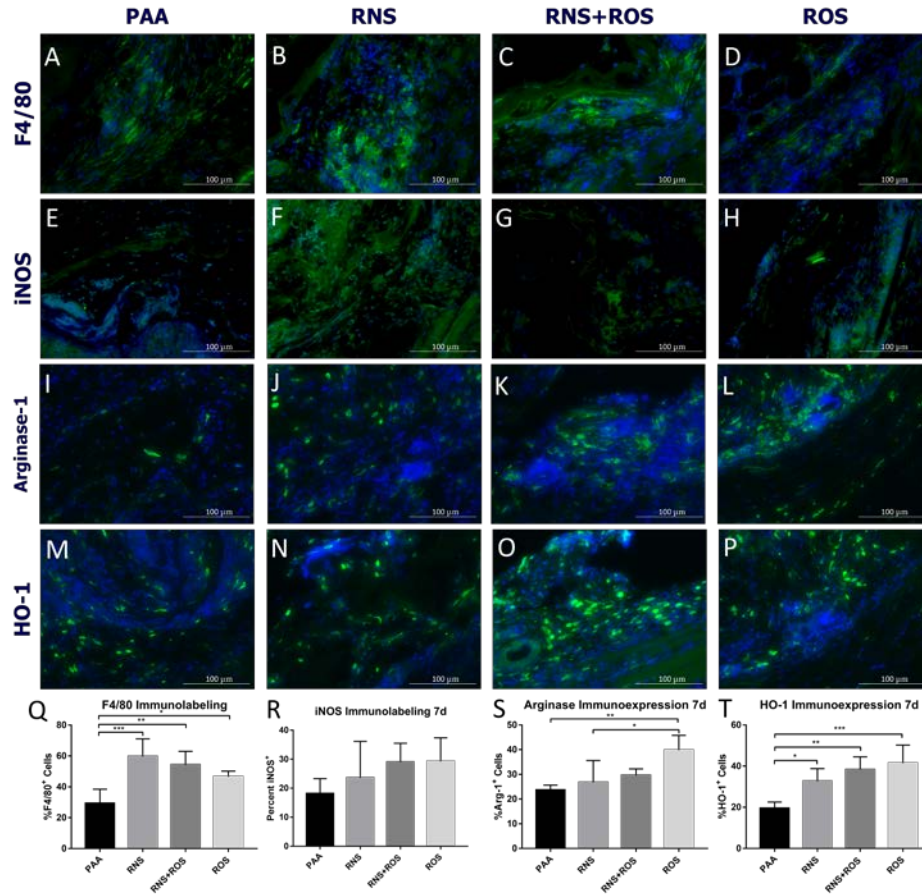
Figure 97: Immuno-labeling of 7 day explants for macrophage polarization markers.

Representative 20X images of immunofluorescent staining of 7 day explants for F4/80 (A-D), iNOS (E-H), arginase-1 (I-L) and heme oxygenase-1 (M-P). Cell Profiler quantification of immunofluorescent staining for F4/80 (Q), iNOS (R), arginase-1 (S) and heme oxygenase-1 (T). Scale bars = 100 μm. Results presented as mean ± S.D. (* represents $p < 0.05$, ** $p < 0.01$, *** $p < 0.001$, **** $p < 0.0001$)

A.3.6   Evaluation of Chronic Remodeling Outcomes

Explants from ECM repair of abdominal wall defects were taken 90 days post-implantation to assess the effect of FR decellularization upon constructive remodeling outcomes. Hematoxylin & eosin staining was performed to assess gross morphology and cellularity during chronic remodeling (Figure 98A-D). There were no significant differences in cellularity at 90 days, suggesting there were no differences in ongoing inflammation (Figure 98Q). There were no differences in Masson's trichrome staining, which suggests that there was no significant differences in fibrotic outcomes (Figure 98R). FR-ECM implantation resulted in a significant increase in Alcian blue staining at 90 days, indicative of increased glycosaminoglycan deposition (Figure 6S). Glycosaminoglycans are important factors in wound healing, which assist with growth factor sequestration and activity, capillary growth and collagen formation [323, 375]. Picrosirius red staining imaged with circularly polarized light was used to assess collagen alignment (Figure 98I-L). RNS ECM had increased levels of red fibers, indicating more highly aligned collagen fibrils than the other ECM types (Figure 98U). There were no significant differences in any of the other groups of fiber alignment (Figure 98V-X). In order to assess quality of muscle healing following regeneration, fast and slow muscle fibers were identified via immunohistochemistry (Figure 98M-P). RNS and ROS ECM had significantly lower fast:slow muscle fiber ratio at 90 days compared to RNS+ROS ECM (Figure 98T). This could be due to unresolved muscle healing as there is an increased presence of slow muscle fibers during acute muscle injury [327].
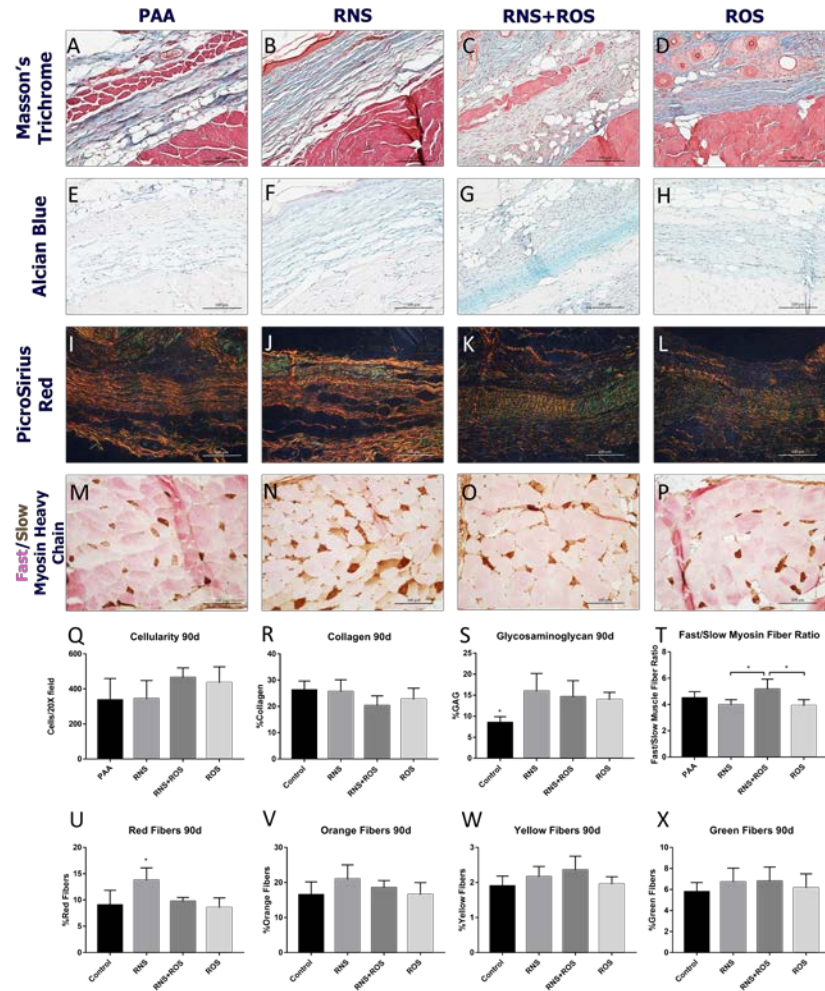
Figure 98: Histologic characterization of chronic 90 day ECM repair of abdominal wall defect.

Histologic stains of 90 day explants for Masson's trichrome (A-D), Alcian blue (E-H), and polarized light microscopy of PicroSirius red (I-L). Immunohistochemical staining for fast (pink) and slow (brown) myosin heavy chain (M-P). Quantification of cellularity (Q), collagen (R), glycosaminoglycan (S), and fast/slow myosin fiber ratio (T). Quantification of red (U), orange (V), yellow (W) and green (X) fiber types from polarized light-imaged PicroSirius Red tissue sections. Scale bars = 100 μm. Results presented as mean ± S.D. (* represents $p < 0.05$, ** $p < 0.01$, *** $p < 0.001$, **** $p < 0.0001$).

A.4   DISCUSSION

The present study sought to investigate the feasibility of decellularizing ECM biomaterials using radical inflammatory species, as well as the effect of these ECM on macrophage responses *in vitro* and within an *in vivo* model of abdominal wall repair. The results presented herein suggest that reactive nitrogen species, reactive oxygen species or the combination of the two are effective reagents for the decellularization of extracellular matrix biomaterials. These reagents also functionalized ECM biomaterials with natural nitroxidative and oxidative modifications similar to those produced during a normal inflammatory event. These modifications could be useful for tailoring ECM biomaterials to have an enhanced inflammatory response that could be beneficial in certain wound repair or disease treatment.

While a basic biochemical assessment was performed, further investigation is necessary to understand how these decellularization agents modified the ECM biomaterials. Hydroxyproline and glycosaminoglycan content were reduced in free radical decellularization methods. It is unclear whether this is due to modification of these biomolecules resulting in lack of detection or whether there is more cellular debris within the scaffolds causing reduced concentration of ECM as a percentage of total mass. Mass spectrometry analysis would be useful in order to determine the retention of different ECM molecules with these methods, but also to understand which biomolecules are being modified by these reagents and how.

Radical inflammatory species-decellularized ECM showed to have an overall antioxidant effect upon macrophages *in vitro* and *in vivo*. This appears to be Nrf2-dependent mechanism involving heme oxygenase-1 upregulation. However, further mechanistic studies would need to be conducted to prove this response. Heme oxygenase-1 induction has been shown to be beneficial for many wound healing applications [376]. The delayed upregulation of heme

oxygenase in diabetic wounds may benefit from the induction of HO-1 by these biomaterials [377]. In muscle, heme oxygenase-1 induction has been shown to improve symptoms from muscle dystrophy [378]. Heme oxygenase-1 expression has been shown to prevent muscle hypertrophy and prevents uncontrolled muscle acceleration of muscle repair [379].

The effect of FR-ECM on the reduction of nitric oxide production in pro-inflammatory conditions also shows the antioxidant potential of this decellularization method. This can be beneficial for preventing further oxidative damage in existing wounds. However, the lack of nitric oxide signaling could affect healing if it is not provided by the modifications created within the biomaterial. It is not evident if this reduction in nitric oxide production is due to heme oxygenase-1 or another antioxidant effect. More testing is needed to understand the direct effect of these ECM scaffolds upon the antioxidant effect of macrophages or other cell types.

Implantation of FR-ECM into an abdominal wound defect model altered the host response observed from a standard ECM control. The increased cellular infiltration observed with RNS and ROS decellularized ECM suggests that those decellularization methods created damage signals that attracted cells to the site of implantation [286]. Reactive oxygen species have been shown to induce cellular migration through a number of pathways [380]. This increased migration could be beneficial in individuals with compromised immune systems such as the elderly or diabetics whose wounds heal more slowly [381, 382].

The acute host response to ECM decellularized with RNS or ROS resulted in increased presence of F4/80$^+$ macrophages. ROS have been shown to induce a CCL2-dependent migratory response in monocytes [383-385]. As macrophage presence is required for proper muscle healing, an enhanced recruitment of macrophages to the site of injury could be beneficial for individuals with delayed immune cell recruitment [93]. FR-ECM induced increases in both anti-

inflammatory and anti-oxidant responses as assessed by arginase-1 and heme oxygenase-1 antibody labeling. ROS have been shown to induce M2 differentiation via late-phase ERK activation [362]. ROS also induce HO-1 protein production via Nrf2 activation [367]. These results suggest that modification of ECM with RNS or ROS directly triggers an anti-inflammatory and anti-oxidant response.

Chronic studies showed no difference in cellularity at 90 days, suggesting there was no ongoing inflammation in any of the samples. The lack of difference in collagen staining suggesting that no treatment induced fibrosis over the level of control ECM. The increased staining for glycosaminoglycans at 90 days in FR-ECM explants is interesting as fetal wounds have been shown to have increased GAG content [375, 386]. Previous reports have shown that M2 macrophages produce more glycosaminoglycans and lead to more GAG sulfation [365]. Therefore, the increased anti-inflammatory macrophage phenotype associated with FR-ECM could directly cause an increase in glycosaminoglycan production. However, the method for assessing GAG content was Alcian blue which is not stoichiometric. Therefore, the increased staining for Alcian blue does not necessarily represent a similar change in magnitude in GAG content at 90 days. Further biochemical testing would be needed to confirm the increased staining.

The unique host response induced by modification of extracellular matrix biomaterials by RNS, ROS or both lends these materials to be useful for specific applications, such as ischemic injury, aging and diabetes. Diabetic wound healing is enhanced by Nrf2 activation and therefore, FR-ECM has potential in treating diabetic wounds [387]. Nitric oxide levels are low in patients with type II diabetes and nephropathy, which contributes to poor angiogenesis and poor wound healing [388]. Reactive oxygen species are recognized to contribute to many stages of wound

215

healing and angiogenesis [389]. The modification of extracellular matrix proteins and lipids with ROS and RNS may produce DAMPs that guide the host response towards healing.

There are several limitation to the current approach. Firstmost, only one concentration of reactive oxygen or nitrogen species was used for the decellularization of extracellular matrix scaffolds. While a standardized protocol for decellularization using peracetic acid has been established, a range of concentrations and durations need to be tested to confirm the optimal protocol for an appropriate host response. These materials were also tested in a model of partial thickness muscle injury in young mice. In order to understand if these materials benefit the healing of ischemic conditions, these materials must be tested in aged and diabetic animals, as well as various site-specific ischemic injuries including wound healing, myocardial infarction, atherosclerosis and stroke. Further quantification of the alterations in the ECM scaffold composition and modification is necessary using genomics, lipidomics and proteomics. How these changes in composition directly impact the host response, which was not investigated in this study, is important to understand as well. Quantification of the effect on gene expression and more quantitative metrics of alterations in extracellular matrix production are necessary to understand the host response and chronic remodeling more fully. For the use of these reagents upon tissues with higher cellularity, combination protocols with detergents are necessary to determine if their effects are similar following detergent cellular removal.

A.5   CONCLUSION

Reactive oxygen and nitrogen species can serve as effective reagents for the decellularization of extracellular matrix biomaterials. These methods imbue biomolecular modifications that are

characteristic of natural inflammatory reactions. The modification of extracellular matrix biomaterials with these highly reactive RNS and ROS result in a greater macrophage infiltration and a shift toward anti-inflammatory and anti-oxidant macrophage phenotypes *in vitro* and *in vivo*. Chronic remodeling resulted in enhanced production of glycosaminoglycans which can aid in beneficial wound healing responses.

APPENDIX B: EFFECT OF EXTRACELLULAR MATRIX SOURCE TISSUE TYPE UPON REMODELING OF TEMPOROMANDIBULAR JOINT MENISCUS REPLACEMENT DEVICE

B.1   INTRODUCTION

The extracellular matrix consists of the myriad secreted proteins, glycosaminoglycan and other molecules that provide structural and signaling functions to a tissue. The extracellular matrix (ECM) is a heterogeneous, dynamic material that is affected by degradation and synthesis by cells and in turn provides signaling cues that affect cell phenotype. Due to this inherent relationship with the cells in a tissue, the ECM has been harvested as a natural biomaterial for reconstruction of various tissues. When effectively prepared and decellularized, ECM biomaterials have been shown to promote constructive remodeling, the site-appropriate formation of new functional host tissue [124]. This regenerative capacity has been demonstrated in many tissues, including esophagus, skeletal muscle, heart, brain, bone and connective tissue among others [390-395].

Recently, devices composed of ECM biomaterials have been successfully used to reconstruct the temporomandibular joint (TMJ) meniscus. Implantation of an acellular, porcine urinary bladder-derived ECM device into a canine model of TMJ meniscus replacement resulted in the formation of site-appropriate, functional host tissue at 6 months that mimicked the native TMJ disc [396]. A more robust study confirmed these previous findings using a canine, urinary bladder ECM device implanted into a porcine model of TMJ meniscus replacement. This study showed a robust, hypercellular response at 1 month post-implantation characteristic of an

218

inflammatory response. The response was resolved by 3 months as the scaffold was completely remodeled into new host tissue at this time. By 6 months, the new remodeled host tissue resembled that of the native TMJ fibrocartilage (cite).

The extracellular matrix composition is unique to its resident tissue. Therefore, ECM biomaterials derived from different tissue types can result in varied cellular responses upon implantation. Cells have been shown to have increased proliferation when they were cultured on ECM harvested from their source tissue [397, 398]. Stem cells grown or administered on tissue specific ECM have shown improved survivability [399]. ECM tissue specificity has become of interest in the natural biomaterial field for these reasons. ECM tissue source has been observed to affect the ability of ECM scaffolds to promote constructive remodeling phenotypes downstream of implantation. When implanted into a rat abdominal wall muscle reconstruction model, faster degrading ECM scaffolds such as small intestine submucosa (SIS) and urinary bladder matrix (UBM) showed more anti-inflammatory macrophage phenotypes at early time points of 14 days, compared to slower degrading scaffolds made from dermis ECM. This was related to better constructive remodeling outcomes at downstream time points of 35 days in the faster degrading scaffolds [59]. ECM tissue source is important for the remodeling response which plays a large role in the success of the TMJ meniscus replacement described above.

Therefore, the present study investigates the promotion of constructive remodeling when the TMJ meniscus replacement device is derived from three different ECM sources: urinary bladder, small intestine and dermis. These sources were chosen due to their use in many clinically available ECM-based products. Previous TMJ meniscus reconstruction studies were performed only with urinary bladder-derived ECM which does not match the tissue type of the TMJ fibrocartilage. A comparative study of the effects of ECM tissue source upon constructive

remodeling of the TMJ meniscus replacement is important for selecting the best material for translating this technology into the clinic.

B.2   MATERIALS & METHODS

B.2.1   Animal Tissue Harvest

Skin, small intestine and urinary bladder were obtained from mongrel dogs of age _____ at time of euthanasia. Tissues were stored at -20°C until needed for further use.

B.2.2   Tissue Decellularization

Small intestine submucosa was prepared as previously described [128]. Briefly, the stratum compactum, muscularis mucosa, and tunica submucosa were mechanically delaminated from adjacent layers in the small intestine. Remaining tissue was thoroughly washed in type 1 water. Following washing, the tissue was decellularized using 0.1% peracetic acid/4% ethanol for 2 hours then alternatively washed with type 1 H_2O and 1X PBS for 15 mins each. All washes were performed under mechanical agitation on a rotary shaker at 300 rpm.

Urinary bladder matrix was prepared as previously described [400]. Briefly, connective and adipose tissue were removed from the serosal side of the urinary bladder. Remnant urine was washed out with tap water. Urinary bladders were mechanically delaminated to disrupt bonds between muscular and connective tissue with the underlying epithelia. The tunica serosa, tunica

220

muscularis externa, tunica submucosa, and most of the tunica muscularis mucosa were mechanically removed. Isolated tissues were washed in type 1 H_2O thoroughly. Decellularization was performed using 0.1% peracetic acid/4% ethanol for 2 hours followed by alternating washes in type 1 H_2O and 1X PBS. All washes were performed under mechanical agitation on a rotary shaker at 300 rpm.

Dermis was prepared as previously described [219]. Briefly, full-thickness skin was delaminated to remove subcutaneous fat, connective tissue, and the epidermis. Dermis was decellularized using incubations on a rotary shaker at 300 rpm in the following solutions: 0.25% trypsin, 6 hours, 1x; deionized water, 15 minutes, 3x; 70% ethanol, 10-12 hours, 1x; 3% H_2O_2, 15 minutes, 1x; deionized water, 15 minutes, 2x; 1% Triton X-100/0.26% EDTA/0.69% Tris, 6 hours, 1x then overnight, 1x; deionized water, 15 minutes, 3x; 0.1% peracetic acid/4% ethanol, 2 hours, 1x; PBS, 15 minutes, 2x; deionized water, 15 minutes, 2x.

Native samples were obtained by processing tissues up to the step before decellularization started. This was done to compare the same layers of tissues together. Samples to be used for biochemical assessment were lyophilized and powdered.

B.2.3 TMJ Device Fabrication

Temporomandibular joint meniscus replacement devices were fabricated as previously described [396]. Briefly, decellularized ECM was frozen at -80°C and then lyophilized. Lyophilized ECM was powdered using a Wiley mill. Sheets of hydrated ECM (2 for UBM and SIS, 1 for dermis) were placed over a mold shaped to the size of a pig TMJ meniscus. Hydrated ECM powder was placed into the mold recess. The ECM powder was then covered with additional sheets of hydrated ECM (2 for UBM and SIS, 1 for dermis). Implants were wrapped in cheesecloth then

vacuum-pressed until sheets were dry. Implants were then frozen and lyophilized until ECM powder was fully dry. Devices used for implantation were sterilized using ethylene oxide.

B.2.4 Histological Assessment

Fresh native and decellularized tissues were fixed in 10% neutral buffered formalin for 3 days prior to being embedded in paraffin wax. Tissue sections were deparaffinized in xylenes 3 times for 3 minutes and then rehydrated using decreasing concentrations of ethanol then tap water. Slides were stained with hematoxylin & eosin staining to confirm removal of nuclei and preservation of native extracellular matrix architecture. Briefly, H&E staining was accomplished with 8 minutes Harris hematoxylin, 2 x 30 seconds dH_2O, 1 minute 5% glacial acetic acid, 2 x 30 seconds dH_2O, 15 seconds Scott's H_2O, 2 x 1 minute dH_2O, 2 minutes alcoholic Eosin, 2 x 30 seconds 95% ethanol, 2 x 30 seconds 100% ethanol, 2 x 1 minute Xylenes, and then fixed with permount.

B.2.5 DNA Content Analysis

Paraffin sections mounted on glass slides were deparaffinized and stained with DAPI. This stain was used to confirm reduction in nuclei and nuclear material from the decellularized scaffolds. Reduction in DNA was quantified using a PicoGreen assay. Briefly, DNA was extracted from lyophilized native and decellularized samples using several repetitions of a 25:24:1 phenol: chloroform: isoamyl alcohol extraction solution. Samples were precipitated using sodium acetate and ethanol and washed in 70% ethanol. DNA pellets were resuspended in Tris-EDTA (TE)

buffer. Samples were diluted and combined with PicoGreen reagent and fluorescence intensity was measured (excitation = 485 nm, emission = 525 nm).

B.2.6   DNA Fragmentation Analysis

Fragmentation of remnant DNA was assessed using an agarose gel. Briefly, a 2% agarose gel was created using 0.5X TBE buffer. DNA extracts were diluted with a 6X DNA Loading Buffer (Novagen) and compared to a 1kD – 0.1 kD DNA standard curve (Fisher Scientific). Gels were imaged on a UV gel imaging machine (_____).

B.2.7   Hydroxyproline Content Analysis

Lyophilized native and decellularized samples were digested in papain digestion buffer (0.125 mg/mL papain; 0.100 M cysteine; 0.100 M Na_2HPO_4; 0.010 M Na_2EDTA) at 50 °C overnight. Fifty microliters of digested were added to screw-top microcentrifuge tubes and combined with 50 μL 2N NaOH and hydrolyzed for 18 hours at 110 °C. Samples were reconstituted with 10.5 μL dH_2O. The following solutions were added to each tube and then thoroughly vortexed after each addition: 20 μL 5N HCl, 100 μL 0.1M Cu_2SO_4, 100 μL 2.5 N NaOH, 100 μL 6% H_2O_2. 400 μL of 3N H_2SO_4 was added to each tube, vortexed and incubated at 80 °C for 5 minutes. Following cooling, 200 μL of freshly prepared 5% p-DMAB in n-propanol was added to each sample and then incubated at 70 °C for 15 minutes. Samples were transferred to a 96 well plate and measured for absorbance at 525 nm.

B.2.8 Glycosaminoglycan Content Analysis

Papain digested samples were pipetted into 96 well plates in triplicate with 50 µL per well. Di-methyl-methylene blue dye was added to each well at 250 µL per well. The absorbance of each well was measured at 540 nm and compared to a standard curve of chondroitin-6-sulfate.

B.2.9 Protein Gel Electrophoresis

Powdered ECM or native tissue was digested for 48 hours under constant stir in a 1mg/mL pepsin solution in 0.01N HCl to create a 10mg/mL ECM digest. ECM digests were diluted to 1mg/mL then loaded into a NuPAGE™ 4-12% Bis-Tris Protein Gel (Thermo) and then ran until protein bands reached end of gel. Gel was stained with Coumassie Blue and then washed with water.

B.2.10 Mechanical Testing

Uniaxial tensile testing was performed on rehydrated TMJ devices using an Instron mechanical testing device. Hydrated extracellular matrix scaffold were stretched under constant strain rate until failure.

B.2.11 Temporomandibular Joint Meniscus Replacement

Pigs underwent unilateral temporomandibular joint meniscus replacement with ECM TMJ meniscus replacement devices as previously described. Remodeled ECM devices were explanted

at 1 month and fixed in 10% neutral buffered formalin. Samples were embedded in paraffin wax, sectioned and then stained with hematoxylin and eosin.

B.2.12 Statistics

All quantitative results were analyzed statistically using a two-way ANOVA with Tukey post-hoc testing. Significance was indicated if p-value was below 0.05.

B.3   RESULTS

B.3.1   Histological Assessment

Hematoxylin & eosin stains of native tissues revealed characteristic physiology of native tissue with intact epidermis and hair follicles in dermis, mucosa and muscularis layers in small intestine and detrusor muscle in bladder. Following decellularization, all tissues exhibited removal of tissues adjacent to the basement membrane as well as resident cells, leaving behind only extracellular matrix (Figure 99). Histological assessment of TMJ meniscus replacement devices show highly aligned extracellular matrix sheets devoid of cellular content.
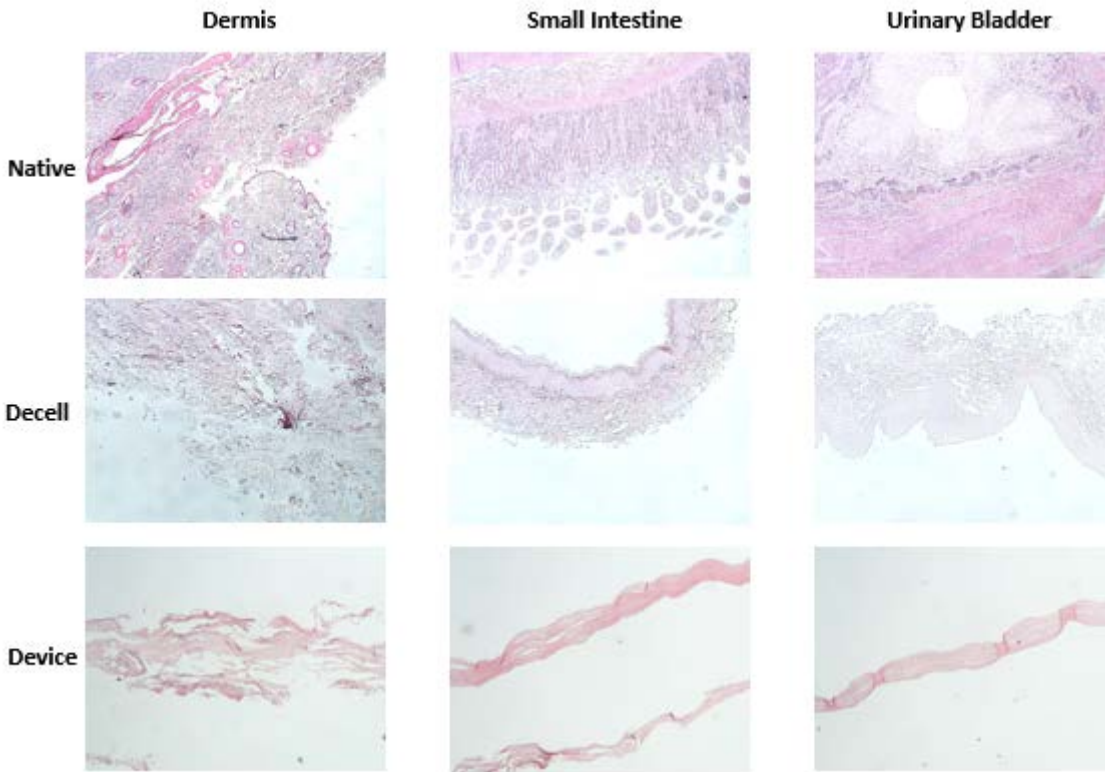
Figure 99: Hematoxylin & eosin staining of native canine dermis, small intestine and urinary bladder, respective decellularized ECM and TMJ meniscus replacement devices created from these ECM.

B.3.2 DAPI Nuclear Stain

Staining of tissue sections with DAPI nuclear stain revealed normal levels of cellular content in native samples. Decellularized ECM and TMJ meniscus replacement devices showed reduced amounts of DAPI staining indicative of a largely decellularized scaffold (Figure 100).
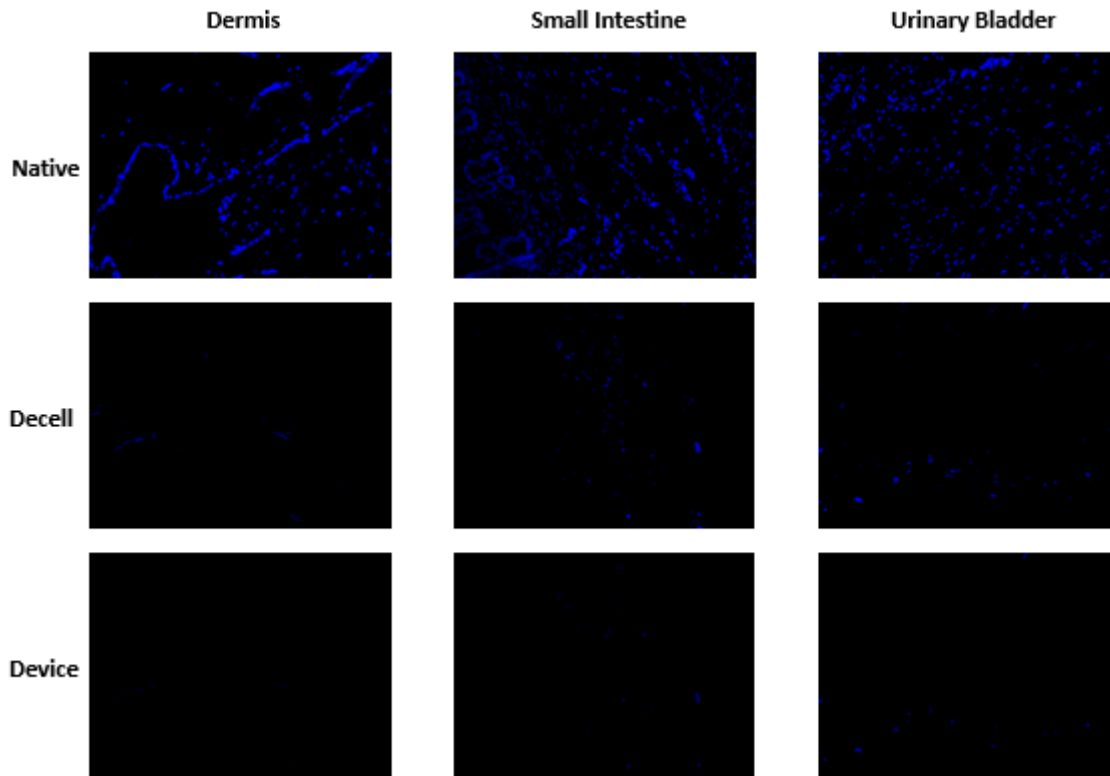
Figure 100: DAPI nuclear staining of native canine dermis, small intestine and urinary bladder, respective decellularized ECM and TMJ meniscus replacement devices created from these ECM.

B.3.3 DNA Quantification and Gel Electrophoresis

DNA gel electrophoresis showed large amounts of high molecular weight DNA in native tissue as expected. DNA extracts from decellularized ECM showed large reductions in levels of DNA (Figure 101A). Remnant DNA was also largely fragmented in all ECM. Quantification of double-stranded DNA content revealed significant reduction in DNA content in all decellularized samples (Figure 101B).
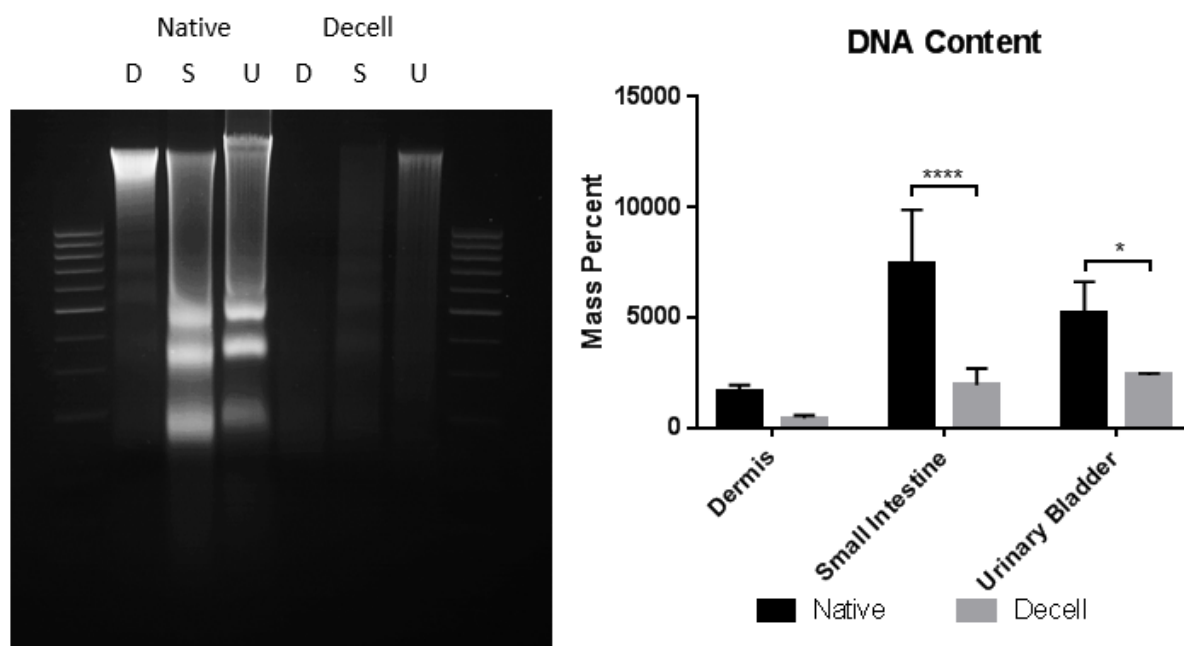
Figure 101: Electrophoresis of DNA extracts on a 2.5% agarose gel (A) and PicoGreen double-stranded DNA quantification of DNA extracts from native and decellularized ECM (B).

B.3.4 Biochemical Analysis

Native and decellularized samples were digested in a pepsin/HCl solution and then ran on a polyacrylamide gel in order to view protein banding. Small intestine and urinary bladder appeared to be most similar in both native and decellularized samples. Dermis had some similarities in protein banding most likely associated with collagen protein. DMMB assay of sulfated glycosaminoglycan content did not reveal any differences between tissues or as a result of decellularization. Hydroxyproline content was enriched in all samples following decellularization. However, there were no significant differences in hydroxyproline content between any of the tissue types.
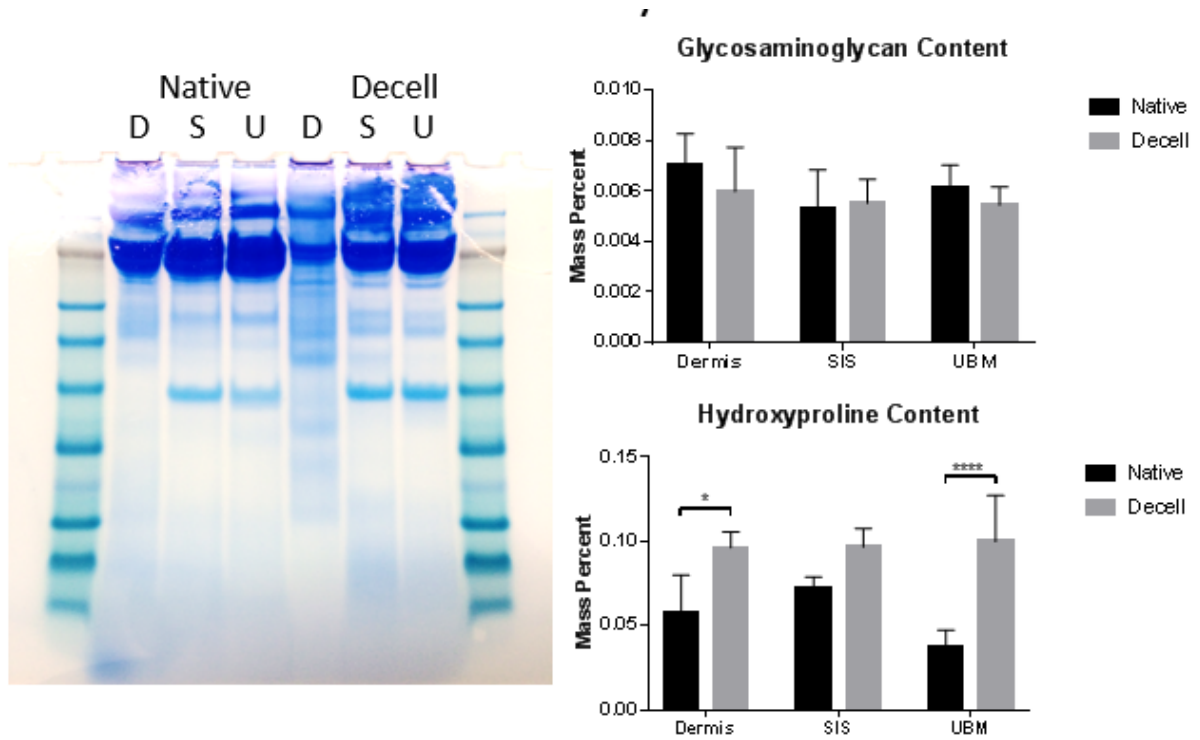
Figure 102: Polyacrylamide gel electrophoresis of ECM pepsin digests (A), DMMB assay of sulfated glycosaminoglycan content (B) and hydroxyproline content (C).

B.3.5 Biomechanical Analysis

Uniaxial tensile testing under constant strain rate was performed on rehydrated devices to failure. Urinary bladder devices carried the least peak load while dermis devices carried the highest peak load. The elastic modulus was similar for small intestine and dermis devices while urinary bladder had a significantly lower elastic modulus than both small intestine and dermis.
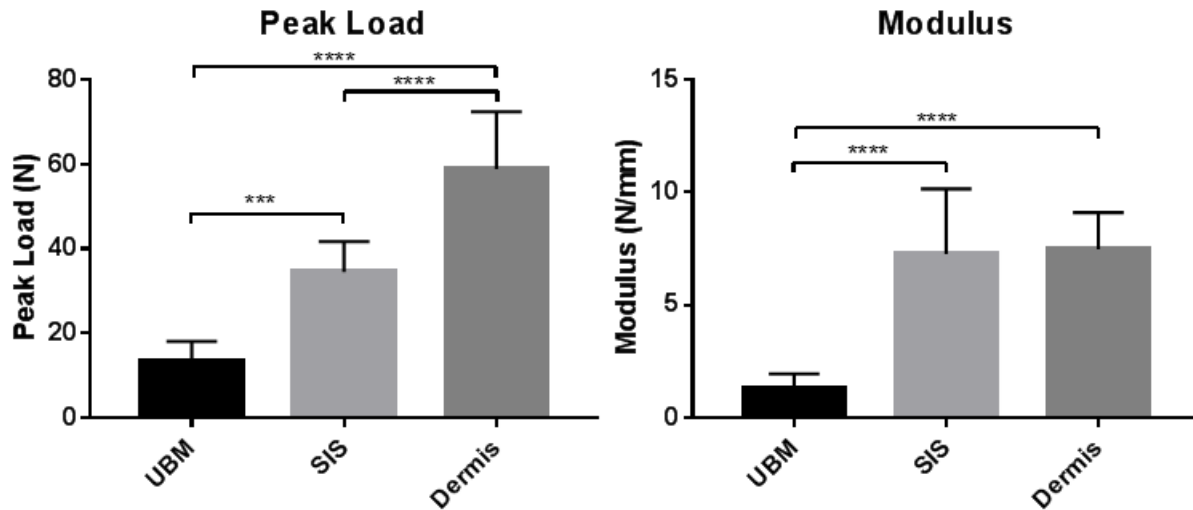
Figure 103: Uniaxial tensile testing under constant strain rate performed on rehydrated devices. Peak load (A) and elastic modulus (B) of urinary bladder, small intestine and dermis devices.

B.3.6 Porcine Model of TMJ Meniscus Replacement

A porcine model was used to evaluate the potential for these devices made from different source tissue to act as a regenerative therapy for TMJ meniscus replacement. Devices were explanted after 1 month for histological evaluation. Hematoxylin & eosin staining revealed that all devices had reduced cellularity and reorganization of matrix into a tissue resembling that of the native TMJ fibrocartilage. However, these samples may suggest that dermis remodels slower than small intestine and urinary bladder counterparts.
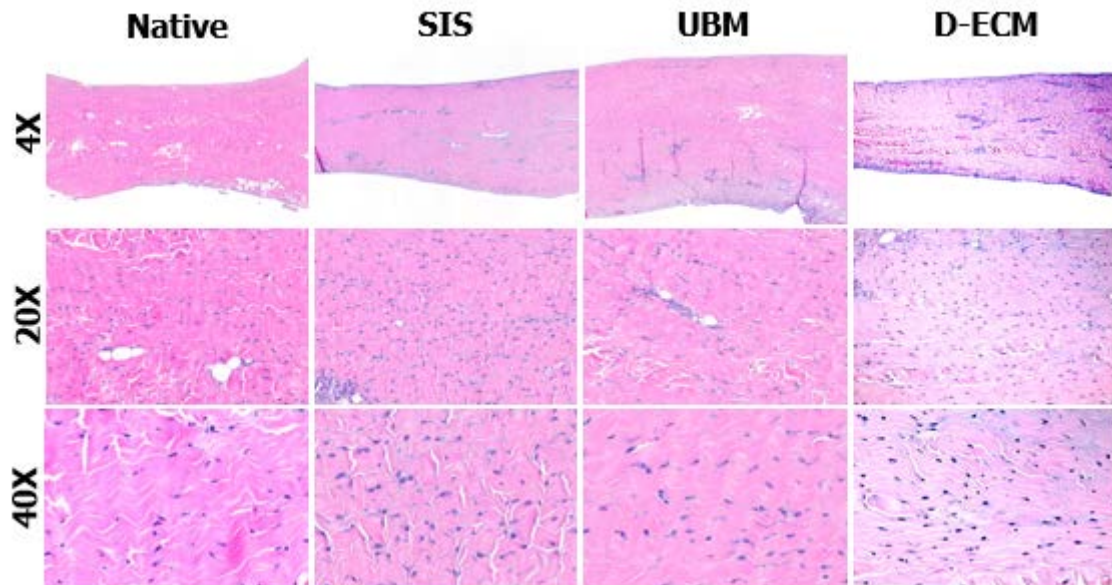
Figure 104: Hematoxylin & eosin staining of 1 month explants from porcine TMJ meniscus replacement and native porcine TMJ meniscus.

B.4   DISCUSSION

Extracellular matrix biomaterials have been proven to successfully remodel into functional site-appropriate host tissue in numerous applications and tissues [137, 390, 396, 401]. Extracellular matrix is known to be tissue specific, having altered protein composition, structure and biomechanics which helps maintain tissue homeostasis [111, 329]. Tissue specific extracellular matrix has been shown to enhance tissue specific proliferation and differentiation [397]. Therefore, it has been posited that the use of tissue-specific ECM biomaterials for regenerative medicine therapies would be beneficial. However, few studies have investigated the comparative success of ECM biomaterials derived from different source tissues. This study seeks to determine the effect of fabricating ECM devices from different tissues in a recently established therapy for temporomandibular joint meniscus replacement.

231

Previous studies have shown that a device fabricated from sheets and powdered urinary bladder-derived ECM was successfully used as a replacement therapy for the temporomandibular joint meniscus in a canine model [396, 402]. Following 6 months of implantation, the acellular device was infiltrated and remodeled into a tissue resembling the fibrocartilage of the native TMJ disc. In order to investigate whether this successful result could be replicated with ECM derived from other tissues, devices were made from urinary bladder as well as small intestine and dermis ECM. These types of ECM have been successful clinically as they have been commercialized into FDA-approved medical devices [215, 403, 404]. All of these scaffolds are also derived from the basement membrane which is rich in ECM ligands that promote cell adhesion and migration [405, 406].

This study showed that the TMJ meniscus replacement device was able to be successfully fabricated from dermis, small intestine submucosa or urinary bladder ECM. ECM was prepared from canine sources in order to preserve xenogenicity in the porcine model used in this study. All three types of ECM were successfully decellularized as indicated by hematoxylin & eosin, DAPI, agarose gel electrophoresis and PicoGreen assay. This is important to prevent potential pro-inflammatory responses from significant amounts of remnant cellular material [223].

Biochemical analysis of decellularized ECM showed no significant differences in sulfated glycosaminoglycan or hydroxyproline content. Further characterization using proteomics would be necessary to determine the specific differences in ECM composition. Gel electrophoresis of pepsin-digested ECM showed some differences in protein banding in dermis samples whereas small intestine and urinary bladder were very similar. This could be due in part to the more extensive decellularization procedure necessary to remove the epidermis and remove cells from the thicker dermal layer. The dermal decellularization procedure involves trypsin

232

which could cleave certain ECM proteins as well as detergents which could denature these proteins as well. This could lead to some differences in the cellular response to the TMJ meniscus replacement device.

Biomechanical analysis of ECM devices showed differences in peak load and elastic modulus. UBM devices were weaker under tensile stress in both peak load and modulus compared to SIS and dermis. SIS was similar to dermis in modulus but had a lower peak load. These biomechanical results suggest that these different ECM biomaterials provide different mechanics to the cells that infiltrate them. Engler et al. showed that differences in matrix stiffness could lead to changes in stem cell differentiation lineage [407]. Changes in integrin ligand density or arrangement could affect cell mechanotransduction. However, the presence or spatial profile of integrin ligands was not investigated. As the temporomandibular joint meniscus mainly possesses a mechanical function reliant upon its unique fibrocartilage tissue structure, the mechanics of the implant before and after remodeling is important [408].

Implantation of TMJ meniscus replacement devices into a porcine model of meniscus replacement showed similar results across devices derived from different tissues. Explants from 1 month showed a reduced cellularity and reorganization of the device ECM into a tissue resembling native TMJ fibrocartilage. However, further investigation will be necessary to show the presence of fibrocartilage specific ECM components. Despite differences in pre-implantation device biomechanics, all devices remodeled similarly. Further studies are necessary to investigate whether all remodeled devices possess similar biomechanics that are appropriate for the TMJ space. This initial data, however, seems to suggest that successful outcomes are achievable in the application of TMJ meniscus replacement when acellular devices are derived from dermis, small intestine or urinary bladder sources.

233

APPENDIX C: EFFECT OF FIBROBLAST SIGNALING UPON MACROPHAGE POLARIZATION

C.1   INTRODUCTION

The processes of wound healing and fibrosis are governed by well-organized stages in order to achieve hemostasis, inflammatory protection, proliferation and restoration of tissue function [409]. Disruption or dysregulation of these processes can lead to aberrant or hypertrophic matrix deposition which results in fibrotic healing [259]. Major orchestrators of wound healing processes include macrophages and fibroblasts [410, 411]. Tissue-resident and monocyte-derived macrophages are recruited to wounds, contributing to pro-inflammatory defense, inflammatory resolution and recruitment of other cells [412]. Fibroblasts are known to contribute to extracellular matrix production needed to protect the wound, release proteases for provisional matrix remodeling, and release cytokines necessary for wound healing and angiogenesis [413].

Macrophages follow neutrophils to wound sites during the first few days following injury and persist for weeks to months. Macrophages help to orchestrate the inflammatory processes associated with wound healing and are responsible for proper immune resolution [414]. Macrophages are now known to exist in a spectrum of phenotypes known as macrophage polarization, existing between M1 and M2 extremes which are characterized as macrophages stimulated with interferon gamma and TLR ligands or interleukin-4, respectively [415]. Normal wound healing necessitates the timely shift of macrophages from the pro-inflammatory M1 to the anti-inflammatory M2 phenotype, leading to inflammatory resolution [416]. However, M2 macrophage phenotypes have been associated with fibrosis due to their production of pro-fibrotic

mediators [417]. Macrophage production of matrix metalloproteinases (MMPs), which degrade and remodel matrix components, plays a large role in wound healing and fibrotic outcomes [418]. Macrophages secrete chemokines which recruit endothelial cells, stem cells and fibroblasts [419]. Based on these conflicting influences, the role of macrophage polarization in wound healing and fibrosis is important but not yet fully understood.

Fibroblasts play an important role in the orchestration of matrix production during wound healing and fibrosis. Proliferation of fibroblasts occurs during the transition from pro-inflammatory to anti-inflammatory responses and as immune cell chemotaxis reduces [420]. Fibroblasts produce many matrix components including collagens, fibronectins, tenascin C, entactin and laminins [421-423]. These cells also produce a variety of chemokines such as CCL2, MIP-1, and IP-10 and growth factors including FGF, PDGF and TGF-β that affect macrophages [424, 425]. These factors can influence macrophage polarization and likely contribute to a phenotype that cannot be simply explained by classical M1 or M2 cytokine stimulus. Additionally, the changes in fibroblast phenotype from resting to activated can also influence signaling production which in turn affects their effect on macrophages [426]. Fibroblast proliferation during the proliferative phase of wound healing is triggered by many factors created during the host response to injury including PDGF, TGF-β, IL-13, eicosanoids, and inhibited by PGE-2 [426]. Fibroblast differentiation into myofibroblasts, usually via TGF-β, is directly associated with fibrotic outcomes [427]. Understanding how fibroblasts and their activation states affect macrophage polarization is important to fully recapitulate normal wound healing pathways and to identify the complex pathways that contribute to fibrosis and scarring.

This study seeks to comprehensively look at the influence of fibroblast signaling upon macrophage polarization. Some work has identified important relationships and effects between

macrophages and fibroblasts but each have been isolated in approach. One study showed that macrophage fibroblast interactions, which are close in normal skin, are interrupted in burn wounds [428]. These macrophage fibroblast interactions occur before collagen production and could factor into matrix production alterations [429]. Previous work has shown that conditioned media from pulmonary fibroblasts alters the production of IL-12 and IL-10 from peripheral blood monocytes [430]. These data suggest that juxtacrine, paracrine and cell contact signaling could be important mediators of macrophage-fibroblast interactions. They also suggest that fibroblasts could play an immunomodulatory role during wound healing, a hypothesis which has been posited previously [431-433]. In this study, a robust approach analyzing the paracrine and juxtacrine effects of fibroblasts upon macrophage polarization will be performed in order to establish pathways of fibroblast immunomodulation during wound healing.

C.2   MATERIALS & METHODS

C.2.1   Fibroblast Conditioned Media

Primary dermal fibroblasts and bone marrow derived macrophages (BMDMs) were isolated from wild-type C57BL6/J mice (Jackson Laboratories). Fibroblast cells were cultured in a 5% CO_2 atmosphere, at 37°C in DMEM medium (Corning 10-013 CM) containing normal glucose (4.5 g/L), 10% fetal calf serum, 1% pen/strep (Gibco 25030-081) and 1% L-glutamate (Gibco 15240-062) either independently or in Corning 0.4-μm Transwell plates (Sigma CLS3407). Fibroblast conditioned media was created from two fibroblast conditions: basal (unactivated) and activated. Basal fibroblasts were cells in basic fibroblast media. Activated fibroblasts were stimulated with

TGF-β. Cells were stimulated and then fresh media was added to cells for an additional 24 hours in order to condition the media with their secreted products (Figure 105A).

C.2.2 Bone Marrow Macrophage Isolation

Bone marrow-derived macrophages were harvested from 2 month C57/BL6 mice as previously described [221]. Briefly, femurs and tibiae were harvested and separated from muscle and connective tissue. Bones were cut at either end to expose bone marrow. Sterile syringe and needles were used to flush out bone marrow using macrophage differentiation media (DMEM/10% FBS/10% L-929 Supernatant/1% PenStrep/2% MEM non-essential amino acids/1% HEPES/0.1% 55μM β-2 mercaptoethanol). Bone marrow lysate was reconstituted in media and filtered through a sterile cell filter. Cells were plated in 96 well plates at a concentration of 200,000 cells per well. Cells were cultured for 7 days in media to differentiate them into macrophages, changing differentiation media every 2 days.

C.2.3 Macrophage Treatment

Following 7 days of differentiation culture as described above, macrophages were treated with acute polarizing regimens to distinguish phenotypes over 24 hours. Naïve macrophage (M0) controls were treated with basal media for 24 hours. M1 (20 ng/mL IFN-γ and 100 ng/mL LPS) and M2 (20 ng/mL IL-4) polarizing cytokines were used to create positive controls for classical pro- and anti-inflammatory macrophages. Macrophages were also treated with conditioned media from fibroblasts for 24 hours (FBCM) (Figure 1B). In order to determine sequential or synergistic effects of macrophage polarizing cytokines and the effects of fibroblast conditioned

media, cytokines and/or conditioned media were added in different combinations. Conditioned media was added for 24 hours, removed and then M1 or M2 macrophage media was added for an additional 24 hours (FBCM→M1Mφ and FBCM→M2Mφ, respectively). Basal, M1 or M2 macrophage media was added for 24 hours, removed and then conditioned media was added for an additional 24 hours (M1Mφ→FBCM, M2Mφ→FBCM, respectively) (Figure 1B). Conditioned media was also added with M1 or M2 polarizing cytokines simultaneously for 24 hours (FBCM+M1Mφ or FBCM+M2Mφ) (Figure 1C).
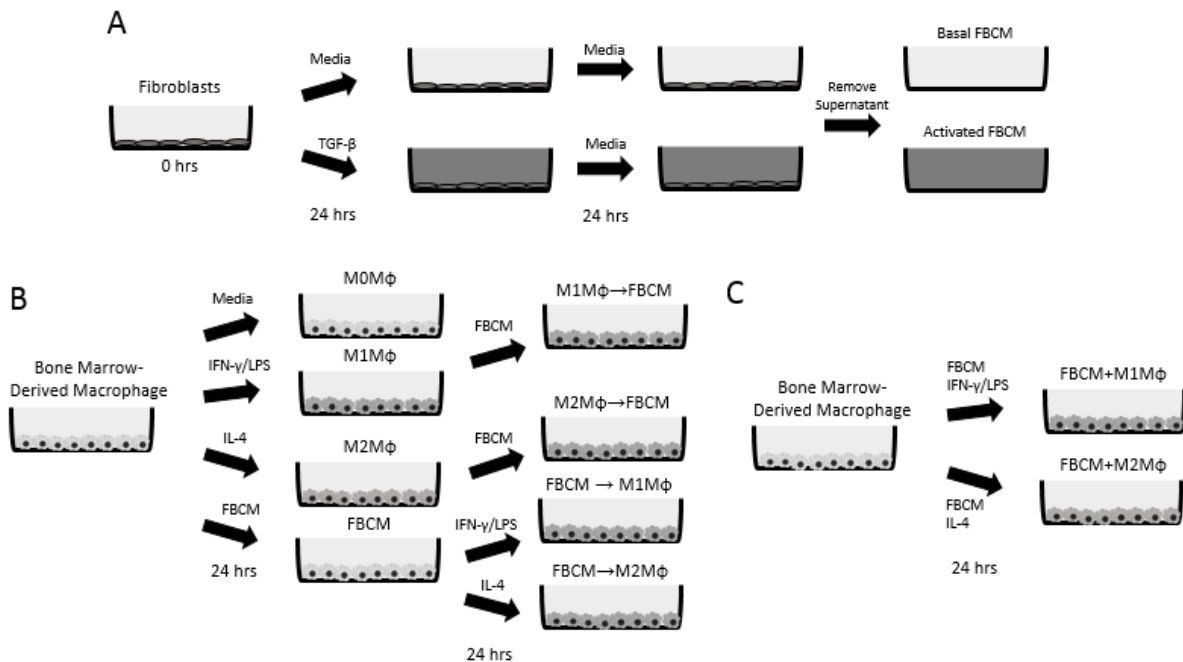
Figure 105: Experimental design for preparation of fibroblast conditioned media (A), sequential treatment of macrophages with fibroblast conditioned media and polarizing cytokines (B), and concurrent treatment of macrophages with fibroblast conditioned media and polarizing cytokines (C).

C.2.4   Transswell Macrophage & Fibroblast Culture

Macrophages were cultured in 6 well plates and stimulated with either M0, M1 or M2 polarizing media. Following stimulation for 24 hours, normal media was added and fibroblasts seeded in 3μm pore transwells were added to the tops of these wells. Following 24 hours of co-culture, media was collected for cytokine analysis and macrophages were harvested for RNA.

C.2.5   Indirect Immunofluorescent Antibody Staining

Cells were fixed with 2% paraformaldehyde (PFA) for 30 minutes then washed in 1XPBS. Cells were incubated in blocking buffer (2% donkey serum, 1% bovine serum albumin (BSA), 0.1% Tween-20) for 1 hour at room temperature. Primary antibodies were diluted in this blocking buffer as follows and incubated overnight at 4 °C: iNOS (1:100, Abcam 3523) Arginase-1 (1:200, Abcam 91279). iNOS is a classical M1 macrophage markers whereas Arginase-1 is a classical M2 macrophage marker. Cells were washed in 1XPBS then incubated in the appropriate fluorescently-labeled secondary antibody solution in blocking buffer for 1 hour at room temperature (1:300 donkey anti-rabbit Alexa Fluor 488 (Abcam 150073)). Cell nuclei were counterstained with DAPI. Six sets of cells were imaged 30 times across each well at 10X magnification using automated position capture function to remove bias from subjective image location acquisition. This set of 30 images per well was counted as one biological replicate. All imaging was performed on an Axio observer T1 microscope. Mean fluorescence intensity of cells was analyzed using Cell Profiler software (Broad Institute). Briefly, DAPI images were used by the program to identify cell nuclei then FITC images were used to identify cell borders around the identified nuclei. The mean fluorescent intensity was calculated by averaging the

pixel intensities (scale of 0 to 1) across the entire cell area. Mean fluorescence intensity values were averaged for all imaged cells in each well.

C.2.6   Phagocytosis Assay

Following treatments, cells were assayed for phagocytic ability using Vybrant Phagocytosis Assay Kit (Invitrogen). Cells were incubated in FITC-labeled dead E. Coli particles for 2 hours in the cell culture incubator. Following washing, the cells were fixed with 2% PFA for 30 minutes then washed with 1X PBS. Cells were counterstained with DAPI then imaged and analyzed as described above.

C.2.7   Taqman Gene Expression Analysis

Following treatments, macrophages (n=5 biological replicates from 5 young (2 month) and 5 aged (18 month) mice) were harvested for RNA using Qiagen RNEasy MiniPrep RNA Isolation Columns following standard protocol. RNA was quantified using a NanoDrop Lite Spectrophotometer (Thermo). cDNA templates were created from 1 μg of RNA using Invitrogen High Capacity RNA-to-cDNA kits (Thermo). Taqman Gene Expression Assays (Thermo) were performed for the following commonly reported M1 and M2 macrophage genes: Nos2 (Mm00440502_m1), IL1b (Mm00434228_m1), IL12b (Mm01288989_m1), TNFa (Mm00443258_m1), MHC-II (Mm01181326_m1), Arg (Mm00475988_m1), Retlna (Fizz1) (Mm00445109_m1), Mrc1 (Mm01329362_m1), IL10 (Mm01288386_m1), and PPARg (Mm00440940_m1).

C.2.8   Nitric Oxide Assay

Following treatments, 50 µL of supernatant from macrophages were transferred into a fresh plate. Nitrite, a stable form of nitric oxide, content was assayed using a Greiss Reagent system. Briefly, 50 µL of sulfanilamide (1% in 5% phosphoric acid) was added to supernatants for 10 minutes. Then, 50 µL of 0.1% N-1-napthylethylenediamine in water was added to the mixture for an additional 10 minutes. The absorbance at 540 nm was measured using a BioTek SYNERGY HTX spectrophotometer.

C.2.9   Arginase Activity Assay

Following treatments, media was removed and macrophages were lysed in 50µL 0.001% Triton X-100 in type 1 H_2O with 1X Halt Protease Inhibitors (Thermo). Twenty five microliters of lysate was added to 25 µL of arginase activation solution (10mM $MnCl_2$/50mM Tris-HCl, pH7.5) and incubated at 55°C for 10 minutes. Samples were allowed to cool and then 50 µL of arginine substrate solution (0.5M L-arginine pH 9.7) was added to each well. Samples were incubated at 37°C for 2 hours. A urea standard curve was created via 2 fold serial dilution from 100 mg/mL to 1.5625 mg/mL with a 0 mg/mL blank in lysis buffer. Five microliters of samples or standards were added to a new 96-well plate and 200 µL of urea detection solution (513 mg/L primaquine, 100 mg/L phthalaldehyde, 2.5 mol/L sulfuric acid, 2.5 g/L boric acid, 0.03% Brij35) was added to each well. Absorbance of samples was analyzed using a plate spectrophotometer at 430 nm between 5-20 minutes following addition of detection solution.

C.2.10 Cytokine Array

Fibroblast conditioned media was removed and spun down for 3 minutes at X,000g. Total protein concentration and purity was measured using a Nano drop (A260/A280 ratio). Equal amounts of protein were used for the analysis- using a max volume of the lowest concentrated protein sample in a volume of 250 ml. A Proteome Profiler Antibody Array was used (R&D Systems AA006)- Mouse Cytokine Array Panel 1. The Proteome Profiler Mouse Cytokine Array Kit, Panel A is a membrane-based sandwich immunoassay. Samples are mixed with a cocktail of biotinylated detection antibodies and then incubated with the array membrane which is spotted in duplicate with capture antibodies to 40 specific target proteins. Captured proteins were visualized using chemiluminescent detection reagents. The signal produced is proportional to the amount of analyte bound. Arrays were analyzed using the Microarray Profiler Plugin for ImageJ to quantify the integrated density of the antibody spots on the array. The image was Inverted, values were measured, and background (average of values from array dots F23 and F24) was subtracted from the values, and normalized to control treatment cells baseline cytokines. The identity of the dots was found by referencing the ARY006 R&D product manual.

C.2.11 Statistical Analysis

Quantitative results were analyzed using a one-way ANOVA with Tukey post-hoc analysis using GraphPad PRISM 7 software. Significance was determined at a p-value less than 0.05.

C.3.1   Effects of Fibroblast Conditioned Media on Naïve Macrophages

In order to determine the effects of fibroblast conditioned media upon macrophage gene expression, bone marrow macrophages were treated with basal media (M0), IFN-γ/LPS (M1), IL-4 (M2) or conditioned media for 24 hours. Taqman gene expression assays were performed on these samples for *Nos2* and *Arg1*. . iNOS is a classical M1 macrophage marker, which metabolizes arginine to produce nitric oxide. Arginase is a classical M2 marker, which competes away arginine from iNOS for the production of polyamines used for collagen synthesis. Treatment with IFN-γ/LPS resulted in significantly higher *Nos2* gene expression compared to M0 and M2 controls as expected (Figure 106A). Conditioned media promoted enhanced transcription of *Nos2* at 24 hours with basal or activated CM promoting a 4.6 or 2.7 fold increase in *Nos2* gene expression over M0 control (Figure 106A). Macrophage treatment with IL-4 resulted in a significant increase in *Arg1* gene expression compared to M0 and M1 controls as expected (Figure 2B). Macrophage treatment with IFN-γ/LPS resulted in a 108-fold increase in *Arg1* gene expression. Conditioned media promoted increased *Arg1* gene expression with basal and activated FBCM inciting a 61- and 1015-fold increase, respectively (Figure 106B). Overall, fibroblast conditioned media has a striking activation of anti-inflammatory macrophage phenotype with some pro-inflammatory effects as well, suggesting that fibroblasts have a role in influencing immune responses during injury.

To assess the effect of conditioned media upon protein expression, macrophages were stained for iNOS and arginase immunoexpression following treatment. M1 macrophages and M2 macrophages both showed increases in iNOS immunoexpression compared to M0 controls with

M1 higher than M2 as well (Figure 2C). Activated conditioned media treatment alone increased iNOS immunoexpression from basal CM as well as the M0 baseline (Figure 106C). Interleukin-4 stimulation produced a significant increase in arginase-1 immunoexpression, as expected from M2 macrophages. Stimulation with interferon-y and lipopolysaccharides resulted in a reduced immunoexpression compared to M0 controls, as expected from M1 macrophages (Figure 106D). Conditioned media treatment alone resulted in significantly lower arginase-1 immunoexpression with basal CM compared to activated CM and M0 controls (Figure 106D). Overall, fibroblast signaling did not produce a strong M1 or M2 phenotype. Though the effect on phenotype appeared to be more pro-inflammatory with activated FBCM increasing iNOS and basal FBCM decreasing arginase-1 immunoexpression.

While treatment with conditioned media produced significant changes in macrophage phenotype, we next wanted to prove that these changes also resulted in altered macrophage function. Pro-inflammatory (M1) macrophages are known to produce nitric oxide in order to produce cytotoxicity in pathogens. Nitric oxide production was indirectly measured through presence of the stable end product of nitric oxide, nitrite, using the Greiss reagent system. Nitrite content was analyzed in supernatants of macrophages following treatment. Stimulus with IFN-γ/LPS produced significantly increased nitrite production compared to naïve and IL-4 stimulated macrophages, which produced no nitrite (Figure 106E). Conditioned media treatment alone led to little nitrite production; however both FBCM groups produced more nitric oxide than M0 controls. This small increase in nitric oxide production in the sub-micromolar range could elicit anti-oxidant pathways that are protective to cells [434].

To assess arginase-1 functionality, urea production was measured from macrophage lysates following treatment as urea is produced by arginase-1. Interleukin-4 treatment caused a

significant increase in urea production compared to M0 and M1 controls as expected (Figure 106F). Conditioned media treatment alone resulted in a significant increase in urea production from activated fibroblasts over basal (Figure 106F). Arginase activity can lead to increased proliferation and collagen production [435]. The increased urea production from activated FBCM suggests activated fibroblasts could enhance fibrosis through increased arginase activity in macrophages.

Macrophages are classically known as phagocytes which uptake pathogens during injury and inflammation. To test changes in macrophage phagocytic function, we cultured macrophages with FITC-labeled E. Coli beads for 2 hours following treatments. Stimulus with IFN-γ/LPS resulted in significantly higher phagocytosis compared to M0 and M2 controls, as expected (Figure 106G). Conditioned media treatment alone had no effect upon phagocytosis. Phagocytosis is important in both the clearance of foreign particles during inflammation and debris during resolution [436]. The lack of effect on phagocytosis suggests fibroblast signaling does not incite a phagocytic phenotype in naïve macrophages regardless of fibroblast activation state.
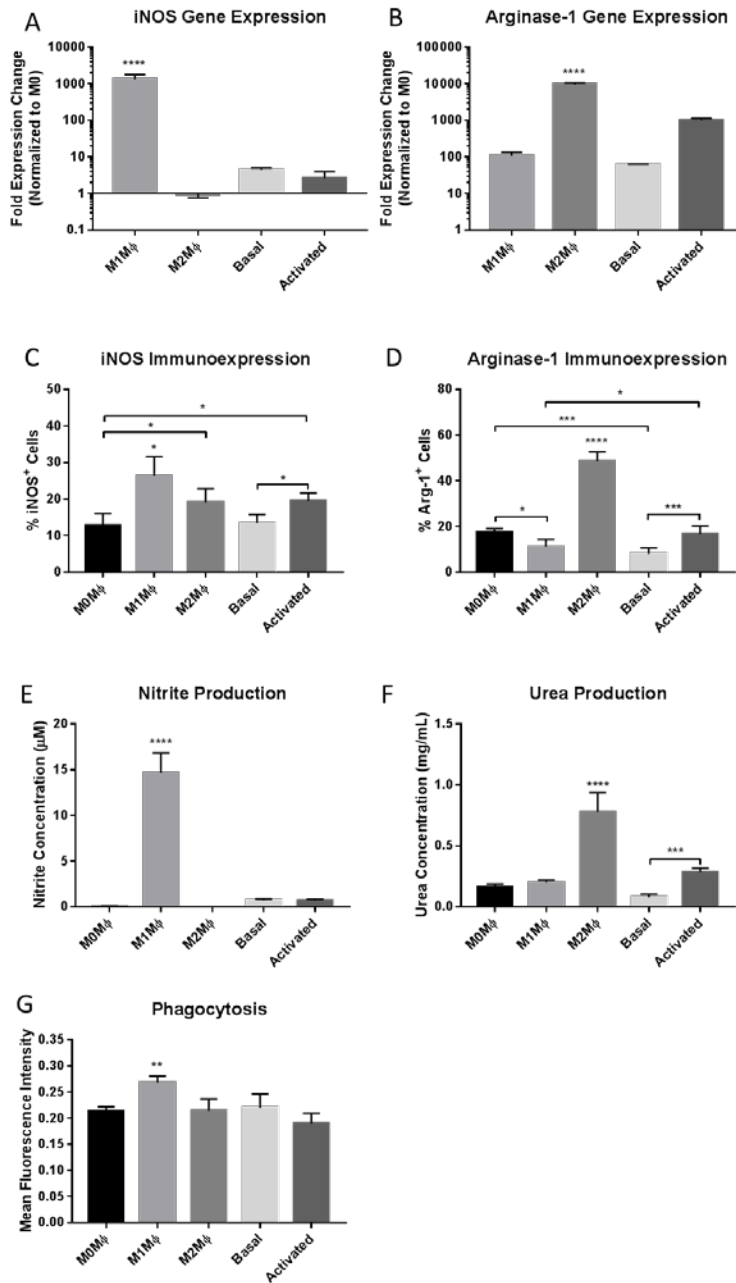
Figure 106: Taqman gene expression for iNOS (A) and arginase (B) of bone marrow derived macrophages treated with basal media (M0), IFN-y/LPS (M1), IL-4 (M2), or conditioned media for 24 hrs. Immunofluorescent antibody labeling of macrophages for iNOS (C). Immunofluorescent antibody labeling for Arginase-1 of bone marrow derived macrophages (D). Greiss reagent system detection of supernatant nitrite levels at 24 hrs (E). Arginase activity assay for urea production of macrophages (F). Vybrant phagocytosis assay on macrophages (G).

C.3.2   Effect of Fibroblast Signaling on Pro-Inflammatory Macrophage Polarization

Following analysis of the effects of fibroblast secretions upon basal macrophage phenotype and function, we next analyzed how fibroblast conditioned media affected polarization to pro-inflammatory M1 extremes. Macrophages were stimulated with fibroblast conditioned media concurrently with (FBCM+M1Mφ), prior to (FBCM→M1Mφ), or following (M1Mφ→FBCM) IFN-γ/LPS treatment. Co-delivery of FBCM and M1 polarizing cytokines resulted in higher iNOS immunoexpression from activated FBCM over basal CM (Figure 107A). Sequential delivery of M1 polarizing cytokines then conditioned media resulted in a significant increase in iNOS immunoexpression with activated FBCM over basal as well as M1→M0 controls (Figure 107B). Sequential delivery of conditioned media then M1 polarizing media resulted in significantly increased iNOS immunoexpression with activated or basal CM and M1 controls (Figure 107C). Fibroblast signaling appears to maintain pro-inflammatory macrophage signaling when it occurs simultaneously. Activated fibroblast signaling appears to extend M1 macrophage phenotype when following pro-inflammatory response while basal and activated fibroblasts can prime macrophages for an enhanced pro-inflammatory response.

Co-stimulus with CM and M1 cytokines did not change arginase immunoexpression (Figure 107D). Stimulation of macrophages with IFN-γ/LPS followed by basal FBCM resulted in significantly less arginase positive cells compared to M1 or activated FBCM (Figure 107E). There was no alteration in arginase immunoexpression with FBCM→M1Mφ treatment (Figure 107F). Similarly to iNOS immunoexpression, fibroblast signaling maintained arginase protein levels when it was delivered concurrently with M1 cytokines. Opposite to iNOS

immunolabeling, arginase immunoexpression was inhibited with basal conditioned media suggesting a further promotion of pro-inflammatory responses.

Activated FBCM enhanced while basal FBCM reduced nitric oxide production when delivered simultaneously with M1 cytokines (Figure 107G). Delivery of conditioned media following M1 stimulus produced overall lower nitrite production compared to M1 stimulus alone while activated was higher than basal (Figure 107H). In M1→CM treatments, activated FBCM again enhanced nitric oxide production while basal decreased it (Figure 107I). The nitric oxide data is most telling of an inhibition of pro-inflammatory responses by basal fibroblasts and a promotion of pro-inflammatory response by activated fibroblast signaling. Interestingly, activated fibroblast signaling enhances nitric oxide production when provided simultaneously or prior to inflammatory stimulus but reduces nitric oxide when following inflammatory stimulus. This spectrum of responses suggests that fibroblast activation can dramatically impact the severity and timing of pro-inflammatory responses.

Urea production with IFN-γ/LPS stimulus was low regardless of stimulation order. With simultaneous treatment, basal FBCM reduced urea production compared to M1 macrophages while activated FBCM enhanced it (Figure 3J). Stimulus with IFN-γ/LPS then FBCM resulted in reduced urea production from basal CM compared to M1 or activated FBCM (Figure 107K). Conditioned media treatment then M1 stimulus resulted in a reduction in urea production from basal FBCM compared to activated FBCM and M1 controls (Figure 107L). The small changes in urea production with M1 cytokines responses suggest fibroblast signaling affect anti-inflammatory function but nitric oxide effects dominate in pro-inflammatory responses.

Co-treatment with CM and M1 cytokines resulted in reduction of phagocytosis compared to M1 controls in all groups (Figure 107M). Conditioned media treatment following M1 stimulus

did not change phagocytosis (Figure 107N). Activated FBCM reduced phagocytosis when followed with IFN-γ/LPS stimulus compared to M1 controls (Figure 107O). These results suggest that signaling from activated fibroblasts can reduce phagocytic macrophage phenotypes but only if it occurs simultaneously or prior to pro-inflammatory signaling.
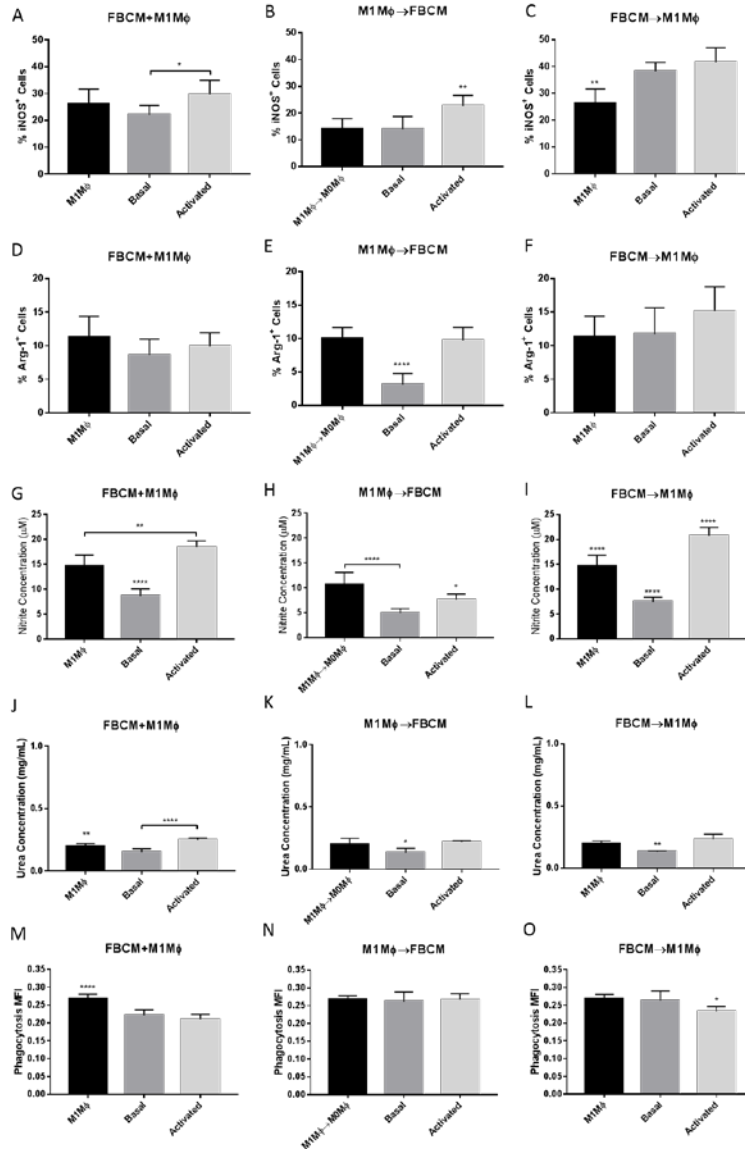
Figure 107: Immunofluorescent antibody labeling for iNOS of bone marrow derived macrophages treated with CM+M1 (A), M1→CM (B) or CM→M1 (C). Immunofluorescent antibody labeling for Arginase-1 of bone marrow derived macrophages treated with CM+M1 (D), M1→CM (E) or CM→M1 (F). Greiss reagent system detection of supernatant nitrite levels at 24 hrs with CM+M1 (G), M1→CM (H) or CM→M1 (I). Arginase activity assay for urea production of macrophages treated with CM+M1 (J), M1→CM (K) or CM→M1 (L). Vybrant phagocytosis assay on macrophages treated with CM+M1 (M), M1→CM (N) or CM→M1 (O).

C.3.3   Effect of Fibroblast Signaling on Anti-Inflammatory Macrophage Polarization

We next analyzed how fibroblast conditioned media affected polarization to an anti-inflammatory M2 phenotype. Co-delivery of conditioned media and IL-4 resulted in decreased iNOS immunoexpression with basal CM stimulation (Figure 108A). Sequential delivery of M2 polarizing cytokines then condition media resulted in significant increases in iNOS immunoexpression from activated over basal CM and M2→M0 controls (Figure 108B). Sequential delivery of conditioned media then M2 polarizing cytokines resulted in significantly higher iNOS immunoexpression with activated FBCM over basal FBCM and M2 controls (Figure 108C). This data suggests that the presence of fibroblasts prior to anti-inflammatory stimulus enhances pro-inflammatory responses while only activated fibroblasts enhance pro-inflammatory macrophage phenotype following IL-4 signaling. Fibroblast activation in anti-inflammatory settings may contribute to mixed macrophage phenotypes observed *in vivo* [437].

Simultaneous delivery of FBCM and M2 polarizing cytokines resulted in increased arginase-1 immunoexpression from activated FBCM while basal FBCM decreased immunoexpression (Figure 108D). M2 cytokine stimulus followed by activated CM resulted in significantly higher arginase-1 immunoexpression than basal and M2 controls (Figure 108E). Sequential treatment of activated CM then M2 polarizing cytokines resulted in significantly increased arginase-1 positive cells over basal and M2 controls (Figure 108F). Overall, activated FBCM tended to increase arginase-1 immunoexpression over basal FBCM with IL-4 stimulus, suggesting an enhanced promotion of an anti-inflammatory macrophage phenotype.

Simultaneous treatment or CM treatment following IL-4 exposure resulted in more nitric oxide production compared to M2 controls (Figure 4G, H). However, the nitric oxide levels were low in magnitude. There was no significant nitric oxide production in FBCM→M2 groups

251

(Figure 108I). Simultaneous delivery of IL-4 and FBCM resulted in enhanced urea production compared to IL-4 alone, while activated FBCM enhanced urea over basal FBCM (Figure 108J). Interleukin-4 treatment followed by activated FB CM resulted in significantly higher urea production compared to basal treatment as well as M2→M0 controls (Figure 108K). Conditioned media treatment prior to IL-4 stimulus resulted in an increased production of urea from activated fibroblast conditioned media compared to IL-4 treatment alone while basal FB CM promoted a decrease (Figure 108L). TGF-beta fibroblast activation caused relatively increased urea production in all treatments suggesting it induces fibroblast phenotypes that enhance anti-inflammatory macrophage responses. This could lead to a synergistic effect of anti-inflammatory macrophages and TGF-β activated fibroblasts to enhance collagen production in fibrosis [438].

With conditioned media and IL-4 co-stimulation, basal and activated CM reduced phagocytosis from M2 controls (Figure 108M). Activated conditioned media promoted reductions in phagocytosis compared to basal CM and M2 controls when condition media was provided before or after M2 stimulus (Figure 108N, O). Activated fibroblast signaling may further turn down phagocytosis in an anti-inflammatory environment.
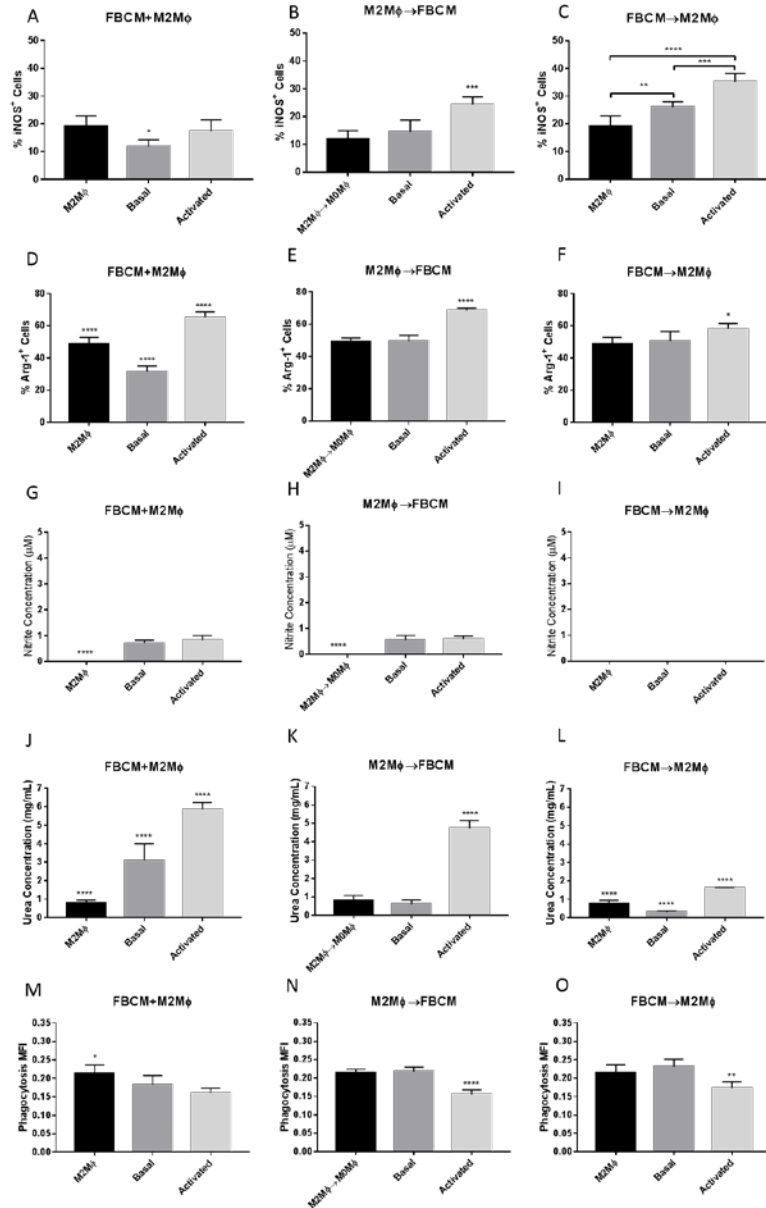
Figure 108: Immunofluorescent antibody labeling for iNOS of bone marrow derived macrophages treated with CM+M2 (A), M2→CM (B) or CM→M2 (C). Immunofluorescent antibody labeling for Arginase-1 of bone marrow derived macrophages treated with CM+M2 (D), M2→CM (E) or CM→M2 (F). Greiss reagent system detection of supernatant nitrite levels at 24 hrs with CM+M2 (G), M2→CM (H) or CM→M2 (I). Arginase activity assay for urea production of macrophages treated with CM+M2 (J), M2→CM (K) or CM→M2 (L). Vybrant phagocytosis assay on macrophages treated with CM+M2 (M), M2→CM (N) or CM→M2 (O).

C.3.4 Characterization of Fibroblast Conditioned Media

In order to determine changes in inflammatory protein expression in unactivated versus activated fibroblasts, conditioned media was assayed using cytokine arrays. TGF-β activation of fibroblasts increased protein expression of the interleukin-1 family, with IL-1ra having the highest increase (Figure 109A). The higher levels of IL-1ra suggest an inhibition of interleukin-1 signaling overall, but further testing would need to be performed. Activated fibroblasts upregulated protein expression of a number of class I cytokines with IL-3 (~300 fold) having the highest increase (Figure 109B). Interleukin-3 is involved in There were also large increases in IL-4 (~10 fold), an anti-inflammatory cytokine, and IL-27 (~7 fold). Fibroblasts stimulated with TGF-β increased IFN-γ and IL-10 protein expression to similar levels (Figure 109C). Of the CC chemokines tested, only CCL17 had a striking increase in protein expression in activated fibroblasts (Figure 109D). CCL17 is a Th2 chemokine, often associated with fibrosis [439]. Fibroblast activation led to increases in the CXC chemokines, CXCL10 and CXCL12 (Figure 109E). CXCL10 is upregulated during fibrosis but has been shown to inhibit fibrotic responses [440]. CXCL12 has been shown to promote fibrosis through CXCR4 signaling [441].
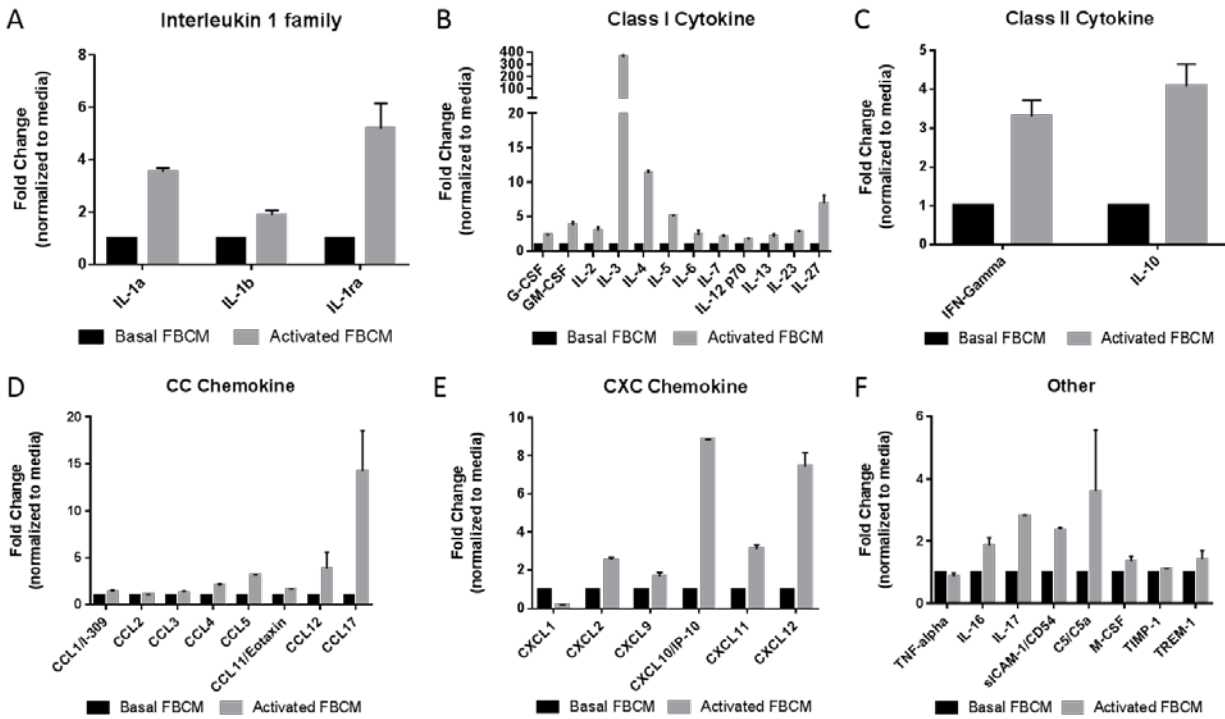
Figure 109: Cytokine array of conditioned media from basal or TGF-β activated fibroblasts. Fold change in protein levels normalized to basal fibroblasts for interleukin 1 cytokines (A), class 1 (hematopoietin) cytokines (B), class II (interferon) cytokines (C), CC chemokines (D), CXC chemokines (E) or members of other cytokine families (F).

C.3.5 Bi-directional signaling between fibroblasts and macrophages

In order to determine real-time communication between macrophages and fibroblasts, fibroblasts were cultured in transwells above macrophages polarized to M0, M1 or M2 phenotypes. Following 24 hours of culture together, conditioned media from macrophages was collected and analyzed using cytokine arrays (Figure 110). Cytokine expression was normalized to M0 macrophages without fibroblast influence. M1 macrophages alone caused increased levels of IL-6, IL-10, GM-CSF, and TNFa while decreasing IFN-g, IL-1b, CCL3, CCL4, CXCL2 and CXCL12 compare to M0 alone. M2 macrophages alone caused increased levels of IL-1b, GM-

CSF and TNF-a cytokine expression while decreasing IFN-g, IL-6, IL-10, CCL3, CCL4, CXCL1, CXCL2 and CXCL12. Addition of fibroblasts above M0 macrophages caused increases in IL-b, IL-6, CXCL2 and TNF-a while reducing IFN-g, IL-10, CCL3, and CCL4 compare to M0 alone. Addition of fibroblasts above M1 macrophages increased IL-1b, IL-6, CXCL2, GM-CSF and TNFa while decreasing IL-10 compared to M1 alone. Addition of fibroblasts above M2 macrophages increased cytokine expression of IL-6 and CXCL1 while reducing IFN-g, IL-1b, CCL3, CCL4, CXCL2, and GM-CSF compared to M2 alone. Addition of fibroblasts seemed to enhance pro-inflammatory responses in M0 and M1 macrophages while tuning down pro-inflammatory responses in M2 macrophages.
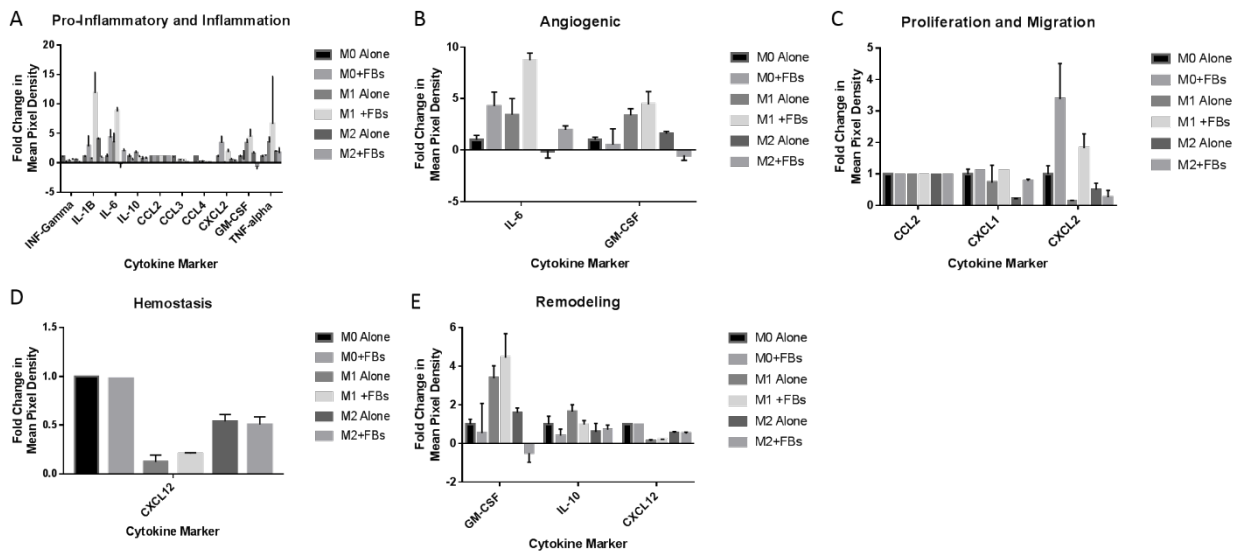
Figure 110: Cytokine array analysis of macrophages cultured with and without fibroblasts in transwells above.

C.4   DISCUSSION

The host response following injury involves many cells and phases in order to orchestrate proper healing. Macrophages are well known orchestrators of the innate inflammatory response while fibroblasts orchestrate the proliferative and remodeling phases of wound healing. While much is known about how the invasion, activation and resolution of these cell populations affects the wound healing process, how they affect each other is largely unknown. This study sought to understand how signaling from fibroblasts influences macrophage phenotype and function. Therapies targeting an anti-inflammatory response may have varying responses based on the cellular microenvironment caused by other host response cells such as fibroblasts. Understanding the pathways controlling this interaction is crucial to optimizing therapies or reducing fibrosis.

Conditioned media from resting, proliferating and activated fibroblasts had profound differences on macrophage phenotype and function as assessed by these *in vitro* assays. Cytokines produced by proliferative and activated fibroblasts enhanced macrophage iNOS immunoexpression in basal, pro- and anti-inflammatory states, suggesting that fibroblast activation can incite or propagate pro-inflammatory phenotypes. Fibroblast activation has been associated with pro-inflammatory responses, including from macrophage-derived TNFα, in atherosclerosis [442]. In contrast, depletion of macrophages from ischemic heart injury prevents fibroblast activation and fibrosis, as well as appropriate healing [443]. While previous studies have shown that pro-inflammatory macrophages activate fibroblasts in wound healing, our results suggest that fibroblast activation, in turn, can promote inflammation in the absence of other signals.

Anti-inflammatory macrophage immunoexpression was mainly affected by fibroblast signaling in basal and IL-4 environments. Interestingly, TGF-β is chiefly produced by

257

macrophages when in an anti-inflammatory state [444]. The reduction in arginase-1 immunoexpression in naïve macrophages promoted by basal and proliferative fibroblast signaling suggests that these signals promote a pro-inflammatory environment. Interestingly, basal and proliferative fibroblast signaling reduced arginase immunoexpression when combined with IL-4 stimulation, suggesting an inhibitory role in anti-inflammation if fibroblasts are present during alternative macrophage activation. The sweeping enhancement of arginase immunoexpression when combined with activated fibroblast signaling suggests that myofibroblasts can prolong alternative activation, which in turn could prolong fibrosis.

Gene expression analysis showed that basal fibroblast conditioned media promoted an enhanced iNOS expression where activation enhanced arginase gene expression. While all conditioned media promoted enhanced iNOS and arginase gene expression, this data suggests a spectrum of macrophage phenotypes promoted by the spectrum of fibroblast activation from a pro-inflammatory macrophage incited by basal fibroblasts and anti-inflammatory macrophage promoted by myofibroblasts.

Our results suggest that fibroblast signaling not only affects macrophage protein and gene expression, but also functional metrics of nitric oxide production and arginase activity. Fibroblast conditioned media led to slight production when macrophages were treated with it alone, with IL-4 simultaneously or after IL-4 stimulation. Despite these nitric oxide levels being quite low compared to pro-inflammatory macrophage levels, nitric oxide is known to have cyto-protective activity at nanomolar concentrations [445]. Fibroblast signaling with pro-inflammatory stimulus had contrasting effects on nitric oxide production depending on the timing of exposure. Conditioned media exposure following pro-inflammatory stimulus reduced nitric oxide production suggesting fibroblasts can reduce macrophage cytotoxicity and transition to anti-

inflammatory activation. Conditioned media exposure before pro-inflammatory stimulus inhibited nitric oxide production with basal fibroblasts and enhanced NO production with activated fibroblasts. This suggests promotion of distinct phenotypes with the presence of difference fibroblast activation states prior to inflammation. Similarly, basal and proliferative fibroblast signaling inhibited while activated promoted nitric oxide signaling when provided simultaneously with IFN-γ and LPS. This also suggests fibroblast presence as well as its spectrum of activation can have strong effects on macrophage function during ongoing inflammation as well as influence the transition to anti-inflammatory phenotypes.

Urea production, an indicator of arginase activity, was also strongly affected by fibroblast signaling. Arginase also produces ornithine which is used to form polyamines and L-proline, both of which are needed for collagen production. Enhanced arginase activity elicited by activated fibroblasts may compound the already fibrotic characteristics of these cells. The presence of basal or activated fibroblasts during or activated fibroblasts after IL-4 mediated alternative macrophage activation drastically enhances this arginase activity *in vitro*. These specific cellular interactions may be a cause for fibrosis where macrophages and fibroblasts are synergistically causing collagen deposition. The presence of basal or proliferating fibroblasts prior to alternative activation may prevent this drastic increase in arginase activity and may prevent excess collagen production.

Fibroblast signaling also had effects on the phagocytic function of macrophages, which is important in the clearance of debris as well as uptake and presentation of antigens [446]. Phagocytosis of apoptotic neutrophils leads to the down-regulation of pro-inflammatory factors IL-1β, IL-8, IL-10, GM-CSF and TNFα while increasing TGF-β and PGE-2, factors that lead to fibroblast activation [447]. Our data shows that proliferative and activated fibroblast signaling

259

decreases macrophage phagocytosis suggesting that these signals provide a feedback loop shifting macrophages from clearance and surveillance to focus on repair and resolution. The lack of inhibition of phagocytosis when CM was presented followed by pro-inflammatory stimuli suggests fibroblast signaling is not strong enough to inhibit phagocytosis after pathogens are already detected. However, simultaneous or previous fibroblast conditioning can steer macrophages away from this phenotype.

Transwell experiments where macrophage and fibroblast signaling was allowed to occur in real-time showed interesting effects on cytokine production. The addition of fibroblasts above macrophages enhanced several pro-inflammatory cytokines including IL-1β and IL-6 in all macrophages while only increasing TNFα in M1 macrophages, suggesting fibroblasts may enhance pro-inflammatory responses from macrophages. Fibroblast transwell addition also reduced IFN-γ and IL-10 cytokine levels. The increase in CXCL2 levels with fibroblast co-culture suggests enhanced migratory signals which would lead to higher recruitment of inflammatory cells to the site of injury [448]. The decreased levels of CCL3, an inhibitor of stem cells, with fibroblast addition may lead to enhanced tissue repair [449]. Overall, fibroblast co-culture enhanced pro-inflammatory cytokine production indicative of an ongoing injury response.

Macrophage and fibroblast responses are crucial to the inflammatory and remodeling processes that occur following injury. Many studies focus on how factors or treatments affect one of these cell populations separately. This study highlights how fibroblast signaling can have drastically different impacts on macrophage phenotype and function based on fibroblast activation state and when fibroblast signaling is presented to these macrophages. More robust

analysis of both macrophages and fibroblasts as well as their interactions is necessary to understand the response to injury and therapeutic interventions designed to improve outcomes.

BIBLIOGRAPHY

[1] C. Lopez-Otin, M.A. Blasco, L. Partridge, M. Serrano, G. Kroemer, The hallmarks of aging, Cell 153(6) (2013) 1194-217.

[2] S. Joanisse, J.P. Nederveen, T. Snijders, B.R. McKay, G. Parise, Skeletal Muscle Regeneration, Repair and Remodelling in Aging: The Importance of Muscle Stem Cells and Vascularization, Gerontology 63(1) (2017) 91-100.

[3] P. Sousa-Victor, L. Garcia-Prat, A.L. Serrano, E. Perdiguero, P. Munoz-Canoves, Muscle stem cell aging: regulation and rejuvenation, Trends in endocrinology and metabolism: TEM 26(6) (2015) 287-96.

[4] B.B. Groen, H.M. Hamer, T. Snijders, J. van Kranenburg, D. Frijns, H. Vink, L.J. van Loon, Skeletal muscle capillary density and microvascular function are compromised with aging and type 2 diabetes, Journal of applied physiology (Bethesda, Md. : 1985) 116(8) (2014) 998-1005.

[5] M.F. O'Leary, A. Vainshtein, S. Iqbal, O. Ostojic, D.A. Hood, Adaptive plasticity of autophagic proteins to denervation in aging skeletal muscle, American journal of physiology. Cell physiology 304(5) (2013) C422-30.

[6] M. Velders, P. Diel, How sex hormones promote skeletal muscle regeneration, Sports medicine (Auckland, N.Z.) 43(11) (2013) 1089-100.

[7] M.A. Bouzid, O. Hammouda, R. Matran, S. Robin, C. Fabre, Changes in oxidative stress markers and biological markers of muscle injury with aging at rest and in response to an exhaustive exercise, PLoS One 9(3) (2014) e90420.

[8] D. Baron, A. Magot, G. Ramstein, M. Steenman, G. Fayet, C. Chevalier, P. Jourdon, R. Houlgatte, F. Savagner, Y. Pereon, Immune response and mitochondrial metabolism are commonly deregulated in DMD and aging skeletal muscle, PLoS One 6(11) (2011) e26952.

[9] K.M. Stearns-Reider, A. D'Amore, K. Beezhold, B. Rothrauff, L. Cavalli, W.R. Wagner, D.A. Vorp, A. Tsamis, S. Shinde, C. Zhang, A. Barchowsky, T.A. Rando, R.S. Tuan, F. Ambrosio, Aging of the skeletal muscle extracellular matrix drives a stem cell fibrogenic conversion, Aging Cell 16(3) (2017) 518-528.

[10] E. Marty, Y. Liu, A. Samuel, O. Or, J. Lane, A review of sarcopenia: Enhancing awareness of an increasingly prevalent disease, Bone 105 (2017) 276-286.

[11] B. Cire, World's older population grows dramatically, 2016. https://www.nih.gov/news-events/news-releases/worlds-older-population-grows-dramatically. (Accessed September 11, 2018.

[12] M. Iannuzzi-Sucich, K.M. Prestwood, A.M. Kenny, Prevalence of Sarcopenia and Predictors of Skeletal Muscle Mass in Healthy, Older Men and Women, The Journals of Gerontology: Series A 57(12) (2002) M772-M777.

[13] H.P. Patel, H.E. Syddall, K. Jameson, S. Robinson, H. Denison, H.C. Roberts, M. Edwards, E. Dennison, C. Cooper, A. Aihie Sayer, Prevalence of sarcopenia in community-dwelling older people in the UK using the European Working Group on Sarcopenia in Older People (EWGSOP) definition: findings from the Hertfordshire Cohort Study (HCS), Age and Ageing 42(3) (2013) 378-384.

[14] C. Beaudart, M. Zaaria, F. Pasleau, J.Y. Reginster, O. Bruyere, Health Outcomes of Sarcopenia: A Systematic Review and Meta-Analysis, PLoS One 12(1) (2017) e0169548.

[15] I. Janssen, D.S. Shepard, P.T. Katzmarzyk, R. Roubenoff, The healthcare costs of sarcopenia in the United States, Journal of the American Geriatrics Society 52(1) (2004) 80-5.

[16] E.D. Schejter, M.K. Baylies, Born to run: creating the muscle fiber, Current opinion in cell biology 22(5) (2010) 566-74.

[17] A. Mauro, Satellite cell of skeletal muscle fibers, The Journal of biophysical and biochemical cytology 9 (1961) 493-5.

[18] X. Shi, D.J. Garry, Muscle stem cells in development, regeneration, and disease, Genes & development 20(13) (2006) 1692-708.

[19] J.R. Beauchamp, L. Heslop, D.S. Yu, S. Tajbakhsh, R.G. Kelly, A. Wernig, M.E. Buckingham, T.A. Partridge, P.S. Zammit, Expression of CD34 and Myf5 defines the majority of quiescent adult skeletal muscle satellite cells, The Journal of cell biology 151(6) (2000) 1221-34.

[20] J. Dhawan, T.A. Rando, Stem cells in postnatal myogenesis: molecular mechanisms of satellite cell quiescence, activation and replenishment, Trends in cell biology 15(12) (2005) 666-73.

[21] S. Tajbakhsh, E. Bober, C. Babinet, S. Pournin, H. Arnold, M. Buckingham, Gene targeting the myf-5 locus with nlacZ reveals expression of this myogenic factor in mature skeletal muscle

fibres as well as early embryonic muscle, Developmental dynamics : an official publication of the American Association of Anatomists 206(3) (1996) 291-300.

[22] R. Tatsumi, J.E. Anderson, C.J. Nevoret, O. Halevy, R.E. Allen, HGF/SF is present in normal adult skeletal muscle and is capable of activating satellite cells, Developmental biology 194(1) (1998) 114-28.

[23] Z. Yablonka-Reuveni, M.E. Danoviz, M. Phelps, P. Stuelsatz, Myogenic-specific ablation of Fgfr1 impairs FGF2-mediated proliferation of satellite cells at the myofiber niche but does not abolish the capacity for muscle regeneration, Frontiers in aging neuroscience 7 (2015) 85.

[24] J. Tonkin, L. Temmerman, R.D. Sampson, E. Gallego-Colon, L. Barberi, D. Bilbao, M.D. Schneider, A. Musaro, N. Rosenthal, Monocyte/Macrophage-derived IGF-1 Orchestrates Murine Skeletal Muscle Regeneration and Modulates Autocrine Polarization, Molecular therapy : the journal of the American Society of Gene Therapy 23(7) (2015) 1189-1200.

[25] R. Buono, C. Vantaggiato, V. Pisa, E. Azzoni, M.T. Bassi, S. Brunelli, C. Sciorati, E. Clementi, Nitric oxide sustains long-term skeletal muscle regeneration by regulating fate of satellite cells via signaling pathways requiring Vangl2 and cyclic GMP, Stem cells (Dayton, Ohio) 30(2) (2012) 197-209.

[26] E. Meadows, J.-H. Cho, J.M. Flynn, W.H. Klein, Myogenin regulates a distinct genetic program in adult muscle stem cells, Developmental Biology 322(2) (2008) 406-414.

[27] S.M. Abmayr, G.K. Pavlath, Myoblast fusion: lessons from flies and mice, Development (Cambridge, England) 139(4) (2012) 641-656.

[28] B. Cadot, V. Gache, E. Vasyutina, S. Falcone, C. Birchmeier, E.R. Gomes, Nuclear movement during myotube formation is microtubule and dynein dependent and is regulated by Cdc42, Par6 and Par3, EMBO reports 13(8) (2012) 741-9.

[29] H. Yin, F. Price, M.A. Rudnicki, Satellite cells and the muscle stem cell niche, Physiological reviews 93(1) (2013) 23-67.

[30] V. Dubowitz, Muscle biopsy--technical and diagnostic aspects, Ann Clin Res 6(2) (1974) 69-79.

[31] C.R. Capers, Multinucleation of skeletal muscle in vitro, The Journal of biophysical and biochemical cytology 7 (1960) 559-66.

[32] J.C. Bruusgaard, K. Liestol, M. Ekmark, K. Kollstad, K. Gundersen, Number and spatial distribution of nuclei in the muscle fibres of normal mice studied in vivo, The Journal of physiology 551(Pt 2) (2003) 467-78.

[33] L.L. Englander, L.L. Rubin, Acetylcholine receptor clustering and nuclear movement in muscle fibers in culture, The Journal of cell biology 104(1) (1987) 87-95.

[34] M. Jevsek, A. Jaworski, L. Polo-Parada, N. Kim, J. Fan, L.T. Landmesser, S.J. Burden, CD24 is expressed by myofiber synaptic nuclei and regulates synaptic transmission, Proc Natl Acad Sci U S A 103(16) (2006) 6374-9.

[35] B. Wang, J. Li, X. Xiao, Adeno-associated virus vector carrying human minidystrophin genes effectively ameliorates muscular dystrophy in mdx mouse model, Proc Natl Acad Sci U S A 97(25) (2000) 13714-9.

[36] L. Gueneau, A.T. Bertrand, J.P. Jais, M.A. Salih, T. Stojkovic, M. Wehnert, M. Hoeltzenbein, S. Spuler, S. Saitoh, A. Verschueren, C. Tranchant, M. Beuvin, E. Lacene, N.B. Romero, S. Heath, D. Zelenika, T. Voit, B. Eymard, R. Ben Yaou, G. Bonne, Mutations of the FHL1 gene cause Emery-Dreifuss muscular dystrophy, American journal of human genetics 85(3) (2009) 338-53.

[37] J. Ehrhardt, J. Morgan, Regenerative capacity of skeletal muscle, Current opinion in neurology 18(5) (2005) 548-53.

[38] G. Shefer, D.P. Van de Mark, J.B. Richardson, Z. Yablonka-Reuveni, Satellite-cell pool size does matter: Defining the myogenic potency of aging skeletal muscle, Developmental Biology 294(1) (2006) 50-66.

[39] I.M. Conboy, M.J. Conboy, A.J. Wagers, E.R. Girma, I.L. Weissman, T.A. Rando, Rejuvenation of aged progenitor cells by exposure to a young systemic environment, Nature 433(7027) (2005) 760-4.

[40] K. Day, G. Shefer, A. Shearer, Z. Yablonka-Reuveni, The depletion of skeletal muscle satellite cells with age is concomitant with reduced capacity of single progenitors to produce reserve progeny, Developmental Biology 340(2) (2010) 330-343.

[41] S.E. Alway, H. Degens, D.A. Lowe, G. Krishnamurthy, Increased myogenic repressor Id mRNA and protein levels in hindlimb muscles of aged rats, American Journal of Physiology-Regulatory, Integrative and Comparative Physiology 282(2) (2002) R411-R422.

[42] A. Bigot, V. Jacquemin, F. Debacq-Chainiaux, G.S. Butler-Browne, O. Toussaint, D. Furling, V. Mouly, Replicative aging down-regulates the myogenic regulatory factors in human myoblasts, Biology of the Cell 100(3) (2012) 189-199.

[43] I.M. Conboy, M.J. Conboy, G.M. Smythe, T.A. Rando, Notch-Mediated Restoration of Regenerative Potential to Aged Muscle, Science 302(5650) (2003) 1575.

265

[44] C.M. Fearing, D.W. Melton, X. Lei, H. Hancock, H. Wang, Z.U. Sarwar, L. Porter, M. McHale, L.M. McManus, P.K. Shireman, Increased Adipocyte Area in Injured Muscle With Aging and Impaired Remodeling in Female Mice, The journals of gerontology. Series A, Biological sciences and medical sciences (2015).

[45] K. Krajnak, S. Waugh, R. Miller, B. Baker, K. Geronilla, S.E. Alway, R.G. Cutlip, Proapoptotic factor Bax is increased in satellite cells in the tibialis anterior muscles of old rats, Muscle & Nerve 34(6) (2006) 720-730.

[46] C. Sonnet, P. Lafuste, L. Arnold, M. Brigitte, F. Poron, F. Authier, F. Chrétien, R.K. Gherardi, B. Chazaud, Human macrophages rescue myoblasts and myotubes from apoptosis through a set of adhesion molecular systems, Journal of Cell Science 119(12) (2006) 2497.

[47] B. Przybyla, C. Gurley, J.F. Harvey, E. Bearden, P. Kortebein, W.J. Evans, D.H. Sullivan, C.A. Peterson, R.A. Dennis, Aging alters macrophage properties in human skeletal muscle both at rest and in response to acute resistance exercise, Experimental gerontology 41(3) (2006) 320-7.

[48] P.A. Della Gatta, A.P. Garnham, J.M. Peake, D. Cameron-Smith, Effect of exercise training on skeletal muscle cytokine expression in the elderly, Brain, Behavior, and Immunity 39 (2014) 80-86.

[49] B.R. Dumke, S.J. Lees, Age-related impairment of T cell-induced skeletal muscle precursor cell function, American Journal of Physiology-Cell Physiology 300(6) (2011) C1226-C1233.

[50] Y. Kharraz, J. Guerra, C.J. Mann, A.L. Serrano, P. Munoz-Canoves, Macrophage plasticity and the role of inflammation in skeletal muscle repair, Mediators of inflammation 2013 (2013) 491497.

[51] J.G. Tidball, S.A. Villalta, Regulatory interactions between muscle and the immune system during muscle regeneration, American journal of physiology. Regulatory, integrative and comparative physiology 298(5) (2010) R1173-87.

[52] S. Mahbub, C.R. Deburghgraeve, E.J. Kovacs, Advanced age impairs macrophage polarization, Journal of interferon & cytokine research : the official journal of the International Society for Interferon and Cytokine Research 32(1) (2012) 18-26.

[53] Y. Wang, M. Wehling-Henricks, G. Samengo, J.G. Tidball, Increases of M2a macrophages and fibrosis in aging muscle are influenced by bone marrow aging and negatively regulated by muscle-derived nitric oxide, Aging Cell 14(4) (2015) 678-88.

[54] C.S. Tam, L.M. Sparks, D.L. Johannsen, J.D. Covington, T.S. Church, E. Ravussin, Low macrophage accumulation in skeletal muscle of obese type 2 diabetics and elderly subjects, Obesity (Silver Spring, Md.) 20(7) (2012) 1530-3.

[55] H. Wang, D.W. Melton, L. Porter, Z.U. Sarwar, L.M. McManus, P.K. Shireman, Altered macrophage phenotype transition impairs skeletal muscle regeneration, The American journal of pathology 184(4) (2014) 1167-84.

[56] Y.C. Liu, X.B. Zou, Y.F. Chai, Y.M. Yao, Macrophage polarization in inflammatory diseases, International journal of biological sciences 10(5) (2014) 520-9.

[57] P.J. Murray, Macrophage Polarization, Annual review of physiology 79 (2017) 541-566.

[58] E. Rigamonti, P. Zordan, C. Sciorati, P. Rovere-Querini, S. Brunelli, Macrophage plasticity in skeletal muscle repair, BioMed research international 2014 (2014) 560629.

[59] B.N. Brown, R. Londono, S. Tottey, L. Zhang, K.A. Kukla, M.T. Wolf, K.A. Daly, J.E. Reing, S.F. Badylak, Macrophage phenotype as a predictor of constructive remodeling following the implantation of biologically derived surgical mesh materials, Acta biomaterialia 8(3) (2012) 978-87.

[60] R. Gentek, K. Molawi, M.H. Sieweke, Tissue macrophage identity and self-renewal, Immunological reviews 262(1) (2014) 56-73.

[61] F. Ginhoux, S. Jung, Monocytes and macrophages: developmental pathways and tissue homeostasis, Nature reviews. Immunology 14(6) (2014) 392-404.

[62] H. Tsutsui, S. Nishiguchi, Importance of Kupffer cells in the development of acute liver injuries in mice, International journal of molecular sciences 15(5) (2014) 7711-30.

[63] L. Morales-Nebreda, A.V. Misharin, H. Perlman, G.R. Budinger, The heterogeneity of lung macrophages in the susceptibility to disease, European respiratory review : an official journal of the European Respiratory Society 24(137) (2015) 505-9.

[64] K. Fujiu, J. Wang, R. Nagai, Cardioprotective function of cardiac macrophages, Cardiovascular research 102(2) (2014) 232-9.

[65] J.M. den Haan, G. Kraal, Innate immune functions of macrophage subpopulations in the spleen, Journal of innate immunity 4(5-6) (2012) 437-45.

[66] C.C. Bain, A.M. Mowat, The monocyte-macrophage axis in the intestine, Cellular immunology 291(1-2) (2014) 41-8.

[67] K.E. McGrath, J.M. Frame, J. Palis, Early hematopoiesis and macrophage development, Seminars in immunology 27(6) (2015) 379-387.

[68] K. Molawi, Y. Wolf, P.K. Kandalla, J. Favret, N. Hagemeyer, K. Frenzel, A.R. Pinto, K. Klapproth, S. Henri, B. Malissen, H.R. Rodewald, N.A. Rosenthal, M. Bajenoff, M. Prinz, S. Jung, M.H. Sieweke, Progressive replacement of embryo-derived cardiac macrophages with age, The Journal of Experimental Medicine 211(11) (2014) 2151-8.

[69] K. Molawi, M.H. Sieweke, Monocytes compensate Kupffer cell loss during bacterial infection, Immunity 42(1) (2015) 10-2.

[70] K. Taut, C. Winter, D.E. Briles, J.C. Paton, J.W. Christman, R. Maus, R. Baumann, T. Welte, U.A. Maus, Macrophage Turnover Kinetics in the Lungs of Mice Infected with Streptococcus pneumoniae, American journal of respiratory cell and molecular biology 38(1) (2008) 105-13.

[71] E.E. Ghosn, A.A. Cassado, G.R. Govoni, T. Fukuhara, Y. Yang, D.M. Monack, K.R. Bortoluci, S.R. Almeida, L.A. Herzenberg, L.A. Herzenberg, Two physically, functionally, and developmentally distinct peritoneal macrophage subsets, Proc Natl Acad Sci U S A 107(6) (2010) 2568-73.

[72] S. Yona, K.W. Kim, Y. Wolf, A. Mildner, D. Varol, M. Breker, D. Strauss-Ayali, S. Viukov, M. Guilliams, A. Misharin, D.A. Hume, H. Perlman, B. Malissen, E. Zelzer, S. Jung, Fate mapping reveals origins and dynamics of monocytes and tissue macrophages under homeostasis, Immunity 38(1) (2013) 79-91.

[73] D.W. Cain, E.G. O'Koren, M.J. Kan, M. Womble, G.D. Sempowski, K. Hopper, M.D. Gunn, G. Kelsoe, Identification of a tissue-specific, C/EBPbeta-dependent pathway of differentiation for murine peritoneal macrophages, Journal of immunology (Baltimore, Md. : 1950) 191(9) (2013) 4665-75.

[74] V. Dioszeghy, M. Rosas, B.H. Maskrey, C. Colmont, N. Topley, P. Chaitidis, H. Kuhn, S.A. Jones, P.R. Taylor, V.B. O'Donnell, 12/15-Lipoxygenase regulates the inflammatory response to bacterial products in vivo, Journal of immunology (Baltimore, Md. : 1950) 181(9) (2008) 6514-24.

[75] M.L. Novak, E.M. Weinheimer-Haus, T.J. Koh, Macrophage Activation and Skeletal Muscle Healing Following Traumatic Injury, The Journal of pathology 232(3) (2014) 344-355.

[76] S. Gordon, P.R. Taylor, Monocyte and macrophage heterogeneity, Nature reviews. Immunology 5(12) (2005) 953-64.

[77] C. Auffray, D. Fogg, M. Garfa, G. Elain, O. Join-Lambert, S. Kayal, S. Sarnacki, A. Cumano, G. Lauvau, F. Geissmann, Monitoring of Blood Vessels and Tissues by a Population of Monocytes with Patrolling Behavior, Science 317(5838) (2007) 666.

[78] C. Sunderkötter, T. Nikolic, M.J. Dillon, N. van Rooijen, M. Stehling, D.A. Drevets, P.J.M. Leenen, Subpopulations of Mouse Blood Monocytes Differ in Maturation Stage and Inflammatory Response, The Journal of Immunology 172(7) (2004) 4410.

[79] M.A. Ingersoll, R. Spanbroek, C. Lottaz, E.L. Gautier, M. Frankenberger, R. Hoffmann, R. Lang, M. Haniffa, M. Collin, F. Tacke, A.J.R. Habenicht, L. Ziegler-Heitbrock, G.J. Randolph, Comparison of gene expression profiles between human and mouse monocyte subsets, Blood 115(3) (2010) e10.

[80] S.-M. Ong, E. Hadadi, T.-M. Dang, W.-H. Yeap, C.T.-Y. Tan, T.-P. Ng, A. Larbi, S.-C. Wong, The pro-inflammatory phenotype of the human non-classical monocyte subset is attributed to senescence, Cell Death & Disease 9(3) (2018) 266.

[81] M. Brigitte, C. Schilte, A. Plonquet, Y. Baba-Amer, A. Henri, C. Charlier, S. Tajbakhsh, M. Albert, R.K. Gherardi, F. Chretien, Muscle resident macrophages control the immune cell reaction in a mouse model of notexin-induced myoinjury, Arthritis and rheumatism 62(1) (2010) 268-79.

[82] C.F. Nathan, H.W. Murray, M.E. Wiebe, B.Y. Rubin, Identification of interferon-gamma as the lymphokine that activates human macrophage oxidative metabolism and antimicrobial activity, The Journal of Experimental Medicine 158(3) (1983) 670-89.

[83] S.L. Abramson, J.I. Gallin, IL-4 inhibits superoxide production by human mononuclear phagocytes, Journal of immunology (Baltimore, Md. : 1950) 144(2) (1990) 625-30.

[84] M. Stein, S. Keshav, N. Harris, S. Gordon, Interleukin 4 potently enhances murine macrophage mannose receptor activity: a marker of alternative immunologic macrophage activation, The Journal of Experimental Medicine 176(1) (1992) 287-92.

[85] J.P. Edwards, X. Zhang, D.M. Mosser, The expression of heparin-binding epidermal growth factor-like growth factor by regulatory macrophages, Journal of immunology (Baltimore, Md. : 1950) 182(4) (2009) 1929-39.

[86] A. Classen, J. Lloberas, A. Celada, Macrophage activation: classical versus alternative, Methods in molecular biology (Clifton, N.J.) 531 (2009) 29-43.

[87] F.A.W. Verreck, T. de Boer, D.M.L. Langenberg, M.A. Hoeve, M. Kramer, E. Vaisberg, R. Kastelein, A. Kolk, R. de Waal-Malefyt, T.H.M. Ottenhoff, Human IL-23-producing type 1 macrophages promote but IL-10-producing type 2 macrophages subvert immunity to

(myco)bacteria, Proceedings of the National Academy of Sciences of the United States of America 101(13) (2004) 4560.

[88] S. Gordon, Alternative activation of macrophages, Nature reviews. Immunology 3(1) (2003) 23-35.

[89] S. Goerdt, C.E. Orfanos, Other Functions, Other Genes: Alternative Activation of Antigen-Presenting Cells, Immunity 10(2) (1999) 137-142.

[90] A. Mantovani, A. Sica, S. Sozzani, P. Allavena, A. Vecchi, M. Locati, The chemokine system in diverse forms of macrophage activation and polarization, Trends in immunology 25(12) (2004) 677-86.

[91] P.J. Murray, J.E. Allen, S.K. Biswas, E.A. Fisher, D.W. Gilroy, S. Goerdt, S. Gordon, J.A. Hamilton, L.B. Ivashkiv, T. Lawrence, M. Locati, A. Mantovani, F.O. Martinez, J.-L. Mege, D.M. Mosser, G. Natoli, J.P. Saeij, J.L. Schultze, K.A. Shirey, A. Sica, J. Suttles, I. Udalova, J.A. van Ginderachter, S.N. Vogel, T.A. Wynn, Macrophage activation and polarization: nomenclature and experimental guidelines, Immunity 41(1) (2014) 14-20.

[92] L. Arnold, A. Henry, F. Poron, Y. Baba-Amer, N. van Rooijen, A. Plonquet, R.K. Gherardi, B. Chazaud, Inflammatory monocytes recruited after skeletal muscle injury switch into antiinflammatory macrophages to support myogenesis, The Journal of Experimental Medicine 204(5) (2007) 1057-69.

[93] W. Xiao, Y. Liu, P. Chen, Macrophage Depletion Impairs Skeletal Muscle Regeneration: the Roles of Pro-fibrotic Factors, Inflammation, and Oxidative Stress, Inflammation 39(6) (2016) 2016-2028.

[94] B.A. St Pierre, J.G. Tidball, Differential response of macrophage subpopulations to soleus muscle reloading after rat hindlimb suspension, Journal of applied physiology (Bethesda, Md. : 1985) 77(1) (1994) 290-7.

[95] M. Saclier, H. Yacoub-Youssef, A.L. Mackey, L. Arnold, H. Ardjoune, M. Magnan, F. Sailhan, J. Chelly, G.K. Pavlath, R. Mounier, M. Kjaer, B. Chazaud, Differentially activated macrophages orchestrate myogenic precursor cell fate during human skeletal muscle regeneration, Stem cells (Dayton, Ohio) 31(2) (2013) 384-96.

[96] H. Degens, The role of systemic inflammation in age-related muscle weakness and wasting, Scandinavian journal of medicine & science in sports 20(1) (2010) 28-38.

[97] A.C. Hearps, G.E. Martin, T.A. Angelovich, W.J. Cheng, A. Maisa, A.L. Landay, A. Jaworowski, S.M. Crowe, Aging is associated with chronic innate immune activation and dysregulation of monocyte phenotype and function, Aging cell 11(5) (2012) 867-75.

[98] S. Seidler, H.W. Zimmermann, M. Bartneck, C. Trautwein, F. Tacke, Age-dependent alterations of monocyte subsets and monocyte-related chemokine pathways in healthy adults, BMC Immunol 11 (2010) 30.

[99] G.S. Ashcroft, M.A. Horan, M.W. Ferguson, Aging alters the inflammatory and endothelial cell adhesion molecule profiles during human cutaneous wound healing, Laboratory investigation; a journal of technical methods and pathology 78(1) (1998) 47-58.

[100] C. Herrero, C. Sebastian, L. Marques, M. Comalada, J. Xaus, A.F. Valledor, J. Lloberas, A. Celada, Immunosenescence of macrophages: reduced MHC class II gene expression, Experimental gerontology 37(2-3) (2002) 389-94.

[101] G. Zissel, M. Schlaak, J. Muller-Quernheim, Age-related decrease in accessory cell function of human alveolar macrophages, Journal of investigative medicine : the official publication of the American Federation for Clinical Research 47(1) (1999) 51-6.

[102] D. Wu, S.N. Meydani, Mechanism of age-associated up-regulation in macrophage PGE2 synthesis, Brain, behavior, and immunity 18(6) (2004) 487-94.

[103] D. van Duin, S. Mohanty, V. Thomas, S. Ginter, R.R. Montgomery, E. Fikrig, H.G. Allore, R. Medzhitov, A.C. Shaw, Age-associated defect in human TLR-1/2 function, Journal of immunology 178(2) (2007) 970-5.

[104] E.D. Boehmer, M.J. Meehan, B.T. Cutro, E.J. Kovacs, Aging negatively skews macrophage TLR2- and TLR4-mediated pro-inflammatory responses without affecting the IL-2-stimulated pathway, Mechanisms of ageing and development 126(12) (2005) 1305-13.

[105] M. De La Fuente, Changes in the macrophage function with aging, Comparative biochemistry and physiology. A, Comparative physiology 81(4) (1985) 935-8.

[106] E. Linehan, Y. Dombrowski, R. Snoddy, P.G. Fallon, A. Kissenpfennig, D.C. Fitzgerald, Aging impairs peritoneal but not bone marrow-derived macrophage phagocytosis, Aging Cell 13(4) (2014) 699-708.

[107] D.J. Holt, D.W. Grainger, Senescence and quiescence induced compromised function in cultured macrophages, Biomaterials 33(30) (2012) 7497-507.

[108] E. Alvarez, A. Machado, F. Sobrino, C. Santa Maria, Nitric oxide and superoxide anion production decrease with age in resident and activated rat peritoneal macrophages, Cell Immunol 169(1) (1996) 152-5.

[109] D. Hachim, N. Wang, S.T. LoPresti, E.C. Stahl, R. Rege, Y. Umeda, S. Carey, D. Mani, B.N. Brown, Effects of Aging upon the Host Response to Implants, J Biomed Mater Res A In Press. (2017).

[110] S.T. LoPresti, B.N. Brown, Effect of Source Animal Age upon Macrophage Response to Extracellular Matrix Biomaterials, Journal of immunology and regenerative medicine 1 (2018) 57-66.

[111] C. Frantz, K.M. Stewart, V.M. Weaver, The extracellular matrix at a glance, Journal of Cell Science 123(24) (2010) 4195-4200.

[112] I.A. Janson, A.J. Putnam, Extracellular matrix elasticity and topography: material-based cues that affect cell function via conserved mechanisms, Journal of biomedical materials research. Part A 103(3) (2015) 1246-58.

[113] J.D. Humphrey, E.R. Dufresne, M.A. Schwartz, Mechanotransduction and extracellular matrix homeostasis, Nature reviews. Molecular cell biology 15(12) (2014) 802-12.

[114] J. Halper, M. Kjaer, Basic components of connective tissues and extracellular matrix: elastin, fibrillin, fibulins, fibrinogen, fibronectin, laminin, tenascins and thrombospondins, Advances in experimental medicine and biology 802 (2014) 31-47.

[115] N. De Franceschi, H. Hamidi, J. Alanko, P. Sahgal, J. Ivaska, Integrin traffic - the update, Journal of cell science 128(5) (2015) 839-52.

[116] M.J. Bissell, J. Aggeler, Dynamic reciprocity: how do extracellular matrix and hormones direct gene expression?, Progress in clinical and biological research 249 (1987) 251-62.

[117] Y.S. Kanwar, J. Wada, S. Lin, F.R. Danesh, S.S. Chugh, Q. Yang, T. Banerjee, J.W. Lomasney, Update of extracellular matrix, its receptors, and cell adhesion molecules in mammalian nephrogenesis, American journal of physiology. Renal physiology 286(2) (2004) F202-15.

[118] B. Leitinger, Discoidin domain receptor functions in physiological and pathological conditions, International review of cell and molecular biology 310 (2014) 39-87.

[119] D. Vigetti, E. Karousou, M. Viola, S. Deleonibus, G. De Luca, A. Passi, Hyaluronan: biosynthesis and signaling, Biochimica et biophysica acta 1840(8) (2014) 2452-9.

[120] M. Ala-Kapee, H. Nevanlinna, M. Mali, M. Jalkanen, J. Schroder, Localization of gene for human syndecan, an integral membrane proteoglycan and a matrix receptor, to chromosome 2, Somatic cell and molecular genetics 16(5) (1990) 501-5.

[121] P. Bornstein, E.H. Sage, Matricellular proteins: extracellular modulators of cell function, Current opinion in cell biology 14(5) (2002) 608-16.

[122] M.F. Brizzi, G. Tarone, P. Defilippi, Extracellular matrix, integrins, and growth factors as tailors of the stem cell niche, Current opinion in cell biology 24(5) (2012) 645-51.

[123] J.M. Wells, A. Gaggar, J.E. Blalock, MMP generated matrikines, Matrix biology : journal of the International Society for Matrix Biology 44-46 (2015) 122-9.

[124] B.N. Brown, S.F. Badylak, Extracellular matrix as an inductive scaffold for functional tissue reconstruction, Translational research : the journal of laboratory and clinical medicine 163(4) (2014) 268-85.

[125] T.J. Keane, I.T. Swinehart, S.F. Badylak, Methods of tissue decellularization used for preparation of biologic scaffolds and in vivo relevance, Methods (San Diego, Calif.) 84 (2015) 25-34.

[126] F.X. Maquart, Extracellular matrix: a major partner of wound healing, Bulletin de l'Academie nationale de medecine 199(7) (2015) 1199-1209.

[127] N.J. Turner, A.J. Yates, Jr., D.J. Weber, I.R. Qureshi, D.B. Stolz, T.W. Gilbert, S.F. Badylak, Xenogeneic extracellular matrix as an inductive scaffold for regeneration of a functioning musculotendinous junction, Tissue engineering. Part A 16(11) (2010) 3309-17.

[128] S.F. Badylak, G.C. Lantz, A. Coffey, L.A. Geddes, Small intestinal submucosa as a large diameter vascular graft in the dog, The Journal of surgical research 47(1) (1989) 74-80.

[129] S. Badylak, K. Kokini, B. Tullius, A. Simmons-Byrd, R. Morff, Morphologic study of small intestinal submucosa as a body wall repair device, The Journal of surgical research 103(2) (2002) 190-202.

[130] A.V. Boruch, A. Nieponice, I.R. Qureshi, T.W. Gilbert, S.F. Badylak, Constructive remodeling of biologic scaffolds is dependent on early exposure to physiologic bladder filling in a canine partial cystectomy model, The Journal of surgical research 161(2) (2010) 217-25.

[131] N.E. Gentile, K.M. Stearns, E.H. Brown, J.P. Rubin, M.L. Boninger, C.L. Dearth, F. Ambrosio, S.F. Badylak, Targeted rehabilitation after extracellular matrix scaffold transplantation for the treatment of volumetric muscle loss, American journal of physical medicine & rehabilitation / Association of Academic Physiatrists 93(11 Suppl 3) (2014) S79-87.

[132] T.J. Keane, J. Dziki, E. Sobieski, A. Smoulder, A. Castleton, N. Turner, L.J. White, S.F. Badylak, Restoring Mucosal Barrier Function and Modifying Macrophage Phenotype with an

Extracellular Matrix Hydrogel: Potential Therapy for Ulcerative Colitis, Journal of Crohn's & colitis (2016).

[133] P. Lin, W.C. Chan, S.F. Badylak, S.N. Bhatia, Assessing porcine liver-derived biomatrix for hepatic tissue engineering, Tissue engineering 10(7-8) (2004) 1046-53.

[134] A. Nieponice, F.F. Ciotola, F. Nachman, B.A. Jobe, T. Hoppo, R. Londono, S. Badylak, A.E. Badaloni, Patch esophagoplasty: esophageal reconstruction using biologic scaffolds, The Annals of thoracic surgery 97(1) (2014) 283-8.

[135] N.T. Remlinger, C.A. Czajka, M.E. Juhas, D.A. Vorp, D.B. Stolz, S.F. Badylak, S. Gilbert, T.W. Gilbert, Hydrated xenogeneic decellularized tracheal matrix as a scaffold for tracheal reconstruction, Biomaterials 31(13) (2010) 3520-6.

[136] J.M. Wainwright, R. Hashizume, K.L. Fujimoto, N.T. Remlinger, C. Pesyna, W.R. Wagner, K. Tobita, T.W. Gilbert, S.F. Badylak, Right ventricular outflow tract repair with a cardiac biologic scaffold, Cells, tissues, organs 195(1-2) (2012) 159-70.

[137] Y. Wu, J. Wang, Y. Shi, H. Pu, R.K. Leak, A.K. Liou, S.F. Badylak, Z. Liu, J. Zhang, J. Chen, L. Chen, Implantation of Brain-derived Extracellular Matrix Enhances Neurological Recovery after Traumatic Brain Injury, Cell transplantation (2016).

[138] N.A. Kissane, K.M. Itani, A decade of ventral incisional hernia repairs with biologic acellular dermal matrix: what have we learned?, Plastic and reconstructive surgery 130(5 Suppl 2) (2012) 194s-202s.

[139] A.W. Peled, R.D. Foster, E.R. Garwood, D.H. Moore, C.A. Ewing, M. Alvarado, E.S. Hwang, L.J. Esserman, The effects of acellular dermal matrix in expander-implant breast reconstruction after total skin-sparing mastectomy: results of a prospective practice improvement study, Plastic and reconstructive surgery 129(6) (2012) 901e-908e.

[140] G. Nicoletti, F. Brenta, M. Bleve, T. Pellegatta, A. Malovini, A. Faga, P. Perugini, Long-term in vivo assessment of bioengineered skin substitutes: a clinical study, Journal of tissue engineering and regenerative medicine 9(4) (2015) 460-8.

[141] H. Lev-Tov, C.S. Li, S. Dahle, R.R. Isseroff, Cellular versus acellular matrix devices in treatment of diabetic foot ulcers: study protocol for a comparative efficacy randomized controlled trial, Trials 14 (2013) 8.

[142] K.M. Lee, H. Kim, J.G. Nemeno, W. Yang, J. Yoon, S. Lee, J.I. Lee, Natural cardiac extracellular matrix sheet as a biomaterial for cardiomyocyte transplantation, Transplantation proceedings 47(3) (2015) 751-6.

[143] N. Hibino, P. McConnell, T. Shinoka, M. Malik, M. Galantowicz, Preliminary Experience in the Use of an Extracellular Matrix (CorMatrix) as a Tube Graft: Word of Caution, Seminars in thoracic and cardiovascular surgery 27(3) (2015) 288-95.

[144] H.J. Kim, S. Lee, H.W. Yun, X.Y. Yin, S.H. Kim, B.H. Choi, Y.J. Kim, M.S. Kim, B.H. Min, In vivo degradation profile of porcine cartilage-derived extracellular matrix powder scaffolds using a non-invasive fluorescence imaging method, Journal of biomaterials science. Polymer edition 27(2) (2016) 177-90.

[145] J. Tien, L. Li, O. Ozsun, K.L. Ekinci, Dynamics of Interstitial Fluid Pressure in Extracellular Matrix Hydrogels in Microfluidic Devices, Journal of biomechanical engineering 137(9) (2015).

[146] E.A. Rommer, M. Peric, A. Wong, Urinary bladder matrix for the treatment of recalcitrant nonhealing radiation wounds, Advances in skin & wound care 26(10) (2013) 450-5.

[147] J.M. Riganti, F. Ciotola, A. Amenabar, D. Craiem, S. Graf, A. Badaloni, T.W. Gilbert, A. Nieponice, Urinary bladder matrix scaffolds strengthen esophageal hiatus repair, The Journal of surgical research 204(2) (2016) 344-350.

[148] W.K. Abu Saleh, O. Al Jabbari, B. Ramlawi, B.A. Bruckner, M. Loebe, M.J. Reardon, Case Report: Cardiac Tumor Resection And Repair With Porcine Xenograft, Methodist DeBakey cardiovascular journal 12(2) (2016) 116-8.

[149] Y. Toyoda, M.A. Kashem, K. Hisamoto, A. Shiose, Tricuspid valve reconstruction with the extracellular matrix tube technique: a word of caution, The Journal of thoracic and cardiovascular surgery 148(2) (2014) e141-3.

[150] W.K. Abu Saleh, O. Al Jabbari, J. Grande-Allen, M. Ramchandani, Extracellular matrix scaffold as a tubular graft for ascending aorta aneurysm repair, Journal of cardiac surgery 30(8) (2015) 648-50.

[151] J. Wu, Q. Ding, A. Dutta, Y. Wang, Y.H. Huang, H. Weng, L. Tang, Y. Hong, An injectable extracellular matrix derived hydrogel for meniscus repair and regeneration, Acta biomaterialia 16 (2015) 49-59.

[152] H. Ghuman, A.R. Massensini, J. Donnelly, S.M. Kim, C.J. Medberry, S.F. Badylak, M. Modo, ECM hydrogel for the treatment of stroke: Characterization of the host cell infiltrate, Biomaterials 91 (2016) 166-181.

[153] S.B. Seif-Naraghi, M.A. Salvatore, P.J. Schup-Magoffin, D.P. Hu, K.L. Christman, Design and characterization of an injectable pericardial matrix gel: a potentially autologous scaffold for cardiac tissue engineering, Tissue engineering. Part A 16(6) (2010) 2017-27.

[154] S.F. Badylak, D. Taylor, K. Uygun, Whole-organ tissue engineering: decellularization and recellularization of three-dimensional matrix scaffolds, Annual review of biomedical engineering 13 (2011) 27-53.

[155] J.M. Lee, W.Y. Yeong, Design and Printing Strategies in 3D Bioprinting of Cell-Hydrogels: A Review, Advanced healthcare materials 5(22) (2016) 2856-2865.

[156] F. Gattazzo, A. Urciuolo, P. Bonaldo, Extracellular matrix: a dynamic microenvironment for stem cell niche, Biochimica et biophysica acta 1840(8) (2014) 2506-19.

[157] B.F. Goncalves, S.G. Campos, C.F. Costa, W.R. Scarano, R.M. Goes, S.R. Taboga, Key participants of the tumor microenvironment of the prostate: an approach of the structural dynamic of cellular elements and extracellular matrix components during epithelial-stromal transition, Acta histochemica 117(1) (2015) 4-13.

[158] S. Klamer, C. Voermans, The role of novel and known extracellular matrix and adhesion molecules in the homeostatic and regenerative bone marrow microenvironment, Cell adhesion & migration 8(6) (2014) 563-77.

[159] E. Arriazu, M. Ruiz de Galarreta, F.J. Cubero, M. Varela-Rey, M.P. Perez de Obanos, T.M. Leung, A. Lopategi, A. Benedicto, I. Abraham-Enachescu, N. Nieto, Extracellular matrix and liver disease, Antioxidants & redox signaling 21(7) (2014) 1078-97.

[160] C. Shimbori, J. Gauldie, M. Kolb, Extracellular matrix microenvironment contributes actively to pulmonary fibrosis, Current opinion in pulmonary medicine 19(5) (2013) 446-52.

[161] T. Quan, G.J. Fisher, Role of Age-Associated Alterations of the Dermal Extracellular Matrix Microenvironment in Human Skin Aging: A Mini-Review, Gerontology (2015).

[162] Y. Shin, K. Yang, S. Han, H.J. Park, Y. Seok Heo, S.W. Cho, S. Chung, Reconstituting vascular microenvironment of neural stem cell niche in three-dimensional extracellular matrix, Advanced healthcare materials 3(9) (2014) 1457-64.

[163] B.J. Gill, J.L. West, Modeling the tumor extracellular matrix: Tissue engineering tools repurposed towards new frontiers in cancer biology, Journal of biomechanics 47(9) (2014) 1969-78.

[164] K. Garg, M.D. Boppart, Influence of exercise and aging on extracellular matrix composition in the skeletal muscle stem cell niche, Journal of applied physiology (Bethesda, Md. : 1985) 121(5) (2016) 1053-1058.

[165] M. Kjaer, Role of extracellular matrix in adaptation of tendon and skeletal muscle to mechanical loading, Physiological reviews 84(2) (2004) 649-98.

[166] G. Lacraz, A.J. Rouleau, V. Couture, T. Sollrald, G. Drouin, N. Veillette, M. Grandbois, G. Grenier, Increased Stiffness in Aged Skeletal Muscle Impairs Muscle Progenitor Cell Proliferative Activity, PLoS One 10(8) (2015) e0136217.

[167] K.S. Ramaswamy, M.L. Palmer, J.H. van der Meulen, A. Renoux, T.Y. Kostrominova, D.E. Michele, J.A. Faulkner, Lateral transmission of force is impaired in skeletal muscles of dystrophic mice and very old rats, The Journal of physiology 589(Pt 5) (2011) 1195-208.

[168] A.G. Hindle, M. Horning, J.A. Mellish, J.M. Lawler, Diving into old age: muscular senescence in a large-bodied, long-lived mammal, the Weddell seal (Leptonychotes weddellii), The Journal of experimental biology 212(Pt 6) (2009) 790-6.

[169] V. Kovanen, H. Suominen, J. Risteli, L. Risteli, Type IV collagen and laminin in slow and fast skeletal muscle in rats--effects of age and life-time endurance training, Collagen and related research 8(2) (1988) 145-53.

[170] J.S. Pattison, L.C. Folk, R.W. Madsen, T.E. Childs, F.W. Booth, Transcriptional profiling identifies extensive downregulation of extracellular matrix gene expression in sarcopenic rat soleus muscle, Physiological genomics 15(1) (2003) 34-43.

[171] R.A. Dennis, B. Przybyla, C. Gurley, P.M. Kortebein, P. Simpson, D.H. Sullivan, C.A. Peterson, Aging alters gene expression of growth and remodeling factors in human skeletal muscle both at rest and in response to acute resistance exercise, Physiological genomics 32(3) (2008) 393-400.

[172] M.H. Snow, The effects of aging on satellite cells in skeletal muscles of mice and rats, Cell and tissue research 185(3) (1977) 399-408.

[173] J. Labat-Robert, Age-dependent remodeling of connective tissue: role of fibronectin and laminin, Pathologie-biologie 51(10) (2003) 563-8.

[174] A.S. Brack, P. Muñoz-Cánoves, The ins and outs of muscle stem cell aging, Skeletal Muscle 6 (2015).

[175] S. Tottey, S.A. Johnson, P.M. Crapo, J.E. Reing, L. Zhang, H. Jiang, C.J. Medberry, B. Reines, S.F. Badylak, The effect of source animal age upon extracellular matrix scaffold properties, Biomaterials 32(1) (2011) 128-36.

[176] B.M. Sicari, S.A. Johnson, B.F. Siu, P.M. Crapo, K.A. Daly, H. Jiang, C.J. Medberry, S. Tottey, N.J. Turner, S.F. Badylak, The effect of source animal age upon the in vivo remodeling characteristics of an extracellular matrix scaffold, Biomaterials 33(22) (2012) 5524-33.

[177] C. Ott, K. Jacobs, E. Haucke, A. Navarrete Santos, T. Grune, A. Simm, Role of advanced glycation end products in cellular signaling, Redox biology 2 (2014) 411-29.

[178] M. Kasper, R.H. Funk, Age-related changes in cells and tissues due to advanced glycation end products (AGEs), Arch Gerontol Geriatr 32(3) (2001) 233-43.

[179] W.G. John, E.J. Lamb, The Maillard or browning reaction in diabetes, Eye (Lond) 7 (Pt 2) (1993) 230-7.

[180] D. Badenhorst, M. Maseko, O.J. Tsotetsi, A. Naidoo, R. Brooksbank, G.R. Norton, A.J. Woodiwiss, Cross-linking influences the impact of quantitative changes in myocardial collagen on cardiac stiffness and remodelling in hypertension in rats, Cardiovasc Res 57(3) (2003) 632-41.

[181] J.V. Valencia, S.C. Weldon, D. Quinn, G.H. Kiers, J. DeGroot, J.M. TeKoppele, T.E. Hughes, Advanced glycation end product ligands for the receptor for advanced glycation end products: biochemical characterization and formation kinetics, Anal Biochem 324(1) (2004) 68-78.

[182] H. Vlassara, J. Uribarri, Advanced glycation end products (AGE) and diabetes: cause, effect, or both?, Curr Diab Rep 14(1) (2014) 453.

[183] F. Zhang, K.C. Kent, D. Yamanouchi, Y. Zhang, K. Kato, S. Tsai, R. Nowygrod, A.M. Schmidt, B. Liu, Anti-receptor for advanced glycation end products therapies as novel treatment for abdominal aortic aneurysm, Ann Surg 250(3) (2009) 416-23.

[184] Y. Chen, E.M. Akirav, W. Chen, O. Henegariu, B. Moser, D. Desai, J.M. Shen, J.C. Webster, R.C. Andrews, A.M. Mjalli, R. Rothlein, A.M. Schmidt, R. Clynes, K.C. Herold, RAGE ligation affects T cell activation and controls T cell differentiation, J Immunol 181(6) (2008) 4272-8.

[185] K. Kierdorf, G. Fritz, RAGE regulation and signaling in inflammation and beyond, J Leukoc Biol 94(1) (2013) 55-68.

[186] I.E. Dumitriu, P. Baruah, B. Valentinis, R.E. Voll, M. Herrmann, P.P. Nawroth, B. Arnold, M.E. Bianchi, A.A. Manfredi, P. Rovere-Querini, Release of high mobility group box 1 by dendritic cells controls T cell activation via the receptor for advanced glycation end products, J Immunol 174(12) (2005) 7506-15.

[187] A. Pollreisz, B.I. Hudson, J.S. Chang, W. Qu, B. Cheng, P.N. Papapanou, A.M. Schmidt, E. Lalla, Receptor for advanced glycation endproducts mediates pro-atherogenic responses to periodontal infection in vascular endothelial cells, Atherosclerosis 212(2) (2010) 451-6.

[188] Y. Liu, C. Liang, X. Liu, B. Liao, X. Pan, Y. Ren, M. Fan, M. Li, Z. He, J. Wu, Z. Wu, AGEs increased migration and inflammatory responses of adventitial fibroblasts via RAGE, MAPK and NF-kappaB pathways, Atherosclerosis 208(1) (2010) 34-42.

[189] M. Neeper, A.M. Schmidt, J. Brett, S.D. Yan, F. Wang, Y.C. Pan, K. Elliston, D. Stern, A. Shaw, Cloning and expression of a cell surface receptor for advanced glycosylation end products of proteins, J Biol Chem 267(21) (1992) 14998-5004.

[190] T. Chavakis, A. Bierhaus, N. Al-Fakhri, D. Schneider, S. Witte, T. Linn, M. Nagashima, J. Morser, B. Arnold, K.T. Preissner, P.P. Nawroth, The pattern recognition receptor (RAGE) is a counterreceptor for leukocyte integrins: a novel pathway for inflammatory cell recruitment, J Exp Med 198(10) (2003) 1507-15.

[191] R. Kokkola, A. Andersson, G. Mullins, T. Ostberg, C.J. Treutiger, B. Arnold, P. Nawroth, U. Andersson, R.A. Harris, H.E. Harris, RAGE is the major receptor for the proinflammatory activity of HMGB1 in rodent macrophages, Scand J Immunol 61(1) (2005) 1-9.

[192] L. Webster, E.A. Abordo, P.J. Thornalley, G.A. Limb, Induction of TNF alpha and IL-1 beta mRNA in monocytes by methylglyoxal- and advanced glycated endproduct-modified human serum albumin, Biochem Soc Trans 25(2) (1997) 250S.

[193] J.K. Juranek, M.S. Geddis, F. Song, J. Zhang, J. Garcia, R. Rosario, S.F. Yan, T.H. Brannagan, A.M. Schmidt, RAGE deficiency improves postinjury sciatic nerve regeneration in type 1 diabetic mice, Diabetes 62(3) (2013) 931-43.

[194] X. Jin, T. Yao, Z. Zhou, J. Zhu, S. Zhang, W. Hu, C. Shen, Advanced Glycation End Products Enhance Macrophages Polarization into M1 Phenotype through Activating RAGE/NF-kappaB Pathway, BioMed research international 2015 (2015) 732450.

[195] N. Shanmugam, Y.S. Kim, L. Lanting, R. Natarajan, Regulation of cyclooxygenase-2 expression in monocytes by ligation of the receptor for advanced glycation end products, J Biol Chem 278(37) (2003) 34834-44.

[196] J.S. Chang, T. Wendt, W. Qu, L. Kong, Y.S. Zou, A.M. Schmidt, S.F. Yan, Oxygen deprivation triggers upregulation of early growth response-1 by the receptor for advanced glycation end products, Circ Res 102(8) (2008) 905-13.

[197] M. Mittal, M.R. Siddiqui, K. Tran, S.P. Reddy, A.B. Malik, Reactive oxygen species in inflammation and tissue injury, Antioxidants & redox signaling 20(7) (2014) 1126-67.

[198] J. Mattana, L. Margiloff, L. Chaplia, Oxidation of extracellular matrix modulates susceptibility to degradation by the mesangial matrix metalloproteinase-2, Free radical biology & medicine 27(3-4) (1999) 315-21.

[199] S. Kar, S. Subbaram, P.M. Carrico, J.A. Melendez, Redox-control of matrix metalloproteinase-1: a critical link between free radicals, matrix remodeling and degenerative disease, Respiratory physiology & neurobiology 174(3) (2010) 299-306.

[200] A. Herchenhan, F. Uhlenbrock, P. Eliasson, M. Weis, D. Eyre, K.E. Kadler, S.P. Magnusson, M. Kjaer, Lysyl Oxidase Activity Is Required for Ordered Collagen Fibrillogenesis by Tendon Cells, The Journal of biological chemistry 290(26) (2015) 16440-50.

[201] V. Barry-Hamilton, R. Spangler, D. Marshall, S. McCauley, H.M. Rodriguez, M. Oyasu, A. Mikels, M. Vaysberg, H. Ghermazien, C. Wai, C.A. Garcia, A.C. Velayo, B. Jorgensen, D. Biermann, D. Tsai, J. Green, S. Zaffryar-Eilot, A. Holzer, S. Ogg, D. Thai, G. Neufeld, P. Van Vlasselaer, V. Smith, Allosteric inhibition of lysyl oxidase-like-2 impedes the development of a pathologic microenvironment, Nature medicine 16(9) (2010) 1009-17.

[202] J. Behmoaras, S. Slove, S. Seve, R. Vranckx, P. Sommer, M.P. Jacob, Differential expression of lysyl oxidases LOXL1 and LOX during growth and aging suggests specific roles in elastin and collagen fiber remodeling in rat aorta, Rejuvenation research 11(5) (2008) 883-9.

[203] Y. Jiang, W. Zong, H. Luan, J.H. Liu, A.Z. Zhang, X.L. Li, S.Y. Liu, S.Q. Zhang, J.G. Gao, Decreased expression of elastin and lysyl oxidase family genes in urogenital tissues of aging mice, The journal of obstetrics and gynaecology research 40(8) (2014) 1998-2004.

[204] J.S. Nyman, A. Roy, R.L. Acuna, H.J. Gayle, M.J. Reyes, J.H. Tyler, D.D. Dean, X. Wang, Age-related effect on the concentration of collagen crosslinks in human osteonal and interstitial bone tissue, Bone 39(6) (2006) 1210-7.

[205] M. Rahmati, G. Nalesso, A. Mobasheri, M. Mozafari, Aging and osteoarthritis: Central role of the extracellular matrix, Ageing research reviews 40 (2017) 20-30.

[206] M. Nita, B. Strzalka-Mrozik, A. Grzybowski, U. Mazurek, W. Romaniuk, Age-related macular degeneration and changes in the extracellular matrix, Medical science monitor : international medical journal of experimental and clinical research 20 (2014) 1003-16.

[207] P. Balasubramanian, V.D. Longo, Growth Factors, aging and age-related diseases, Growth hormone & IGF research : official journal of the Growth Hormone Research Society and the International IGF Research Society 28 (2016) 66-68.

[208] M. Gueugneau, C. Coudy-Gandilhon, L. Theron, B. Meunier, C. Barboiron, L. Combaret, D. Taillandier, C. Polge, D. Attaix, B. Picard, J. Verney, F. Roche, L. Feasson, J.C. Barthelemy, D. Bechet, Skeletal muscle lipid content and oxidative activity in relation to muscle fiber type in aging and metabolic syndrome, The journals of gerontology. Series A, Biological sciences and medical sciences 70(5) (2015) 566-76.

[209] B. Brown, K. Lindberg, J. Reing, D.B. Stolz, S.F. Badylak, The basement membrane component of biologic scaffolds derived from extracellular matrix, Tissue engineering 12(3) (2006) 519-26.

[210] J. Labat-Robert, L. Robert, Longevity and aging. Mechanisms and perspectives, Pathologie-biologie 63(6) (2015) 272-6.

[211] R. Bucala, Diabetes, aging, and their tissue complications, The Journal of clinical investigation 124(5) (2014) 1887-8.

[212] F. Corica, G. Bianchi, A. Corsonello, N. Mazzella, F. Lattanzio, G. Marchesini, Obesity in the Context of Aging: Quality of Life Considerations, PharmacoEconomics 33(7) (2015) 655-72.

[213] B.J. North, D.A. Sinclair, The intersection between aging and cardiovascular disease, Circulation research 110(8) (2012) 1097-108.

[214] A. Clough, J. Ball, G.S. Smith, S. Leibman, Porcine small intestine submucosa matrix (Surgisis) for esophageal perforation, The Annals of thoracic surgery 91(2) (2011) e15-6.

[215] M. Cosentino, A. Kanashiro, A. Vives, J. Sanchez, M.F. Peraza, D. Moreno, J. Perona, V. De Marco, E. Ruiz-Castane, J. Sarquella, Surgical treatment of Peyronie's disease with small intestinal submucosa graft patch, International journal of impotence research 28(3) (2016) 106-9.

[216] S.M. Cazzell, D.L. Lange, J.E. Dickerson, H.B. Slade, The Management of Diabetic Foot Ulcers with Porcine Small Intestine Submucosa Tri-Layer Matrix: A Randomized Controlled Trial, Advances in Wound Care 4(12) (2015) 711-718.

[217] J. Simon, R. de Petriconi, M. Meilinger, R.E. Hautmann, G. Bartsch, Optimized haemostasis in nephron-sparing surgery using small-intestine submucosa, BMC Urology 8 (2008) 8-8.

[218] H.-K. Lin, S.Y. Godiwalla, B. Palmer, D. Frimberger, Q. Yang, S.V. Madihally, K.-M. Fung, B.P. Kropp, Understanding Roles of Porcine Small Intestinal Submucosa in Urinary Bladder Regeneration: Identification of Variable Regenerative Characteristics of Small Intestinal Submucosa, Tissue Engineering. Part B, Reviews 20(1) (2014) 73-83.

[219] J.E. Reing, B.N. Brown, K.A. Daly, J.M. Freund, T.W. Gilbert, S.X. Hsiong, A. Huber, K.E. Kullas, S. Tottey, M.T. Wolf, S.F. Badylak, The effects of processing methods upon mechanical and biologic properties of porcine dermal extracellular matrix scaffolds, Biomaterials 31(33) (2010) 8626-33.

[220] R. Roy, A. Boskey, L.J. Bonassar, Processing of type I collagen gels using nonenzymatic glycation, Journal of biomedical materials research. Part A 93(3) (2010) 843-51.

[221] B.M. Sicari, J.L. Dziki, B.F. Siu, C.J. Medberry, C.L. Dearth, S.F. Badylak, The promotion of a constructive macrophage phenotype by solubilized extracellular matrix, Biomaterials 35(30) (2014) 8605-12.

[222] T.W. Gilbert, A.M. Stewart-Akers, J. Sydeski, T.D. Nguyen, S.F. Badylak, S.L. Woo, Gene expression by fibroblasts seeded on small intestinal submucosa and subjected to cyclic stretching, Tissue engineering 13(6) (2007) 1313-23.

[223] T.J. Keane, R. Londono, N.J. Turner, S.F. Badylak, Consequences of ineffective decellularization of biologic scaffolds on the host response, Biomaterials 33(6) (2012) 1771-81.

[224] M. Guthridge, M. Wilson, J. Cowling, J. Bertolini, M.T. Hearn, The role of basic fibroblast growth factor in skeletal muscle regeneration, Growth factors (Chur, Switzerland) 6(1) (1992) 53-63.

[225] M.C. Leroy, J. Perroud, B. Darbellay, L. Bernheim, S. Konig, Epidermal Growth Factor Receptor Down-Regulation Triggers Human Myoblast Differentiation, PLOS ONE 8(8) (2013) e71770.

[226] K.J. Miller, D. Thaloor, S. Matteson, G.K. Pavlath, Hepatocyte growth factor affects satellite cell activation and differentiation in regenerating skeletal muscle, American journal of physiology. Cell physiology 278(1) (2000) C174-81.

[227] A. Costa, J.D. Naranjo, R. Londono, S.F. Badylak, Biologic Scaffolds, Cold Spring Harbor perspectives in medicine 7(9) (2017).

[228] H. Christensen, T.T. Andreassen, H. Oxlund, Age-related alterations in the strength and collagen content of left colon in rats, International journal of colorectal disease 7(2) (1992) 85-8.

[229] M. Stahl, J. Schupp, B. Jager, M. Schmid, G. Zissel, J. Muller-Quernheim, A. Prasse, Lung collagens perpetuate pulmonary fibrosis via CD204 and M2 macrophage activation, PLoS One 8(11) (2013) e81382.

[230] D. Hachim, N. Wang, S.T. Lopresti, E.C. Stahl, Y.U. Umeda, R.D. Rege, S.T. Carey, D. Mani, B.N. Brown, Effects of Aging upon the Host Response to Implants, Journal of Biomedical Materials Research Part A (2017) n/a-n/a.

[231] M. Dimitrijevic, S. Stanojevic, V. Blagojevic, I. Curuvija, I. Vujnovic, R. Petrovic, N. Arsenovic-Ranin, V. Vujic, G. Leposavic, Aging affects the responsiveness of rat peritoneal macrophages to GM-CSF and IL-4, Biogerontology 17(2) (2016) 359-71.

[232] H.M. Blau, B.D. Cosgrove, A.T. Ho, The central role of muscle stem cells in regenerative failure with aging, Nature medicine 21(8) (2015) 854-62.

[233] E. Koike, T. Kobayashi, K. Mochitate, M. Murakami, Effect of aging on nitric oxide production by rat alveolar macrophages, Experimental gerontology 34(7) (1999) 889-94.

[234] M.E. Swift, A.L. Burns, K.L. Gray, L.A. DiPietro, Age-related alterations in the inflammatory response to dermal injury, The Journal of investigative dermatology 117(5) (2001) 1027-35.

[235] G.S. Ashcroft, S.J. Mills, J.J. Ashworth, Ageing and wound healing, Biogerontology 3(6) (2002) 337-45.

[236] M.E. Swift, H.K. Kleinman, L.A. DiPietro, Impaired wound repair and delayed angiogenesis in aged mice, Laboratory investigation; a journal of technical methods and pathology 79(12) (1999) 1479-87.

[237] M.J. Reed, N. Karres, D. Eyman, R.B. Vernon, J.M. Edelberg, Age-related differences in repair of dermal wounds and myocardial infarcts attenuate during the later stages of healing, In vivo (Athens, Greece) 20(6b) (2006) 801-6.

[238] B. Zhang, W.M. Bailey, K.J. Braun, J.C. Gensel, Age decreases macrophage IL-10 expression: Implications for functional recovery and tissue repair in spinal cord injury, Experimental neurology 273 (2015) 83-91.

[239] L. Rodriguez-Menocal, M.H. Faridi, L. Martinez, L.A. Shehadeh, J.C. Duque, Y. Wei, A. Mesa, A. Pena, V. Gupta, S.M. Pham, R.I. Vazquez-Padron, Macrophage-derived IL-18 and increased fibrinogen deposition are age-related inflammatory signatures of vascular remodeling, American journal of physiology. Heart and circulatory physiology 306(5) (2014) H641-53.

[240] L. Huleihel, G.S. Hussey, J.D. Naranjo, L. Zhang, J.L. Dziki, N.J. Turner, D.B. Stolz, S.F. Badylak, Matrix-bound nanovesicles within ECM bioscaffolds, Science advances 2(6) (2016) e1600502.

[241] C. Meschiari, O.K. Ero, H. Pan, T. Finkel, M.L. Lindsey, The Impact of Aging on Cardiac Extracellular Matrix, GeroScience 39(1) (2017) 7-18.

[242] K.M. Stearns-Reider, A. D'Amore, K. Beezhold, B. Rothrauff, L. Cavalli, W.R. Wagner, D.A. Vorp, A. Tsamis, S. Shinde, C. Zhang, A. Barchowsky, T.A. Rando, R.S. Tuan, F. Ambrosio, Aging of the skeletal muscle extracellular matrix drives a stem cell fibrogenic conversion, Aging Cell 16(3) (2017) 518-528.

[243] A. Branco, A. Todorovic Fabro, T.M. Goncalves, R.H. Garcia Martins, Alterations in extracellular matrix composition in the aging larynx, Otolaryngology--head and neck surgery : official journal of American Academy of Otolaryngology-Head and Neck Surgery 152(2) (2015) 302-7.

[244] S.L. Voytik-Harbin, A.O. Brightman, M.R. Kraine, B. Waisner, S.F. Badylak, Identification of extractable growth factors from small intestinal submucosa, Journal of cellular biochemistry 67(4) (1997) 478-91.

[245] K.J. Rowland, P.M. Choi, B.W. Warner, The Role of Growth Factors in Intestinal Regeneration and Repair in Necrotizing Enterocolitis, Seminars in pediatric surgery 22(2) (2013) 101-111.

[246] L. Drozdowski, A.B.R. Thomson, Aging and the intestine, World Journal of Gastroenterology : WJG 12(47) (2006) 7578-7584.

[247] O. Spadaro, C.D. Camell, L. Bosurgi, K.Y. Nguyen, Y.H. Youm, C.V. Rothlin, V.D. Dixit, IGF1 Shapes Macrophage Activation in Response to Immunometabolic Challenge, Cell reports 19(2) (2017) 225-234.

[248] M. Hollmén, S. Karaman, S. Schwager, A. Lisibach, A.J. Christiansen, M. Maksimow, Z. Varga, S. Jalkanen, M. Detmar, G-CSF regulates macrophage phenotype and associates with poor overall survival in human triple-negative breast cancer, Oncoimmunology 5(3) (2016) e1115177.

[249] G. Zhao, L. Liu, R.M. Peek, Jr., X. Hao, D.B. Polk, H. Li, F. Yan, Activation of Epidermal Growth Factor Receptor in Macrophages Mediates Feedback Inhibition of M2 Polarization and Gastrointestinal Tumor Cell Growth, The Journal of biological chemistry 291(39) (2016) 20462-72.

[250] L. Bosch, M. Tor, J. Reixach, J. Estany, Age-related changes in intramuscular and subcutaneous fat content and fatty acid composition in growing pigs using longitudinal data, Meat science 91(3) (2012) 358-63.

[251] D. Namgaladze, B. Brune, Macrophage fatty acid oxidation and its roles in macrophage polarization and fatty acid-induced inflammation, Biochimica et biophysica acta 1861(11) (2016) 1796-1807.

[252] C. Gladine, M. Zmojdzian, L. Joumard-Cubizolles, M.A. Verny, B. Comte, A. Mazur, The omega-3 fatty acid docosahexaenoic acid favorably modulates the inflammatory pathways and macrophage polarization within aorta of LDLR(-/-) mice, Genes & nutrition 9(5) (2014) 424.

[253] M.Y. Song, J. Wang, Y. Lee, J. Lee, K.S. Kwon, E.J. Bae, B.H. Park, Enhanced M2 macrophage polarization in high n-3 polyunsaturated fatty acid transgenic mice fed a high-fat diet, Molecular nutrition & food research 60(11) (2016) 2481-2492.

[254] H.Y. Chang, H.N. Lee, W. Kim, Y.J. Surh, Docosahexaenoic acid induces M2 macrophage polarization through peroxisome proliferator-activated receptor gamma activation, Life sciences 120 (2015) 39-47.

[255] M. Gessel, J.M. Spraggins, P. Voziyan, B.G. Hudson, R.M. Caprioli, Decellularization of intact tissue enables MALDI imaging mass spectrometry analysis of the extracellular matrix, Journal of mass spectrometry : JMS 50(11) (2015) 1288-93.

[256] S. Dalle, L. Rossmeislova, K. Koppo, The Role of Inflammation in Age-Related Sarcopenia, Frontiers in Physiology 8 (2017) 1045.

[257] I. Beyer, T. Mets, I. Bautmans, Chronic low-grade inflammation and age-related sarcopenia, Current opinion in clinical nutrition and metabolic care 15(1) (2012) 12-22.

[258] M.C. de Medeiros, S.C.T. Frasnelli, A.d.S. Bastos, S.R.P. Orrico, C. Rossa Junior, Modulation of cell proliferation, survival and gene expression by RAGE and TLR signaling in cells of the innate and adaptive immune response: role of p38 MAPK and NF-KB, Journal of Applied Oral Science 22(3) (2014) 185-193.

[259] T.J. Shaw, K. Kishi, R. Mori, Wound-associated skin fibrosis: mechanisms and treatments based on modulating the inflammatory response, Endocrine, metabolic & immune disorders drug targets 10(4) (2010) 320-30.

[260] S.F. Badylak, D.O. Freytes, T.W. Gilbert, Extracellular matrix as a biological scaffold material: Structure and function, Acta biomaterialia 5(1) (2009) 1-13.

[261] M.T. Wolf, K.A. Daly, J.E. Reing, S.F. Badylak, Biologic scaffold composed of skeletal muscle extracellular matrix, Biomaterials 33(10) (2012) 2916-25.

[262] L.K. Wood, E. Kayupov, J.P. Gumucio, C.L. Mendias, D.R. Claflin, S.V. Brooks, Intrinsic stiffness of extracellular matrix increases with age in skeletal muscles of mice, Journal of applied physiology (Bethesda, Md. : 1985) 117(4) (2014) 363-9.

[263] R.H. Houtkooper, C. Argmann, S.M. Houten, C. Cantó, E.H. Jeninga, P.A. Andreux, C. Thomas, R. Doenlen, K. Schoonjans, J. Auwerx, The metabolic footprint of aging in mice, Scientific reports 1 (2011) 134-134.

[264] M.Z. Tucker, L.P. Turcotte, Impaired fatty acid oxidation in muscle of aging rats perfused under basal conditions, American journal of physiology. Endocrinology and metabolism 282(5) (2002) E1102-9.

[265] B.A. Baker, An Old Problem: Aging and Skeletal-Muscle-Strain Injury, Journal of sport rehabilitation 26(2) (2017) 180-188.

[266] L. Garcia-Prat, P. Sousa-Victor, P. Munoz-Canoves, Functional dysregulation of stem cells during aging: a focus on skeletal muscle stem cells, The FEBS journal 280(17) (2013) 4051-62.

[267] P. Hasty, J. Campisi, J. Hoeijmakers, H. van Steeg, J. Vijg, Aging and genome maintenance: lessons from the mouse?, Science (New York, N.Y.) 299(5611) (2003) 1355-9.

[268] B.N. Ames, Delaying the mitochondrial decay of aging, Annals of the New York Academy of Sciences 1019 (2004) 406-11.

[269] T.R. Golden, D.A. Hinerfeld, S. Melov, Oxidative stress and aging: beyond correlation, Aging Cell 1(2) (2002) 117-23.

[270] D.E. Harrison, Long-term erythropoietic repopulating ability of old, young, and fetal stem cells, The Journal of Experimental Medicine 157(5) (1983) 1496-504.

[271] A.S. Brack, M.J. Conboy, S. Roy, M. Lee, C.J. Kuo, C. Keller, T.A. Rando, Increased Wnt signaling during aging alters muscle stem cell fate and increases fibrosis, Science 317(5839) (2007) 807-10.

[272] D. Wilson, T. Jackson, E. Sapey, J.M. Lord, Frailty and sarcopenia: The potential role of an aged immune system, Ageing research reviews 36 (2017) 1-10.

[273] Y. Oishi, I. Manabe, Macrophages in age-related chronic inflammatory diseases, Npj Aging And Mechanisms Of Disease 2 (2016) 16018.

[274] J. Chen, J.S. Alexander, A.W. Orr, Integrins and their extracellular matrix ligands in lymphangiogenesis and lymph node metastasis, International journal of cell biology 2012 (2012) 853703.

[275] C. Franceschi, J. Campisi, Chronic Inflammation (Inflammaging) and Its Potential Contribution to Age-Associated Diseases, The Journals of Gerontology: Series A 69(Suppl_1) (2014) S4-S9.

[276] J.M. Wainwright, C.A. Czajka, U.B. Patel, D.O. Freytes, K. Tobita, T.W. Gilbert, S.F. Badylak, Preparation of Cardiac Extracellular Matrix from an Intact Porcine Heart, Tissue Engineering. Part C, Methods 16(3) (2010) 525-532.

[277] J.C. Kutten, D. McGovern, C.M. Hobson, S.A. Luffy, A. Nieponice, K. Tobita, R.J. Francis, S.D. Reynolds, J.S. Isenberg, T.W. Gilbert, Decellularized Tracheal Extracellular Matrix Supports Epithelial Migration, Differentiation, and Function, Tissue Engineering. Part A 21(1-2) (2015) 75-84.

[278] M.T. Wolf, K.A. Daly, J.E. Reing, S.F. Badylak, Biologic scaffold composed of skeletal muscle extracellular matrix, Biomaterials 33(10) (2012) 2916-2925.

[279] K.S. Putt, R.B. Pugh, A High-Throughput Microtiter Plate Based Method for the Determination of Peracetic Acid and Hydrogen Peroxide, PLoS ONE 8(11) (2013) e79218.

[280] P. Niethammer, C. Grabher, A.T. Look, T.J. Mitchison, A tissue-scale gradient of hydrogen peroxide mediates rapid wound detection in zebrafish, Nature 459(7249) (2009) 996-9.

[281] C.C. Winterbourn, A.J. Kettle, M.B. Hampton, Reactive Oxygen Species and Neutrophil Function, Annual review of biochemistry 85 (2016) 765-92.

[282] R.C. Melo, D.L. Fabrino, H. D'Avila, H.C. Teixeira, A.P. Ferreira, Production of hydrogen peroxide by peripheral blood monocytes and specific macrophages during experimental infection with Trypanosoma cruzi in vivo, Cell biology international 27(10) (2003) 853-61.

[283] R.H. Burdon, Superoxide and hydrogen peroxide in relation to mammalian cell proliferation, Free radical biology & medicine 18(4) (1995) 775-94.

[284] S. Lee, E. Tak, J. Lee, M.A. Rashid, M.P. Murphy, J. Ha, S.S. Kim, Mitochondrial H2O2 generated from electron transport chain complex I stimulates muscle differentiation, Cell research 21(5) (2011) 817-34.

[285] H. Sies, Hydrogen peroxide as a central redox signaling molecule in physiological oxidative stress: Oxidative eustress, Redox biology 11 (2017) 613-619.

[286] D. Weismann, C.J. Binder, The innate immune response to products of phospholipid peroxidation, Biochimica et biophysica acta 1818(10) (2012) 2465-75.

[287] I. Lorenzen, L. Mullen, S. Bekeschus, E.-M. Hanschmann, Redox Regulation of Inflammatory Processes Is Enzymatically Controlled, Oxidative medicine and cellular longevity 2017 (2017) 8459402-8459402.

[288] E.M. Hanschmann, J.R. Godoy, C. Berndt, C. Hudemann, C.H. Lillig, Thioredoxins, glutaredoxins, and peroxiredoxins--molecular mechanisms and health significance: from cofactors to antioxidants to redox signaling, Antioxidants & redox signaling 19(13) (2013) 1539-605.

[289] A. Silva-Palacios, M. Konigsberg, C. Zazueta, Nrf2 signaling and redox homeostasis in the aging heart: A potential target to prevent cardiovascular diseases?, Ageing research reviews 26 (2016) 81-95.

[290] A. Kammeyer, R.M. Luiten, Oxidation events and skin aging, Ageing research reviews 21 (2015) 16-29.

[291] E. Barreiro, C. Coronell, B. Lavina, A. Ramirez-Sarmiento, M. Orozco-Levi, J. Gea, Aging, sex differences, and oxidative stress in human respiratory and limb muscles, Free radical biology & medicine 41(5) (2006) 797-809.

[292] O. Pansarasa, L. Bertorelli, J. Vecchiet, G. Felzani, F. Marzatico, Age-dependent changes of antioxidant activities and markers of free radical damage in human skeletal muscle, Free radical biology & medicine 27(5-6) (1999) 617-22.

[293] O. Pansarasa, L. Castagna, B. Colombi, J. Vecchiet, G. Felzani, F. Marzatico, Age and sex differences in human skeletal muscle: role of reactive oxygen species, Free radical research 33(3) (2000) 287-93.

[294] B. McDonagh, G.K. Sakellariou, N.T. Smith, P. Brownridge, M.J. Jackson, Differential Cysteine Labeling and Global Label-Free Proteomics Reveals an Altered Metabolic State in Skeletal Muscle Aging, Journal of Proteome Research 13(11) (2014) 5008-5021.

[295] S.K. Powers, J. Duarte, A.N. Kavazis, E.E. Talbert, Reactive oxygen species are signalling molecules for skeletal muscle adaptation, Experimental physiology 95(1) (2010) 1-9.

[296] O. Nedic, S.I. Rattan, T. Grune, I.P. Trougakos, Molecular effects of advanced glycation end products on cell signalling pathways, ageing and pathophysiology, Free radical research 47 Suppl 1 (2013) 28-38.

[297] A. Gautieri, A. Redaelli, M.J. Buehler, S. Vesentini, Age- and diabetes-related nonenzymatic crosslinks in collagen fibrils: candidate amino acids involved in Advanced Glycation End-products, Matrix biology : journal of the International Society for Matrix Biology 34 (2014) 89-95.

[298] G. Aldini, G. Vistoli, M. Stefek, N. Chondrogianni, T. Grune, J. Sereikaite, I. Sadowska-Bartosz, G. Bartosz, Molecular strategies to prevent, inhibit, and degrade advanced glycoxidation and advanced lipoxidation end products, Free radical research 47 Suppl 1 (2013) 93-137.

[299] G. Llaurado, V. Ceperuelo-Mallafre, C. Vilardell, R. Simo, P. Gil, A. Cano, J. Vendrell, J.M. Gonzalez-Clemente, Advanced glycation end products are associated with arterial stiffness in type 1 diabetes, The Journal of endocrinology 221(3) (2014) 405-13.

[300] J.C. Tobon-Velasco, E. Cuevas, M.A. Torres-Ramos, Receptor for AGEs (RAGE) as mediator of NF-kB pathway activation in neuroinflammation and oxidative stress, CNS & neurological disorders drug targets 13(9) (2014) 1615-26.

[301] T.S. Girton, T.R. Oegema, R.T. Tranquillo, Exploiting glycation to stiffen and strengthen tissue equivalents for tissue engineering, Journal of biomedical materials research 46(1) (1999) 87-92.

[302] P. Lu, K. Takai, V.M. Weaver, Z. Werb, Extracellular matrix degradation and remodeling in development and disease, Cold Spring Harbor perspectives in biology 3(12) (2011) 10.1101/cshperspect.a005058 a005058.

[303] B. Sutariya, D. Jhonsa, M.N. Saraf, TGF-beta: the connecting link between nephropathy and fibrosis, Immunopharmacology and immunotoxicology 38(1) (2016) 39-49.

[304] I. Sen, O. Bozkurt, E. Aras, S. Heise, G.A. Brockmann, F. Severcan, Lipid profiles of adipose and muscle tissues in mouse models of juvenile onset of obesity without high fat diet induction: a Fourier transform infrared (FT-IR) spectroscopic study, Applied spectroscopy 69(6) (2015) 679-88.

[305] R.D. Semba, E.J. Nicklett, L. Ferrucci, Does Accumulation of Advanced Glycation End Products Contribute to the Aging Phenotype?, The Journals of Gerontology Series A: Biological Sciences and Medical Sciences 65A(9) (2010) 963-975.

[306] V.P. Singh, A. Bali, N. Singh, A.S. Jaggi, Advanced Glycation End Products and Diabetic Complications, The Korean Journal of Physiology & Pharmacology : Official Journal of the Korean Physiological Society and the Korean Society of Pharmacology 18(1) (2014) 1-14.

[307] A. Bierhaus, P.M. Humpert, M. Morcos, T. Wendt, T. Chavakis, B. Arnold, D.M. Stern, P.P. Nawroth, Understanding RAGE, the receptor for advanced glycation end products, Journal of molecular medicine (Berlin, Germany) 83(11) (2005) 876-86.

[308] H. Vlassara, H. Fuh, Z. Makita, S. Krungkrai, A. Cerami, R. Bucala, Exogenous advanced glycosylation end products induce complex vascular dysfunction in normal animals: a model for diabetic and aging complications, Proc Natl Acad Sci U S A 89(24) (1992) 12043-7.

[309] N.C. Avery, A.J. Bailey, Enzymic and non-enzymic cross-linking mechanisms in relation to turnover of collagen: relevance to aging and exercise, Scandinavian journal of medicine & science in sports 15(4) (2005) 231-40.

[310] N. Verzijl, J. DeGroot, S.R. Thorpe, R.A. Bank, J.N. Shaw, T.J. Lyons, J.W. Bijlsma, F.P. Lafeber, J.W. Baynes, J.M. TeKoppele, Effect of collagen turnover on the accumulation of advanced glycation end products, The Journal of biological chemistry 275(50) (2000) 39027-31.

[311] Y. Wei, L. Chen, J. Chen, L. Ge, R.Q. He, Rapid glycation with D-ribose induces globular amyloid-like aggregations of BSA with high cytotoxicity to SH-SY5Y cells, BMC Cell Biology 10 (2009) 10-10.

[312] M. Aragno, R. Mastrocola, Dietary Sugars and Endogenous Formation of Advanced Glycation Endproducts: Emerging Mechanisms of Disease, Nutrients 9(4) (2017) 385.

[313] J. Jensen, P.I. Rustad, A.J. Kolnes, Y.-C. Lai, The Role of Skeletal Muscle Glycogen Breakdown for Regulation of Insulin Sensitivity by Exercise, Frontiers in Physiology 2 (2011) 112.

[314] P.J. Keller, Q. Le Van, S.U. Kim, D.H. Bown, H.C. Chen, A. Kohnle, A. Bacher, H.G. Floss, Biosynthesis of riboflavin: mechanism of formation of the ribitylamino linkage, Biochemistry 27(4) (1988) 1117-1120.

[315] A.D. Broom, L.B. Townsend, J.W. Jones, R.K. Robins, Purine Nucleosides. VI. Further Methylation Studies of Naturally Occurring Purine Nucleosides*, Biochemistry 3(4) (1964) 494-500.

[316] M. Mauser, H.M. Hoffmeister, C. Nienaber, W. Schaper, Influence of ribose, adenosine, and "AICAR" on the rate of myocardial adenosine triphosphate synthesis during reperfusion after coronary artery occlusion in the dog, Circulation research 56(2) (1985) 220-30.

[317] T. Matsuda, A. Kubo, T. Taguchi, K. Mizumura, ATP decreases mechanical sensitivity of muscle thin-fiber afferents in rats, Neuroscience research 97 (2015) 36-44.

[318] T. Chavakis, A. Bierhaus, P.P. Nawroth, RAGE (receptor for advanced glycation end products): a central player in the inflammatory response, Microbes and infection 6(13) (2004) 1219-25.

[319] D. Arias-Salvatierra, E.K. Silbergeld, L.C. Acosta-Saavedra, E.S. Calderon-Aranda, Role of nitric oxide produced by iNOS through NF-kappaB pathway in migration of cerebellar granule neurons induced by Lipopolysaccharide, Cellular signalling 23(2) (2011) 425-35.

[320] C. Laflamme, G.B. Mailhot, M. Pouliot, Age-related decline of the acute local inflammation response: a mitigating role for the adenosine A(2A) receptor, Aging (Albany NY) 9(10) (2017) 2083-2097.

[321] E. Sapey, H. Greenwood, G. Walton, E. Mann, A. Love, N. Aaronson, R.H. Insall, R.A. Stockley, J.M. Lord, Phosphoinositide 3-kinase inhibition restores neutrophil accuracy in the elderly: toward targeted treatments for immunosenescence, Blood 123(2) (2014) 239-248.

[322] K. Hamada, E. Vannier, J.M. Sacheck, A.L. Witsell, R. Roubenoff, Senescence of human skeletal muscle impairs the local inflammatory cytokine response to acute eccentric exercise, FASEB journal : official publication of the Federation of American Societies for Experimental Biology 19(2) (2005) 264-6.

[323] S. Ghatak, E.V. Maytin, J.A. Mack, V.C. Hascall, I. Atanelishvili, R. Moreno Rodriguez, R.R. Markwald, S. Misra, Roles of Proteoglycans and Glycosaminoglycans in Wound Healing and Fibrosis, International journal of cell biology 2015 (2015) 834893.

[324] H. Wang, D.W. Melton, L. Porter, Z.U. Sarwar, L.M. McManus, P.K. Shireman, Altered Macrophage Phenotype Transition Impairs Skeletal Muscle Regeneration, The American Journal of Pathology 184(4) (2014) 1167-1184.

[325] S. Umadevi, V. Gopi, V. Elangovan, Regulatory mechanism of gallic acid against advanced glycation end products induced cardiac remodeling in experimental rats, Chemico-biological interactions 208 (2014) 28-36.

[326] A. Yuen, C. Laschinger, I. Talior, W. Lee, M. Chan, J. Birek, E.W. Young, K. Sivagurunathan, E. Won, C.A. Simmons, C.A. McCulloch, Methylglyoxal-modified collagen promotes myofibroblast differentiation, Matrix biology : journal of the International Society for Matrix Biology 29(6) (2010) 537-48.

[327] T. Matsuura, Y. Li, J.P. Giacobino, F.H. Fu, J. Huard, Skeletal muscle fiber type conversion during the repair of mouse soleus: potential implications for muscle healing after injury, Journal of orthopaedic research : official publication of the Orthopaedic Research Society 25(11) (2007) 1534-40.

[328] P. Marin, B. Andersson, M. Krotkiewski, P. Bjorntorp, Muscle fiber composition and capillary density in women and men with NIDDM, Diabetes care 17(5) (1994) 382-6.

[329] V.Z. Beachley, M.T. Wolf, K. Sadtler, S.S. Manda, H. Jacobs, M.R. Blatchley, J.S. Bader, A. Pandey, D. Pardoll, J.H. Elisseeff, Tissue matrix arrays for high-throughput screening and systems analysis of cell function, Nature methods 12(12) (2015) 1197-204.

[330] C. Bonnans, J. Chou, Z. Werb, Remodelling the extracellular matrix in development and disease, Nature reviews. Molecular cell biology 15(12) (2014) 786-801.

[331] S. Ozbek, P.G. Balasubramanian, R. Chiquet-Ehrismann, R.P. Tucker, J.C. Adams, The evolution of extracellular matrix, Molecular biology of the cell 21(24) (2010) 4300-4305.

[332] J.A. Fishman, L. Scobie, Y. Takeuchi, Xenotransplantation-associated infectious risk: a WHO consultation, Xenotransplantation 19(2) (2012) 72-81.

[333] Y. Ji, Z. Wu, Z. Dai, X. Wang, J. Li, B. Wang, G. Wu, Fetal and neonatal programming of postnatal growth and feed efficiency in swine, Journal of animal science and biotechnology 8 (2017) 42-42.

[334] C.K. Abrass, M.J. Adcox, G.J. Raugi, Aging-associated changes in renal extracellular matrix, The American Journal of Pathology 146(3) (1995) 742-52.

[335] B. Bartling, M. Desole, S. Rohrbach, R.E. Silber, A. Simm, Age-associated changes of extracellular matrix collagen impair lung cancer cell migration, FASEB journal : official publication of the Federation of American Societies for Experimental Biology 23(5) (2009) 1510-20.

[336] M.L. Burgess, J.C. McCrea, H.L. Hedrick, Age-associated changes in cardiac matrix and integrins, Mechanisms of ageing and development 122(15) (2001) 1739-56.

[337] J.D. Furber, Extracellular glycation crosslinks: prospects for removal, Rejuvenation research 9(2) (2006) 274-8.

[338] A. Kurtz, S.J. Oh, Age related changes of the extracellular matrix and stem cell maintenance, Preventive medicine 54 Suppl (2012) S50-6.

[339] J. Berrou, I. Tostivint, F. Verrecchia, C. Berthier, E. Boulanger, A. Mauviel, H.P. Marti, M.P. Wautier, J.L. Wautier, E. Rondeau, A. Hertig, Advanced glycation end products regulate extracellular matrix protein and protease expression by human glomerular mesangial cells, International journal of molecular medicine 23(4) (2009) 513-20.

[340] J. Peake, P. Della Gatta, D. Cameron-Smith, Aging and its effects on inflammation in skeletal muscle at rest and following exercise-induced muscle injury, American journal of physiology. Regulatory, integrative and comparative physiology 298(6) (2010) R1485-95.

[341] A.I. Serban, L. Stanca, O.I. Geicu, M.C. Munteanu, M. Costache, A. Dinischiotu, Extracellular matrix is modulated in advanced glycation end products milieu via a RAGE receptor dependent pathway boosted by transforming growth factor-beta1 RAGE, Journal of diabetes 7(1) (2015) 114-24.

[342] M.P. Krause, D. Al-Sajee, D.M. D'Souza, I.A. Rebalka, J. Moradi, M.C. Riddell, T.J. Hawke, Impaired macrophage and satellite cell infiltration occurs in a muscle-specific fashion following injury in diabetic skeletal muscle, PLoS One 8(8) (2013) e70971.

[343] S.E. Abdel, I. Abdel-Meguid, S. Korraa, Markers of oxidative stress and aging in Duchene muscular dystrophy patients and the possible ameliorating effect of He:Ne laser, Acta myologica : myopathies and cardiomyopathies : official journal of the Mediterranean Society of Myology 26(1) (2007) 14-21.

[344] S. Jeddi, S. Khalifi, M. Ghanbari, F. Bageripour, A. Ghasemi, Effects of Nitrate Intake on Myocardial Ischemia-Reperfusion Injury in Diabetic Rats, Arquivos brasileiros de cardiologia 107(4) (2016) 339-347.

[345] A. Vasilaki, M.J. Jackson, Role of reactive oxygen species in the defective regeneration seen in aging muscle, Free radical biology & medicine 65 (2013) 317-323.

[346] S. Fujimaki, T. Wakabayashi, T. Takemasa, M. Asashima, T. Kuwabara, Diabetes and stem cell function, BioMed research international 2015 (2015) 592915-592915.

[347] C.F. McKenna, C.S. Fry, Altered satellite cell dynamics accompany skeletal muscle atrophy during chronic illness, disuse, and aging, Current opinion in clinical nutrition and metabolic care 20(6) (2017) 447-452.

[348] R. Berria, L. Wang, D.K. Richardson, J. Finlayson, R. Belfort, T. Pratipanawatr, E.A. De Filippis, S. Kashyap, L.J. Mandarino, Increased collagen content in insulin-resistant skeletal muscle, American journal of physiology. Endocrinology and metabolism 290(3) (2006) E560-5.

[349] C.A. Stuart, M.P. McCurry, A. Marino, M.A. South, M.E.A. Howell, A.S. Layne, M.W. Ramsey, M.H. Stone, Slow-twitch fiber proportion in skeletal muscle correlates with insulin responsiveness, The Journal of clinical endocrinology and metabolism 98(5) (2013) 2027-2036.

[350] P.M. Crapo, T.W. Gilbert, S.F. Badylak, An overview of tissue and whole organ decellularization processes, Biomaterials 32(12) (2011) 3233-43.

[351] R. Rutkowski, S.A. Pancewicz, K. Rutkowski, J. Rutkowska, [Reactive oxygen and nitrogen species in inflammatory process], Polski merkuriusz lekarski : organ Polskiego Towarzystwa Lekarskiego 23(134) (2007) 131-6.

[352] Q. Huang, R.A. Dawson, D.E. Pegg, J.N. Kearney, S. Macneil, Use of peracetic acid to sterilize human donor skin for production of acellular dermal matrices for clinical use, Wound repair and regeneration : official publication of the Wound Healing Society [and] the European Tissue Repair Society 12(3) (2004) 276-87.

[353] N. Poornejad, J.J. Nielsen, R.J. Morris, J.R. Gassman, P.R. Reynolds, B.L. Roeder, A.D. Cook, Comparison of four decontamination treatments on porcine renal decellularized extracellular matrix structure, composition, and support of human renal cortical tubular epithelium cells, Journal of biomaterials applications 30(8) (2016) 1154-67.

[354] E.A. Wrona, R. Peng, H. Born, M.R. Amin, R.C. Branski, D.O. Freytes, Derivation and characterization of porcine vocal fold extracellular matrix scaffold, The Laryngoscope 126(4) (2016) 928-35.

[355] V. Oliveira-Marques, H.S. Marinho, L. Cyrne, F. Antunes, Role of hydrogen peroxide in NF-kappaB activation: from inducer to modulator, Antioxidants & redox signaling 11(9) (2009) 2223-43.

[356] F. Gruber, C.M. Ornelas, S. Karner, M.S. Narzt, I.M. Nagelreiter, M. Gschwandtner, V. Bochkov, E. Tschachler, Nrf2 deficiency causes lipid oxidation, inflammation, and matrix-protease expression in DHA-supplemented and UVA-irradiated skin fibroblasts, Free radical biology & medicine 88(Pt B) (2015) 439-451.

[357] S. Garcia-Santamarina, S. Boronat, E. Hidalgo, Reversible cysteine oxidation in hydrogen peroxide sensing and signal transduction, Biochemistry 53(16) (2014) 2560-80.

[358] J.W. Seo, E.J. Yang, K.H. Yoo, I.H. Choi, Macrophage Differentiation from Monocytes Is Influenced by the Lipid Oxidation Degree of Low Density Lipoprotein, Mediators of inflammation 2015 (2015) 235797.

[359] S. Yoganarasimha, W.R. Trahan, A.M. Best, G.L. Bowlin, T.O. Kitten, P.C. Moon, P.A. Madurantakam, Peracetic acid: a practical agent for sterilizing heat-labile polymeric tissue-engineering scaffolds, Tissue engineering. Part C, Methods 20(9) (2014) 714-23.

[360] M. Zhou, N. Zhang, X. Liu, Y. Li, Y. Zhang, X. Wang, B. Li, B. Li, Tendon allograft sterilized by peracetic acid/ethanol combined with gamma irradiation, Journal of orthopaedic science : official journal of the Japanese Orthopaedic Association 19(4) (2014) 627-36.

[361] E. Park, C. Lee, M. Bisesi, J. Lee, Efficiency of peracetic acid in inactivating bacteria, viruses, and spores in water determined with ATP bioluminescence, quantitative PCR, and culture-based methods, Journal of water and health 12(1) (2014) 13-23.

[362] Y. Zhang, S. Choksi, K. Chen, Y. Pobezinskaya, I. Linnoila, Z.-G. Liu, ROS play a critical role in the differentiation of alternatively activated macrophages and the occurrence of tumor-associated macrophages, Cell Research 23 (2013) 898.

[363] W.J. Lee, S. Tateya, A.M. Cheng, N. Rizzo-DeLeon, N.F. Wang, P. Handa, C.L. Wilson, A.W. Clowes, I.R. Sweet, K. Bomsztyk, M.W. Schwartz, F. Kim, M2 Macrophage Polarization Mediates Anti-inflammatory Effects of Endothelial Nitric Oxide Signaling, Diabetes 64(8) (2015) 2836-46.

[364] M.A. Rahat, B. Hemmerlein, Macrophage-tumor cell interactions regulate the function of nitric oxide, Frontiers in physiology 4 (2013) 144.

[365] P. Martinez, A. Denys, M. Delos, A.S. Sikora, M. Carpentier, S. Julien, J. Pestel, F. Allain, Macrophage polarization alters the expression and sulfation pattern of glycosaminoglycans, Glycobiology 25(5) (2015) 502-13.

[366] G. Lu, R. Zhang, S. Geng, L. Peng, P. Jayaraman, C. Chen, F. Xu, J. Yang, Q. Li, H. Zheng, K. Shen, J. Wang, X. Liu, W. Wang, Z. Zheng, C.F. Qi, C. Si, J.C. He, K. Liu, S.A. Lira,

A.G. Sikora, L. Li, H. Xiong, Myeloid cell-derived inducible nitric oxide synthase suppresses M1 macrophage polarization, Nature communications 6 (2015) 6676.

[367] A. Loboda, M. Damulewicz, E. Pyza, A. Jozkowicz, J. Dulak, Role of Nrf2/HO-1 system in development, oxidative stress response and diseases: an evolutionarily conserved mechanism, Cellular and molecular life sciences : CMLS 73(17) (2016) 3221-47.

[368] J.L. Dziki, D.S. Wang, C. Pineda, B.M. Sicari, T. Rausch, S.F. Badylak, Solubilized extracellular matrix bioscaffolds derived from diverse source tissues differentially influence macrophage phenotype, Journal of biomedical materials research. Part A 105(1) (2017) 138-147.

[369] B. Sicari, N. Turner, S.F. Badylak, An in vivo model system for evaluation of the host response to biomaterials, Methods in molecular biology (Clifton, N.J.) 1037 (2013) 3-25.

[370] B.N. Brown, J.E. Valentin, A.M. Stewart-Akers, G.P. McCabe, S.F. Badylak, Macrophage phenotype and remodeling outcomes in response to biologic scaffolds with and without a cellular component, Biomaterials 30(8) (2009) 1482-91.

[371] M. Rath, I. Muller, P. Kropf, E.I. Closs, M. Munder, Metabolism via Arginase or Nitric Oxide Synthase: Two Competing Arginine Pathways in Macrophages, Frontiers in Immunology 5 (2014) 532.

[372] Y. Naito, T. Takagi, Y. Higashimura, Heme oxygenase-1 and anti-inflammatory M2 macrophages, Archives of biochemistry and biophysics 564 (2014) 83-8.

[373] D.M. Faulk, R. Londono, M.T. Wolf, C.A. Ranallo, C.A. Carruthers, J.D. Wildemann, C.L. Dearth, S.F. Badylak, ECM hydrogel coating mitigates the chronic inflammatory response to polypropylene mesh, Biomaterials 35(30) (2014) 8585-95.

[374] A. Dos Anjos Cassado, F4/80 as a Major Macrophage Marker: The Case of the Peritoneum and Spleen, Results and problems in cell differentiation 62 (2017) 161-179.

[375] B.J. Larson, M.T. Longaker, H.P. Lorenz, Scarless Fetal Wound Healing: A Basic Science Review, Plastic and reconstructive surgery 126(4) (2010) 1172-1180.

[376] D.M.S. Lundvig, S. Immenschuh, F.A.D.T.G. Wagener, Heme Oxygenase, Inflammation, and Fibrosis: The Good, the Bad, and the Ugly?, Frontiers in Pharmacology 3 (2012) 81.

[377] A. Grochot-Przeczek, R. Lach, J. Mis, K. Skrzypek, M. Gozdecka, P. Sroczynska, M. Dubiel, A. Rutkowski, M. Kozakowska, A. Zagorska, J. Walczynski, H. Was, J. Kotlinowski, J. Drukala, K. Kurowski, C. Kieda, Y. Herault, J. Dulak, A. Jozkowicz, Heme oxygenase-1 accelerates cutaneous wound healing in mice, PLoS One 4(6) (2009) e5803.

[378] K. Pietraszek-Gremplewicz, M. Kozakowska, I. Bronisz-Budzynska, M. Ciesla, O. Mucha, P. Podkalicka, M. Madej, U. Glowniak, K. Szade, J. Stepniewski, M. Jez, K. Andrysiak, K. Bukowska-Strakova, A. Kaminska, A. Kostera-Pruszczyk, A. Jozkowicz, A. Loboda, J. Dulak, Heme Oxygenase-1 Influences Satellite Cells and Progression of Duchenne Muscular Dystrophy in Mice, Antioxidants & redox signaling 29(2) (2018) 128-148.

[379] M. Kozakowska, K. Pietraszek-Gremplewicz, M. Ciesla, M. Seczynska, I. Bronisz-Budzynska, P. Podkalicka, K. Bukowska-Strakova, A. Loboda, A. Jozkowicz, J. Dulak, Lack of Heme Oxygenase-1 Induces Inflammatory Reaction and Proliferation of Muscle Satellite Cells after Cardiotoxin-Induced Skeletal Muscle Injury, The American Journal of Pathology 188(2) (2018) 491-506.

[380] T.R. Hurd, M. DeGennaro, R. Lehmann, Redox regulation of cell migration and adhesion, Trends in cell biology 22(2) (2012) 107-115.

[381] S. Mahbub, A.L. Brubaker, E.J. Kovacs, Aging of the Innate Immune System: An Update, Current immunology reviews 7(1) (2011) 104-115.

[382] D.T. Graves, R.A. Kayal, Diabetic complications and dysregulated innate immunity, Frontiers in bioscience : a journal and virtual library 13 (2008) 1227-1239.

[383] D. Hackel, D. Pflucke, A. Neumann, J. Viebahn, S. Mousa, E. Wischmeyer, N. Roewer, A. Brack, H.L. Rittner, The connection of monocytes and reactive oxygen species in pain, PLoS One 8(5) (2013) e63564.

[384] S. Ullevig, Q. Zhao, C.F. Lee, H. Seok Kim, D. Zamora, R. Asmis, NADPH oxidase 4 mediates monocyte priming and accelerated chemotaxis induced by metabolic stress, Arteriosclerosis, thrombosis, and vascular biology 32(2) (2012) 415-26.

[385] C.F. Lee, S. Ullevig, H.S. Kim, R. Asmis, Regulation of Monocyte Adhesion and Migration by Nox4, PLoS One 8(6) (2013) e66964.

[386] M.T. Longaker, E.S. Chiu, N.S. Adzick, M. Stern, M.R. Harrison, R. Stern, Studies in fetal wound healing. V. A prolonged presence of hyaluronic acid characterizes fetal wound fluid, Annals of surgery 213(4) (1991) 292-6.

[387] M. Long, M. Rojo de la Vega, Q. Wen, M. Bharara, T. Jiang, R. Zhang, S. Zhou, P.K. Wong, G.T. Wondrak, H. Zheng, D.D. Zhang, An Essential Role of NRF2 in Diabetic Wound Healing, Diabetes 65(3) (2016) 780-93.

[388] P. Tessari, D. Cecchet, A. Cosma, M. Vettore, A. Coracina, R. Millioni, E. Iori, L. Puricelli, A. Avogaro, M. Vedovato, Nitric Oxide Synthesis Is Reduced in Subjects With Type 2 Diabetes and Nephropathy, Diabetes 59(9) (2010) 2152-9.

[389] D. André-Lévigne, A. Modarressi, M.S. Pepper, B. Pittet-Cuénod, Reactive Oxygen Species and NOX Enzymes Are Emerging as Key Players in Cutaneous Wound Repair, International Journal of Molecular Sciences 18(10) (2017) 2149.

[390] S.F. Badylak, T. Hoppo, A. Nieponice, T.W. Gilbert, J.M. Davison, B.A. Jobe, Esophageal preservation in five male patients after endoscopic inner-layer circumferential resection in the setting of superficial cancer: a regenerative medicine approach with a biologic scaffold, Tissue engineering. Part A 17(11-12) (2011) 1643-50.

[391] B.M. Sicari, J.P. Rubin, C.L. Dearth, M.T. Wolf, F. Ambrosio, M. Boninger, N.J. Turner, D.J. Weber, T.W. Simpson, A. Wyse, E.H. Brown, J.L. Dziki, L.E. Fisher, S. Brown, S.F. Badylak, An acellular biologic scaffold promotes skeletal muscle formation in mice and humans with volumetric muscle loss, Science translational medicine 6(234) (2014) 234ra58.

[392] S.B. Seif-Naraghi, J.M. Singelyn, M.A. Salvatore, K.G. Osborn, J.J. Wang, U. Sampat, O.L. Kwan, G.M. Strachan, J. Wong, P.J. Schup-Magoffin, R.L. Braden, K. Bartels, J.A. DeQuach, M. Preul, A.M. Kinsey, A.N. DeMaria, N. Dib, K.L. Christman, Safety and efficacy of an injectable extracellular matrix hydrogel for treating myocardial infarction, Science translational medicine 5(173) (2013) 173ra25.

[393] C.J. Medberry, P.M. Crapo, B.F. Siu, C.A. Carruthers, M.T. Wolf, S.P. Nagarkar, V. Agrawal, K.E. Jones, J. Kelly, S.A. Johnson, S.S. Velankar, S.C. Watkins, M. Modo, S.F. Badylak, Hydrogels derived from central nervous system extracellular matrix, Biomaterials 34(4) (2013) 1033-40.

[394] M.J. Sawkins, W. Bowen, P. Dhadda, H. Markides, L.E. Sidney, A.J. Taylor, F.R. Rose, S.F. Badylak, K.M. Shakesheff, L.J. White, Hydrogels derived from demineralized and decellularized bone extracellular matrix, Acta biomaterialia 9(8) (2013) 7865-73.

[395] T. Zantop, T.W. Gilbert, M.C. Yoder, S.F. Badylak, Extracellular matrix scaffolds are repopulated by bone marrow-derived cells in a mouse model of achilles tendon reconstruction, Journal of orthopaedic research : official publication of the Orthopaedic Research Society 24(6) (2006) 1299-309.

[396] B.N. Brown, W.L. Chung, A.J. Almarza, M.D. Pavlick, S.N. Reppas, M.W. Ochs, A.J. Russell, S.F. Badylak, Inductive, scaffold-based, regenerative medicine approach to reconstruction of the temporomandibular joint disk, Journal of oral and maxillofacial surgery : official journal of the American Association of Oral and Maxillofacial Surgeons 70(11) (2012) 2656-68.

[397] Y. Zhang, Y. He, S. Bharadwaj, N. Hammam, K. Carnagey, R. Myers, A. Atala, M. Van Dyke, Tissue-specific extracellular matrix coatings for the promotion of cell proliferation and maintenance of cell phenotype, Biomaterials 30(23-24) (2009) 4021-8.

[398] T.L. Sellaro, A. Ranade, D.M. Faulk, G.P. McCabe, K. Dorko, S.F. Badylak, S.C. Strom, Maintenance of human hepatocyte function in vitro by liver-derived extracellular matrix gels, Tissue engineering. Part A 16(3) (2010) 1075-82.

[399] P. Chandra, S.J. Lee, Synthetic Extracellular Microenvironment for Modulating Stem Cell Behaviors, Biomarker Insights 10(Suppl 1) (2015) 105-16.

[400] D.O. Freytes, R.S. Tullius, S.F. Badylak, Effect of storage upon material properties of lyophilized porcine extracellular matrix derived from the urinary bladder, Journal of biomedical materials research. Part B, Applied biomaterials 78(2) (2006) 327-33.

[401] N. Han, M.A. Yabroudi, K. Stearns-Reider, W. Helkowski, B.M. Sicari, J.P. Rubin, S.F. Badylak, M.L. Boninger, F. Ambrosio, Electrodiagnostic Evaluation of Individuals Implanted With Extracellular Matrix for the Treatment of Volumetric Muscle Injury: Case Series, Physical therapy 96(4) (2016) 540-9.

[402] B.N. Brown, W.L. Chung, M. Pavlick, S. Reppas, M.W. Ochs, A.J. Russell, S.F. Badylak, Extracellular matrix as an inductive template for temporomandibular joint meniscus reconstruction: a pilot study, Journal of oral and maxillofacial surgery : official journal of the American Association of Oral and Maxillofacial Surgeons 69(12) (2011) e488-505.

[403] J.S. Roth, C. Brathwaite, K. Hacker, K. Fisher, J. King, Complex ventral hernia repair with a human acellular dermal matrix, Hernia : the journal of hernias and abdominal wall surgery 19(2) (2015) 247-52.

[404] Y. Puckett, T. Pham, S. McReynolds, C.A. Ronaghan, Porcine Urinary Bladder Matrix for Management of Infected Radiation Mastectomy Wound, Cureus 9(7) (2017) e1451.

[405] Y.Y. Li, H.T. Cheung, Basement membrane and its components on lymphocyte adhesion, migration, and proliferation, Journal of immunology (Baltimore, Md. : 1950) 149(10) (1992) 3174-81.

[406] E. Korpos, C. Wu, J. Song, R. Hallmann, L. Sorokin, Role of the extracellular matrix in lymphocyte migration, Cell and tissue research 339(1) (2010) 47-57.

[407] A.J. Engler, S. Sen, H.L. Sweeney, D.E. Discher, Matrix elasticity directs stem cell lineage specification, Cell 126(4) (2006) 677-89.

[408] R.F. MacBarb, A.L. Chen, J.C. Hu, K.A. Athanasiou, Engineering functional anisotropy in fibrocartilage neotissues, Biomaterials 34(38) (2013) 9980-9.

[409] J.M. Reinke, H. Sorg, Wound repair and regeneration, European surgical research. Europaische chirurgische Forschung. Recherches chirurgicales europeennes 49(1) (2012) 35-43.

[410] M.P. Rodero, K. Khosrotehrani, Skin wound healing modulation by macrophages, International journal of clinical and experimental pathology 3(7) (2010) 643-53.

[411] P. Bainbridge, Wound healing and the role of fibroblasts, Journal of wound care 22(8) (2013) 407-8, 410-12.

[412] T.J. Koh, L.A. DiPietro, Inflammation and wound healing: the role of the macrophage, Expert reviews in molecular medicine 13 (2011) e23.

[413] I.A. Darby, T.D. Hewitson, Fibroblast differentiation in wound healing and fibrosis, International review of cytology 257 (2007) 143-79.

[414] A. Mantovani, S.K. Biswas, M.R. Galdiero, A. Sica, M. Locati, Macrophage plasticity and polarization in tissue repair and remodelling, The Journal of pathology 229(2) (2013) 176-85.

[415] A. Mantovani, A. Sica, M. Locati, Macrophage polarization comes of age, Immunity 23(4) (2005) 344-6.

[416] R.E. Mirza, M.M. Fang, M.L. Novak, N. Urao, A. Sui, W.J. Ennis, T.J. Koh, Macrophage PPARgamma and impaired wound healing in type 2 diabetes, The Journal of pathology 236(4) (2015) 433-44.

[417] T.T. Braga, J.S.H. Agudelo, N.O.S. Camara, Macrophages During the Fibrotic Process: M2 as Friend and Foe, Frontiers in Immunology 6 (2015).

[418] C.M. Minutti, J.A. Knipper, J.E. Allen, D.M.W. Zaiss, Tissue-specific contribution of macrophages to wound healing, Seminars in Cell & Developmental Biology 61 (2017) 3-11.

[419] T. Lucas, A. Waisman, R. Ranjan, J. Roes, T. Krieg, W. Muller, A. Roers, S.A. Eming, Differential roles of macrophages in diverse phases of skin repair, Journal of immunology (Baltimore, Md. : 1950) 184(7) (2010) 3964-77.

[420] I.A. Darby, B. Laverdet, F. Bonté, A. Desmoulière, Fibroblasts and myofibroblasts in wound healing, Clinical, Cosmetic and Investigational Dermatology 7 (2014) 301-311.

[421] G. Baneyx, L. Baugh, V. Vogel, Fibronectin extension and unfolding within cell matrix fibrils controlled by cytoskeletal tension, Proc Natl Acad Sci U S A 99(8) (2002) 5139-43.

[422] S. Chakravarti, M.F. Tam, A.E. Chung, The basement membrane glycoprotein entactin promotes cell attachment and binds calcium ions, The Journal of biological chemistry 265(18) (1990) 10597-603.

[423] B. Steffensen, L. Hakkinen, H. Larjava, Proteolytic events of wound-healing--coordinated interactions among matrix metalloproteinases (MMPs), integrins, and extracellular matrix molecules, Critical reviews in oral biology and medicine : an official publication of the American Association of Oral Biologists 12(5) (2001) 373-98.

[424] S. Barrientos, O. Stojadinovic, M.S. Golinko, H. Brem, M. Tomic-Canic, Growth factors and cytokines in wound healing, Wound repair and regeneration : official publication of the Wound Healing Society [and] the European Tissue Repair Society 16(5) (2008) 585-601.

[425] N.W. Lukacs, S.L. Kunkel, R. Allen, H.L. Evanoff, C.L. Shaklee, J.S. Sherman, M.D. Burdick, R.M. Strieter, Stimulus and cell-specific expression of C-X-C and C-C chemokines by pulmonary stromal cell populations, The American journal of physiology 268(5 Pt 1) (1995) L856-61.

[426] R.T. Kendall, C.A. Feghali-Bostwick, Fibroblasts in fibrosis: novel roles and mediators, Frontiers in Pharmacology 5(123) (2014).

[427] M.-L. Bochaton-Piallat, G. Gabbiani, B. Hinz, The myofibroblast in wound healing and fibrosis: answered and unanswered questions, F1000Research 5 (2016) F1000 Faculty Rev-752.

[428] T. Oka, K. Ohta, T. Kanazawa, K. Nakamura, Interaction between Macrophages and Fibroblasts during Wound Healing of Burn Injuries in Rats, The Kurume medical journal 62(3-4) (2016) 59-66.

[429] A.B. Shekhter, G.N. Berchenko, A.V. Nikolaev, [Macrophage-fibroblast interaction and its possible role in regulating collagen metabolism during wound healing], Biulleten' eksperimental'noi biologii i meditsiny 83(5) (1977) 627-30.

[430] C. Vancheri, C. Mastruzzo, V. Tomaselli, M.A. Sortino, L. D'Amico, G. Bellistrí, M.P. Pistorio, E.T. Salinaro, F. Palermo, A. Mistretta, N. Crimi, Normal Human Lung Fibroblasts Differently Modulate Interleukin-10 and Interleukin-12 Production by Monocytes, American Journal of Respiratory Cell and Molecular Biology 25(5) (2001) 592-599.

[431] S. Van Linthout, K. Miteva, C. Tschöpe, Crosstalk between fibroblasts and inflammatory cells, Cardiovascular Research 102(2) (2014) 258-269.

[432] M. Jordana, B. Sarnstrand, P.J. Sime, I. Ramis, Immune-inflammatory functions of fibroblasts, The European respiratory journal 7(12) (1994) 2212-22.

[433] L.A. Bautista-Hernández, J.L. Gómez-Olivares, B. Buentello-Volante, V.M.B.-d. Lucio, Fibroblasts: the unknown sentinels eliciting immune responses against microorganisms, European Journal of Microbiology and Immunology 7(3) (2017) 151-157.

[434] D.A. Wink, K.M. Miranda, M.G. Espey, R.M. Pluta, S.J. Hewett, C. Colton, M. Vitek, M. Feelisch, M.B. Grisham, Mechanisms of the antioxidant effects of nitric oxide, Antioxidants & redox signaling 3(2) (2001) 203-13.

[435] R.W. Caldwell, P.C. Rodriguez, H.A. Toque, S.P. Narayanan, R.B. Caldwell, Arginase: A Multifaceted Enzyme Important in Health and Disease, Physiological reviews 98(2) (2018) 641-665.

[436] M. Rodrigues, G. Gurtner, Black, White, and Gray: Macrophages in Skin Repair and Disease, Current pathobiology reports 5(4) (2017) 333-342.

[437] A. Sica, A. Mantovani, Macrophage plasticity and polarization: in vivo veritas, The Journal of clinical investigation 122(3) (2012) 787-95.

[438] T.A. Wynn, L. Barron, Macrophages: master regulators of inflammation and fibrosis, Seminars in liver disease 30(3) (2010) 245-57.

[439] J.A. Belperio, M. Dy, L. Murray, M.D. Burdick, Y.Y. Xue, R.M. Strieter, M.P. Keane, The role of the Th2 CC chemokine ligand CCL17 in pulmonary fibrosis, Journal of immunology (Baltimore, Md. : 1950) 173(7) (2004) 4692-8.

[440] A.M. Tager, R.L. Kradin, P. LaCamera, S.D. Bercury, G.S. Campanella, C.P. Leary, V. Polosukhin, L.H. Zhao, H. Sakamoto, T.S. Blackwell, A.D. Luster, Inhibition of pulmonary fibrosis by the chemokine IP-10/CXCL10, American journal of respiratory cell and molecular biology 31(4) (2004) 395-404.

[441] F. Li, H. Dai, J. Geng, X. Xu, Inhibiting CXCR4/CXCL12 axis attenuates lung fibrosis both in vitro and in vivo, European Respiratory Journal 40(Suppl 56) (2012).

[442] C.E. Brokopp, R. Schoenauer, P. Richards, S. Bauer, C. Lohmann, M.Y. Emmert, B. Weber, S. Winnik, E. Aikawa, K. Graves, M. Genoni, P. Vogt, T.F. Luscher, C. Renner, S.P. Hoerstrup, C.M. Matter, Fibroblast activation protein is induced by inflammation and degrades type I collagen in thin-cap fibroatheromata, European heart journal 32(21) (2011) 2713-22.

[443] M. Nahrendorf, F.K. Swirski, E. Aikawa, L. Stangenberg, T. Wurdinger, J.-L. Figueiredo, P. Libby, R. Weissleder, M.J. Pittet, The healing myocardium sequentially mobilizes two monocyte subsets with divergent and complementary functions, The Journal of Experimental Medicine 204(12) (2007) 3037.

[444] L.A. Murray, Q. Chen, M.S. Kramer, D.P. Hesson, R.L. Argentieri, X. Peng, M. Gulati, R.J. Homer, T. Russell, N. van Rooijen, J.A. Elias, C.M. Hogaboam, E.L. Herzog, TGF-beta

driven lung fibrosis is macrophage dependent and blocked by Serum amyloid P, The international journal of biochemistry & cell biology 43(1) (2011) 154-62.

[445] E.E. Benarroch, Nitric oxide, Neurology 77(16) (2011) 1568.

[446] A. Aderem, D.M. Underhill, Mechanisms of phagocytosis in macrophages, Annual review of immunology 17 (1999) 593-623.

[447] V.A. Fadok, D.L. Bratton, A. Konowal, P.W. Freed, J.Y. Westcott, P.M. Henson, Macrophages that have ingested apoptotic cells in vitro inhibit proinflammatory cytokine production through autocrine/paracrine mechanisms involving TGF-beta, PGE2, and PAF, The Journal of Clinical Investigation 101(4) (1998) 890-898.

[448] C. Rouault, V. Pellegrinelli, R. Schilch, A. Cotillard, C. Poitou, J. Tordjman, H. Sell, K. Clément, D. Lacasa, Roles of Chemokine Ligand-2 (CXCL2) and Neutrophils in Influencing Endothelial Cell Function and Inflammation of Human Adipose Tissue, Endocrinology 154(3) (2013) 1069-1079.

[449] T. Baba, N. Mukaida, Role of macrophage inflammatory protein (MIP)-1α/CCL3 in leukemogenesis, Molecular & Cellular Oncology 1(1) (2014) e29899.